6. SITE 650: MARSILI BASIN[1]

Shipboard Scientific Party[2]

HOLE 650A

Date occupied: 2 January 1986

Date departed: 9 January 1986

Time on hole: 6 days, 17 hr

Position: 39° 21.40′N.; 13° 54.05′E.

Water depth (sea level, corrected m, echo-sounding): 3516.3

Water depth (rig floor, corrected m, echo-sounding): 3526.3

Bottom felt (m, drill pipe length from rig floor): 3529

Total depth (m): 4162.8

Penetration (m): 633.8

Number of cores: 69

Total length of cored section (m): 633.8

Total core recovered (m): 315.6

Core recovery (%): 49.7

Deepest sedimentary unit cored:
Depth sub-bottom (m): 565
Nature: Nannofossil ooze and green-grey mudstone
Age: late Pliocene
Measured vertical sound velocity (km/s): 1.6 to 2.3

Igneous or metamorphic basement:
Depth sub-bottom (m): 601.9 (top); 633.8 (bottom of the hole)
Nature: Vesicular basalt
Velocity range (km/s): 2.8 to 3.2

HOLE 650B

Date occupied: 9 January 1986

Date departed: 10 January 1986

Time on hole: 1 day, 6.3 hr

Position: 39° 21.40′N.; 13° 54.05′E.

Water depth (sea level, corrected m, echo-sounding): 3516.3

Water depth (rig floor, corrected m, echo-sounding): 3526.3

Bottom felt (m, drill pipe length from rig floor): 3529

Total depth (m): 3631.5

Penetration (m): 102.5

Number of cores: 0

Total length of cored section (m): 0

Total core recovered (m): 0

Core recovery (%): 0

Deepest sedimentary unit cored: None

Igneous or metamorphic basement: None

Principal results: Site 650 was located near the western rim of the Marsili Basin, which is the eastern of two deep basins in the Tyrrhenian Sea (Fig. 1). Drilling established the presence of vesicular basalt beneath an unexpectedly young sedimentary cover of late Pliocene to Pleistocene age.

Two major sedimentary units were recovered between the seafloor and 602 mbsf, and basalt was recovered between 602 m and 634 mbsf (Fig. 2). The lithologic units were as follows:

Sedimentary Unit I: Depth: 0–354 mbsf; age: <0.45 m.y. (NN19/NN20). Normally graded sequences of gravel to sand-sized clastics with low carbonate content, with thicknesses on the order of decimeters and meters, intercalated with muds. The normally graded sequences are interpreted as turbidites. Coarse basal portions of the turbidites are dominated by volcaniclastic components (glass and pumice fragments). The fine-grained upper portion of each turbidite is a calcareous mud, occasionally containing volcanic ash. A thick pumice layer, as much as 32 m thick, occurs in the middle of the unit.

Sedimentary Unit II: Depth: 354–602 mbsf; age: from late Pleistocene (0.45 m.y.) to late Pliocene (~2.0 m.y.). The upper part of Unit II (354–546 mbsf) is predominantly calcareous mud and mudstones, interbedded with thin normally graded clastic sequences interpreted as volcaniclastic turbidites. The lower part (546–602 mbsf) consists of nannofossil ooze, calcareous muds, pebbly mudstones, thin sapropels, and slump deposits. A 10-m-thick basal unit of red-brown to grayish-green nannofossil ooze, possibly a metalliferous facies, lies in contact with basalt.

Vesicular basalt: Cores: 107-650A-66X, to -69X; Depth: 602–634 mbsf. The top part of the basalt unit consists of strongly altered glass containing a few scattered skeletal Ca-plagioclase crystals and pseudomorphs after olivine. Further down in the section, the crystallinity increases and the basalt shows intersertal to intergranular

---

[1] Kastens, K. A., Mascle, J, Auroux, C., et al., 1987. *Proc., Init. Repts. (Pt. A), ODP*, 107.

[2] Kim A. Kastens (Co-Chief Scientist), Lamont-Doherty Geological Observatory, Palisades, NY 10964; Jean Mascle (Co-Chief Scientist), Laboratoire de Géodynamique Sous-Marine, Université Pierre et Marie Curie, BP 48, 06230 Villefranche-sur-Mer, France; Christian Auroux, Staff Scientist, Ocean Drilling Program, Texas A&M University, College Station, TX 77843; Enrico Bonatti, Lamont-Doherty Geological Observatory, Palisades, NY 10964; Cristina Broglia, Lamont-Doherty Geological Observatory, Palisades, NY 10964; James Channell, Department of Geology, 1112 Turlington Hall, University of Florida, Gainesville, FL 32611; Pietro Curzi, Istituto di Geologia Marina, Via Zamboni, 65, 40127 Bologna, Italy; Kay-Christian Emeis, Ocean Drilling Program, Texas A&M University, College Station, TX 77843; Georgette Glaçon, Laboratoire de Stratigraphie et de Paleoécologie, Centre Saint-Charles, Université de Provence, 3, Place Victor Hugo, 13331 Marseille Cedex, France; Shiro Hasegawa, Institute of Geology, Faculty of Science, Tohoku University, Aobayama, Sendai, 980, Japan; Werner Hieke, Lehrstuhl für Allgemeine, Angewandte und Ingenieur-Geologie, Abt. Sedimentforschung und Meeresgeologie, Technische Universität München, Lichtenbergstrasse 4, D-8046 Garching, Federal Republic of Germany; Floyd McCoy, Lamont-Doherty Geological Observatory, Palisades, NY 10964; Judith McKenzie, Department of Geology, University of Florida, 1112 Turlington Hall, Gainesville, FL 32611; Georges Mascle, Institut Dolomieu, Université Scientifique et Médicale de Grenoble, 15 Rue Maurice Gignoux, 38031 Grenoble Cedex, France; James Mendelson, Earth Resources Laboratory E34-366, Department of Earth, Atmospheric and Planetary Sciences, Massachusetts Institute of Technology, 42 Carleton Street, Cambridge, MA 02142; Carla Müller, Geol.-Paläont. Institut, Universität Frankfurt/Main, 32–34 Senckenberg-Anlage, D-6000 Frankfurt/Main 1, Federal Republic of Germany (current address: 1 Rue Martignon, 92500 Rueil-Malmaison, France); Jean-Pierre Réhault, Laboratoire de Géodynamique Sous-Marine, Université Pierre et Marie Curie, BP 48, 06230 Villefranche-sur-Mer, France; Alastair Robertson, U.S. Geological Survey, 345 Middlefield Road, Menlo Park, CA 94025 (current address: Department of Geology, Grant Institute, University of Edinburgh, Edinburgh, EH9 3JW, United Kingdom); Renzo Sartori, Istituto di Geologia Marina, Via Zamboni, 65, 40127 Bologna, Italy; Rodolfo Sprovieri, Istituto di Geologia, Corso Tukory, 131, Palermo, Italy; Masayuki Torii, Department of Geology and Mineralogy, Faculty of Science, Kyoto University, Kyoto, 606, Japan.

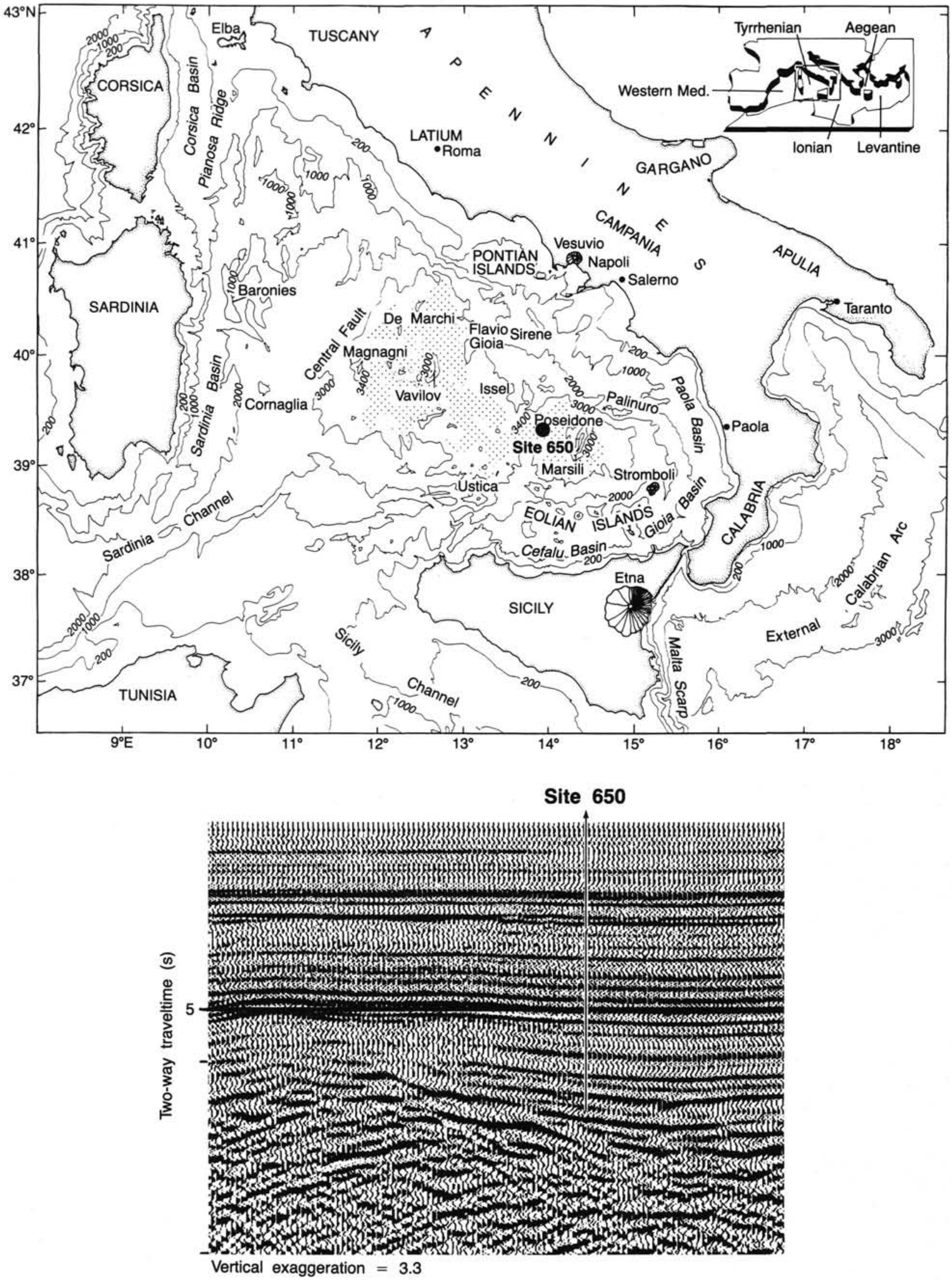

Figure 1. Location of Site 650 on bathymetric map and on MCS Line ST14. Bathymetry in meters.

texture. Vesicles are large (2–3 mm diameter) and abundant (about 20% of rock volume).

Three successful heat flow measurements gave a linear thermal gradient of 14C°/100 m implying a heat flow of approximately 147 mW/m^2.

BACKGROUND AND OBJECTIVES

Background

Site 650 lies near the western edge of the Marsili Basin in the southeastern Tyrrhenian Sea (Fig. 3). The Marsili Basin is bounded on the northeast and east by the continental slope of southern Italy, and on the south by the north-facing flanks of the Eolian Islands. To the west, a structural and bathymetric sill separates Marsili Basin from the rest of the Tyrrhenian Sea. The basin floor comprises a small (100 km across) bathyal plain (water depth 3500 m), bisected by a prominent (2500 m high) north-northeast-trending elongate volcano, Marsili Seamount.

Marsili Basin is the southeastern of two deep basins in the central Tyrrhenian Sea. Both basins are believed to be underlain by oceanic-type crust because of their high heat flow (Erickson et al., 1977; Della Vedova et al., 1984; Hutchinson et al., 1985), relatively high amplitude magnetic anomalies (Bolis et al., 1981), thin crust (Panza et al., 1980; Recq et al., 1984; Ferrucci et al., 1982; Steinmetz et al., 1983), and the recovery of basalt in dredge hauls from seamounts (Colantoni et al., 1981). In the northwestern (Vavilov) basin, the existence of oceanic-type crust has been further supported by recovery of tholeiitic basalt at DSDP Site 373A (Dietrich et al., 1978). In the Marsili Basin, tholeiitic basalt with ages as young as 0.1–0.2 m.y. has been dredged from Marsili Seamount; however the existence and extent of basaltic crust away from the seamount had not been documented prior to Leg 107. In the vicinity of Site 650, the thickness of the crust is 7 to 9 km (Fig. 4). Heat flow values near Site 650 are high but variable, ranging from 120 to 350 mW/m^2 (Fig. 5).

Single channel and multichannel seismic reflection profiles (Fig. 6) across Marsili Basin show a strongly diffractive and irregular acoustic basement at about 4 km below sea level. Interval velocities within this unit range from 2.7 km/sec to 4.5 km/sec (see "Seismic Stratigraphy" section, this chapter). Acoustic basement is overlain by as much as 500 m of well-layered, flat-lying sediments, which have interval velocities of 1.6 km/s and 2.4 km/s. These basin-filling units had been interpreted as ponded turbidites, ash layers, and hemipelagic sediments. Their age was presumed to be Pliocene through Quaternary.

Objectives

Basin Formation

The primary objectives at Site 650 were to ascertain the nature of the acoustic basement and thus constrain the mode of formation of the basin; to date the basement and the sediments immediately overlying basement and thus constrain the age of formation of the basin; and then to compare these results with results from a similar site in Vavilov Basin (Site 651).

Five hypotheses had been considered for the nature of the acoustic basement of Marsili Basin:

1. The acoustic basement represents the uppermost part of typical oceanic crust, i.e., tholeiitic pillow basalts emplaced at an accretionary center.
2. The acoustic basement represents sediments interbedded with sills of basaltic composition, emplaced at an accretionary center in an area of extremely rapid terrigenous sedimentation. An analogy can be drawn with the Gulf of California (Curray, Moore et al., 1982).
3. The acoustic basement comprises pyroclastic material erupted by extensive subaerial volcanism, possibly during the Messinian desiccation event from an eruptive center ancestral to the present Marsili Seamount.
4. The acoustic basement contains or underlies subaerial clastic deposits emplaced during the Messinian (Malinverno, 1981).
5. The acoustic basement consists of highly deformed material, within which any coherent layering has been destroyed tectonically. Such material could be of either sedimentary or magmatic origin, and of almost any age. Deformation could have occurred either during extensional tectonism connected with the most recent phase of thinning of continental crust or during earlier compressional phases (e.g., during Appeninic collision).

The age of the contact between the oldest ponded sediments and the basement is a significant constraint on the tectonic evolution of the Tyrrhenian Basin. Because heat flow increases from west to east, Hutchinson et al. (1985) suggested that the eastern Tyrrhenian basin is younger than the western region. The inference of a younger age for the easternmost Tyrrhenian is also compatible with tectonic models which couple extension in the back-arc region with seaward retreat of the subduction zone (e.g., Kanamori, 1977). By drilling to basement in both Vavilov Basin and Marsili Basin, we hoped to compare the ages of the eastern and western deep basins.

A final source of insight into the evolution of Marsili Basin was expected to come from dating prominent reflectors within the basin-filling sedimentary sequence. Moussat (1983) has worked out a subsidence history based on the dip-slip displacement of prominent reflectors across faults around the margin of the Tyrrhenian Basin. By assigning absolute dates to Moussat's key horizons, we hoped to quantify the rate and timing of vertical displacements.

Tephrochronology

A secondary objective of Site 650 was to develop a tephrochronology for erupta from the numerous circum-Tyrrhenian volcanoes (Fig. 7). We felt that such a chronology could serve three purposes. First, since volcanism in convergent plate margins is broadly associated with tectonic activity, tephra studies should hold clues to tectonic history. Thus frequency and timing of episodes of explosive volcanism could be related (although the relation might be complex) to the frequency and timing of tectonic pulses. In the eastern Mediterranean, the geochemistry of tephras is sufficiently diverse that source areas for individual ash layers can be identified (Keller et al., 1978). Geochemical fingerprinting thus has the potential to allow us to examine the spatial variability of volcanicity in the circum-Tyrrhenian, as well as its temporal variability, looking for migration in the locus of intense volcanism over time. In addition, we planned to look for changes through time in the chemistry of ashes derived from individual volcanic centers; such changes might be similar to the evolution from tholeiitic to calc-alkaline chemistry which have been inferred for Marsili Seamount (Selli et al., 1977; Colantoni et al., 1981) or the evolution from calc-alkaline to shoshonitic chemistry as reported from the Eolian Islands (Barberi et al., 1974).

Secondly, we felt that tephra studies could provide a basis of stratigraphic correlation between the Tyrrhenian Basin and eastern Mediterranean basins. Whereas a biostratigraphic or geochemical datum could be diachronous in these two adjacent semi-enclosed basins, an ashfall is independent of paleoceanographic conditions. A high percentage of the well-documented ash layers in the eastern Mediterranean are thought to come from volcanoes in Italy (Keller et al., 1978); thus the probability of recovering correlative tephras at Site 650 seemed high.

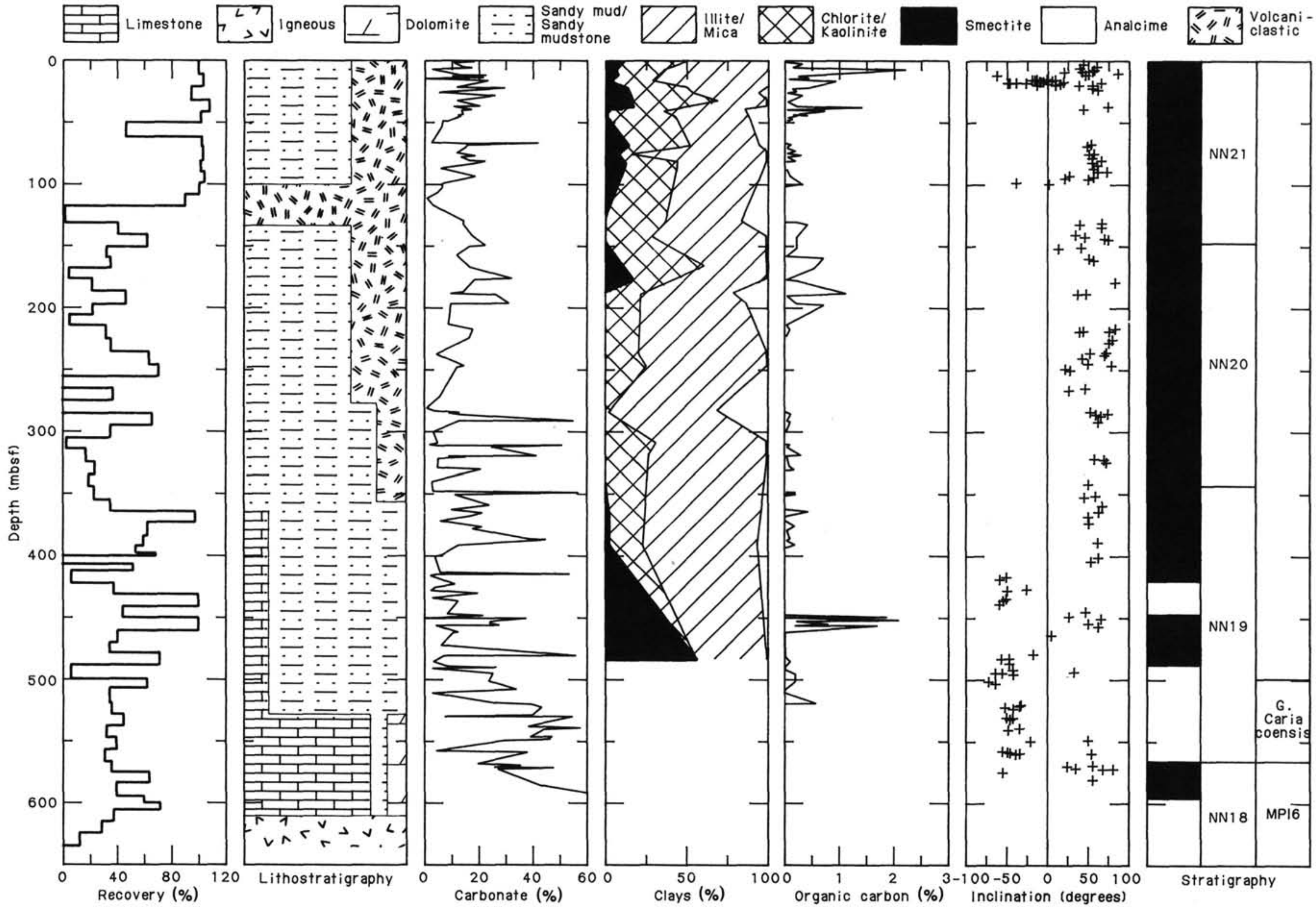

Limestone
Igneous
Dolomite
Sandy mud/ Sandy mudstone
Illite/ Mica
Chlorite/ Kaolinite
Smectite
Analcime
Volcani-clastic
Depth (mbsf)
0
100
200
300
400
500
600
0 40 80 120
Recovery (%)
Lithostratigraphy
0 20 40 60
Carbonate (%)
0 50 100
Clays (%)
0 1 2 3
Organic carbon (%)
-100 -50 0 50 100
Inclination (degrees)
NN21
NN20
NN19
NN18
G. Caria coensis
MPl6
Stratigraphy

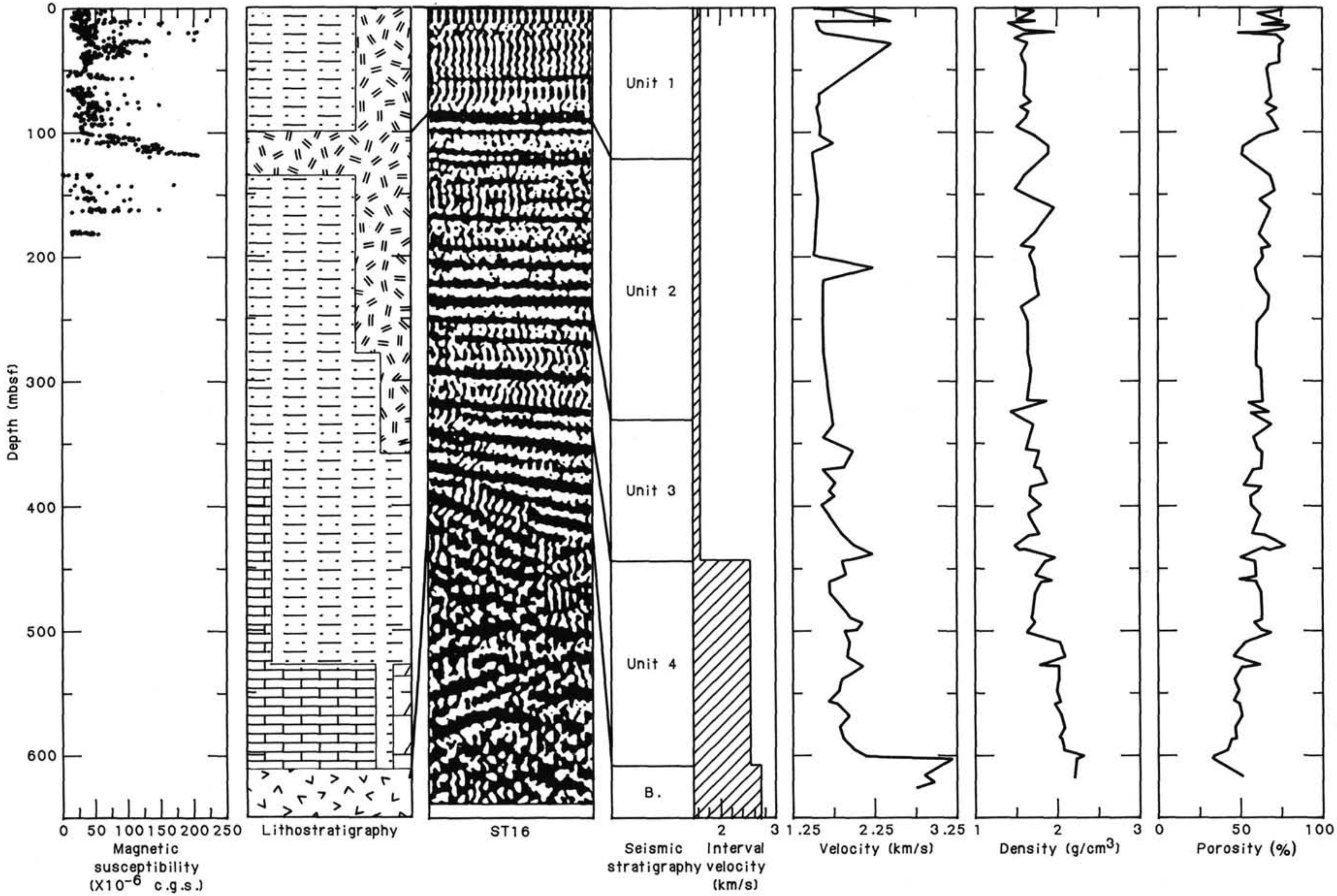

Figure 2. Summary of measurements made on cores recovered at Site 650.

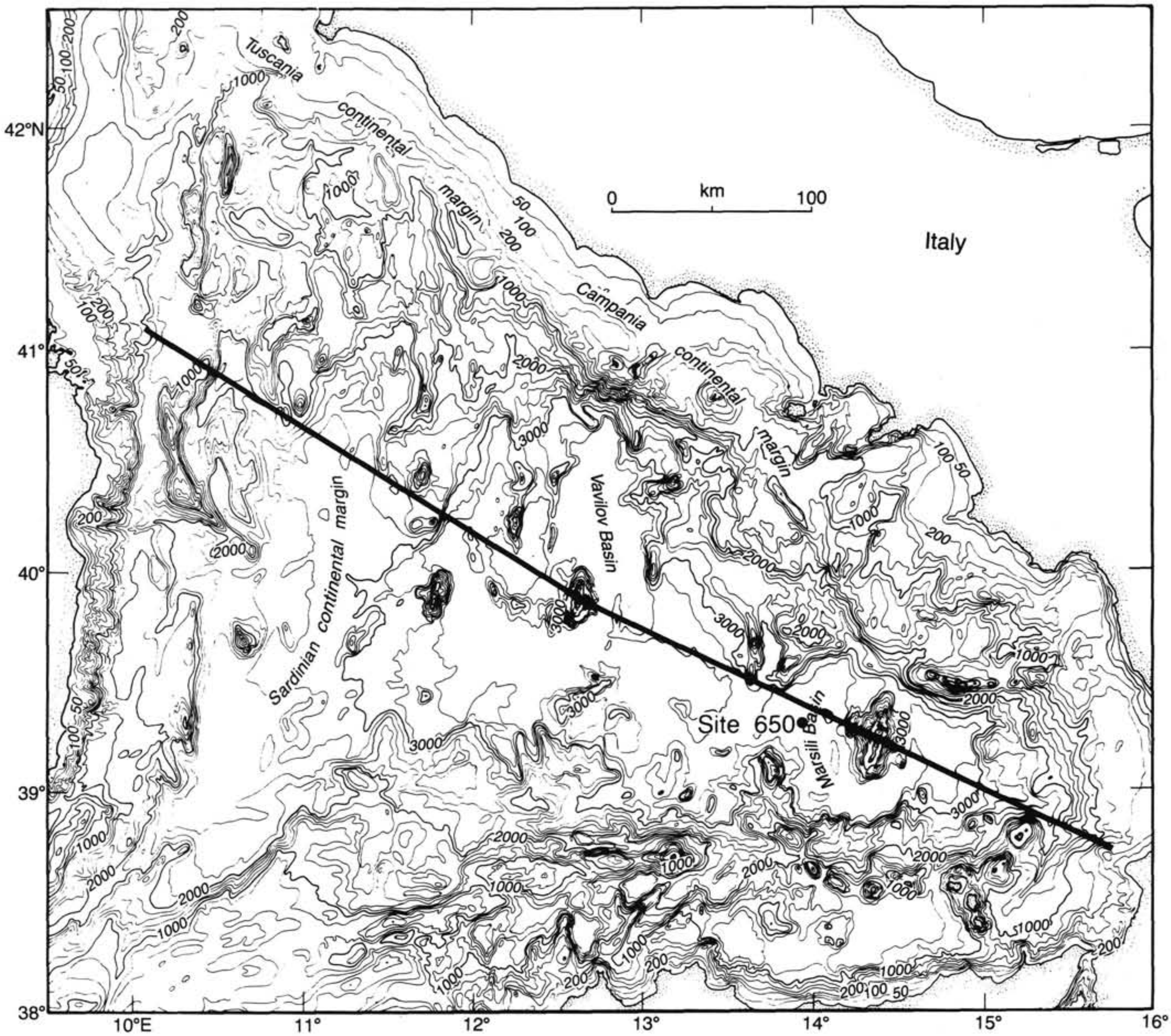

Figure 3. Site 650 is located near the western rim of the eastern of the two deep Tyrrhenian basins (Marsili Basin). Marsili Basin floor is a 3500-m-deep bathyal plain, bisected by a north-northeast-trending seamount (Marsili Seamount). Heavy line shows position of profile in Figure 4.

Third, sampling of tephras in the Tyrrhenian Sea would fill in an empty quadrant in our knowledge of the distributions of ashfalls from Italian volcanoes. Accurate and complete plan-view mapping of distribution and thickness of ash layers is a necessary prerequisite for reconstructing the processes by which volcaniclastics are erupted, transported, and deposited. The Mediterranean is ideally suited for such studies because of its numerous identifiable volcanic provinces.

Site Selection

The proposed site was located near the western rim of the bathyal plain. Three considerations guided the site selection: we wanted to sample "real basement" rather than flows from Marsili Seamount; we wanted to minimize the thickness of basin fill turbidites to penetrate; and yet we wanted to sample the oldest sediment overlying basement. A site meeting these criteria was selected (Fig. 8) at the intersection of multichannel seismic lines ST14 and ST16.

OPERATIONS

Prelude

The *JOIDES Resolution* (*Sedco/BP 471*) departed Malaga, Spain, on December 30, 1985, with the last line off at 2020 hours. Because of complications in shipping and customs clearances over the Christmas/New Year's holiday, several significant items were missing from the planned equipment inventory at the time of departure including the ODP air freight, the Sedco/Forex air freight, a spare armature for the Top Drive, a special order of liquid helium to replenish limited supplies on board for the cryogenic magnetometer, a shipment of supplies for the drill pipe severing system, and a new 3.5-kHz transducer system. Since no firm date could be estimated for the arrival of the missing shipments, the vessel debarked as scheduled with the plan of receiving the materials by boat transfer as soon as possible while on site near Naples.

The original operations plan had been to occupy the selected first-priority sites in a general west-to-east direction starting with

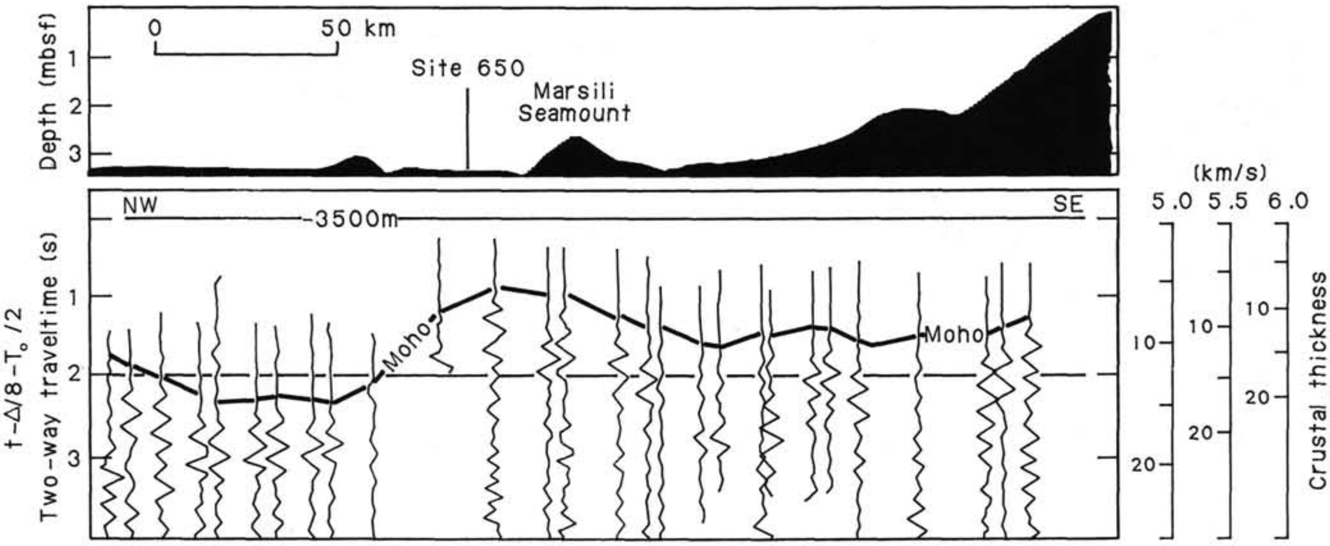

Figure 4. Profile of the depth to Moho, obtained from seismic refraction experiment using ocean-bottom seismometers as receivers (after Steinmetz et al., 1983). Position of the profile is shown in Figure 3; the data set continues westward to the continental slope. In its entirety, Steinmetz's profile shows two regions of thin crust, one beneath Marsili Basin and one beneath Vavilov Basin, with a region of thicker crust underlying the bathymetric sill between the two basins. At Site 650, the depth to Moho is between 7 km and 9 km, depending on the assumed crustal velocity.

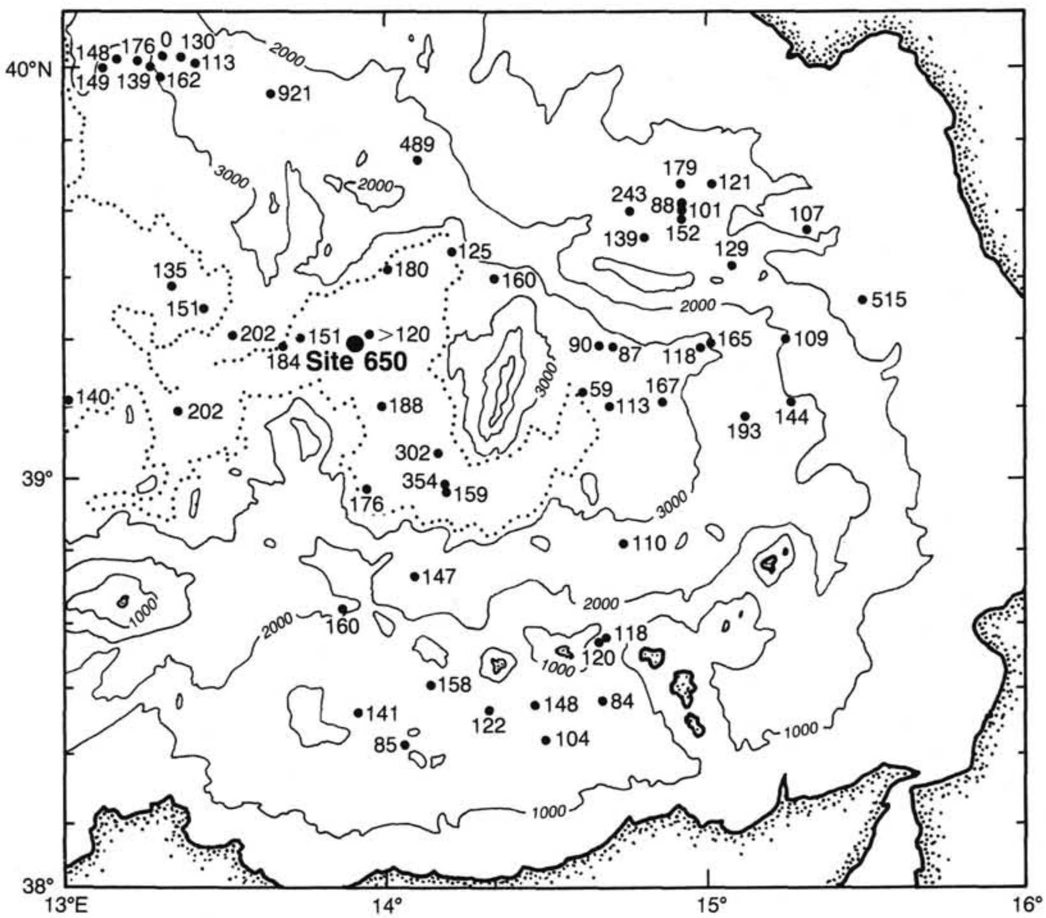

Figure 5. Heat flow in the Marsili Basin is high and variable. Measurements are in mW/m^2, from Erickson et al. (1977) and Della Vadova et al. (1984). Dotted line marks 3400-m bathymetric contour, which approximately outlines the limits of the bathyal plain.

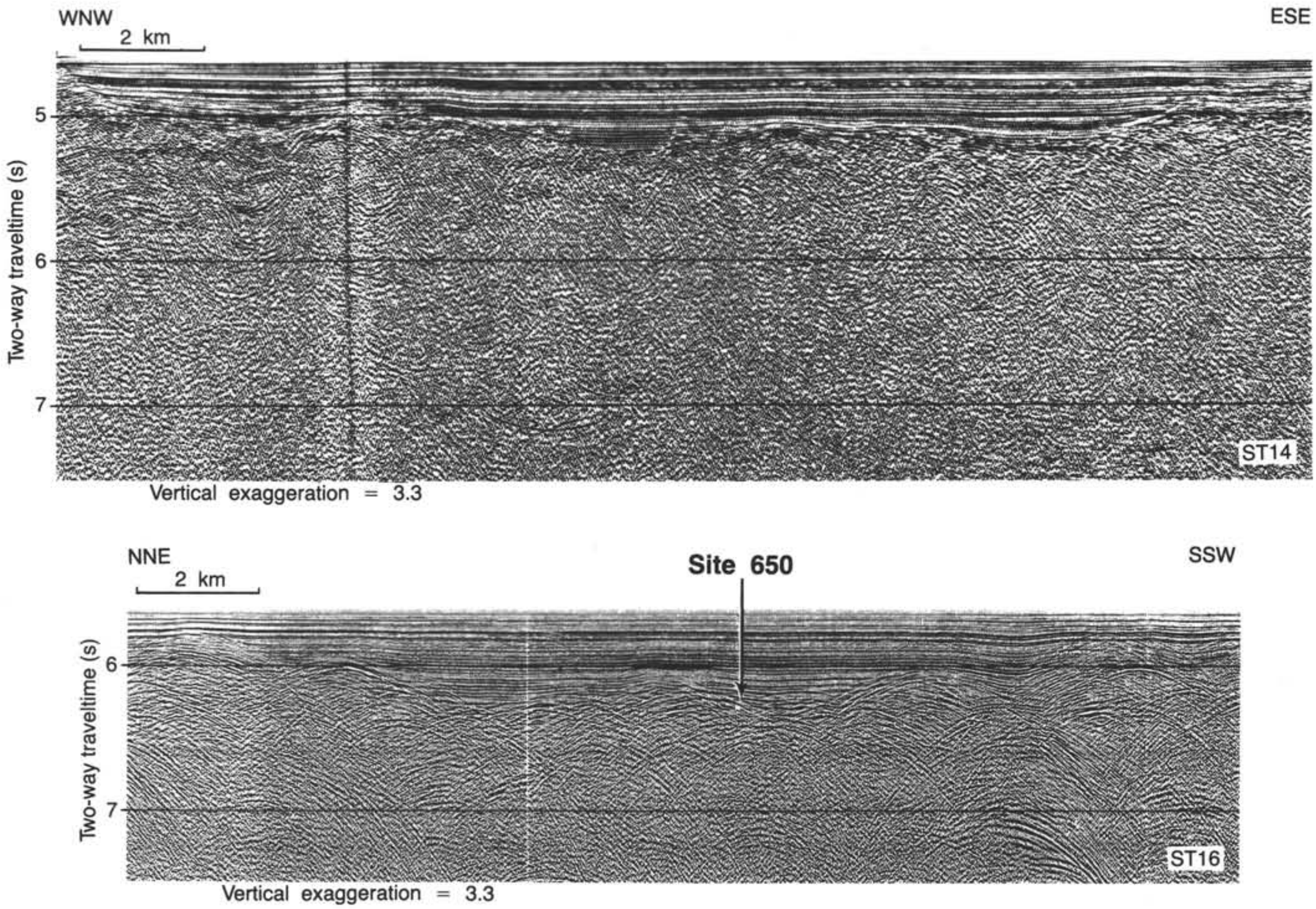

Figure 6. Multichannel seismic profiles across the western Marsili Basin collected during the French site survey cruise. Site 650 is located at the intersection of ST14 and ST16 (location in Fig. 8). In this area there is as much as 500 ms of well-layered, flat-lying sedimentary fill with close-spaced, laterally continuous, high-amplitude internal reflectors. The basin-filling sediment overlies an irregular, strongly diffracting acoustic basement. Identifying the nature of this acoustic basement was one of the primary objectives at Site 650.

Site TYR 2, and then to use any remaining time to occupy second-priority sites while heading back west toward Marseilles. After the problems during the Malaga port call, the plan was reversed and the easternmost site, TYR 7B (Site 650), was selected to be first. The foreseen advantages of the east-to-west program were that (1) the vessel would be close to Italy during the first several weeks to expedite the boat transfer of the missing material; (2) drilling of Site TYR 1B (Site 654), for which final safety panel approval was still pending, would be delayed for several weeks; and (3) work at Site TYR 2 (Site 653), for which the cryogenic magnetometer was deemed to be critical, would be delayed until after the liquid helium and magnetometer electronics had arrived by boat. An unforeseen disadvantage of the revised program was that the drastic, last-minute change in plans would jeopardize our clearance to work in Italian waters.

The steaming time from Malaga to Site TYR 7B was a little over 3 days and the vessel arrived in the vicinity of the site on the evening of 2 January 1986.

Strategy

The primary objective of Site 650 was penetration and sampling of an acoustic basement of unknown lithology which was anticipated at approximately 560 mbsf. If the basement was basalt, a single bit rotary core (RCB) hole would be the only logical plan. However, interval velocities of 2.5–2.7 km/s suggested that upper part of the "basement" might be of fairly low density and thus drillable with the extended core barrel (XCB) system. This approach guaranteed higher recovery and less coring disturbance throughout the sedimentary section. Since the XCB and the advanced piston core (APC) system use the same bit and bottom hole assembly, it would be possible to core the softest part of the section, approximately the upper 200 m, with the APC system which gives the least possible coring disturbance. In addition, the APC cores could be oriented with respect to north for determination of paleomagnetic declination, using the "multishot camera" attached to the top of the core barrel. If it turned out that the XCB system reached refusal above the target depth, a conventional RCB system could be washed down with minimum loss of time to complete coring in an adjacent hole.

A heat flow program was planned with stations every 50 m, beginning at 50 mbsf. While the APC system was in use, we would be using the "Von Herzen" heat flow instrument, which has its sensors inside the cutting shoe of the corer. Measurements with the Von Herzen instrument consume only a few minutes, the time for the probe to reach thermal equilibrium with the sediments. After the switch to XCB coring, we would have to use the "Uyeda" heat flow instrument, which is a free-standing, self-contained probe lowered on the wireline. Measurements with the Uyeda instrument require a round trip with the wireline which consumes approximately 70 min at Site 650's water depth.

The planned logging program consisted of three runs in the hole: (1) velocity, resistivity, caliper; (2) lithodensity, neutron

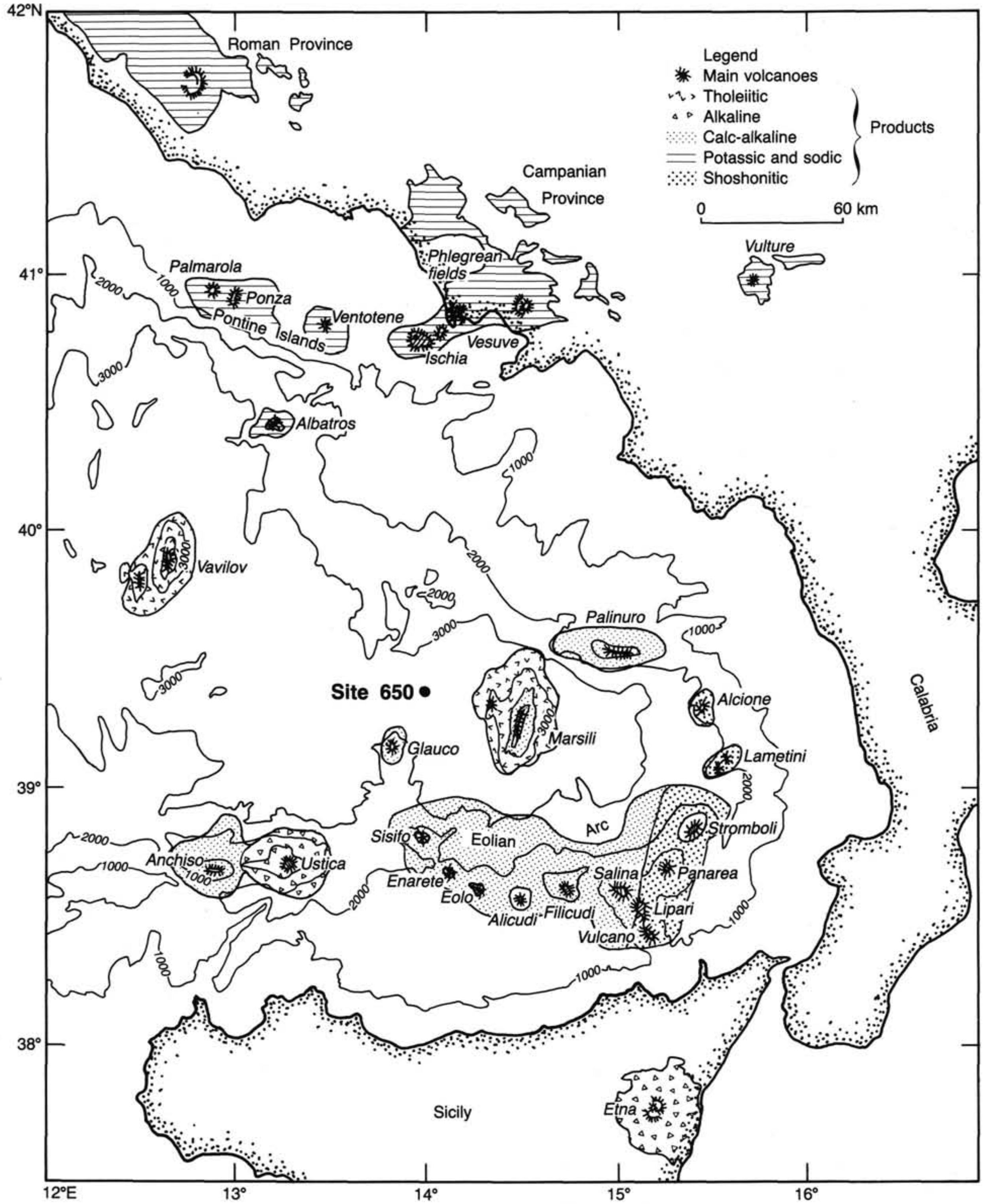

Figure 7. Marsili Basin is surrounded by volcanoes which have been active in the Pleistocene. The geochemistry of the volcanic provinces varies sufficiently that it should be possible to identify the source region for volcaniclastic and ash units.

porosity, natural spectral gamma ray; and (3) the LDGO-modified borehole televiewer.

Approach to Site

Site 650 was proposed at the intersection between multichannel seismic (MCS) site survey lines ST14 (shotpoint 3020) and ST16 (shotpoint 1400), at 39°19′N, 13°53′E. The site survey had been navigated using Loran C; however the *Resolution's* Loran C receiver appeared to be unreliable during our 3-day transit onto site. The navigation techniques which we did have available included transit satellites, dead reckoning by gyrocompass and pitlog, and Global Positioning System (GPS) fixes during two windows from approximately 1200 to 1615 and from approximately 2040 to 0300 (local time equals GMT). With GPS

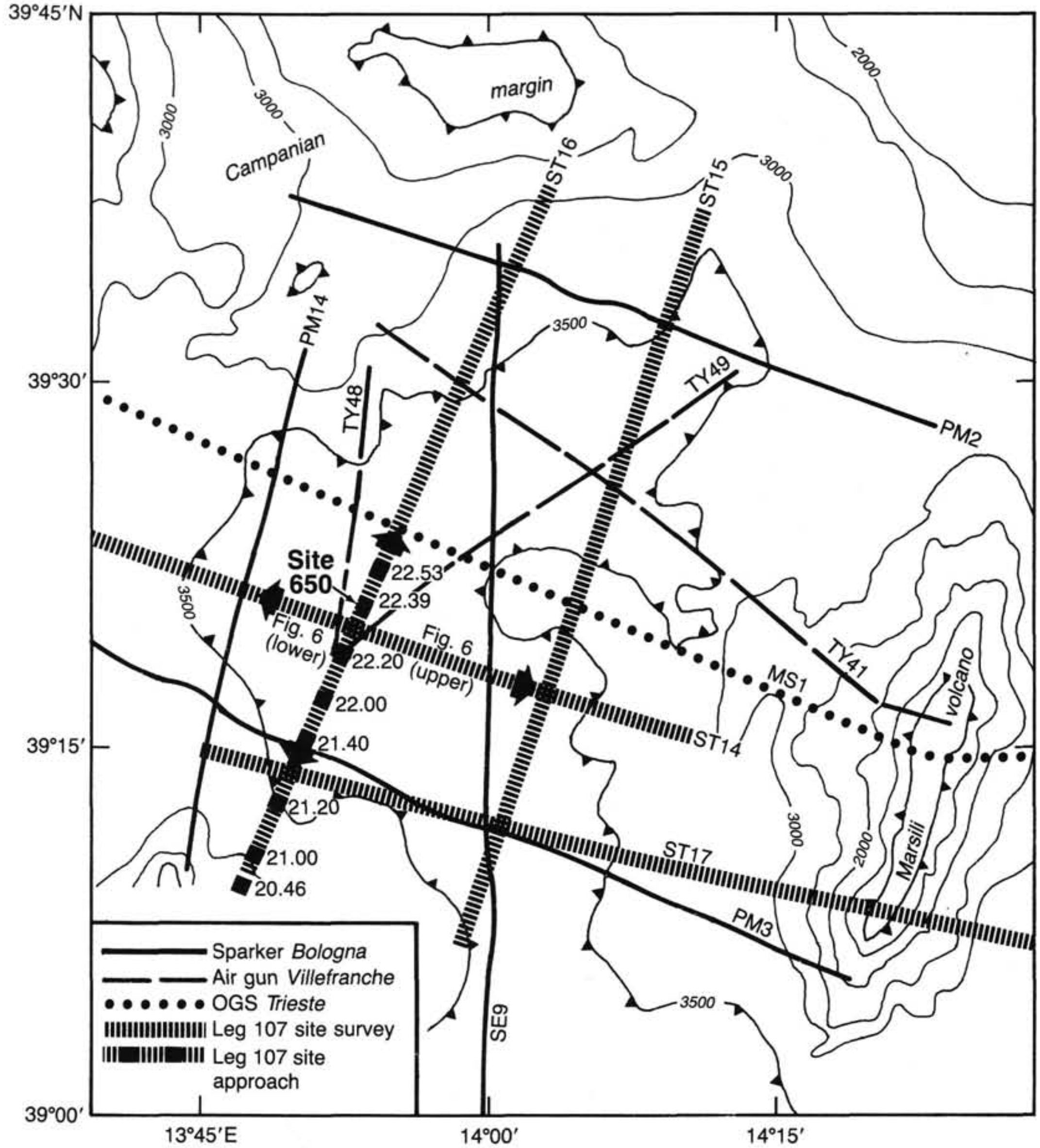

Figure 8. Navigation track chart. Site 650 is located near the intersection of site survey multichannel seismic lines ST14 and ST16. Approach to site was navigated using the Global Positioning System (GPS).

but without Loran we could navigate precisely, but faced the possibility that there might be a systematic offset between our navigation and the navigation of the site survey profiles. Therefore we decided to approach the site along one of the site survey lines in order to match our single channel seismic line with the MCS line. We chose to approach from south to north along line ST16 because the basement topography was more distinctive than on line ST14, and because this strategy required the least extra steaming time.

Starting from the south, MCS line ST16 passes over the north-facing slope of a seamount, followed by the flat-lying bathyal plain. Under the acoustically-laminated, flat-lying bathyal plain turbidites, the acoustic basement has a rugged topography. The proposed Site 650 was located on a slight acoustic-basement swell separating two small basins. The goal was to compare the *Resolution* seismic line with the site survey line and match the distinctive pattern of seamount flank followed by narrow 'basement' basin, followed by broad basement swell, followed by narrow basement basin, followed by the target basement swell.

At 1826 (approximatively 25 nmi from the proposed drill site) we slowed the ship to 6 kt and changed course to 024°. Seismic gear was streamed at 1846. At 2046, approximately 13 nmi south of the site, we received the first GPS fix of the evening window (Fig. 8). From that time until the beacon was dropped the ship was steered by GPS along line ST16, assuming no offset between GPS and Loran C fixes.

At 2226 we reached the latitude at which the Loran-navigated site survey line had placed the target. However, a comparison of the site survey profile ST16 and the *Resolution* water-gun profile suggested that we were still too far south, that we were still on the south side of our target bathymetric high. The beacon was dropped at 2238, on the northern flank of the "basement" swell, in a water depth of 3430 m (uncorrected), or 3509 m (corrected). The GPS position at the time of the beacon drop was 39°21.3′N, 13°54.0′E. The beacon position on the seafloor, derived from GPS and the dynamic position system was 39°21.4′N, 13°54.1′E. While drilling we were able to determine a Loran C position of 39°20.4′N, 13°54.7′E using the X and Y master/slave pairs. The offset between the Loran C and GPS positions is thus 1 minute of latitude and 0.6 minutes of longitude, with the GPS position lying northwest of the Loran C position.

To verify our identification of the basement morphology we prolonged the seismic survey to 39°22.6'N, 13°54.8'E (GPS), 3.5 km north of the drill site. The towed seismic gear was retrieved at 2253. The ship reversed course and returned to the beacon to begin dynamic positioning.

Hole 650A

Hole 650A was spudded with a mud-line APC core at 1435 on 3 January. Cores 107-650A-1H through 107-650A-13H were taken with the APC system (Table 1). APC recovery ranged from >100% to 46%, with the least satisfactory results occurring in units of coarse-grained volcaniclastic turbidites. Very little drilling disturbance could be identified. The multishot camera was deployed to measure orientation of the core on APC Cores 107-650A-2H through 107-650A-12H. However, because of torn film, worn batteries and ambiguity in interpretation of orientation photographs on heat flow runs, the only usable orientations were on Cores 107-650A-6H, -7H and -10H. Von Herzen heat flow measurements were attempted at 42, 71, and 91 mbsf; however, only the measurement at 71 mbsf was successful. The other measurements were unproductive due to operator error and tool problems. Core 107-650A-13H, in a pumice-rich layer, required an unacceptably high overpull to pull out of the mud, so the decision was made to begin XCB operations with Core 107-650A-14X.

XCB coring commenced at 119 mbsf. Uyeda probe-type heat flow measurements were taken at 142 and 190 mbsf. The temperature recorded at 190 mbsf indicated that the probe was in fill and had not penetrated virgin sediment; as a result only the measurement at 142 mbsf was useable. By the time the hole had been deepened to about 200 mbsf the sediments were too stiff to risk inserting the probe type tool. XCB core recovery was extremely variable (0%–96%) in the upper Pleistocene turbidites. The hole remained stable despite strata of moderately unlithified, coarse volcanogenic materials.

Coring continued with relative ease of penetration through the lower Pleistocene and uppermost Pliocene (30–40 minutes per core) until 604 mbsf, where highly vesicular, severely altered basalt was recovered. This new lithology caused the drill string to torque more than had been previously experienced; however the formation penetrated readily. Contact with an even harder material, possibly less altered or less vesicular basalt, occurred at 625.5 mbsf; penetration rate dropped suddenly to 1 m/hr. After 1-1/2 m of laborious penetration we decided to retrieve the core to examine the material recovered and switch to a diamond cutting shoe. However, the core barrel was firmly stuck in the pipe. Repeated attempts to free the barrel were fruitless so the remaining 7.1 m of the joint was drilled down in hopes that the barrel would be worked free. Unfortunately, the core barrel remained fixed, and the only way to extract the stuck barrel was to retrieve the entire drill string. Logging through the pipe was considered. However the shipboard logging scientists felt that the data would be of only marginal value and not worth the time, especially since the crucial basalt/sediment contact would have to be logged through the thick collars of the bottom hole assembly.

Table 1. Coring summary table for Site 650.

Core no.	Date (Jan. 1986)	Time	Sub-bottom depths (m)	Length cored (m)	Length recovered (m)	Recovery (%)
1H	3	1520	0.0-3.0	3.0	3.0	98.3
2H	3	1645	3.0-12.7	9.7	9.6	98.6
3H	3	1840	12.7-22.4	9.7	9.9	102.0
4H	3	1945	22.4-32.8	10.4	9.6	92.6
5H	3	2115	32.8-42.4	9.6	10.2	106.7
6H	3	2230	42.4-52.1	9.7	9.7	100.0
7H	4	0000	52.1-61.8	9.7	4.5	46.0
8H	4	0130	61.8-71.3	9.5	9.6	100.7
9H	4	0230	71.3-81.0	9.7	9.8	101.3
10H	4	0415	81.0-90.7	9.7	9.7	100.3
11H	4	0500	90.7-100.3	9.6	9.9	102.6
12H	4	0600	100.3-109.7	9.4	9.3	99.3
13H	4	0815	109.7-119.4	9.7	8.6	88.8
14X	4	0945	119.4-132.1	12.7	0.1	1.1
15X	4	1115	132.1-141.7	9.6	3.9	40.5
16X	4	1545	141.7-151.3	9.6	5.9	61.8
17X	4	1730	151.3-160.5	9.2	3.0	32.2
18X	4	1900	160.5-170.2	9.7	3.4	34.9
19X	4	2045	170.2-179.8	9.6	0.4	4.2
20X	4	2230	179.8-189.5	9.7	2.0	21.0
21X	5	0145	189.5-199.2	9.7	4.5	46.3
22X	5	0315	199.2-208.9	9.7	2.0	21.0
23X	5	0515	208.9-218.6	9.7	0.4	4.4
24X	5	0700	218.6-228.2	9.6	3.0	31.0
25X	5	0900	228.2-237.8	9.6	3.3	34.4
26X	5	1045	237.8-247.5	9.7	6.1	62.8
27X	5	1230	247.5-257.2	9.7	6.8	70.0
28X	5	1415	257.2-266.8	9.6	0.0	0.0
29X	5	1615	266.8-276.5	9.7	3.5	36.4
30X	5	1745	276.5-286.2	9.7	0.0	0.0
31X	5	1945	286.2-295.8	9.6	6.3	65.5
32X	5	2130	295.8-305.5	9.7	3.3	34.4
33X	6	0000	305.5-315.1	9.6	0.2	2.5
34X	6	0215	315.1-324.8	9.7	1.6	16.7
35X	6	0415	324.8-334.5	9.7	2.2	23.1
36X	6	0615	334.5-344.2	9.7	1.8	18.4
37X	6	0815	344.2-353.9	9.7	2.2	22.3
38X	6	1000	353.9-363.5	9.6	3.3	34.8
39X	6	1145	363.5-373.1	9.6	9.3	96.6
40X	6	1315	373.1-382.8	9.7	6.0	62.1
41X	6	1515	382.8-392.4	9.6	5.7	59.4
42X	6	1730	392.4-397.4	5.0	2.7	53.4
43X	6	1945	397.4-399.4	2.0	1.4	68.0
44X	6	2145	399.4-406.1	6.7	0.0	0.0
45X	6	2330	406.1-411.8	5.7	3.0	51.9
46X	7	0245	411.8-421.5	9.7	0.6	5.8
47X	7	0400	421.5-431.1	9.6	3.5	36.8
48X	7	0600	431.1-440.8	9.7	9.6	99.0
49X	7	0800	440.8-450.4	9.6	4.2	43.8
50X	7	1000	450.4-460.1	9.7	9.6	98.7
51X	7	1200	460.1-469.7	9.6	3.9	40.2
52X	7	1400	469.7-479.3	9.6	3.3	34.4
53X	7	1545	479.3-488.9	9.6	6.8	70.6
54X	7	1745	488.9-498.6	9.7	5.3	54.4
55X	7	2000	498.6-508.2	9.6	6.0	62.4
56X	7	2230	508.2-517.9	9.7	3.3	33.9
57X	8	0015	517.9-527.5	9.6	3.4	35.5
58X	8	0215	527.5-537.2	9.7	4.4	45.1
59X	8	0415	537.2-546.8	9.6	3.0	31.6
60X	8	0630	546.8-556.5	9.7	3.8	39.0
61X	8	0900	556.5-566.1	9.6	2.9	29.7
62X	8	1100	566.1-575.8	9.7	3.4	35.4
63X	8	1300	575.8-584.4	8.6	5.5	63.5
64X	8	1445	584.4-594.1	9.7	3.8	38.9
65X	8	1715	594.1-599.8	5.7	3.4	59.8
66X	8	1900	599.8-604.8	5.0	3.6	71.8
67X	8	2100	604.8-614.5	9.7	3.6	36.7
68X	8	2315	614.5-624.2	9.7	2.7	28.0
69X	9	1930	624.2-633.8	9.6	1.1	11.0

Hole 650B

As 95% of the scientific objectives of Site TYR 7B had been met by drilling at Hole 650A, our preferred plan at this point was to leave Site 650 3 days ahead of schedule and proceed immediately to the next site. The decision to continue with a B-hole was made because of diplomatic delays in getting clearance to move to the next site. The vessel was offset 15 m (50 ft) and an RCB bottom-hole assembly was made up and run to the sea floor with a center bit in place. The plan was to wash to the depth of the Hole 650A and core deeper into the basement to determine whether the basalt encountered in Hole 650A was a sill or truly the top of oceanic layer 2. Within the sedimentary section we planned one spot core to fill in the interval of 107-650A-14 (which had zero recovery in an interesting stratum) and two additional heat flow measurements.

Departure approval from the Italian Navy was received while early in the process of washing down. A single successful heat flow measurement using the Uyeda tool was made at 102.4 mbsf and the pipe was tripped back onboard. The bit was on deck at 2050 on 10 January.

LITHOSTRATIGRAPHY

Sedimentary Units

Two major sedimentary units were recovered between the seafloor and 602 mbsf, and basalt was recovered between 602 and 634 mbsf. Two lithologic units were identified:

Unit I Cores: 107-650A-1H to 107-650A-37X; Depth: 0–354 mbsf; Age: < 0.45 m.y. (NN19/NN20). Thickness: 354 m.

In general, Unit I delineates an interval of episodic input of volcanic glass and pumice (interpreted as indicative of subaerial and shallow-water eruptive activity). Unit I is also characterized by a high input of clay-sized terrigenous material.

Unit I was deposited extremely rapidly, at a sedimentation rate in excess of 50 cm/1000 years.

Subunit Ia: Cores 107-650-1H through 107-650-11H; Depth: 0–100 mbsf; Thickness: 100 m.

Normally graded sequences of clastic layers with low carbonate contents (less than 30%, with an average of 15%–20%), are interpreted as turbidites. The thickness of these turbidites varies between 10 cm and, in one case, about 10 m. The coarser basal portions of the turbidites are dominated by volcaniclastic sand and gravel (glass and pumice fragments). The finer grained upper portion of each turbidite is a calcareous mud, occasionally containing volcanic ash and isolated pumice fragments.

On top of the normally graded sequences there often occur homogeneous muds and calcareous muds. In such cases it is difficult to recognize the upper limit of the turbidites. We believe that the homogeneous muds and calcareous muds are also turbidites rather than hemipelagic because: (1) burrowing structures in these homogenous intervals are infrequently observed, (2) displaced nannoplankton and benthic foraminifera are abundant in these fine-grained layers, and (3) even after deducting the obvious turbidites with coarse-grained basal sections, the sedimentation rate of the remaining sediments appears to be too high. We cannot determine whether the fine-grained, apparently turbiditic, units belong to the same turbiditic event as the underlying normally graded sequences or represent separate turbiditic events. In the latter case, the coarse-grained terrigenous debris mobilized by the respective turbiditic event could have been trapped in small peri-Tyrrhenian basins (Fabbri et al., 1981; Barone et al., 1982).

The volcanic detritus has most likely been derived from the Eolian Islands (Fig. 9).

Subunit Ib: Cores 107-650A-12H to 107-650A-14X; Depth: 100–132 mbsf; Thickness: 32 m.

A thick pumice layer correlates well with a high-amplitude acoustic reflector at about 120 mbsf throughout the Marsili Basin. Pumice particles vary in size from microscopic to gravel, usually supported in a mud or clay matrix. Approximately 10 thin (10 cm thick) normally graded pumice layers, presumably turbidites, occur in the middle of the subunit. Subunit Ib lithologies have been observed only in cores 12 and 13, and in 14 CC. The recovery of core 14 was only 1.1%. Nevertheless, the entire length of core 14 is interpreted to consist of the same lithology. The very poor recovery may be due to the change from APC (cores 1–13) to the XCB system (core 14). Thus the coarse-grained less or non-cohesive volcaniclastics could have been washed out.

Subunit Ic: Cores 107-650A-15X to 107-650A-30X; Depth: 132–286 mbsf; Thickness: 154 m.

This subunit is similar in lithologic characteristics to Subunit Ia, especially with respect to variations in texture and carbonate content, and is interpreted as a series of turbidites containing variable fine-grained volcanic detritus interspersed with intervals of calcareous mud layers. The obviously normally graded sequences are less frequent and form only a few percent of the total subunit. Homogeneous calcareous muds are dominant. However, considering the poor recovery after changing the coring system (Cores 107-650A-1H to -13H were APC, and all successive cores, XCB) it may be assumed that the coarser parts of any turbidite sequence could have been washed out by drilling.

Subunit Id: Cores 107-650A-31X to 107-650A-37X; Depth: 286–354 mbsf; Thickness: 68 m.

Sediments in this interval contain textural and mineralogical characteristics of both Subunits Ia and Ic, and Unit II (described below). Few clastic-rich turbidites occur and those present are thin (about 10 cm) and represent less than a percent of the subunit. Mud turbidites presumably are present but cannot be distinguished by visual criteria. Carbonate contents are generally similar to those of Subunits Ia and Ic, but increase to 57%. Textural characteristics vary in accordance with these allochthonous/autochthonous and compositional variations. Near the base of the subunit (Core 107-650A-36X) two thin (about 5 mm) dark layers occur that are inferred to be sapropels.

Unit II Cores 107-650A-38X to 107-650A-66X; Depth: 354–602 mbsf; Age: Pleistocene to upper Pliocene 0.45 to 2.0 m.y. Thickness: 248 m.

Unit II differs from Unit I by generally higher carbonate contents as well as by thinner and less frequent normally graded clastic sequences interpreted as turbidites. Also the amount of volcanic detritus such as pumice and glass fragments is considerably less than in Unit I, although fine-grained vitric particles remain nearly as abundant as in Unit I. Accordingly, textural variations are less in Unit II with higher clay and lower sand/silt contents. From Core 107-650A-51X downward, a few thin dark layers, inferred to be sapropelitic, occur in discrete horizons. Sedimentation rates (without consideration of compaction) vary from 25 cm/1000 yr in the upper half of the unit to 13 cm/1000 yr in the lower half. Unit II is divided into two subunits on the basis of a distinct downcore trend toward higher carbonate contents.

Subunit IIa: Cores 107-650A-38X to -57X; Depth: 354–527 mbsf; Thickness: 173 m.

Subunit IIa consists predominantly of calcareous mud. The mean carbonate content is 15%–20%. Normally graded clastic sequences interpreted as turbidites form only a few percent of the total thickness of this subunit, and individual turbidite layers are rarely thicker than 10 cm. The amount of coarser grained volcanic detritus is considerably less than in Unit I, but fine-grained ash particles persist. The interpretation of calcareous muds containing allochthonous material corresponds to that given for Subunit Ia.

Subunit IIb: Core 107-650A-58 to -66X; Depth: 527–602 mbsf; Thickness: 75 m.

Subunit IIb consists almost entirely of nannofossil ooze with a few layers of calcareous mud as well as mud. Mean carbonate content is 35%–40%. Pebbly mudstones and slump folds occur in Cores 107-650A-60X and 107-650A-63X. Lithification result-

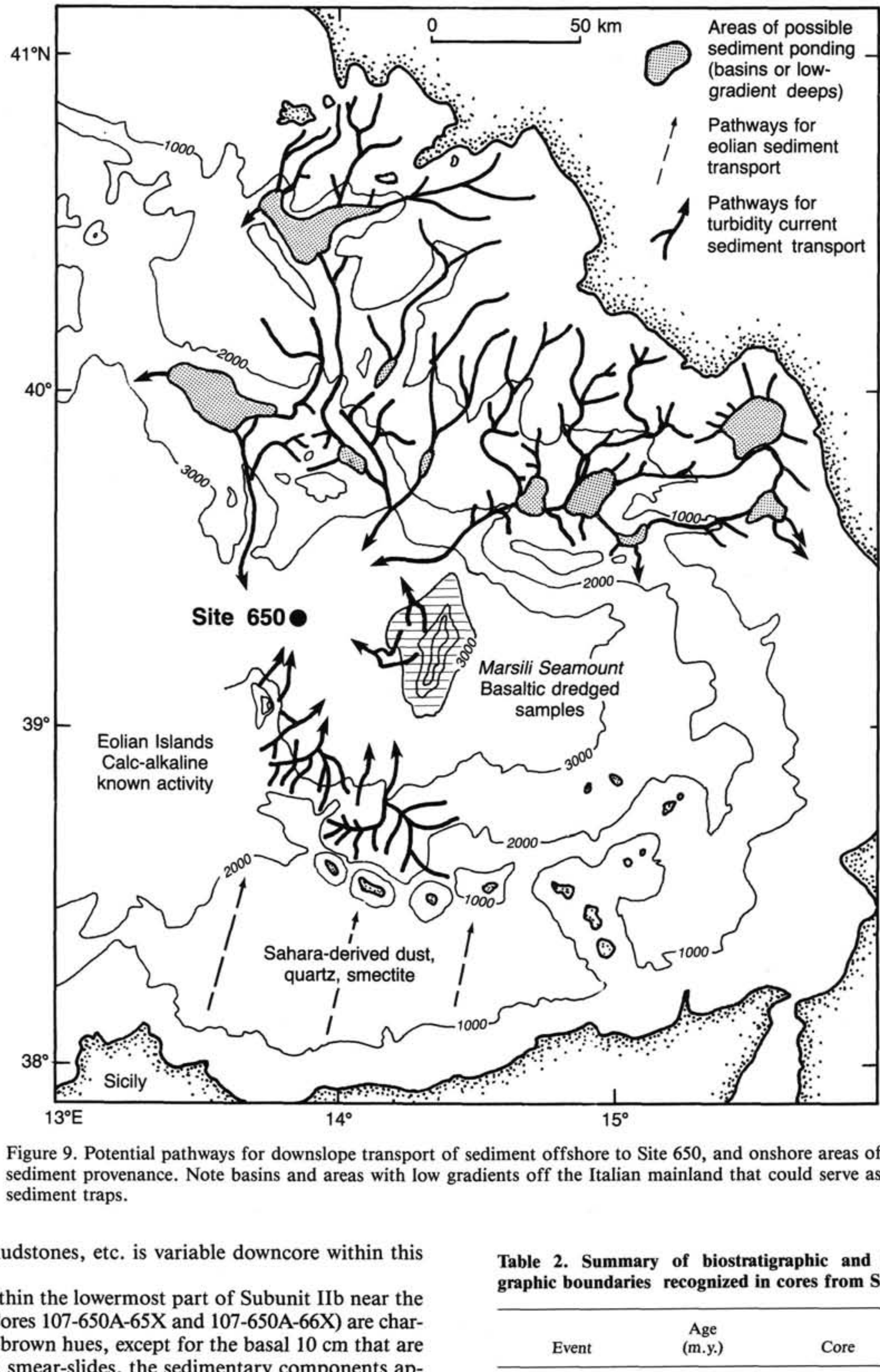

Figure 9. Potential pathways for downslope transport of sediment offshore to Site 650, and onshore areas of sediment provenance. Note basins and areas with low gradients off the Italian mainland that could serve as sediment traps.

ing in chalks, mudstones, etc. is variable downcore within this subunit.

Sediments within the lowermost part of Subunit IIb near the basalt contact (Cores 107-650A-65X and 107-650A-66X) are characterized by red-brown hues, except for the basal 10 cm that are greenish-gray. In smear-slides, the sedimentary components appear to be dominated by euhedral small dolomite crystals, authigenic feldspars (sanidine?, albite?), and zeolites. These changes (color, composition) probably have resulted from low-temperature halmyrolysis of underlying basalts, providing Mg^{++} ions for the formation of dolomites.

Sedimentation Rates

The oldest datable sediments recovered at Site 650 are of latest Pliocene age (near the base of biozone MP16) (Table 2). The

Table 2. Summary of biostratigraphic and magnetostratigraphic boundaries recognized in cores from Site 650.

Event	Age (m.y.)	Core	Depth (mbsf)
Base of E. huxleyi (NN21/NN20)	0.27	107-650A-16X, -17X	151–161
NN19/NN20	0.46	107-650A-36X to -27X	344–353
Brunhes/Matuyama	0.73	107-650A-45X to -47X	409–422
Top of Jaramillo	0.90	107-650A-49X to -50X	455–457
Base of Jaramillo	0.97	107-650A-53X	470–471
Sicilian/Emilian	1.15	107-650A-54X, -55X	498–508
Pleistocene/Pliocene	1.68-1.8	107-650A-61X, -62X	566–578
Top of Olduvai	1.67	107-650A-62X	579–581
Near base of MP16	2.0	107-650A-65X	594–602

upper 30 m of Pliocene sediments are overlain by a predominantly volcaniclastic Pleistocene sequence 566 m thick. The sedimentation rate of the upper Pliocene and lower Pleistocene (1.8–1.20 Ma) hemipelagic sequence vary from 6 to 19 cm/1000 yr.

Sedimentation rates increase throughout the Pleistocene from 25 cm/1000 yr (1.2–0.70 Ma) to 95 cm/1000 yr (0.70–0.47 Ma) within the upper part. The increase is due to the increased input of pumice, volcanic ash, and intercalations of distal turbidites.

X-Ray Diffraction Data

Numerous X-ray diffraction scans were run on Site 650 samples selected from those chosen previously for percentage carbonate analysis. The diffraction patterns were run between 2.0 and 60.0 degree 2-theta using only powder samples with the shipboard diffractometer, a Philips PW1729/ADP3720 with Ni-filtered Cu_{Kalpha} radiation. For this report, two subsets of data from the analyses were collated in order to (1) study general mineralogic trends in the sediments of Site 650 and (2) to discern possible mineralogic changes which could be a reflection of late Pleistocene glacial/interglacial cycles.

Mineralogic Trends

X-ray diffraction data from 28 samples representing only the fine-grained sediments (muds, clays, mudstones, and claystones) in the sequence were analyzed to distinguish relative mineralogic abundances and trends of these abundances throughout the sedimentary column of Site 650. For each sample, the peak areas in counts (cts) of the major peaks (degree 2-theta) of selected minerals were grouped according to the following categories:

Group 1—Bulk sample		Group 2—Clays/zeolites	
Calcite	29.37	Smectite/chlorite	5.73–6.31
Dolomite	30.94	Illite/mica	8.75–8.87
Quartz	26.68	Chlorite/kaolinite	12.29–12.55
Feldspars	27.35–28.15 (Sum)	Analcime	15.79
Total clay	Sum of Group 2		

These peaks are the ideal degree 2-theta values for each mineral. For the purpose of this preliminary analysis, these ideal values are assigned to these specific minerals. In practice, a serious problem exists as chlorite and smectite peaks overlap and can only be distinguished by further analysis (glycolation). Since we note below general correlation between relative intensity of the smectite/chlorite peak with redeposited volcaniclastic sediments, we believe the assignment of this peak to smectite is a plausible assumption. The data for each group were normalized to 100% and are graphically displayed in Figure 10. These normalized percentages should not be taken to be absolute abundances. Note that the normalized graphs are interpolations between discrete data points. Between 0 and 200 mbsf (Cores 107-650A-1H to -22X), one sample was taken approximately each 10 m, which represents 1 sample/13,000 yr assuming a constant sedimentation rate of 77 cm/1000 yr. Between 200 and 500 mbsf (Cores 107-650A-22X to -54X) the number and spacing of samples decreased to ~1 sample/50 m. There are no data available for the basal sediments because of equipment malfunction.

Several interesting trends in the data can be seen in Figure 10 (note that these data are only for fine-grained sediment layers; obvious coarse-grained basal portions of turbidites were not studied). Calcite does not show extreme fluctuations. By contrast, much greater variations in percent carbonate exist when sediments of all grain sizes are included (see "Geochemistry" section, this chapter). Between 0 and 200 mbsf (Cores 107-650A-1H to -22X), small amounts of dolomite are sometimes present in the sediments, approximately 1%–4% of the normalized minerals. Below approximately 200 mbsf, dolomite disappears from the sediments. The dolomite may or may not be authigenic. In smear slides, the dolomite appears as clear, rhombohedral (10μm–40μm) crystals. They do not have rounded corners and, thus, do not appear to have been transported.

Above 200 mbsf, smectite/chlorite is a significant component of the clay mineral assemblage but disappears below this depth. The sharp increase in smectite at 494 mbsf (Core 107-650A-54X) may be an artifact as only one sample in the present data set shows this increase. An increase in the feldspar composition of the sediments below 400 mbsf is seen in two samples at 432 and 494 mbsf (Cores 107-650A-48X and -54X).

The presence of analcime was first noted in a smear slide from a "sapropel" layer at 335.7 mbsf (Core 107-650A-36-1, 115 cm). The diffraction pattern of this thin discrete layer confirmed analcime to be present. Subsequently, the characteristic major peak for analcime was recognized in other bulk samples, as shown in Figure 10. Without more extensive X-ray diffraction analyses of the sediments, it is impossible to separate and quantify the chlorite and kaolinite peaks, but the occurrence of a secondary chlorite peak suggests its presence.

Fluctuations of the smectite/chlorite content in the fine-grained sediments of the upper 200 mbsf, in the interval between 0 and 120 mbsf where the hydraulic piston corer was used, are particularly well-documented because 48 samples for X-ray diffraction analysis were taken in this interval. Thus, a higher stratigraphic resolution of the smectite/chlorite was possible through the different lithologies of varying grain sizes in this interval. Figure 11 shows a plot of smectite/chlorite peak area (cts) against depth below seafloor (mbsf). These clays were not detected by X-ray diffraction analysis at: 5.11 mbsf, 14.30–14.44 and 15.94–16.50 mbsf, 41.08–47.34 mbsf, 71.04–71.89 mbsf, and 89.00–119.61 mbsf.

Interpretation: Late Pleistocene Cyclicity (?)

Smectite in deep-sea sediments can be detrital or authigenic. It is an alteration product of volcanic material and can be formed either *in situ* in the submarine environment or subaerially and subsequently transported into the marine basin. Its distribution within the sediments could be dependent upon the abundance of volcanic material within individual facies units.

Smectite abundance could relate to the amount of unstable volcanic glass that is available for the *in-situ* formation of smectite. The smectite/chlorite intervals could also represent periods of increased erosional volcaniclastic material on land. This assumption seems reasonable considering that glass fragments observed in smear slides were usually fresh with few indications of weathering or other types of alteration, so the smectite/chlorite variations are unlikely to have been produced *in situ* and thus were transported from the land and reflect climatic events on land.

This general interpretation can be reinforced for this sequence by the magnetic susceptibility data, which indicate the presence of two distinct zones of low susceptibility between 0 and 120 mbsf (~40–50 mbsf and ~90–100 mbsf) (see "Paleomagnetism" section, this chapter). The zones of low magnetic susceptibility are correlated with sediments containing low concentrations of magnetic minerals, primarily magnetite.

In principle, the fluctuations between smectite and nonsmectite intervals could have a climatic, tectonic, or volcanic significance. An attractive possibility is that the cycles could be related to the late Pleistocene glacial/interglacial cycles. During periods of lowered sea level, the continental shelves are exposed to greater amounts of erosion, which brings an increased sediment load onto the continental slopes to be subsequently transported by turbidity currents into the adjoining deeper basins. In general, sea-level regressions enhance processes resulting in the redeposition of clastic sediments. In the case of the Marsili Basin, periods of intensified glaciation (regressions) could be associated

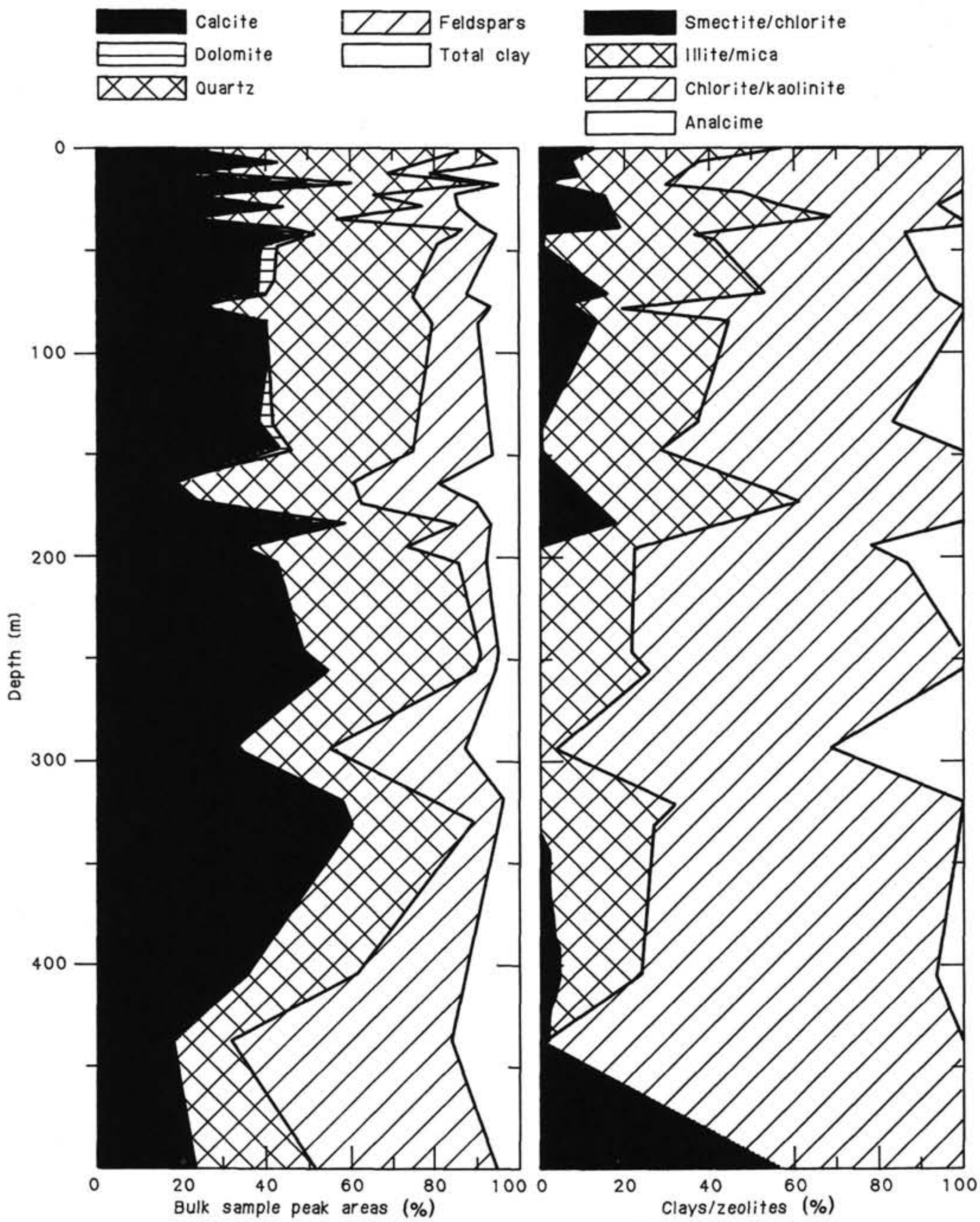

Figure 10. X-ray diffraction peak areas of selected minerals as percentage of bulk sample or clay/zeolite fraction in clays, muds, claystones, and mudstones from Cores 107-650A-1H to -54X.

with intervals of increased volcaniclastic turbidite deposition, while periods of decreased glaciation (transgressions) could be associated with intervals of diminished turbidite deposition which would enhance the background sedimentation through less dilution. In general, intervals showing no detectable smectite/chlorite correlate with intervals showing increases in percentage carbonate and vice versa (Fig. 11). This apparent correlation could be explained by decreased clastic dilution of the background open-marine carbonate sedimentation.

The Pleistocene glacial/interglacial intervals have been divided into isotope stages based on the oxygen-isotope stratigraphy derived from foraminifers in deep-sea cores (Emiliani, 1978). Micropaleontologic studies of the planktonic foraminifers from Pleistocene cores taken in the Mediterranean Sea can also distinguish these glacial/interglacial cycles and are correlatable with the isotope stages (Vergnaud-Grazzini and Glaçon, in press). At Site 650 the presence or absence of warm-water species of planktonic foraminifers gives evidence for these cycles. Of particular interest is the micropaleontologic recognition of Terminations I and II between 3 and 12.7 mbsf (between Cores 107-650A-1H-CC and -2-CC) and at 100.3 mbsf (Core 107-650A-11H-CC), respectively (see "Biostratigraphy" section, this chapter). These terminations represent the rapid transitions from glacial to interglacial conditions as defined by oxygen-isotope stratigraphy.

Based on the limited data set, a tentative correlation between the fluctuations in the smectite/chlorite content of the sediments and the isotope stages can be made (Fig. 11). It is probably not a coincidence that the sediments between 100.3 and

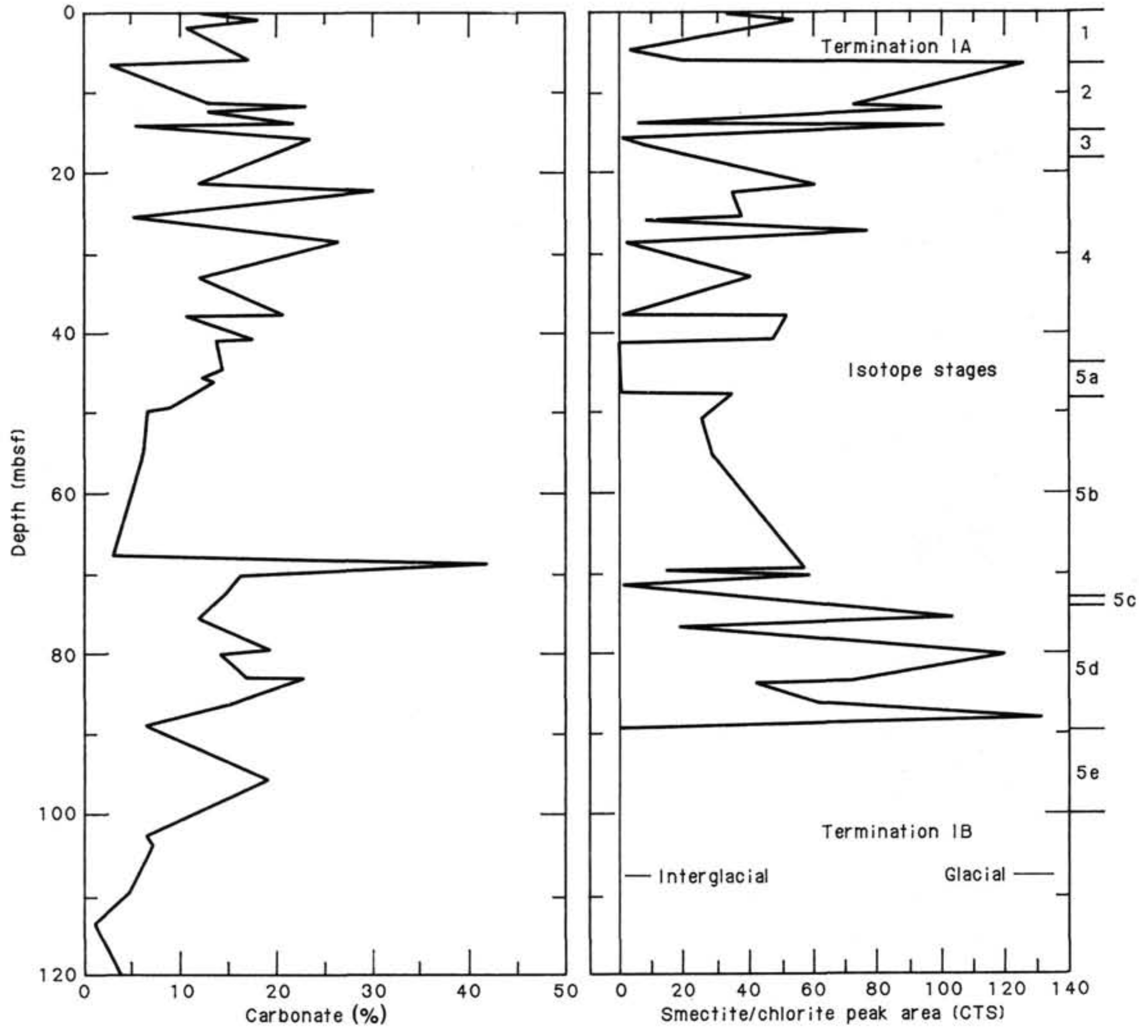

Figure 11. Correlation of the glacial/interglacial isotope stages with concentration of smectite plus chlorite (right graph) and percentage of carbonate (left graph) in sediments from Cores 107-650A-1H to -13H.

89.00 mbsf contain no detectable smectite. The sediments in this interval are tentatively correlated with Termination II and Isotope Stage 5e, an interglacial period climatically similar to the Holocene. Isotope Stage 5 is predominantly a warm period but does contain cooler periods or substages within it. The three warmer substages (5a, 5c, and 5e) are correlated with the following clay-free intervals: 41.08–47.34 mbsf, 71.04–71.89 mbsf, and 89.00–100.3 mbsf, respectively. The cooler substages (5b and 5d) are represented by the intervening occurrences of smectite/chlorite. Glacial Isotope Stages 2 and 4 can also be detected as periods of increased smectite, while the interglacial Isotope Stage 3 is, once again, denoted by a clay-free interval (14.30–14.44 mbsf and 15.94–16.50 mbsf). The late Holocene or maximum interglacial Isotope Stage 1 is apparently missing in the Site 650 cores, but the micropaleontologic recognition of Termination I can be placed on the smectite/chlorite curve at about 6.0 mbsf (Fig. 11). This most recent termination has been subdivided into two events; Termination IA is the rapid deglaciation at 13,000 yr B.P. followed by an intervening renewed glaciation (the Younger Dryas event) and Termination IB at about 10,000 yr B.P. The renewed glaciation between Terminations IA and IB may be reflected by the smectite/chlorite peak observed between 0.20 and 1.13 mbsf (Fig. 11).

Although this correlation of the clay content with late Pleistocene glacial/interglacial cycles is based on limited data, there does appear to be a positive correspondence between the two which demands further investigation. Future, high resolution correlations of bio-, isotope- and clay mineralogic stratigraphies should be able to resolve the climatic and/or tectonic significance of the fluctuations in the smectite content of the Site 650 sediments.

Sedimentary Instabilities Observed in Hole 650A

The following markers have been considered as representative expressions of sediment instabilities:

1. Minor tensional faults were observed but many are thought to result from drilling disturbance. We consider significant only those faults which exhibit a small unconformity with the overlying sediments (Fig. 12); in Cores 107-650A-24X (interval 218.6–228.2 mbsf), 107-650A-38X (interval 353.9-363.5 mbsf), 107-650A-45X (interval 406.1-411.8 mbsf), and in one rock fragment of Core 107-650A-25X (interval 228.2-237.8 mbsf) showing fault-surface slickensides. In this rock fragment there was an indurated wacke, quartzose, arkosic sandstone identical in composition (though not in induration) to the coarser sequence of the turbiditic sediments in Subunit Ic, Cores 107-650-15X to -30X, interval 132–286 mbsf. In addition to the slickensides, one thin section shows obvious microfractures and microstructures suggesting shear.

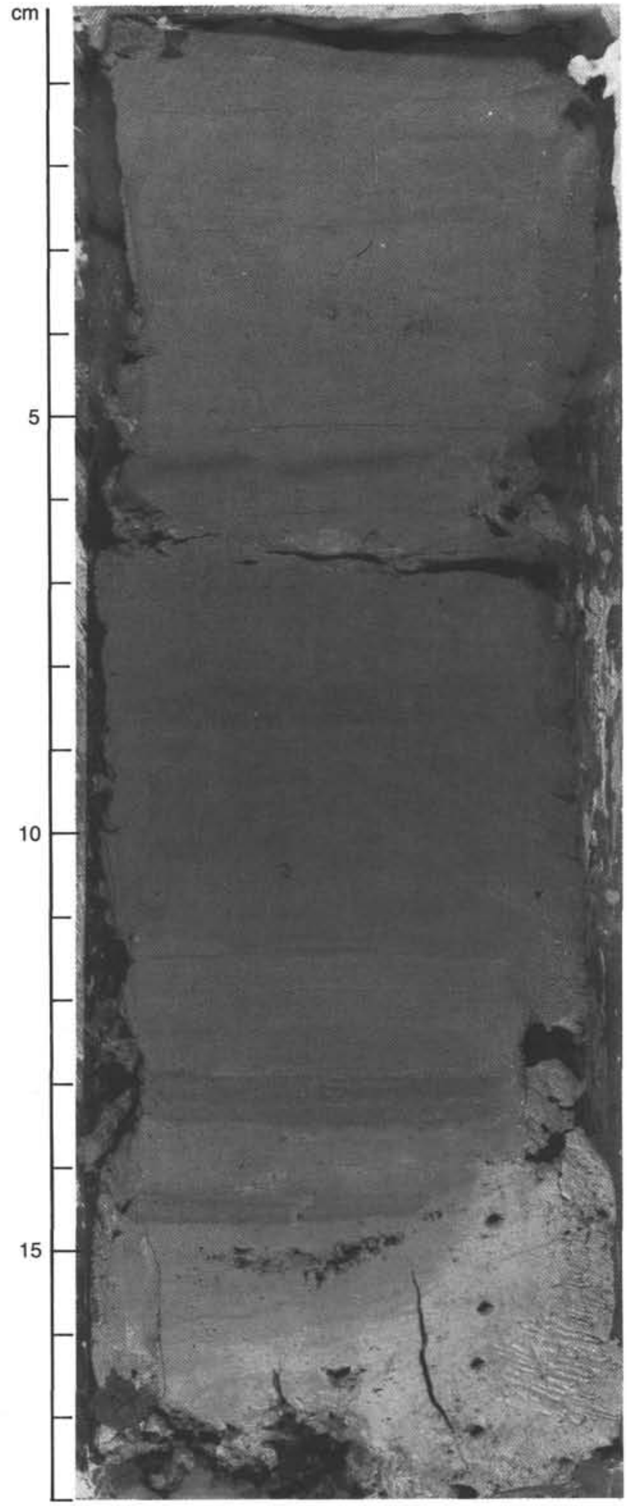

Figure 12. Synsedimentary microfault observed in Sample 107-650A-24X-CC, 6–7 cm (221.6 mbsf).

2. Minor slumps and synsedimentary folds were detected at 22.4–42.4 mbsf (Cores 107-650A-4H to -5H), 344.2–373.1 mbsf (Cores 107-650A-37X to -39X), 546.8–566.1 mbsf (Cores 107-650A-60X to -61X), and 575.8–584.4 mbsf (Core 107-650A-63X) (Fig. 13). Minor structures are also detected within the intervals 71.3–81.0 mbsf (Core 107-650A-9H), 160.5–170.2 mbsf (Core 107-650A-18X), 324.8–334.5 mbsf (Core 107-650A-35X),

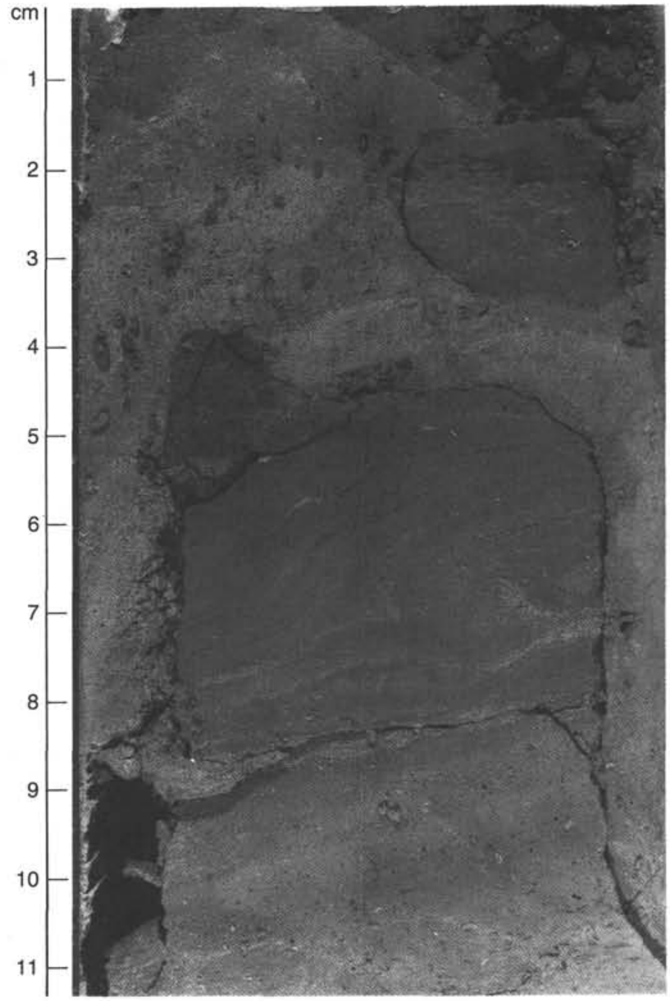

Figure 13. Example of a slump occurring in Sample 107-650A-63X-3, 5–8 cm (578.8 mbsf).

498.6–508.2 mbsf (Core 107-650A-55X), and 584.4–594.1 mbsf (Core 107-650A-64X).

3. Absence, scarcity, or thinness (< 10 cm) of sequences of volcanogenic sands in the intervals 42.4–52.1 mbsf (Core 107-650A-6H), 69.5–73.3 mbsf (part of Core 107-650A-8H), 92.5–109.7 mbsf (part of Cores 107-650A-11H and -12H) (Fig. 14), 132.1–151.3 mbsf (Cores 107-650A-15X to -16X), 237.8–295.8 mbsf (Cores 107-650A-26X to -31X), 360–392.4 mbsf (Cores 107-650A-39X to 107-650A-41X), 411.8–460.1 mbsf (Cores 107-650A-46X to -50X), and 469.7–488.9 (Cores 107-650A-52X to -53X).

Four main periods of relatively active sediment instability are suggested (Fig. 15):

1. 22.4 to 42.4 mbsf (Cores 107-650A-4H to -5H);
2. 218.6 to 237.8 mbsf (Cores 107-650A-24X to -25X);
3. 344.2 to 411.8 mbsf (Cores 107-650A-37X to -45X), which could be subdivided in two subperiods above and below the interval 373.1–392.4 mbsf (Cores 107-650A-40X to -41X);
4. The interval between 546.8 and 599.8 mbsf (Cores 107-650A-60X to -65X).

The end of Periods 4 and 3 corresponds respectively with the proposed limits between sedimentary Units IIb and IIa and between Units II and I. The two other events correspond with

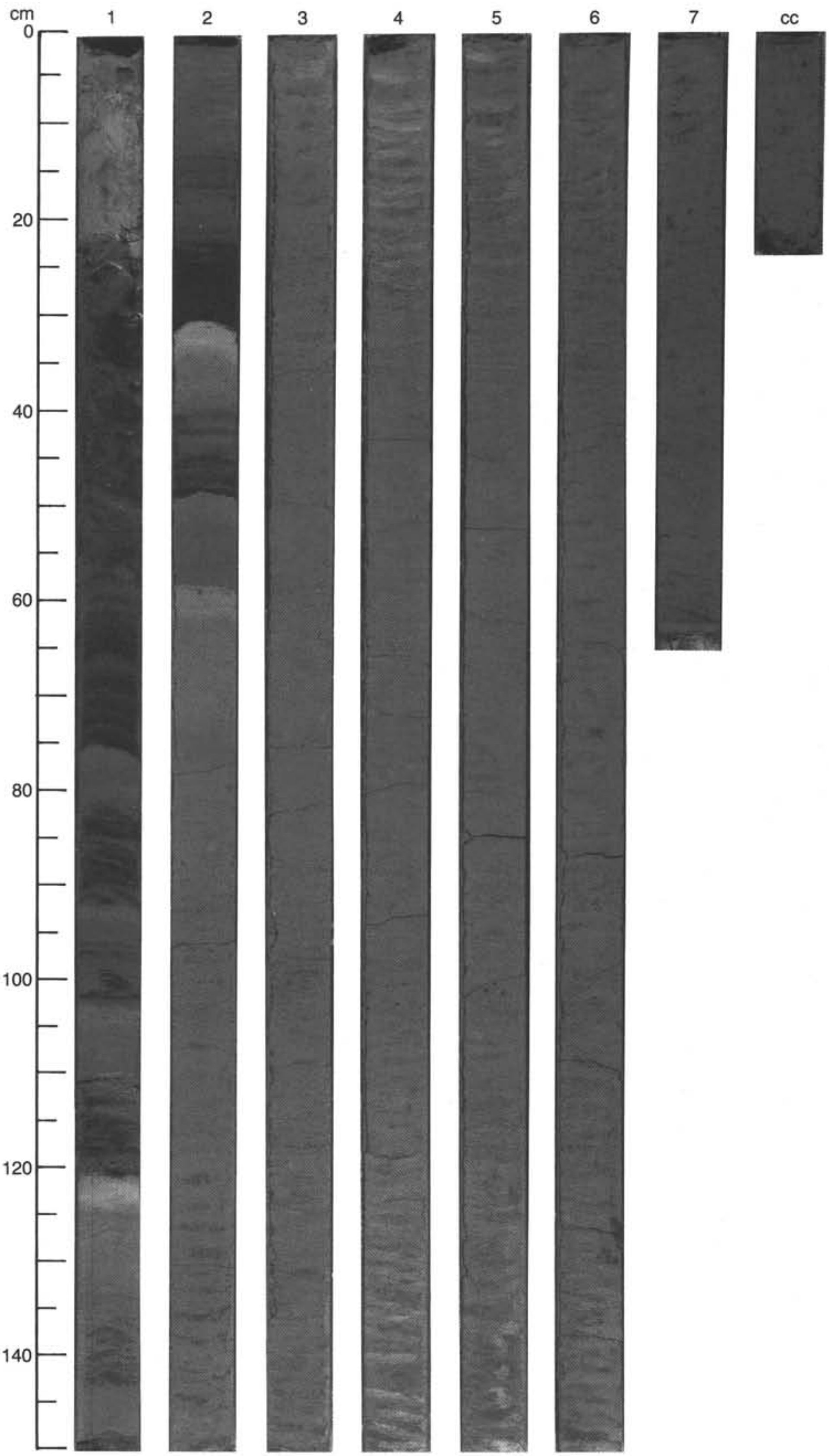

Figure 14. Example of a core with mainly fine detritic content (Sample 107-650A-11H, 90.7–100.3 mbsf), without the abundant volcaniclastic sediments attributed to turbidity current redistribution.

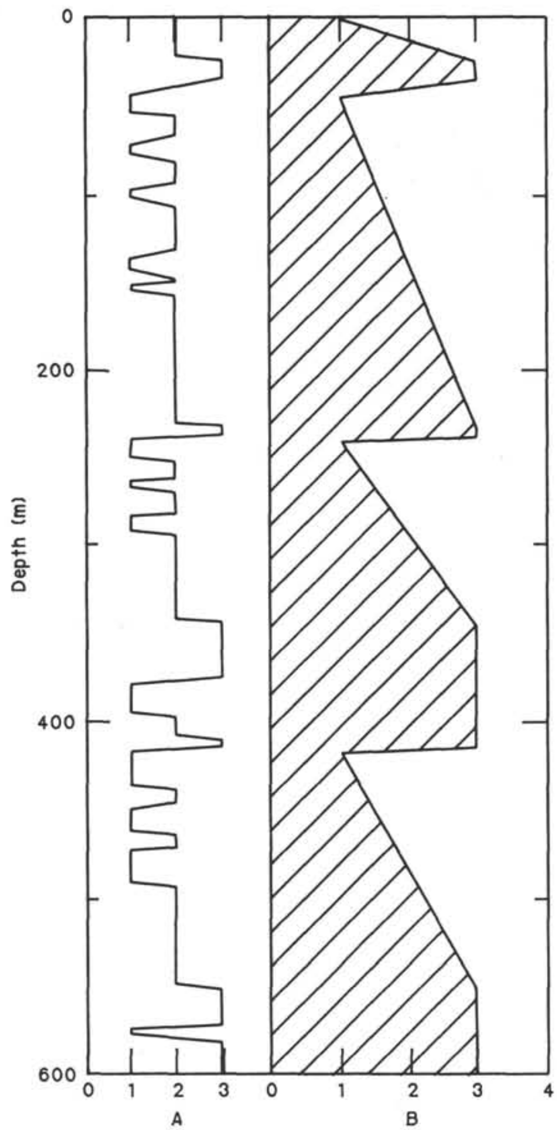

Figure 15. Sedimentary instability vs. depth in Hole 650A. A. Relative sedimentary instability; 1: weakly unstable; 2: moderately unstable; 3: fairly unstable. B. Smoothed curve suggesting first-order instability (same scale as in A).

marked changes of volcaniclastic influx respectively in between Units Ic (event 2) and Units Ia (event 1).

IGNEOUS PETROLOGY

Basalt/Sediment Contact

Basalt was reached at 602 mbsf. For a few meters above the basalt/sediment contact, the sediment (fine-grained nannofossil ooze) is reddish brown in color, due probably to a small Fe hydroxide fraction. Just above the contact a 10–12-cm-thick zone was observed where the sediment is well compacted and pale green to blue in color (Fig. 16). The sediment of this zone consists dominantly of well formed euhedral dolomite rhombs ~5–20 μm in size, and of subhedral to anhedral laths of an alkali feldspar, probably albite.

Description of the Basalt

Basalt was penetrated for a thickness of about 32 m. It appears to be strongly altered and highly vesicular (Fig. 16). The

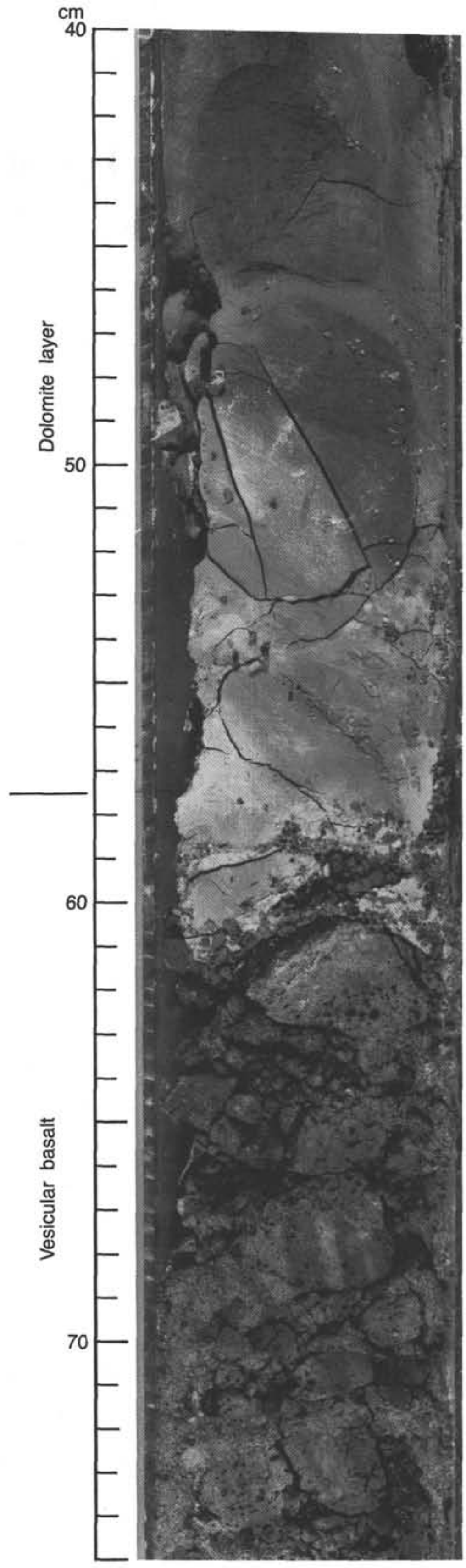

Figure 16. Contact between vesicular basalt and the 10–12-cm thick dolomitic layer, Core 107-650A-66X-2.

diameter of the vesicles ranges from about 3–4 mm to ~100 μm. The degree of vesicularity ranges throughout the cored section from very high (over 30% by volume) to moderate (roughly 10% by volume). Measured values of porosity in hand specimen range from 50% for the highly vesicular samples to 30% for those with moderate vesicularity. Compressional acoustic wave velocity ranges from 2.8 km/s (highly vesicular) to 3.2 km/s (moderately vesicular). The internal surface of the vesicles is coated with carbonates, zeolites, and Fe-hydroxides.

Thin section observations confirm that the rocks are highly altered. Their texture, rather constant throughout the cored section, ranges from intergranular to intersertal (Fig. 17). A network of elongated laths or microliths of Ca-plagioclase encloses a mass of secondary products including phyllosilicates and Fe-hydroxides. The degree of crystallinity varies: at the top of the section and again 145 cm below the top, the rock consists mostly of strongly altered glass with a few skeletal plagioclase microliths and some pseudomorphs after olivine, suggesting former chilled margins marking the tops of flows. Away from these glassy zones the degree of crystallinity of the rock is higher. Pseudomorphs after euhedral or subhedral olivine crystals are frequent at some levels. In a few cases relict clinopyroxene (cpx) crystals were recognized in the groundmass. However, the modal cpx content of the basalt was probably very low even before alteration.

Preliminary Evaluation of the Results

1. The observation of former glass chilled margins and the interpretation of the dolomitic sediment above the basalt as due to gradual alteration and recrystallization are consistent with the basalt having been emplaced on the seafloor and not as a sill. The low acoustic velocity of the basalt may be due to its alteration and vesicularity. This velocity is consistent with the low acoustic velocity measured from MCS velocity analysis (2.7 km/s) for the inferred basement of the Marsili basin (see "Seismic Stratigraphy" section, this chapter). If the basalt drilled at Site 650 is indeed the top of the igneous basement, the Marsili basin must be quite young (approximately 2 m.y.).

2. Given the pressure/dependency of gas solubility in a magma, and even considering that back-arc and/or island arc basalts have a relatively high volatile content (Garcia et al., 1979), the high vesicularity of site 650 basalt suggests that its emplacement took place at a considerably shallower depth than its present level (~4100 m below sea level). This implies that the basin subsided considerably since 2 m.y., when the basalt was apparently emplaced.

3. Given the highly altered state of the rocks, and the lack as yet of a complete set of chemical data on the samples, no firm assessment of the petrochemical affinity of Site 650 basalt can be given. However, some whole rock major element data, as well as preliminary electron probe analyses of relict plagioclase and clinopyroxene minerals, suggest a calc-alkaline affinity for the samples. If this is confirmed by further studies, Site 650 volcanism could be related to the calc-alkaline magmatism of the Eolian arc (Barberi et al., 1974; Beccaluva et al., 1982), and to the younger activity of the Marsili Seamount (Selli et al., 1977). This interpretation would imply that the igneous basement of the Marsili Basin is different not only in age but also in origin from that of the Vavilov Basin, which from data of Leg 42 (Barberi et al., 1977) and Leg 107 Sites 651 and 655 appears to have tholeiitic affinity.

BIOSTRATIGRAPHY

Summary

At Site 650, a sedimentary sequence 602 m thick overlies a vesicular basalt unit (Core 650A-66X). The sedimentary sequence is referred to the latest Pliocene–early Holocene interval (*Disco-*

Figure 17. Photomicrograph of basalt from Site 650, showing intersertal/intergranular texture, with Ca-plagioclase microliths in a groundmass of clay and Fe-hydroxide alteration products. Pseudomorphs after an olivine microphenocryst are visible. Length of olivine pseudomorph is roughly 100 μm. Sample is 107-650A-69X-CC, 10–12 cm.

aster brouweri (NN18)/*Globorotalia inflata* (MPl6) to *Emiliania huxleyi* (NN21)/*Globorotalia truncatulinoides excelsa*) (Fig. 18).

Planktonic foraminifers are generally poorly represented from the top down to 527 mbsf (Core 650A-57X), an interval diluted by a large amount of volcanic glass and pumice. From 527 mbsf to the base of the sequence the foraminiferal assemblages are more common and well diversified.

Distinct changes in planktonic foraminiferal assemblages, mainly during the late and middle Pleistocene, indicate stronger climatic fluctuations during this time interval than during the preglacial Pleistocene. These climatic changes have been used to provide stratigraphic subdivisions for the upper part of the sequence.

Autochthonous benthic foraminifers are very rare throughout the whole series. Displaced specimens from shallower water environments are more or less frequent in some discrete levels.

Radiolarians, sponge spicules, echinoids remains, and otoliths occur sporadically. Pteropods are present in some intervals of the uppermost Pleistocene.

Well-preserved nannoplankton are few to abundant throughout the series. The occurrence of common reworked species from older strata in certain levels makes it possible to recognize distal turbidites.

Planktonic Foraminifers

Holocene

Holocene sediments were recovered from Core 650A-1H. This age was recognized by the presence of *Globorotalia truncatulinoides* right coiling and by the general foraminiferal assemblage indicating a warm-temperate climate, underlain by a cooler climate assemblage in 650A-2H, CC (12.7 mbsf). Termination I is assumed to be in core 2H.

Pleistocene

The Pleistocene interval was recovered from 12.7 mbsf to about 580 mbsf. Two planktonic foraminiferal biozones were recognized (Ruggieri and Sprovieri, 1983; Ruggieri et al., 1984 amended in the Explanatory Notes). *Globorotalia truncatulinoides excelsa* biozone is present from the top to about 508 mbsf. The zonal marker is present only in some samples and is generally rare. The base of this biozone was difficult to recognize since in the pertinent interval the planktonic foraminiferal assemblage is extremely poor.

Globigerina cariacoensis biozone was recognized from about 508 to about 580 mbsf. Again, the nominal marker is always very rare and sparse (Fig. 18).

The Pliocene/Pleistocene boundary was recognized at 580 mbsf, by the strong increase of *Neogloboquadrina pachyderma* left-coiling specimens. Its absolute age has been evaluated at about 1.67 m.y. (Colalongo et al., 1982; Tauxe et al., 1983).

Pliocene

The latest Pliocene (Piacenzian stage) present is between about 580 and about 602 msbf (base of the sedimentary sequence), where the MP16 (*Globorotalia inflata*) biozone (Cita, 1975; Rio et al., 1984a) was recognized. The zonal marker is always abundant. The occurrence of *Globorotalia truncatulinoides truncatulinoides, Globorotalia tosaensis, Globorotalia tosaensis tenuitheca*, and frequent specimens of *Sphaeroidinella dehiscens* (generally rare throughout the Pliocene in the Mediterranean basin) between 594 and 599 msbf would indicate that this interval is near the base of the MP16 biozone.

Benthic Foraminifers

Among the few benthic species that can be considered not displaced (*Pyrgo depressa, Pyrgo lucernula, Oridorsalis stellatus, Gyroidina* spp., *Articulina tubulosa*), only *Articulina tubulosa* is indicative of water depth, since the other species have a rather wide bathymetric range. Within the Mediterranean basin *Articulina tubulosa* is known to range from about 1000 m down to deeper than 3000 m of water (Parker, 1958; Massiota et al., 1976). It is present, always with very few specimens, sporadically from the interval between 22 and 584 m, essentially in samples corresponding to fine-grained sediments. In the sediments above the top of the basalts (Cores 63 to 65) the benthic assemblage is very poor. Nevertheless the absence of an epibathyal assemblage and the absence of *Cibicidoides kullembergi* (a deep species with an upper depth limit around 2000 m in depth), which appears well above, makes it possible to propose a depth range for this interval between 1000 and 2000 m.

Paleoclimatic Approach

Based on changes of planktonic foraminiferal assemblage, we tried to identify the Terminations of Broeker and Van Donk (1970), in order to recognize the isotopic stages. This approach does not allow a real differentiation between "cold" and "warm" intervals, but only a climatic trend. It will be checked against the isotopic curve provided by onshore studies.

This technique for subdividing the upper part of the Pleistocene has been successful in the Eastern Mediterranean (Glaçon, 1983) and it is interesting to test whether the same planktonic foraminiferal "events" can be recognized in the Tyrrhenian Basin. For example, the disappearance of *Globorotalia inflata* during isotope Stage 2 was well documented in Levantine cores (Murat and Glaçon, 1985) and in the Ionian Sea (Muerdter and Kennett, 1983). Even in lithological intervals that can be ascribed to distal turbidites, this method, based on the presence or absence of selected species and not on their relative abundance, can be used. We think, indeed, that such displacements do not substantially modify the specific composition of the planktonic assemblage present in the sediments. Figure 19 shows preliminary results based on studies of the core catchers assemblages only and will be improved later.

Cifelli (1974) recovered a living assemblage (during June) from the Tyrrhenian Sea dominated by *Hastigerina siphonifera* (about 40%) and *Globorotalia truncatulinoides* (15%). Parker (1955), Todd (1958), and Thunell (1978) found in surface sediments a foraminiferal assemblage dominated by *Globigerina bulloides, Neogloboquadrina dutertrei, Globorotalia inflata*, and *Globigerinoides ruber*.

Starting from the present-day assemblage we can recognize the tendency to "cool" climate by the disappearance of *Globigerinoides ruber*, followed by the disappearance of *Globorotalia inflata* and the relative increase of *Globigerinita quinqueloba, Globorotalia scitula*, and *Neogloboquadrina pachyderma*, the later one represented also by some left-coiled specimens. The trend to "warm" climate is not so clear. At Site 650 in the core catcher samples *Globigerina calida* was not found. Only few specimens of *Globigerina praecalida* and *Globigerinoides ruber* with large apertures are present.

Nannoplankton

At Site 650, a late Pliocene (zone NN18) to Quaternary (zone NN21) sequence of 602 m thickness was recovered overlying vesicular basalts.

Nannoplankton zone NN21 (*Emiliania huxleyi* zone) was determined from Core 107-650A-1H·to sample 107-650A-16X-4, 18–20 cm (147 mbsf) by the presence of *Emiliania huxleyi*.

Zone NN20 (*Gephyrocapsa oceanica* zone) was recovered from Sample 107-650A-16X, CC to Sample 107-650A-37X, CC 25–26 cm (353 mbsf). The nannoplankton assemblages of the upper Quaternary are typical for temperate surface water masses influenced by the influx from the Atlantic. Typical warm-water species like *Umbellosphaera tenuis, Discosphaera tubifera, Ooli-*

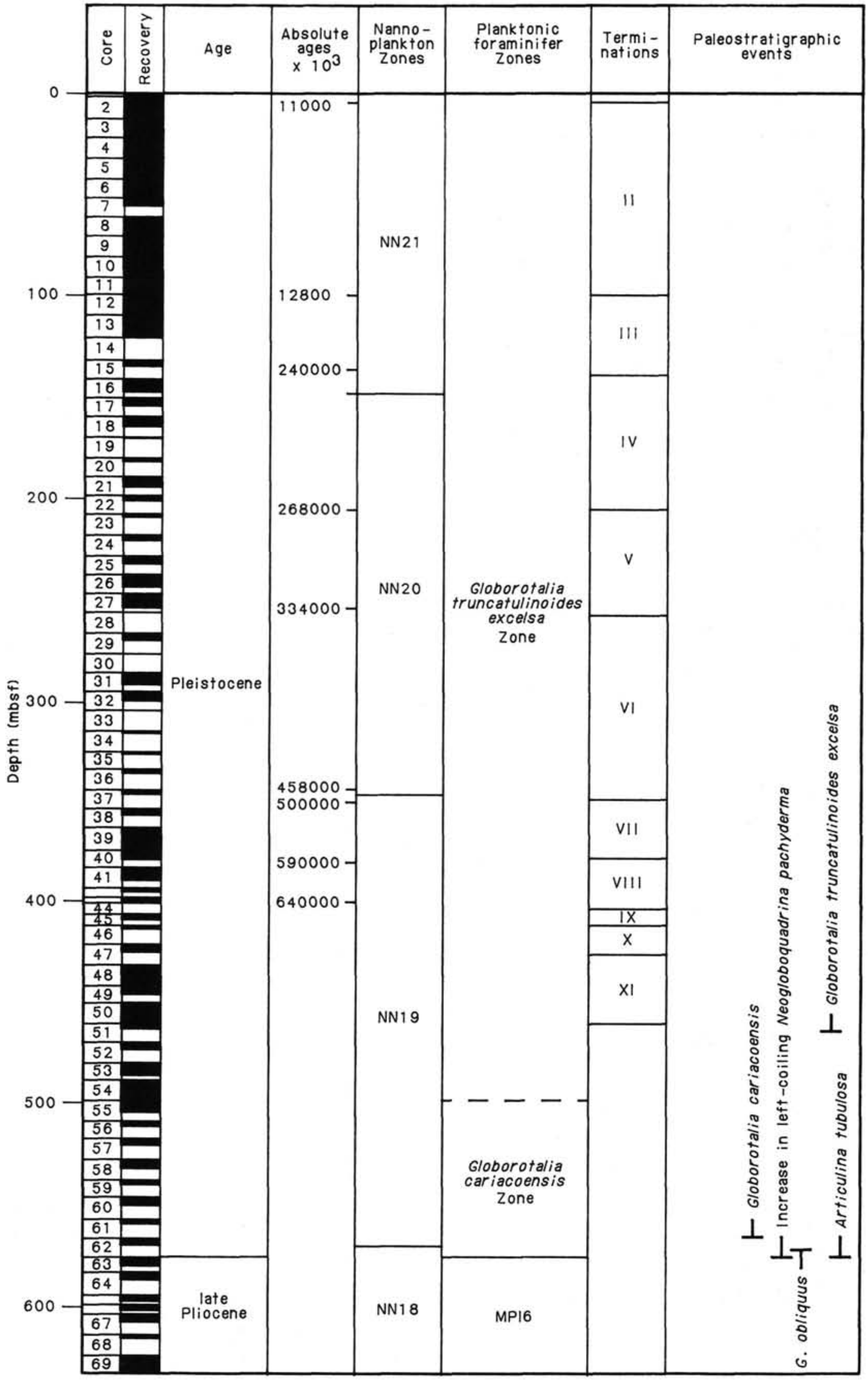

Figure 18. Biostratigraphy of Site 650.

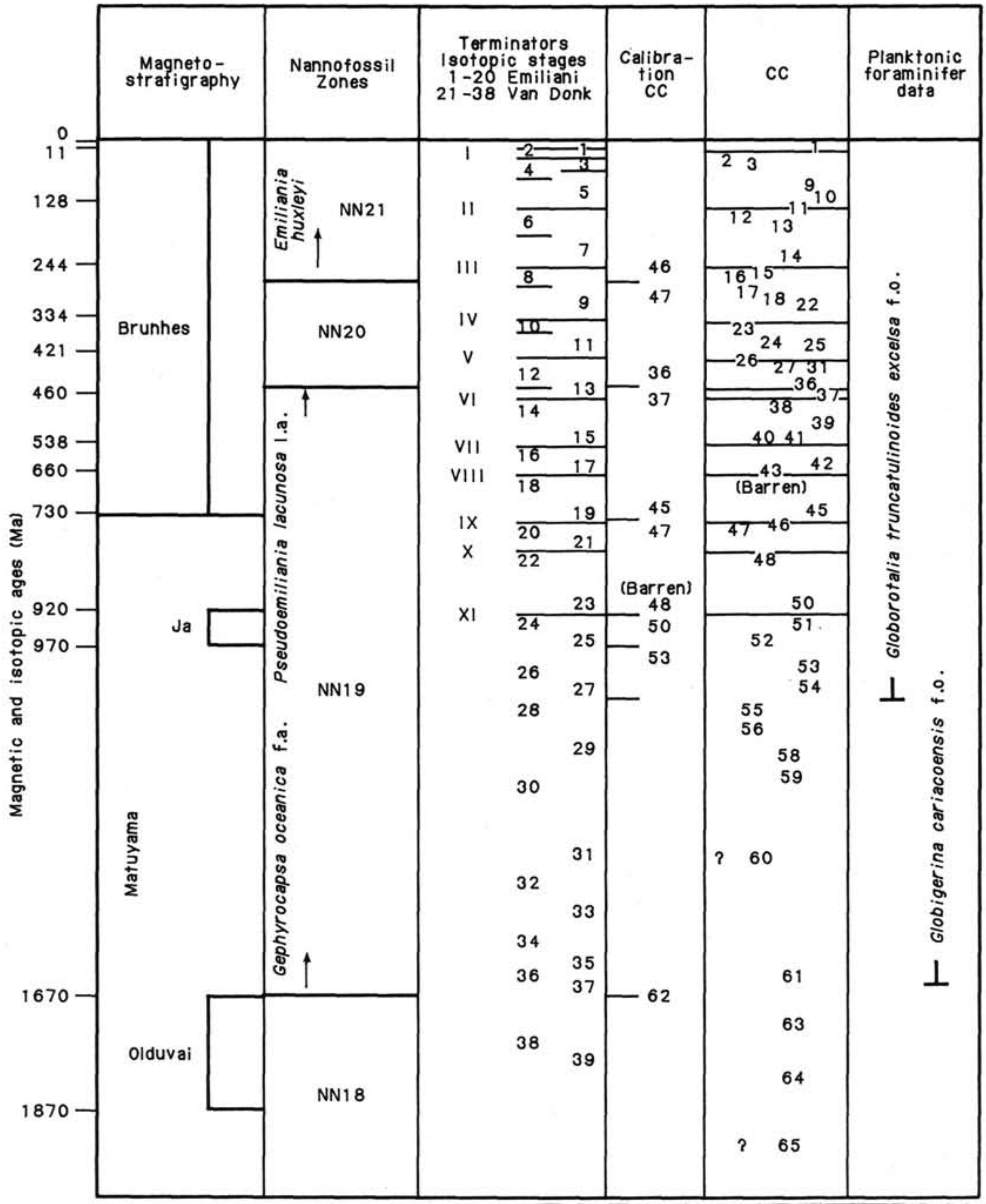

Figure 19. Preliminary time scale to identify the glacial terminations based on foraminiferal assemblages done on board during Leg 107.

tothus fragilis, and *Pontosphaera syracusana* are generally rare or missing. *Coccolithus pelagicus*, a cold-water species, is absent within the uppermost part of the sequence (0–2.5 mbsf) which corresponds to Termination I. Deeper in the section, the abundance of *Coccolithus pelagicus* is variable. It is generally only rare within the Lower Quaternary (zone NN19) but becomes more frequent within the Pliocene.

Nannoplankton zone NN20 is characterized by the dominance of different species of the genus *Gephyrocapsa*. A *Helicosphaera* sp. (with two large pores) is present within the interval from Sample 107-650A-31X-3, 92–94 cm to Sample 107-650A-34X, CC. This species was also observed in all the other sites and seems to be typical for the lower part of zone NN20 where it is restricted to a short interval.

The late Pleistocene sequence consists of alternating hemipelagic sediments and turbidites which are dominated by volcaniclastic components (glass and pumice fragments) in their lower part. The fine-grained upper portion of each turbidite is a calcareous mud often rich in volcanic ash. Nannoplankton are strongly diluted within these turbidites, and reworked Cretaceous to Pliocene species are few to common.

Nannoplankton zone NN19 (*Pseudoemiliania lacunosa* zone) was recognized from Sample 107-650A-37X, CC to Sample 107-650A-61X, CC (354.0–566.0 mbsf). The boundary NN19/NN20 corresponds approximately with a lithological change characterized by downsection higher carbonate contents, less frequent turbidites, and the decrease of volcanic detritus. This change is most probably linked to a climatic change between the preglacial and glacial Quaternary.

Gartner (1977) established a revised nannoplankton zonation for the Quaternary, subdividing the rather long time interval represented by zone NN19 into four zones. Results obtained by this study have shown that they are in good agreement with the described events, and that they are useful for more precise datings. The highest level with the dominance of a very small *Gephyrocapsa* at 0.92 m.y. corresponds approximately with the Jaramillo magnetic event (0.9–0.97 m.y.). At Hole 650A the acme of the small *Gephyrocapsa* was observed from Core 107A-650A-48X-4 to Core 107-650A-52X. The small *Gephyrocapsa* occurs also above and below the acme but less abundantly.

The last occurrence of *Helicosphaera sellii* lies in Sample 107-650A-52, CC just below the acme of the small *Gephyrocapsa*.

The interval near the Jaramillo magnetic event is characterized by the presence of several sapropel layers (Core 107-650A-50 to 107-650A-53). The sapropels are rich in pyrite and organic matter of marine origin. Plant fragments are rare. Some of the sapropels contain rather common reworked nannofossils which might indicate that they are not always autochthonous.

Discolithina japonica, Pontosphaera pacifica, and *Holodiscolithus macroporus* are common within nannoplankton zone NN19 and the upper Pliocene. The same observation was described from the northeast Atlantic (Müller, 1979). *Coccolithus pelagicus* is generally rare to few within this zone. It becomes more abundant within the Pliocene.

Several very thin white layers consisting of almost entirely large specimens of *Braarudosphaera bigelowi* are present around the Pliocene/Pleistocene boundary (107-650A-60-2, and 107-650A-64-1 and -2). The latter ones are intercalated in a sapropel layer. This species is considered to indicate lower salinity of the surface water. This might be related to a warming around the Pliocene/Pleistocene boundary linked with heavy rainfalls and/or a strong influx of fresh water from the rivers.

Time-equivalent levels with common *Braarudosphaera bigelowi* were also mentioned from the eastern Mediterranean (Müller, 1978, 1985). Decreasing salinity of the surface-water masses causes stratification within the water column and stagnation at the bottom with an extremely low oxygen content which allows preservation of organic matter and formation of sapropels. The number of sapropel layers increases upsection around this boundary.

The Pliocene/Pleistocene boundary was recognized by the extinction of *Cyclococcolithus macintyrei* which lies in the Mediterranean near the top of the Olduvai magnetic event. The extinction of *Cyclococcolithus macintyrei* at the top of the Olduvai event was described from the northeast Atlantic (Müller, 1979, 1985) and from the northwest Pacific (Monechi et al., 1986). This shows clearly that the disappearance of this species is synchronous in the Atlantic and the Mediterranean. That means that *Cyclococcolithus macintyrei* is a more useful marker for the Pliocene/Pleistocene boundary than the last occurrence of the discoasters. The latter have an earlier extinction in areas of lower surface water temperature. Discoasters are absent or only rare and mostly restricted to certain levels within the uppermost Pliocene of the western Mediterranean (Bizon and Müller, 1978). The extinction of *Cyclococcolithus macintyrei* falls together with the first occurrence of *Gephyrocapsa oceanica*.

At Hole 650A the Pliocene/Pleistocene boundary lies in Core 107-650A-62X-1, 47 cm at about 567 mbsf.

This boundary at Hole 650A falls almost together with a lithological change from predominantly calcareous mud above to nannofossil ooze below. Some slumping and synsedimentary mud breccias occur in sections 1 and 2 of Core 107-650A-62X. Nannoplankton are abundant within the uppermost Pliocene. However, in several layers they are less common due to fragmentation of the smaller species often linked with an increase of detrital carbonates and the occurrence of reworked nannofossils. These fluctuations are probably also related to climatic oscillations as indicated by variations of the nannoplankton assemblages.

The Pliocene sequence recovered at Hole 650A belongs to the interval of nannoplankton zone NN18 as indicated by the rare occurrence of *Discoaster brouweri* and *Discoaster triradiatus* in several layers.

Nannofossils are almost entirely destroyed within the sediments directly overlying the basalt. Secondary dolomite is abundant.

PALEOMAGNETISM

The electronics for the shipboard cryogenic magnetometer were not on board during the drilling of Site 650. Discrete 7-cm^3 samples were collected throughout the cored sequence. The sampling interval was dictated by the occurrence of drilling disturbance and by the variable core recovery. The average sampling interval through the sedimentary sequence was 3 m. These discrete samples were all measured using the shipboard Molspin fluxgate magnetometer and progressively demagnetized in alternating fields with the Schonstedt GSD-1 demagnetizer. Thermal demagnetization was carried out on shore to refine the magnetostratigraphy.

One hundred eighty-seven 7-cm^3 cubic samples were collected throughout the section and measured on the Molspin magnetometer. The natural remanent magnetization (NRM) of the sediment samples had an average intensity of about 10^{-5} G/cm^3 and a median destructive field of 100–150 Oe. The NRM inclinations were nearly always steep and positive, steeper than the present Earth's field, suggesting that a near-vertical drill-string (viscous) magnetization may have been acquired by the samples. This overprint dominates the NRM directions, but has low coercivity and can be easily removed by peak alternating fields of about 200 Oe. The low median destructive field reflects the low coercivity of this overprint. Alternating field demagnetization at peak fields in the range 200–400 Oe is usually sufficient to isolate a higher coercivity magnetization component which records a well-defined magnetic stratigraphy. The intensity of this component falls below Molspin noise level (equivalent to 10^{-7} G/cm^3) at peak demagnetization fields in the range 400–600 Oe. The coercivity spectrum of this component suggests that it is carried by fine-grained (diameter $< 10^{-6}$m), single domain magnetite. A likely source of this fine-grained magnetite is windblown volcanic detritus. The magnetization intensity is much greater than would be expected from biological input of magnetite for this sedimentation rate.

We have been able to clearly isolate several reversal boundaries on the basis of inclination changes in the higher coercivity component (Table 3). The result is partly confirmed by the shorebased thermal demagnetization.

Three intervals of low and negative inclinations in Cores 107-650A-2H to 107-650A-3H, Core 107-650A-11H-6,- 7, and Core 107-650A-17X-2 conceivably represent short geomagnetic events during the Brunhes normal chron, but more work needs to be done in this interval.

All samples collected from Core 107-650A-64X and below did not yield a magnetization component that could be considered primary. Core 107-650A-64X was very weakly magnetized and, even prior to demagnetization, could not be measured with sufficient precision. Magnetization intensities increased at Core 107-650A-65X-2, 69 cm, and below this level the sediment carries a very high coercivity (hematite) magnetization with steep

Table 3. Preliminary determination of magnetozone boundaries for Site 650. The samples which bracket the magnetozone boundaries are given.

Magnetozone boundary	Core	Section	Interval (cm)	Depth (mbsf)
Base of Brunhes	Between 45X	2	105–107	408.66
	and 47X	1	38–40	421.89
Top of Jaramillo	Between 50X	4	48–50	455.39
	and 50X	5	88–90	457.29
Base of Jaramillo	Between 52X	1	80–82	470.51
	and 52X	2	8–10	470.69
Top of Olduvai	Between 63X	3	34–36	579.15
	and 63X	3	141–143	580.22

positive inclinations. A single sample from the basalt at Core 107-650A-66X-2, 132 cm also carries a steep positive inclination. We consider that these steep positive inclinations from the basal brown metalliferous sediments and from the altered basalt are secondary and cannot be associated with the age of the sediment or basalt. Therefore, the contact between the sediments and the basalt at Hole 650A cannot be directly dated through the polarity time scale, but this contact is between 17.60 and 20.92 m below the base of the Olduvai event.

Cores 107-650A-1H to -20X were passed through the "loop" sensor of the Bartington susceptibility bridge prior to splitting. Measurements were made every 10 cm down to 120 mbsf, and at intervals of 10 or 20 cm below this level (Fig. 20). The susceptibility values probably reflect the concentration of magnetite which in turn reflects the contribution of volcanogenic detritus to the sediments. The volume susceptibility log supports this conclusion. From the top of the core down to 40 mbsf, the susceptibility values are very scattered with a rising trend. Three prominent peaks at 11.5, 19.5, and 26.0 mbsf correlate with prominent volcaniclastic sands in Cores 107-650A-2H-6, 107-650A-3H-6, and 107-650A-4H-3, respectively. The very constant susceptibility values between 39 and 49 mbsf correlate with the occurrence of homogeneous calcareous mud in this interval, which may represent the turbidite-free background sedimentation. A volcanogenic turbidite-rich interval between 60 and 94 mbsf is characterized by variable susceptibility values, below which constant low values again indicate the predominance of turbidite-free background sedimentation. At 99 mbsf, the values begin to rise as the concentration of pumice increases in Cores 107-650A-12H and -13H. The low values between 107 and 109 mbsf reflect a void in the core, interrupting the steady increase in susceptibility as pumice concentration increases. Below 120 mbsf, recovery is very poor.

These data represent a very impressive record of volcanogenic turbidite frequency; prominent individual volcanogenic layers can be spotted as can intervals of turbidite-free background sedimentation. However such records are only of value if recovery is good (the record below 120 mbsf is impossible to interpret) and if the cores are undisturbed by drilling.

PHYSICAL PROPERTIES

Introduction

Coring Site 650 on the Marsili Basin sampled a 601.9-m-thick sedimentary sequence, ranging from Recent to upper Pliocene in age, overlying a vesicular basalt lying from 601.9 mbsf to the bottom of the hole at 633.8 mbsf. Routine physical properties measured on the sedimentary sequence and the basement include porosity, bulk density, vane shear strength, thermal conductivity, and compressional wave velocity (Table 4).

Thermal conductivity measurements were taken on at least one, usually two, sections every two cores where GRAPE records indicated a homogenous interval (see "Explanatory Notes," this volume). Some cored intervals in the uppermost part of Site 650 were not cohesive enough to allow for compressional wave velocity measurements on discrete samples. Therefore, the velocity was measured through the split core liner, parallel to the bedding planes.

Results

GRAPE Density

Bulk density was determined by gamma ray attenuation porosity evaluation (GRAPE) for the entire length of every core.

The upper part of the sedimentary section shows a homogeneous GRAPE density of 1.5 to 1.6 g/cm^3 with some local variation up to 1.9 g/cm^3 (76–92 mbsf, 103–119 mbsf). These values remain constant to about 300 mbsf. Deeper, we observed a gradual increase to as much as 1.7 g/cm^3 at about 400 mbsf. The GRAPE density presents an alternation of values between 1.5 and 2.0 g/cm^3 between 400 and 510 mbsf and is relatively constant (2.0 g/cm^3) even in the basement.

Index Properties

Porosity, bulk density, and grain density are plotted relative to sub-bottom depth in Figures 21 and 22 and are listed in Table 4 with the compressional wave velocity data.

The porosity varies rapidly between 60% and 80% in the first 20 m of the hole and reflects the alternation of volcanic sands and mud. Deeper, four main trends can be recognized (Fig. 21): from 20 to 100 mbsf, 120 to 520 mbsf, 520 to 600 mbsf, and 600 to 615 mbsf, with values of about 70%, 45%–60%, 45%, and 35%–50%, respectively. The relative decrease of porosity (51%) at 117 mbsf has to be noted. The 120-520-mbsf trend is related to a unit with generally high carbonate content. This trend can be divided in two subtrends: (1) 120–330 mbsf (porosity: 60%–70%) and (2) 330–520 mbsf (porosity: 50%–60%).

The bulk density (Fig. 21 and Table 4) values are in good agreement with the porosity values and reflect the same trend changes along the cores. Total range of bulk density is 1.44–2.34 g/cm^3. Here again the uppermost interval of the hole, represented by an alternation of volcanic sands and mud layers, show a density fluctuating between 1.39 and 1.96 g/cm^3.

The grain density (Fig. 22) increases from the mud line to 330 mbsf (2.60–2.77 g/cm^3) and decreases between 330 and 660 mbsf. This result reflects the two main lithostratigraphic units.

Compressional Wave Velocity

The upper 30 m of the hole (Fig. 21) are characterized by velocity ranging from 1.50 to 2.45 km/s. Again, these variations have to be related to the alternation of volcanic layers and soft sediments. Between 30 and 100 mbsf, the velocity stays around 1.60 km/s. A change of velocity occurs between 100 and 120 mbsf. The interval between 120 and 325 mbsf presents very homogeneous velocities (with an artifact at 209 mbsf) gradually increasing to 1.75 km/s. The 355 mbsf and 440 mbsf changes correlate with the seismic stratigraphy (see "Seismic Stratigraphy" section, this chapter) showing velocities of 1.99 and 2.13 km/s, respectively. The episode at 500 mbsf previously noted in the porosity and density data is present here too, and seems to correspond to the top of a relatively homogeneous acoustic sequence with a velocity of about 1.9 km/s. The last velocity change occurs at the sediment-basement contact at 600 mbsf. The vesicular basalt shows velocities of about 2.8–3.2 km/s. Such relatively low velocities were unexpected and reflect the degree of alteration and/or vesicularity of this basalt which shows a high percentage of porosity (32%–50%).

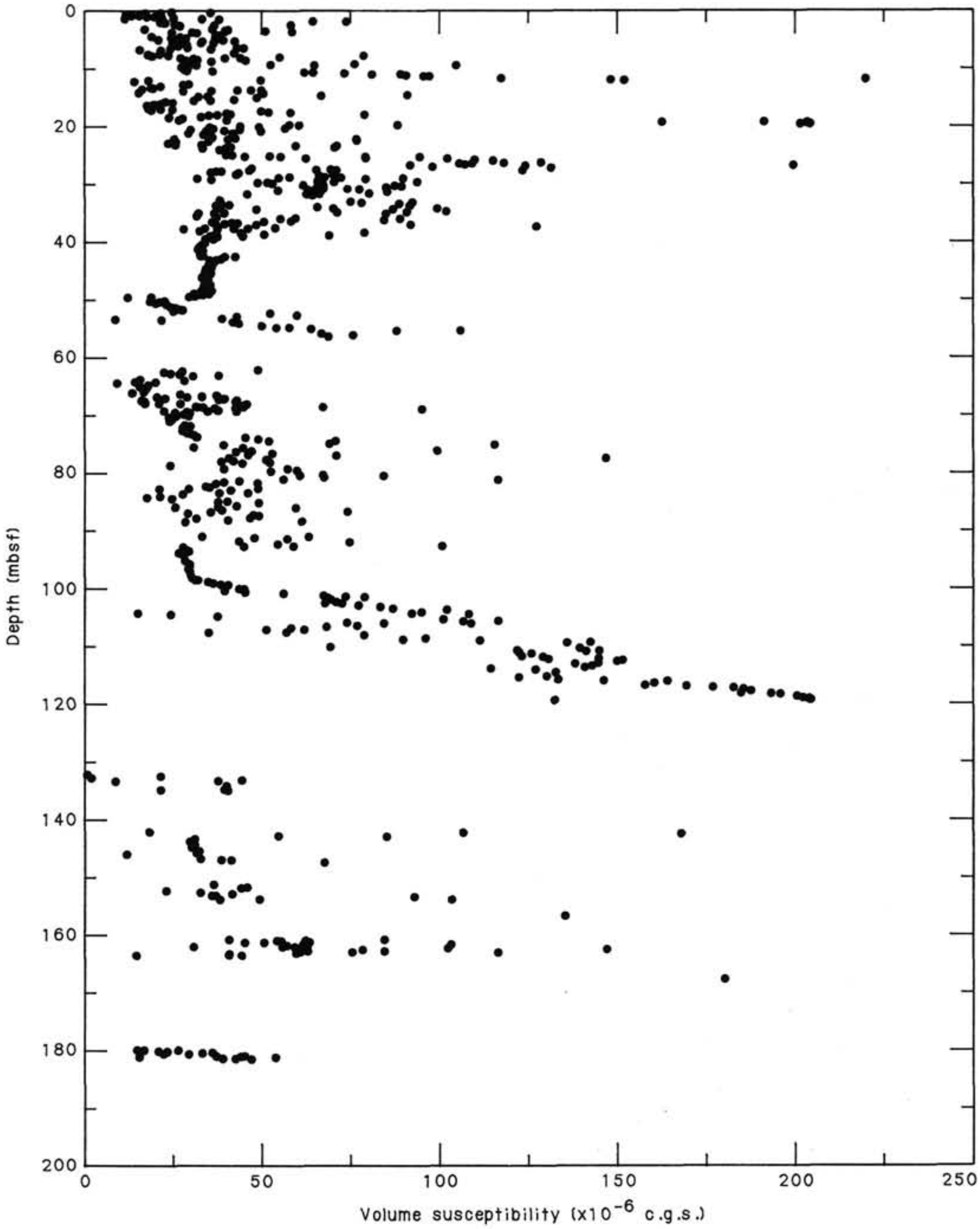

Figure 20. Whole-core measurements of magnetic susceptibility from Hole 650A.

It is interesting to compare the average velocity of each main interval with the velocity analysis of the site survey seismic line used for the choice of Site 650: The average measured compressional velocity of samples from within Seismic Unit 1 (Fig. 26) is 1.80 km/s which is 0.15 km/s higher than the 1.65 km/s velocity computed from the seismic line. The velocities measured on samples from Seismic Unit 2 have an average of 1.67 km/s which is very close to the seismic line velocity analysis (1.65 km/s). Seismic Unit 3 samples have a measured average velocity of 1.80 km/s which is higher than the computed velocities (1.65 km/s). Seismic Unit 4 samples have a measured average of 1.89 km/s. This value is sensibly lower than the computed interval velocity (2.56 km/s). Such a discrepancy (20%) can easily be explained by the drilling disturbances. Finally, the average velocity measured in basalt samples (2.9 km/s) is comparable with the computed interval velocity (2.76 km/s).

Undrained Shear Strength

Undrained shear strength was routinely measured in soft sediments from the mud line to 369.2 mbsf (Table 5 and Fig. 22). Three main intervals can be recognized: a first one occurs between the mud line and 100 mbsf, the shear strength increasing from 1.6 kPa at 1.65 mbsf to 80 kPa at 100 mbsf. The marked interruption of this first trend can be tentatively correlated with the seismic reflector lying at 150 ms sub-bottom ("Background and Objectives" section, this chapter). A second interval ranges from 100 to 191.1 mbsf, and a third unit can be recognized between 241.1 and 369.2 mbsf.

Table 4. Physical properties index from Site 650.

Core section	Depth sub-bottom (m)	Bulk density (g/cm^3)	Porosity (%)	Grain density (g/cm^3)	Compressional wave velocity (km/s)
1H-1	0.35	1.48	75.6	2.85	
1H-2	1.65	1.56	69.7	2.67	1.506
1H-2	2.30	1.71	59.8	2.60	1.845
2H-5	10.05	1.49	77.1	2.79	
2H-6	11.46	1.72	63.7	2.72	2.384
2H-7	12.25	1.39	81.4	2.70	2.446
3H-2	14.95	1.47	77.3	2.62	
3H-5	19.00	1.60	62.6	2.81	1.572
3H-5	19.40	1.96	48.3	2.66	
3H-7	20.64				1.640
4H-2	24.65	1.48	76.7	2.68	
4H-5	29.15	1.62	74.5	2.81	2.440
5H-4	37.95	1.55	74.7	2.78	
5H-6	40.85	1.58	74.7	2.78	
6H-2	44.65	1.58	67.6	2.57	
6H-4	47.35	1.61	66.1	2.57	
8H-6	69.95	1.59	69.1	2.69	1.579
9H-3	75.50	1.68	65.7	2.82	1.579
9H-6	79.75	1.55	72.6	2.76	1.545
10H-2	83.25	1.63	66.4	2.72	
10H-5	87.85	1.61	69.0	2.59	
11H-4	95.85	1.50	74.1	2.65	1.593
12H-2	102.55	1.71	61.4	2.60	1.588
12H-7	111.40	1.89	51.4	2.64	1.739
13H-6	117.50	1.89	50.6	2.66	1.482
15X-2	134.50	1.60	68.4	2.63	
16X-3	145.40	1.49	71.5	2.41	
17X-2	153.30	1.71	61.8	2.65	1.552
18X-1	161.10	1.95	68.7	2.73	
20X-1	180.90	1.72	61.8	2.74	
21X-2	191.50	1.55	68.5	2.57	
22X-1	199.40	1.67	64.2	2.70	1.504
23X-C	209.35	1.73	58.4	2.46	2.239
24X-1	219.00	1.74	60.7	2.72	1.628
25X-2	231.00	1.78	67.7	2.72	
26X-3	240.85	1.56	67.0	2.44	1.618
27X-4	252.70	1.65	60.5	2.76	
29X-C	276.30	1.64	60.3	2.48	1.626
31X-2	287.85	1.67	59.8	2.38	
31X-2	288.85	1.69	62.2	2.37	
34X-1	315.95	1.63	64.5	2.58	1.699
34X-1	316.50	1.89	55.2	2.77	
35X-1	324.90	1.44	67.3	2.10	
35X-1	325.50	1.44	56.2	2.34	
36X-1	335.00	1.72	68.7	2.85	1.751
37X-1	345.25	1.67	57.6	2.80	1.624
38X-1	354.50	1.63	60.5	2.78	
38X-2	356.60	1.79	63.1	2.69	1.994
39X-4	369.40	1.74	62.3	2.74	1.872
39X-6	371.10	1.80	57.5	2.67	1.623
40X-C	382.60	1.90	52.3	2.80	1.771
41X-2	384.89	1.71	62.6	2.60	
41X-4	388.21	1.69	60.3	2.50	1.710
42X-1	392.58	1.68	55.8	2.27	1.747
43X-C	399.30	1.82	56.7	2.67	1.605
45X-1	406.42	1.65	61.7	2.37	
47X-1	422.15	1.80	56.8	2.72	
47X-2	423.70	1.66	65.3	2.53	1.861
48X-1	431.80	1.50	77.6	2.65	2.001
48X-2	433.32	1.60	63.6	2.42	
48X-3	434.90	1.55	68.3	2.24	
48X-6	439.60				2.127
48X-C	440.60				2.084
49X-1	442.11	2.00	49.8	2.73	
49X-3	444.86	1.87	58.3	2.75	1.831
50X-5	456.88	1.75	60.2	2.54	1.900
50X-7	459.72	1.95	49.2	2.76	1.748
51X-1	460.60	1.82	58.6	2.76	1.691
52X-1	469.97	1.74	63.3	2.57	1.703
54X-1	489.74	1.70	63.1	2.50	1.964
54X-4	493.43	1.75	58.3	2.77	2.103
55X-1	498.94	1.66	62.1	2.38	2.040
55X-1	499.4				1.881
55X-2	501.04	1.66	68.0	2.63	1.818
56X-1	508.78	2.05	52.8	2.90	1.941
57X-2	520.70	2.14	45.2	2.68	1.918
58X-1	528.02	1.82	62.1	2.66	
58X-2	529.30	2.05	50.2	2.54	2.106
59X-2	539.40	2.04	45.3	2.74	
60X-1	547.75	2.02	48.7	2.80	1.804
60X-C	556.40	2.06	45.2	2.73	1.689
61X-2	558.05	1.99	48.1	2.75	1.796
62X-2	567.65	2.08	50.6	2.71	1.935
63X-2	577.35	2.12	45.8	2.85	1.829
64X-2	586.10	2.05	46.5	2.69	
64X-2	586.90	2.08	43.7	2.72	1.829
65X-2	595.70	2.11	41.3	2.73	1.853
66X-1	600.65	2.34	34.7	2.74	2.130
66X-2	602.60	2.25	32.7	2.73	3.182
68X-1	615.30	2.23	50.2	2.72	2.850

Thermal Conductivity

Thermal conductivities measured at Site 650 are listed in Table 6 and were used for the evaluation of the heat flow in connection with temperature measurements in the hole (see "Downhole Measurements" section, this chapter). The thermal conductivity measurements were routinely performed from the mud line to a depth of 423.6 mbsf. Below that depth, the drilling disturbances induced a lack of coherence in the measurements. The conductivities measured vary between 1.5 and 3.2×10^{-3} cal $\times$ $cm^{-1} \times s^{-1}$. Three main thermal conductivity units can be distinguished (Fig. 22): (1) the interval from the mud line to about 100 mbsf is characterized by a relatively well defined gradient of increasing conductivity from 1.8 to 2.5×10^{-3} cal $\times$ $cm^{-1} \times s^{-1}$, (2) the 135–220-mbsf interval shows relatively high values: two maxima at about 2.8–2.9×10^{-3} cal $\times$ $cm^{-1} \times s^{-1}$ are separated by low values of 2.3–2.5×10^{-3} cal $\times$ $cm^{-1} \times s^{-1}$, (3) the 240–398.2-mbsf interval is characterized by an alternation of high (2.79×10^{-3} cal $\times$ $cm^{-1} \times s^{-1}$) and low (1.95×10^{-3} cal $\times$ $cm^{-1} \times s^{-1}$) values but shows an overall increase of the thermal conductivity downsection.

Conclusions

The physical-properties analyses of Site 650 underline the main acoustic units of the site survey seismic profile (see "Seismic Stratigraphy" section, this chapter) and point out four significant trend changes at approximately 100–120, 330, 500, and 600 mbsf. Within these trends important value changes occur at 0–20 and 440 mbsf. The interval 0–20 mbsf is related to an alternation of volcanic sands and muds. The interval 100–120 mbsf correlates with both a thick pumice layer and strong seismic reflector. The trend at 440 mbsf is related to an alternation of calcareous mudstone and mudstone levels. The most significant change of the physical properties occurs at the sediment/basalt contact.

GEOCHEMISTRY

Organic Geochemistry

Numerous analyses for the concentration of organic carbon were performed on samples from Site 650 according to the method described in the Explanatory Notes (see Table 7). Because we suspect a leak in the nitrogen system of the Perkin Elmer Elemental Analyzer, numbers given for N_{total} and the ratio of C to N may be erroneous. Several sapropels (C_{org} greater than 2%) and sapropelic (C_{org} greater than 0.5%) mudstones and nannofossil oozes were encountered in the sedimentary section (Fig. 23). They cluster around depth intervals 0–50 mbsf, 150–200 mbsf, and 450–470 mbsf. A maximum value of 2.29 weight % C_{org} was measured in sample 650-2A-3, 53–54 cm at a depth of 6.5 mbsf.

Analyses of gas bubbles extracted from the core liners by vacutainer sampling did not reveal any hydrocarbon gases.

Inorganic Geochemistry

Carbonate Analyses

A total of 203 sediment samples was analyzed for their carbonate content. In addition to samples taken exclusively for this purpose, subsamples of physical properties samples and samples taken adjacent to intervals investigated by smear slide analyses were used employing the method outlined in the Explanatory Notes. Results are shown in Table 7 and Figure 24. Values for carbonate content vary widely from a low of 0.47% in a coarse-grained volcaniclastic turbidite layer of youngest Pleistocene age to a high of 59.8% encountered in a lower Pleistocene nannofossil claystone.

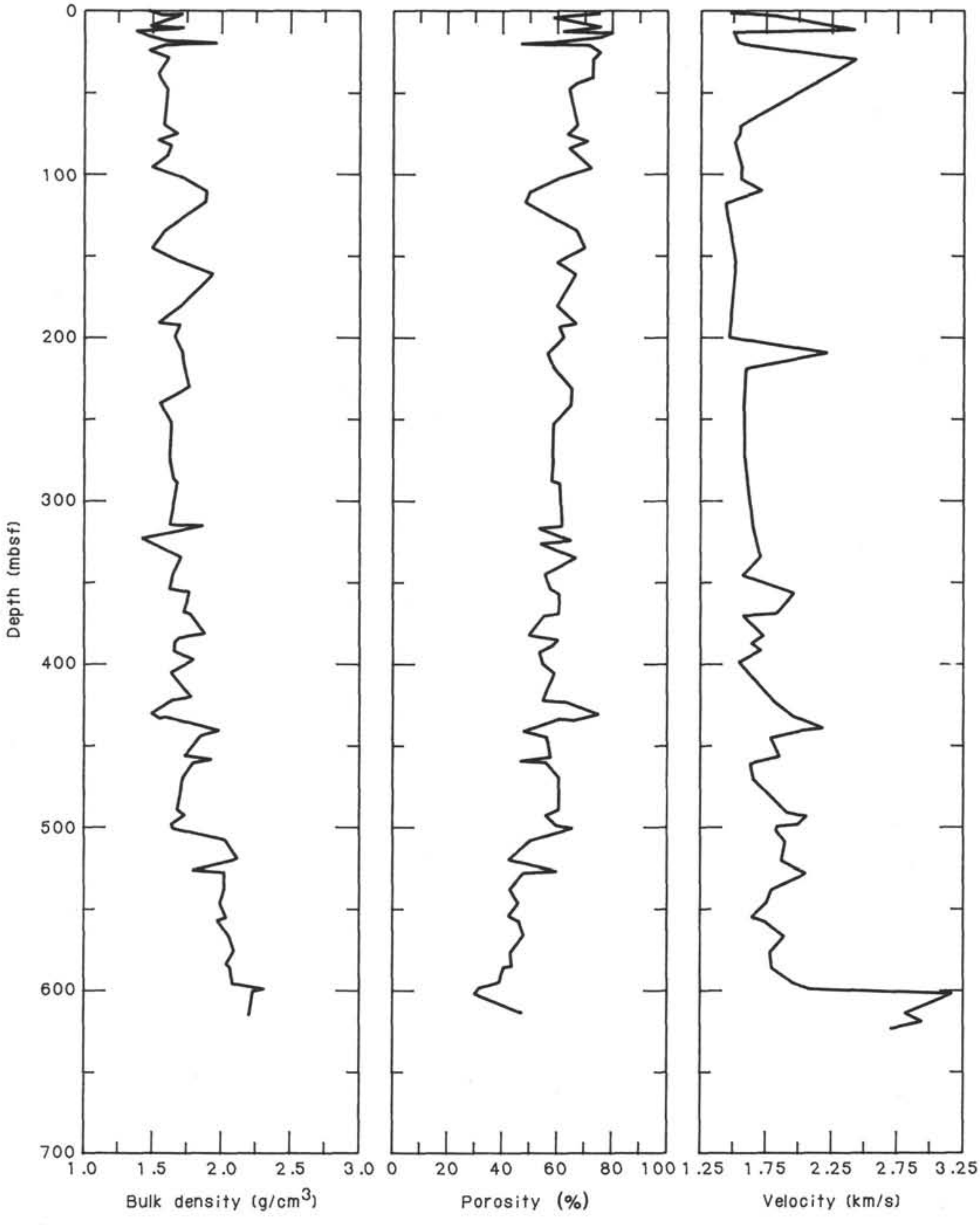

Figure 21. Bulk density, porosity, and velocity vs. depth at Site 650.

Generally, carbonate occurs as fine-grained constituent of clastic allochthonous sediments in turbidites (or as micritic cement). The conspicuous saw-tooth pattern of carbonate concentrations as depicted in Figure 24 reflects the alternation of siliciclastic, coarse turbidite members generally low in $CaCO_3$ (less than 5% calcium carbonate by weight) with progressively finer-grained, carbonate-rich turbidite members or autochthonous sediments. Values in these facies range from 20–30% $CaCO_3$. From Figure 24 it appears that the short-term fluctuations caused by grain size effects during turbidite emplacement (or by varying source of turbidites) are superimposed on cyclic variations in carbonate deposition of longer duration. Three phases of relatively high abundance of carbonate are separated by two phases of carbonate-lean sedimentation, when sedimentation in the Marsili Basin was dominated by siliciclastic or volcanogenic turbidite sedimentation. Sediments of Cores 107-650-1H to 107-650-12H (110 mbsf), and 107-650A-32R (296 mbsf) to 650-66R (604.8 mbsf) are characterized by highly variable carbonate content attributable to dilution by clastics. Carbonate sedimentation patterns in Cores 107-650-13H to 107-650-31X (110–296 mbsf) are less varied in terms of $CaCO_3$ content, but values above 35% are never reached. During times of predominantly nannofossil ooze sedimentation in early Pleistocene times (underlying Core 107-650-48X, below 440 mbsf) sediments are characterized by generally higher concentrations of carbonate, ranging typically from 30% to 40% $CaCO_3$. These sediments are

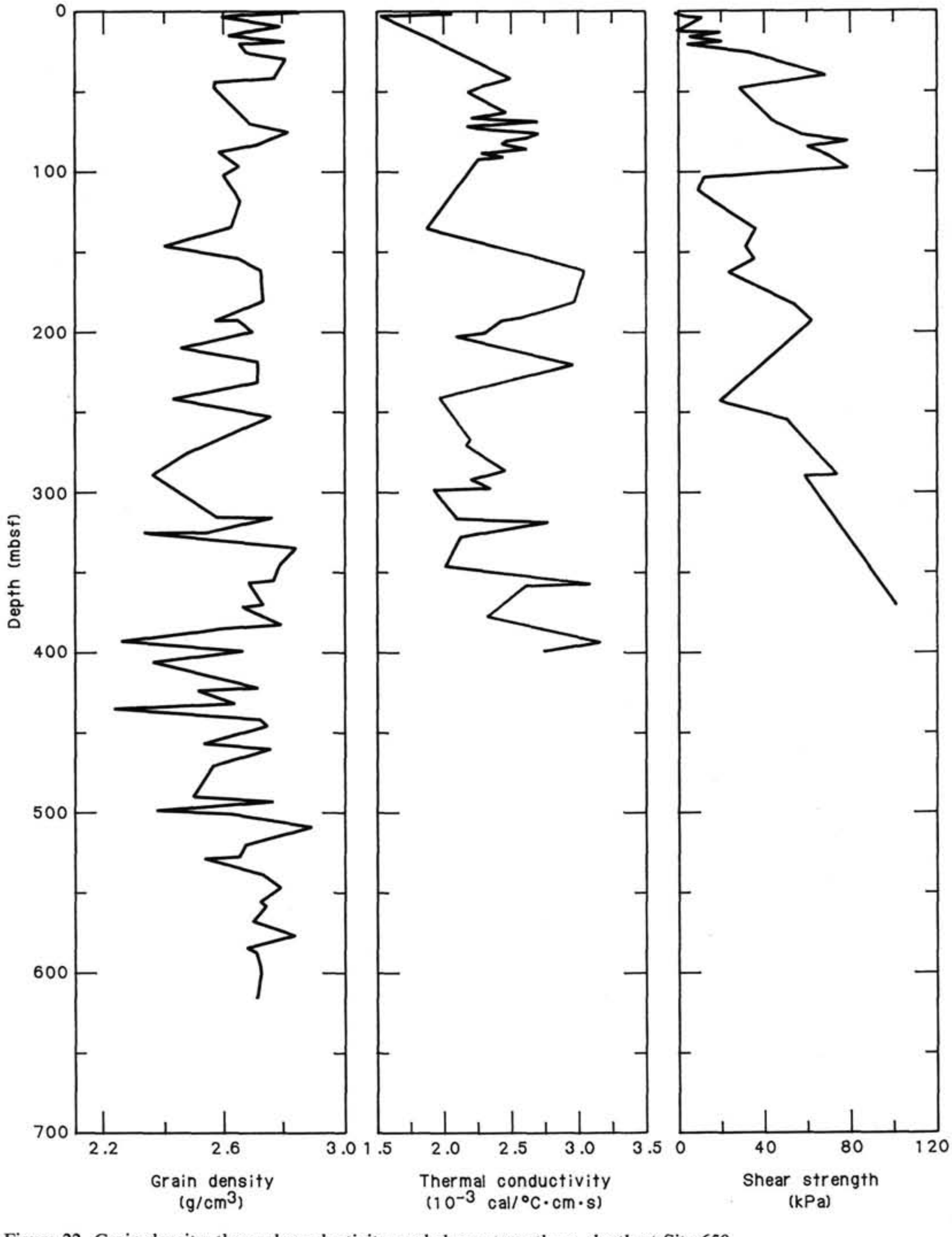

Figure 22. Grain density, thermal conductivity, and shear strength vs. depth at Site 650.

still highly variable in carbonate content and the variability is caused by deposition of carbonate-poor turbidites superimposed on the dominant carbonate-rich lithology.

Interstitial Water Analyses:

Subsamples of interstitial waters squeezed from 12 whole-round core segments of 10-cm length and a reference sample of surface seawater were analyzed on board according to the procedures outlined in the Explanatory Notes. The results of these analyses are listed in Table 8 and depicted as depth plots in Figure 25.

In these depth plots the fluctuations of alkalinity and sulfate in sample 5H-5, 140–150 cm are inferred to be related to bacterial sulfate reduction of sedimentary organic matter at a depth of about 40 mbsf. The relatively low alkalinity value (10.7 mmol/L) may be attributable to generally low abundance of organic material in these sediments. Abundance and type of organic matter available control the extent of sulfate reduction by bacteria, and the accompanying increase in alkalinity (Westrich and Berner, 1984). Further downhole, alkalinity concentrations remain fairly constant, increasing only slightly near basement to values around 4 mmol/L. In contrast, sulfate concentrations are polymodal. The second maximum in sample 25X-1, 140–150 cm corresponds to a pronounced maximum in calcium concentration. This covariance suggests the dissolution of gypsum in the corresponding sediments, although the presence of gypsum could

Table 5. Shear strength measurements from Site 650.

Core section	Interval (cm)	Depth sub-bottom (m)	Shear strength (kPa)
1H-2	12-15	1.7	1.665
1H-2	55-58	2.1	5.618
1H-2	77-80	2.3	13.108
2H-6	93-94	11.5	1.665
2H-7	30-31	12.3	21.431
3H-2	75-78	14.9	6.658
3H-5	28-30	19.0	22.887
3H-5	69-71	19.4	7.074
4H-4	74-75	24.6	35.088
5H-4	74-75	38.1	70.177
6H-4	25-26	47.1	29.862
8H-4	70-71	67.0	45.765
9H-3	115-116	75.5	59.054
9H-6	115-116	79.7	80.276
10H-2	80-81	83.2	61.965
10H-5	82-83	87.8	70.923
11H-4	70-71	95.9	79.882
12H-2	79-80	102.6	13.841
12H-7	11-12	109.4	11.534
13H-6	39-40	117.6	19.377
15X-2	80-81	134.4	38.754
16X-3	56-57	145.3	33.218
17X-2	36-37	153.2	38.075
18X-1	65-66	161.2	26.130
20X-1	82-83	180.6	55.992
21X-2	9-12	191.1	64.138
26X-3	25-26	241.1	21.650
27X-4	77-78	252.8	53.006
29X-3	6-7	274.9	66.470
31X-1	133-134	288.3	75.799
31X-2	107-108	288.6	60.639
39X-4	20-21	369.2	101.454

not be proved in smear slides. Another rather unusual feature of these depth profiles is the inversion of the magnesium depletion in sample 38X-1, 140-150 cm, 355 mbsf. While magnesium decreases steadily in the upper part of the profile—a phenomenon attributed to the uptake of Mg^{2+} substituting for Ca^{2+} in detrital silicates of volcanogenic origin to form smectites (Gieskes, 1975), or to diagenetic dolomitization of calcium carbonate—the profiles of these two elements cross over a second time at approximately 300 mbsf. It was pointed out that amorphous volcanic glass liberates magnesium during halmyrolysis (Bonatti, pers. comm.) and that the observed increase of dissolved magnesium in samples associated with volcaniclastic turbidites and in those close to basement may be an indication of low-temperature alteration of glass. High temperature basalt/seawater interaction usually removes all but a small fraction of magnesium from pore water or seawater (Mottl and Holland, 1978). The spike in magnesium concentration at a depth of 355 mbsf is associated with a pronounced drop in chloride concentration of about 70 mmol. Possibly we encountered a phenomenon similar to that described by Manheim (1967), who detected fresh-water input along conduits in the sedimentary column at distances of as much as 120 km from the coast. Contamination of the sample by surface seawater pumped down the pipe during drilling operations seems unlikely because of the quite distinctly different geochemical fingerprints of surface seawater; at present, we lack a comprehensive and plausible explanation for the observed unusual distribution of magnesium and chloride ions.

SEISMIC STRATIGRAPHY

Introduction

Site 650 is located on MCS Line ST16 (Fig. 8) at shot point 1400. Examination of this seismic line and other lines in the western Marsili Basin (Fig. 6) shows the presence of three widespread seismic reflectors. The reflector sequence can be divided into four acoustic units based on seismic characteristics (Fig. 26).

Table 6. Thermal conductivity measurements from Site 650.

Core section	Interval (cm)	Depth sub-bottom (m)	Thermal conductivity ($cal/°C \times cm^{-1} \times s^{-1}$)
1H-1	112	1.12	2.0901
1H-2	52	2.0	1.5651
3H-3	70	16.4	1.9344
5H-6	79	41.1	2.5142
6H-3	44	45.8	2.3267
6H-5	54	48.9	2.2226
8H-1	20	62.0	2.5006
8H-3	137	66.2	2.2433
8H-5	45	68.2	2.7229
8H-7	9	70.9	2.2250
9H-1	96	72.3	2.2871
9H-3	96	75.3	2.7366
9H-5	61	77.9	2.6551
9H-7	18	80.5	2.5029
10H-1	92	81.9	2.4748
10H-3	78	84.8	2.6299
10H-5	76	87.8	2.3142
10H-7	19	90.2	2.4683
11H-1	18	90.9	2.2914
15X-2	124	134.8	1.8953
17X-1	54	151.8	2.7115
18X-1	60	161.1	3.0777
20X-1	70	180.5	3.0005
21X-1	74	190.2	2.5987
21X-2	74	191.7	2.4571
22X-1	76	200.0	2.3432
22X-2	13	200.8	2.1391
24X-1	69	219.3	3.0015
24X-2	51	220.6	2.9133
26X-2	70	240.0	2.0158
29X-1	70	267.5	2.2344
29X-2	70	269.0	2.2071
31X-3	85	285.8	2.4855
31X-4	85	291.5	2.2435
32X-1	70	296.5	2.3875
32X-2	60	297.9	1.9554
34X-1	89	316.0	2.1359
34X-1	117	317.7	2.8105
35X-1	145	326.2	2.2857
35X-2	20	326.5	2.1677
37X-1	125	345.5	2.0584
38X-1	130	356.7	3.1409
38X-2	70	357.6	2.6538
40X-3	40	376.5	2.3690
42X-1	67	393.1	3.2054
43X-1	78	398.2	2.7956

Description of Units

Seismic Unit One

This unit extends from the seafloor to the top of a prominent, high-amplitude reflector seen throughout the Marsili Basin. The unit is 0.15 s thick and has an interval velocity of 1.65 km/s on the basis of MCS velocity analysis. The base of the unit should be at about 120 mbsf. Apart from a few thin internal reflectors, the unit is almost seismically transparent over much of the basin. There is no variation in thickness of this unit in the basin.

Seismic Unit Two

This unit comprises a number of alternating high- and low-amplitude reflectors interbedded within seismically more transparent layers. Toward the bottom of the unit, one observes a series of flat-lying strong reflectors. Seismic Unit Two, at the site and over most of the basin, has a rather constant thickness of

Table 7. Percentage $CaCO_3$, total C, and organic C of samples from Hole 650.

Core-section-interval	$CaCO_3$ (%)	C_{total} (%)	C_{org}[a] (%)	N_{total} (%)	C/N	Depth (mbsf)
1-1-20-21	9.57	1.23	0.10	0.09	[b]n.d.	0.20
1-1-54-55	10.16	1.42	0.20	0.03	6.7	0.54
1-1-113-115	17.87	2.07	0.00	0.06	n.d.	1.13
1-2-50-51	10.36	1.59	0.33	0.04	8.8	2.00
2-2-61-62	14.58	1.90	0.15	0.03	5.0	5.11
2-3-23-24	17.38	2.38	0.29	0.04	7.3	6.23
2-3-53-54	2.25	2.54	2.29	0.04	57.3	6.53
2-5-130-131	12.60	1.86	0.35	0.03	11.6	11.80
2-7-26-27	23.07	3.02	0.25	0.03	8.4	12.26
2-cc-10-11	9.94	1.47	0.28	0.05	5.6	12.50
3-2-18-19	21.85	3.01	0.39	0.06	6.5	14.38
3-2-24-25	0.47	0.54	0.48	0.00	n.d.	14.44
3-2-31-32	1.17	0.16	0.00	0.04	n.d.	14.51
3-2-71-72	7.49	1.84	0.94	0.06	15.7	14.91
3-3-80-81	23.64	[c]				16.50
3-cc-10-11	11.47	1.79	0.41	0.04	10.3	22.10
4-1-50-51	29.89	3.75	0.16	0.02	8.0	22.90
4-2-72-75	15.99	2.10	0.18	0.00	n.d.	24.60
4-3-54-55	5.19	0.86	0.24	0.03	8.0	25.94
4-3-118-119	5.25	0.46	0.00	0.00	n.d.	26.58
4-4-80-81	16.11	2.19	0.26	0.03	8.5	27.70
4-5-72-75	26.18	3.45	0.31	0.04	7.7	29.12
5-1-80-81	11.60	1.02	0.00	0.02	n.d.	33.60
5-4-65-68	20.67	2.69	0.21	0.09	2.3	37.95
5-4-80-81	10.50	2.71	1.45	0.04	36.2	38.10
5-6-54-57	17.70	2.13	0.01	0.04	n.d.	40.85
5-6-78-79	13.50	2.36	0.74	0.02	37.0	41.08
6-2-75-78	14.28	1.88	0.17	0.00	n.d.	44.65
6-3-29-31	12.23	1.91	0.44	0.09	4.9	45.69
6-3-80-81	13.62	1.79	0.15	0.01	15.0	46.20
6-4-44-47	12.12	1.54	0.08	0.03	n.d.	47.34
6-4-80-81	11.45	1.54	0.17	0.07	2.4	47.70
6-5-117-118	8.95	1.23	0.16	0.04	4.0	49.57
6-6-25-26	6.73	0.87	0.06	0.00	n.d.	50.15
7-3-4-5	6.06	0.82	0.09	0.02	4.6	55.14
8-4-136-137	2.64	0.36	0.04	0.03	n.d.	67.66
8-5-109-110	18.57	2.34	0.11	0.02	5.5	68.89
8-5-115-116	41.83					68.95
8-6-62-65	15.99	2.06	0.14	0.09	n.d.	69.92
8-cc-4-5	15.20					71.04
9-1-59-60	13.83	2.11	0.45	0.02	22.5	71.89
9-3-117-121	11.99	1.71	0.27	0.13	n.d.	75.47
9-4-64-65	12.60					76.44
9-5-118-120	16.84	2.34	0.32	0.12	4.9	78.48
9-6-91-95	18.94	2.42	0.15	0.02	7.3	79.71
9-6-110-111	13.38					79.90
10-2-75-78	16.76	2.24	0.23	0.03	7.6	83.25
10-2-98-99	22.68					83.48
10-4-49-50	16.29					85.99
10-5-86-89	14.53	1.99	0.25	0.03	8.1	87.86
10-6-50-51	5.59	0.63	0.00	0.01	n.d.	89.00
11-4-63-66	19.15	2.44	0.14	0.00	n.d.	95.83
12-2-75-78	6.32	1.07	0.31	0.06	5.2	102.55
12-3-79-81	6.94	0.86	0.00	0.15	n.d.	104.09
12-7-7-10	4.79	0.60	0.02	0.08	n.d.	109.37
13-2-62-64	1.06	0.17	0.04	0.02	n.d.	113.77
13-6-46-49	3.47	0.47	0.05	0.03	n.d.	119.61
15-1-50-51	13.98					132.60
15-2-90-93	14.87	2.06	0.27	0.02	13.5	133.00
15-2-127-129	14.10	2.14	0.45	0.15	3.0	134.87
16-3-70-73	17.88	2.37	0.22	0.03	7.3	145.40
17-1-99-101	22.86	3.52	0.78	0.03	25.9	152.29
17-2-48-51	16.36	2.23	0.27	0.02	13.0	153.28
18-1-59-63	11.83	1.73	0.31	0.05	6.1	161.09
18-1-117-119	13.00	2.35	0.79	0.11	7.2	161.67
19-1-14-15	17.09	2.63	0.58	0.01	n.d.	170.34
20-1-75-76	32.53	3.89	0.00	0.01	n.d.	180.55
20-1-106-111	18.44	2.41	0.20	0.02	10.0	180.86
21-2-23-25	13.82	2.84	1.18	0.09	13.1	191.23
21-2-94-96	22.38	3.55	0.86	0.04	21.5	191.94
21-2-104-107	9.99	1.50	0.30	0.03	10.0	192.04
21-3-23-25	26.23					192.70
22-1-17-20	31.70	4.05	0.24	0.02	12.0	199.37
22-1-112-115	9.96	1.99	0.79	0.04	20.0	200.32
23-cc-27-30	9.07	1.17	0.08	0.05	n.d.	217.57
24-2-86-88	18.40	2.36	0.15	0.03	5.0	220.96
25-1-18-19	16.54	0.52	n.d.	0.04	n.d.	228.38

Table 7 (continued).

Core-section-interval	$CaCO_3$ (%)	C_{total} (%)	C_{org}[a] (%)	N_{total} (%)	C/N	Depth (mbsf)
26-3-6-9	4.97	0.63	0.03	0.15	n.d.	240.86
26-3-97-98	4.70					241.77
27-3-80-82	14.94	1.88	0.09	0.00	n.d.	251.30
27-4-67-71	12.08	1.52	0.07			252.67
29-cc-12-15	5.92	0.70	0.01			276.40
31-1-40-42	1.34			0.03		286.60
31-2-60-63	5.21	0.59	0.04			288.30
31-2-135-139	12.99	1.75	0.19			289.05
31-3-39-41	8.95	1.25	0.18	0.04	4.5	289.59
31-3-108-111	13.64	1.78	0.14	0.00	n.d.	290.90
32-1-32-33	55.32	6.05	0.00	0.02		296.12
32-1-106-108	12.74	1.64	0.11	0.04		296.86
32-cc-14-15	3.49	0.51	0.09	0.04		305.40
33-cc-5-6	5.56	0.74	0.07	0.06	n.d.	314.85
33-cc-14-16	2.51	0.37	0.07	0.03		314.94
34-1-32-33	5.62	0.87	0.19	0.02		315.42
34-1-86-87	5.09	0.69	0.08	0.09	n.d.	315.96
34-1-90-91	6.03	0.80	0.08	0.01	8.0	316.00
34-1-125-127	51.43	6.00	0.17	0.01	17.0	316.35
34-1-138-139	23.83	3.14	0.28			316.48
34-cc-19-20	41.56	5.37	0.38	0.00		324.74
34-cc-27-30	9.07					324.82
35-1-9-10	13.04					324.91
35-1-58-59	15.54	1.90	0.03	0.00	n.d.	325.38
35-1-69-70	13.62	1.74	0.10			325.49
35-1-140-141	5.31	0.69	0.05	0.04	n.d.	326.20
36-1-52-53	20.98					335.02
36-1-58-59	4.93	0.71	0.12	0.05	2.4	335.08
36-1-110-111	21.27	2.76	0.21	0.06	3.5	335.60
36-1-115-116	19.33	2.50	0.18	0.01	18.0	335.65
37-1-122-125	2.69	0.36	0.04			345.42
37-1-127-129	2.87	0.37	0.03			345.47
37-1-129-131	3.03	0.36	0.00	0.08	n.d.	345.49
37-cc-22-23	3.46	0.45	0.03	0.02	n.d.	353.60
38-1-52-55	38.48	4.82	0.21			354.42
38-1-87-89	57.30	6.94	0.06	0.00	n.d.	354.77
38-2-98-99	20.96	2.79	0.27	0.00	n.d.	356.38
38-2-112-114	11.25	1.85	0.50	0.15	3.4	356.52
39-1-123-124	24.48	1.43	?	0.03		364.73
39-4-77-78	12.93	1.61	0.06	0.05	n.d.	368.77
39-4-137-141	9.75	1.57	0.40			369.37
39-6-9-12	22.27	3.08	0.41			371.09
40-1-98-100	17.20	1.97	0.00	0.00	n.d.	374.08
40-4-72-74	5.45	0.70	0.05			378.32
40-cc-26-29	21.85	2.91	0.29			382.76
41-2-109-111	17.61	2.13	0.02	0.00	n.d.	385.39
42-1-52-56	38.86	4.85	0.18	0.01	18.0	392.92
42-1-64-66	45.05	5.42	0.01			393.04
43-1-102-103	17.49	2.30	0.20	0.00	n.d.	398.42
43-cc-3-6	12.90	1.64	0.09			399.17
45-1-25-26	6.44	0.82	0.05	0.00	n.d.	406.35
45-1-30-32	7.73	1.00	0.07			406.40
45-2-30-33	4.35	0.52	0.00	0.00	n.d.	407.90
46-cc-25-30	6.74	0.82	0.01	0.00	n.d.	421.40
47-1-7-8	4.85	0.61	0.03			421.57
47-1-63-65	53.94	6.34	0.00			422.13
47-2-19-20	2.21	0.29	0.02			423.09
47-2-63-65		1.54				423.63
47-cc-28-30	12.24	0.73	0.74	0.03	24.7	431.00
48-2-70-72	4.29	0.53	0.01			433.30
48-3-78-80	3.27	0.41	0.02			434.88
48-4-16-18	3.81	0.44	0.00	0.00	n.d.	435.76
48-4-46-48	3.04	0.38	0.02	0.01	n.d.	436.06
48-4-60-61	2.28	0.29	0.02			436.20
48-4-61-62	2.57	0.30	0.01			436.21
48-5-71-72	20.09	2.50	0.09	0.00	n.d.	437.81
48-cc-28-30	3.25	0.40	0.01	0.02	n.d.	440.60
49-1-98-99	4.37	0.46	0.00			441.78
49-3-98-99	12.81	1.63	0.09			444.78
49-3-103-106	13.23					444.83
50-4-69-70	8.14	1.00	0.02			455.59
50-4-138-141	22.28	4.58	1.91	0.18	10.6	456.28
50-5-45-48	6.19					456.85
50-6-34-37	0.70	0.13	0.05	0.07	n.d.	458.30
50-6-106-108	37.81	6.71	2.17	0.13	16.7	459.02
51-1-47-50	24.36	3.15	0.23	0.08	2.8	460.57

Table 7 (continued).

Core-section-interval	$CaCO_3$ (%)	C_{total} (%)	C_{org}[a] (%)	N_{total} (%)	C/N	Depth (mbsf)
51-2-116-120	23.96	3.69	0.81	0.06	13.6	462.76
51-3-57-58	28.17	3.58	0.20			463.67
51-3-92-94	4.41	2.32	1.79	0.08	22.38	464.02
52-1-24-27	12.95	1.58	0.03			469.94
52-1-29-31	10.94					469.99
53-1-68-69	6.45					479.98
53-5-56-57	32.19					485.86
53-cc-4-5	55.92					488.64
54-1-81-84	8.14	1.00	0.02	0.09		489.71
54-1-88-90	8.12	0.99	0.02			489.78
54-1-96-97	7.4	0.91	0.02			489.86
54-4-1-3	3.02	0.46	0.10			493.99
55-1-30-34	9.91	1.27	0.08			498.90
55-1-107-108	27.00	3.30	0.06			499.67
55-2-90-96	2.72					500.00
55-2-101-102	8.24					501.11
55-4-69-70	25.8	3.36	0.26	0.06	4.3	503.79
56-2-75-76	23.72	3.06	0.21			510.45
57-2-8-9	34.58					517.99
57-2-77-78	2.97					518.68
57-2-126-130	20.65					519.17
58-1-83-84	26.61	3.81	0.62			528.33
58-2-27-30	35.49					529.27
58-2-50-51	39.45					529.50
58-3-82-83	43.3					531.32
59-1-84-85	39.64	4.79	0.03			538.04
59-2-68-70	7.44					539.38
59-2-76-77	55.31					539.46
60-1-66-68	38.20					547.46
60-1-94-97	42.13					547.74
60-2-43-44	57.68					548.73
60-2-115-117	44.12					549.45
60-cc-14-15	38.79					556.37
60-cc-24-27	47.34					556.47
61-1-10-11	45.11					556.60
61-2-85-88	46.71					558.82
61-2-100-103	29.38					559.00
62-2-5-7	7.59					567.65
62-2-114-115	4.66					568.74
62-2-142-143	38.28					569.02
63-2-3-6	35.99					577.23
63-2-143-144	19.87					578.63
63-3-73-74	45.98					580.90
64-1-132-133	47.96					581.48
64-2-17-20	40.85					581.84
64-2-51-53	29.89					582.18
64-2-67-68	25.96					582.34
65-2-32-33	43.07					595.22
66-2-40-42	59.79					601.26

[a] C_{org} = TC − Carbonate − C;
[b] n.d. = not determined;
[c] blank space = not measured.

about 0.25 s. As for Unit One, the internal velocity is 1.65 km/s;this indicates that the base of Unit Two is at about 330 mbsf (210 m thick). The base is marked by a prominent reflector which is slightly unconformable with Unit Three.

Seismic Unit Three

This unit is almost seismically transparent with the exception of a single marked internal reflector; its top corresponds to a slight unconformity and its base to a strong reflector. At Site 650, the thickness of Unit Three is about 0.14 s. The interval velocity is also 1.65 km/s, indicating that the base lies at 440 mbsf (110 m thick).

Seismic Unit Four

This unit is made of a series of pronounced reflectors. It is bounded at the top by Seismic Unit Three and at the bottom by an acoustic basement. On line MCS ST 16, as well as on other lines, Seismic Unit Four appears to fill a series of small basins (Fig. 6) within the irregular topography of the acoustic basement; thickness of this unit varies depending on basement irregularities. In the center of small basins Unit 4 thickness is about 0.15 s. According to velocity analysis based on MCS data, the interval velocity for Unit Four is 2.56 km/s. This gives a base for the unit at 540–630 mbsf (100–190 m thick), depending on the position relative to basement highs and lows.

Acoustic Basement

The lowermost seismic unit is characterized by hyperbolic reflectors in MCS lines as well as in single-channel seismic lines. Prior to Leg 107 this unit was designated as acoustic basement. Several possible natures were considered. Interval velocities available just prior to the cruise gave values of about 2.7 km/s. Therefore it was assumed that the acoustic basement at Site 650 was not a real basement but an unknown layer, which appeared as a major target for the understanding of the area.

Previous Lithologic and Stratigraphic Interpretations

Scientists working on Tyrrhenian Sea seismic data have faced a major difficulty: the seismic characteristics are highly variable from basin to basin and therefore it is difficult to propose a reliable seismic stratigraphic interpretation for the whole area. Nevertheless, Finetti et al. (1970), Fabbri and Curzi (1979), Malinverno et al. (1981), and Moussat (1983) have proposed stratigraphic and/or facies interpretations of seismic records across the Marsili Basin.

Fabbri and Curzi (1979) distinguish two main seismic sequences—A and B (Fig. 26). A is interpreted to be a sedimentary sequence from middle Pliocene to Recent. B is divided into two subunits, B_1 and B_2, attributed respectively to sedimentary sequences from Messinian to middle Pliocene, and to Messinian evaporites. Within the basin, Fabbri and Curzi (1979) as well as Malinverno et al. (1981) believe that the whole Pliocene and Pleistocene sedimentary sequences are present and cover a Messinian unit which is either thin or uncertain (Fabbri and Curzi, 1979). This Messinian unit may consist of lacustrine or clastic sediments (Malinverno et al., 1981). Moussat (1983) also believes that the Pliocene-Pleistocene section is complete but covers terrain of unknown nature and age (volcaniclastics or real volcanic basement). Units One to Three as defined herein can be correlated to Unit A of Fabbri and Curzi (1979), while Unit Four can be correlated to Unit B_1.

Results from Site 650

A synthetic *P*-wave seismogram was calculated based on physical properties measurements of velocity and bulk density. The laboratory results used are shown graphically in Figure 21 of this report. The data were linearly interpolated onto an evenly spaced 1-m grid and then input to a simple 1-D convolutional synthetic seismic program. The wavelet used was 25 Hz Ricker type. Attenuation and spreading effects are unaccounted for in the synthetic seismograms. Internal multiples are included but seabed multiples are not.

The synthetic seismograms calculated here, shown in Figure 27, should be compared with the site survey reflection line ST14, Figure 26. The quality of correlation indicates that synthetic seismograms based on physical properties data are an effective tool for monitoring progress while drilling.

Care must be taken to insure that anomalous physical properties measurements on small or atypical samples do not cause false reflections in the synthetic profile. An example of this is the synthetic reflector at 4.91 s bsl. This reflector is caused by a single high velocity sample at 209.35 mbsf and does not correlate with the site MCS line.

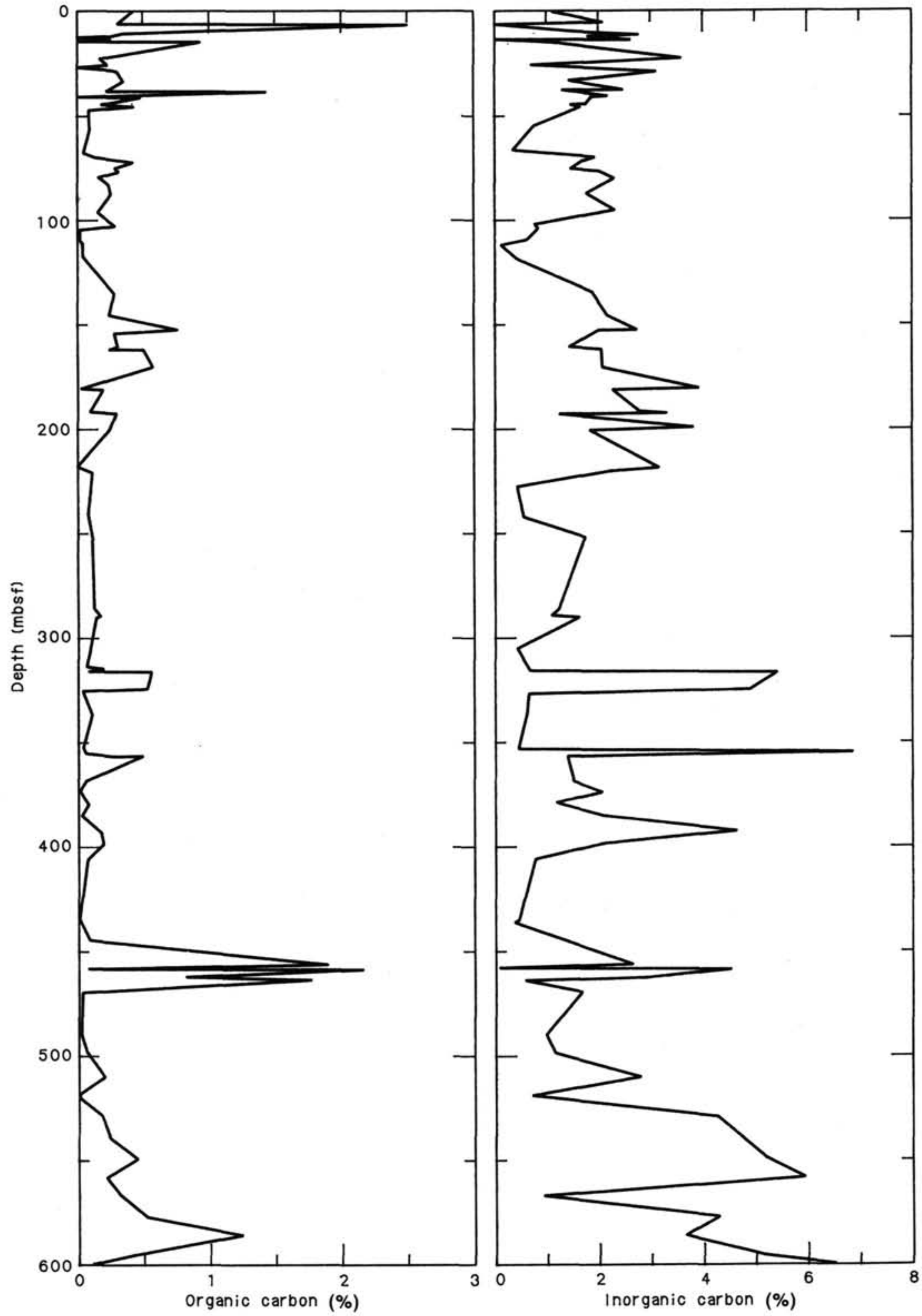

Figure 23. Organic and inorganic carbon percentage vs. depth in samples from Site 650.

A quick comparison between seismic Line ST 16 at Site 650 and the synthetic *P*-wave seismogram points out the following features:

1. The base of Seismic Unit One (4.80 s bsl) appears as a prominent reflector at 120 mbsf on the synthetic seismogram.
2. The base of Seismic Unit Two (5.05 s bsl) is correlatable with small reflector (330 mbsf) of the synthetic seismogram.
3. The base of Seismic Unit Three appears on the synthetic seismogram as a complex interference pattern which is the result of alternating high and low velocity layers. The base of Seismic Unit Three (5.19 s bsl) is the most prominent reflector on the seismic seismogram at about 440 mbsf.
4. The sediment-basement interface (base of Seismic Unit Four, 5.35 s bsl) is marked as a high-amplitude reflector at 600 mbsf on the synthetic seismogram.

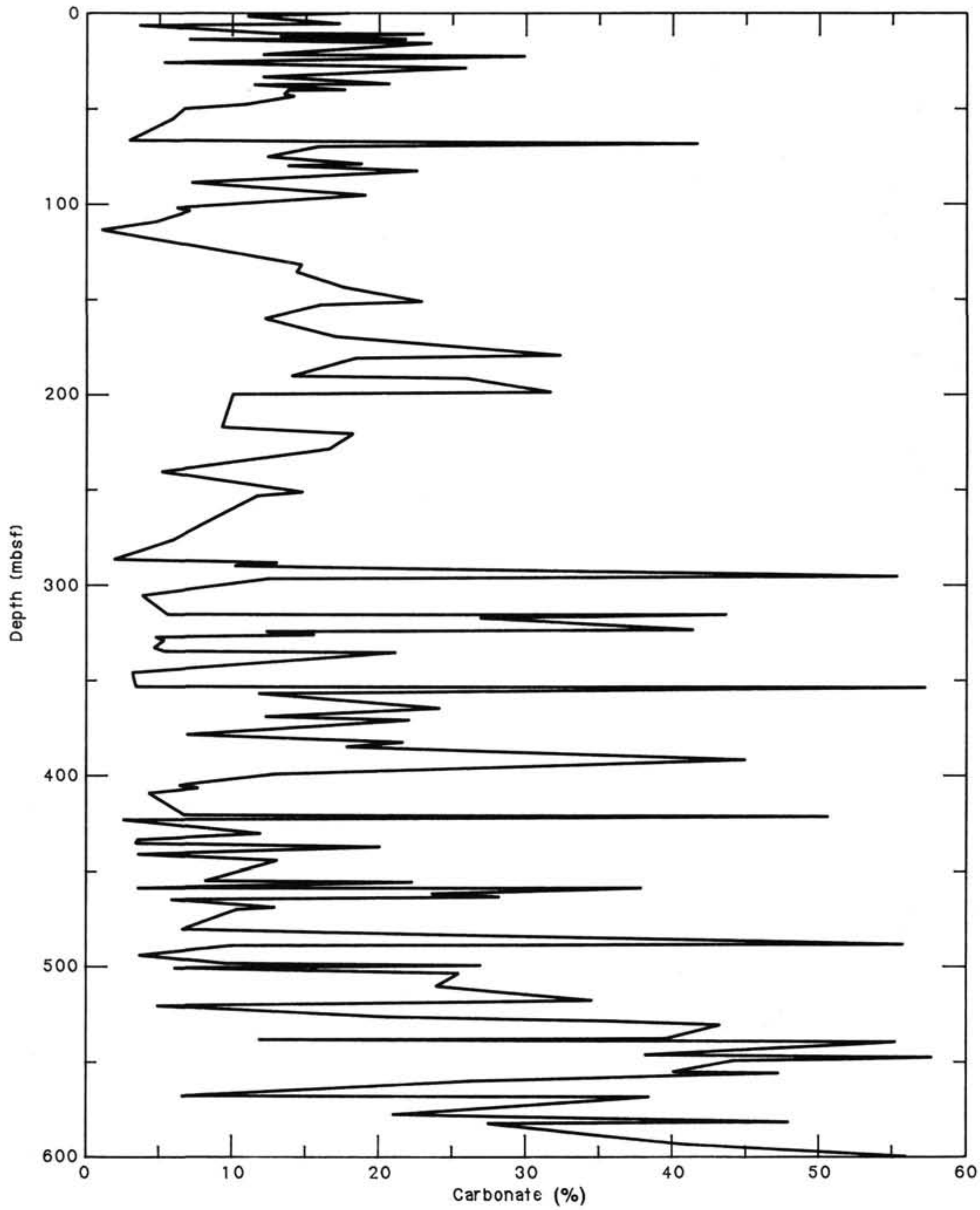

Figure 24. Carbonate percentage vs. depth in samples from Hole 650A.

Conclusions

Drilling at Site 650 established the following points:

1. Seismic Unit One corresponds to dominantly turbiditic sediments (lithostratigraphic Subunit Ia) including abundant volcanic glass and pumice; its base correlates well with a pumice-rich layer, recovered in Cores 107-650A-13H and 107-650A-14X, which may be 15–20 m thick.
2. Seismic Unit Two correlates with a sequence of turbidites with considerable volcaniclastics (lithostratigraphic Subunits Ic and Id), the coarsest parts of which have probably been washed out (poor recovery).
3. Seismic Unit Three is made of more homogeneous claystone, still with thin volcaniclastic turbidites.
4. Seismic Unit Four corresponds to an earlier input of ash layers in more indurated claystones and nannofossil/foraminiferal oozes, including turbiditic sequences (lithostratigraphic Subunit II).
5. Seismic Units One through Three and the upper part of Four are of Pleistocene age. Therefore, Units A and B_1 of Fabbri and Curzi (1979), which correlate easily with our Seismic Units One to Four, are of Pleistocene age. The X discontinuity of Fabbri and Curzi (1979) appears to correlate, depending on the area, with either the base of our seismic Unit Two or the base of Unit Three.

Table 8. Chemical analyses of interstitial water, Site 650.

Sample no.	Depth	Sal.	Alk.	pH	Cl^-	SO_4^{2-}	Ca^{2+}	Mg^{2+}	Ca/Mg
Surface water		39.0	2.27	7.95	541	9.1	10.9	52.6	0.21
1H-1	1.4	36.5	3.88	7.67	551	8.6	10.4	55.7	0.19
5H-5	40.2	35.5	10.74	7.66	570	1.0	6.9	36.2	0.19
10H-5	88.4	36.0	3.00	7.44	552	0.7	16.7	33.4	0.50
15H-2	135.0	38.0	1.39	7.75	553	4.5	29.3	27.4	1.07
25X-1	229.6	40.0	1.09	7.69	636	8.4	46.7	25.5	1.83
31X-1	290.6	42.0	0.75	7.67	651	5.9	46.5	13.3	3.50
38X-1	355.3	38.0	1.25	7.83	582	4.4	27.9	27.1	1.05
45X-1	407.5	39.0	1.29	7.73	627	7.1	27.9	9.6	2.90
50X-5	457.8	39.0	1.98	7.46	750	3.3	29.0	9.6	3.02
55X-3	494.0	40.0	1.79	7.35	712	4.5	33.8	17.3	1.96
60X-2	549.7	42.0	4.17	6.95	881	4.5	34.9	27.4	1.27
64X-2	588.1	44.0	4.14	7.11	812	5.5	40.3	32.5	1.24

Chemical analyses of interstitial water: Leg 107, Hole 650A. Sample no.: Hole 650A, Core-Section, 140–150 cm; Depth below seafloor; Sal. = salinity in parts per thousand; Alk. = alkalinity in mmol/L; Cl^-, SO_4^{2-}, Ca^{2+}, Mg^{2+} in mmol/L.

6. The seismic observations of numerous subparallel, subhorizontal reflectors within Units One through Four are compatible with the relative abundance of turbidites in these units.

7. At the very base of Site 650, near the contact between Unit Four and the acoustic basement, nannofossil ooze was cored. The ooze contained upper Pliocene species. Therefore one may correlate the lower part of Unit Four with the uppermost Pliocene. The site bottomed in a volcanic layer indicating that the upper part of the acoustic basement is made of vesicular basalts.

DOWNHOLE MEASUREMENTS

Because of a stuck core barrel while recovering Core 107-650A-69X (633.8 mbsf) the drill string had to be tripped out. This precluded the acquisition of any logging data at this site.

Heat Flow

Four downhole temperature measurements were made in Hole 650A and one in Hole 650B using first the Von Herzen temperature probe during APC operations (650A HF 1) and later the Uyeda probe during XCB drilling (650A HF 2, 3, 4) and rotary drilling (650B HF 1). See "Explanatory Notes" chapter, this volume, for procedures and equipment. Of these five successful runs, only three gave data which were considered to be equilibrated and reliable in determining *in-situ* thermal gradients (Figs. 28–32).

Temperature Data and In-Situ Thermal Gradient Determination

Measurement 650A-HF 4 shows that the thermistor came more or less into thermal equilibrium with the adjacent sediment while measurement 650A HF 2 was probably not equilibrated. However, these measurements (Figs. 29 and 31) were considered unreasonably low, possibly due to excessive cooling of the bottom hole sediments by vigorous circulation of drilling fluids, but more likely because the probe entered fill or cuttings rather than virgin sediment. These measurements were discarded, although the shape of the plateau of equilibrium temperature looks similar to that of the other measurements 650A HF 1 and 3 and 650B HF 1.

The seafloor water temperature is estimated at about 13.25°C based on data from the thermistor probe as it passed the mud line during its descent to the bottom of the hole and its ascent back to the drill floor. The thermal measurements are listed below; the continuously recorded temperature data for each station are illustrated in Figures 28–32.

Thermal Conductivity

Forty-five thermal conductivities were measured on cores from Hole 650A (Fig. 22). Thermal conductivity is highly variable in the upper 400 m of Hole 650A, which is consistent with the succession of the volcaniclastic turbiditic sequences into rare pelagic or hemipelagic formations.

Between 40 and 90 mbsf, the thermal conductivity is fairly uniform with a mean value of $2.5 \pm 0.25\ 10^{-3}$ cal $\times$ cm^{-1} $\times$ s^{-1} (= 1.046 ± 10 W/m^{-1} K) (10 measurements). Deeper than 90 mbsf, thermal conductivities are more variable but in the same average value. Seventeen measurements into the 240–400 mbsf interval exhibit a clear increase in thermal conductivity with depth (see Fig. 22). The average thermal conductivity at the base of the measured section (near 400 mbsf) is 1.254 W m^{-1} K ($3.0\ 10^{-3}$ cal $\times$ cm^{-1} $\times$ s^{-1}). This conductivity increase appears to relate the porosity decrease with depth (see "Physical Properties" section, this chapter) due to the sediment compaction.

Below 400 m thermal conductivities unfortunately have not been measured because the sediment was too hard for careful penetration of the needle probe. It would be important to obtain some measurements in harder material for modelling of the conductivity structure of the sedimentary sequence and the effects of thermal refraction and lateral diffusion. In fact, conductivity structure evidently is three dimensional. Nevertheless the two dimensional determination of thermal conductivities measured on the cores can provide a good approximate solution. The presence of irregularly distributed high-conductivity layers is a possible explanation for the observed variability in the subsurface heat flux.

An accurate estimation of the sediment corrections or the blanketing effect due to rapidly deposited Pleistocene sediments needs to be precisely estimated post-cruise. In fact we have here an unique opportunity for such a determination through the knowledge of the main physical properties of the sediments (bulk density, porosity, grain density, thermal conductivity, sedimentation rate, estimation of the compaction). See porosity depth dependence defined by:

$$P(z) = Po^{e-z/a}$$

where z = depth; P = porosity; a = compaction constant.

Heat Flow Determination

The thermal gradient for Hole 650A is plotted in Figure 33. A nearly straight line fits both the downhole temperature determinations 650A HF 1(71.3 m) and 650A HF 3 (141.7 m) and the sea-bottom temperature estimate, giving an overall mean gradient of 14°C/100 m. The measurement 650B HF 1 (102.4 m) plots close to this line (0.5°C higher).

Temperature gradients determined for each depth interval are 15°C/100 m from 71.3 m to 102.4 m and 12°C/100 m from 102.5 m to 141.7 m. However, it is questionable whether a linear extrapolation of the temperature data value from the deepest measurement (141.7 m) is reliable with the uppermost value (71.3 m) and with the sea-bottom temperature. The other separate gradients do not fit with the sea-bottom temperature. The slight change in gradient observed at depth 102.4 m from Hole 650B HF 1 measurement may be related to slight changes in the thermal conductivities resulting from the 15-m (50-ft) offset between the two holes. Unfortunately we have only one conductivity measurement between 90 and 150 mbsf.

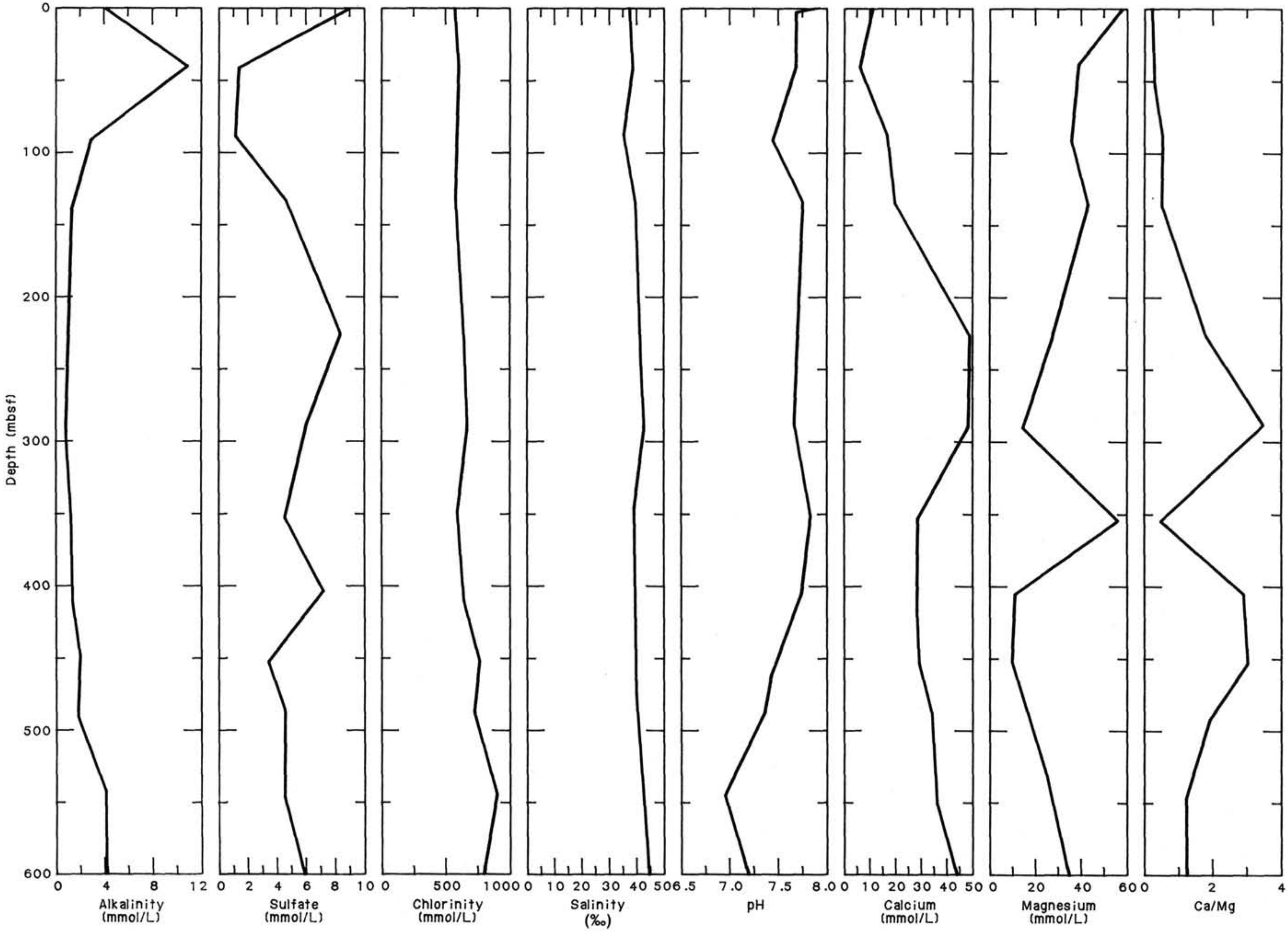

Figure 25. Analyses from interstitial waters extracted from core samples at Hole 650A.

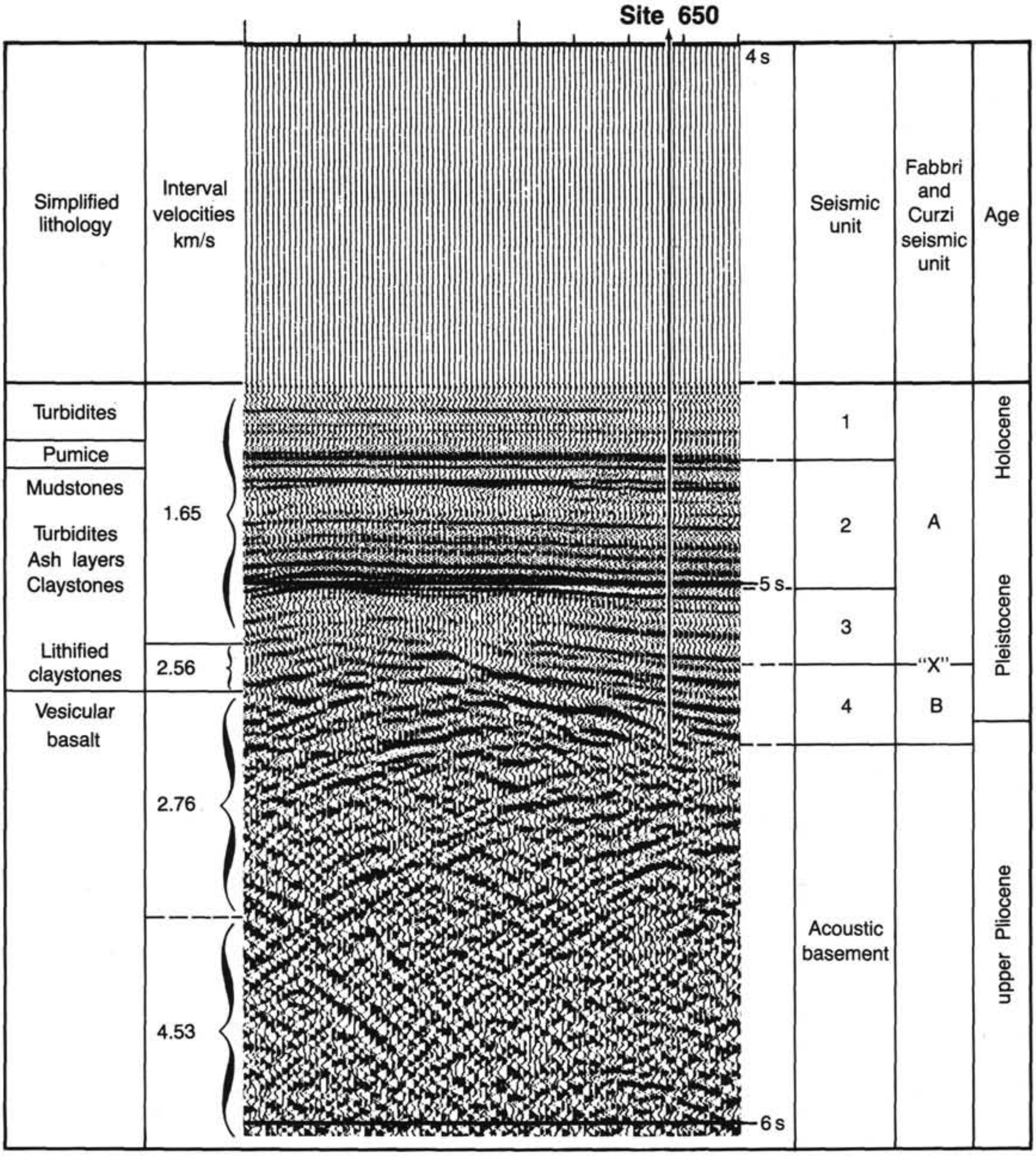

Figure 26. Close-up of a section of MCS line ST16 at Site 650. Correlations with main lithologic units and previous subdivision are given, as well as interval velocities and time scale.

Summary of Heatflow at Site 650

Average gradient = 14° ± 0.5° C/100 m (measured)

Thermal conductivity = 2.3 to 10^{-3} cal × cm × s^{-1} (measured on cores)

= 0.9614 to 1.254 W m^{-1}°K

Observed heat flow = 3.22 HFU < HF Site 650 < 4.22 HFU

134.6 mW/m^2 < HF Site 650 < 175.56 mW/m^2

Using a mean thermal conductivity value of 1.05 Wm^{-1}°K gives

$$\text{mean heat flow} => Q = 147 \pm 14 \text{ mW/m}^2.$$

Sedimentary correction can be estimated at about 10% (Della Vedova et al., 1984; Hutchison et al., 1985). Therefore:

$$\text{Corrected heat flow} = Q_{corr} = 162 \text{ mW/m}^2 = 3.86 \text{ HFU}.$$

Conclusions

1. The downhole temperatures measured at Site 650 indicate nearly equilibrium, and a predominantly conductive geothermal gradient persists through the investigated depth of Hole 650A.

2. If we consider a sedimentary correction of the heat flow due to the effects of sedimentation and compaction at about 10% after Hutchison (1983) and Della Vedova et al. (1984), the average value of 162 mW/m^2 corrected heat flow determined at Site 650 is in good agreement with the main previous shallow-probe heat flow measurements within the Marsili Basin.

3. Downhole determinations, as well as the previous shallow probe measurements (Erickson, 1970; Della Vedova et al., 1984; Hutchison et al., 1985;) indicate a heat flow value considerably lower than that predicted for 2 m.y. old oceanic-type crust. If the prediction is based on a simple one-dimensional cooling lithosphere model (Parsons and Sclater, 1977; Malinverno, 1981), the age estimate is 10–14 m.y. Using a more elaborate two-di-

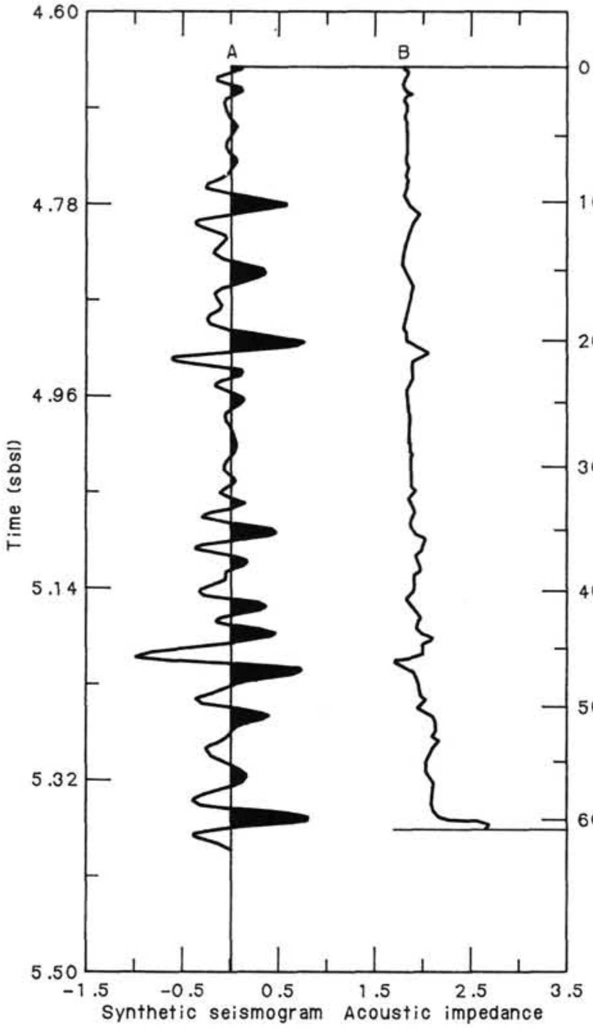

Figure 27. A. Synthetic seismogram. B. Acoustic impedance. The seismograph, calculated from shipboard physical properties measurements, allows correlation of core features with seismic reflectors, and facilitates monitoring of progress while drilling.

mensional model combining thermal effect of progressive continental lithospheric extension, and restricted oceanic accretion and lateral conduction as well as radioactivity, the age estimate is 4–5 m.y. (Rehault et al., 1984). The anomalous low heat flow may be due to hydrothermal fluid circulation.

CONCLUSIONS AND DISCUSSION

Basement

Drilling at Site 650 accomplished its main objective which was to ascertain the nature and age of the acoustic basement that floors the Marsili Basin, and thus provide a constraint to the mode and timing of formation of the basin.

Nature of the Basement

The acoustic basement in the western Marsili Basin has been determined to consist of altered, highly vesicular basalt. The degree of vesicularity varies from 10% to >30% by volume, while the size of the vesicles varies from about 100 μm to 4 mm. Based on preliminary chemical data, it appears that Site 650 basement has a calc-alkaline affinity. If further studies confirm this affinity, Site 650 basalts may be similar in geochemistry to the younger recovered basalts from Marsili Seamount, and to the products of the Eolian Arc. In contrast, the older volcanism of Marsili seamount and the volcanism of the Vavilov Basin as seen at Sites 651, 655, and DSDP 373 are tholeiitic.

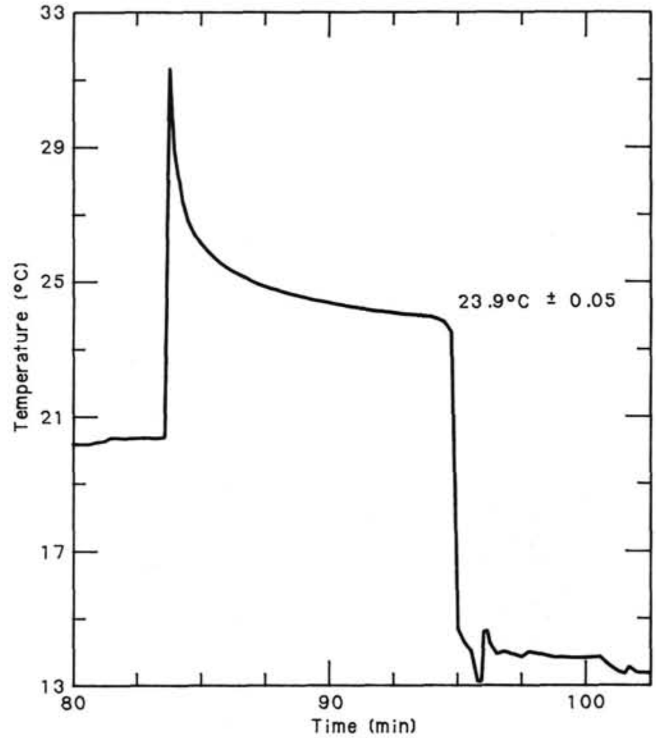

Figure 28. Downhole temperature measurement 650A HF 1 at 71.3 mbsf.

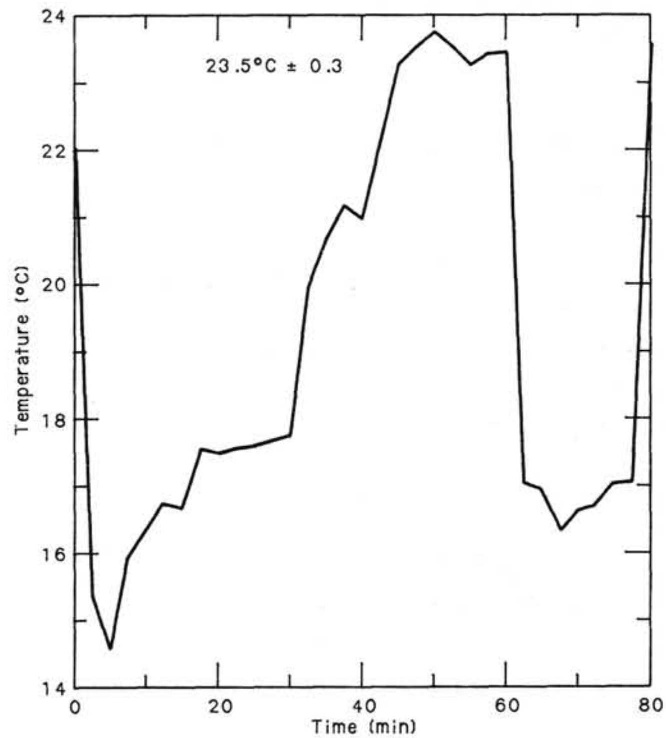

Figure 29. Downhole temperature measurement 650A HF 2 at 90.7 mbsf.

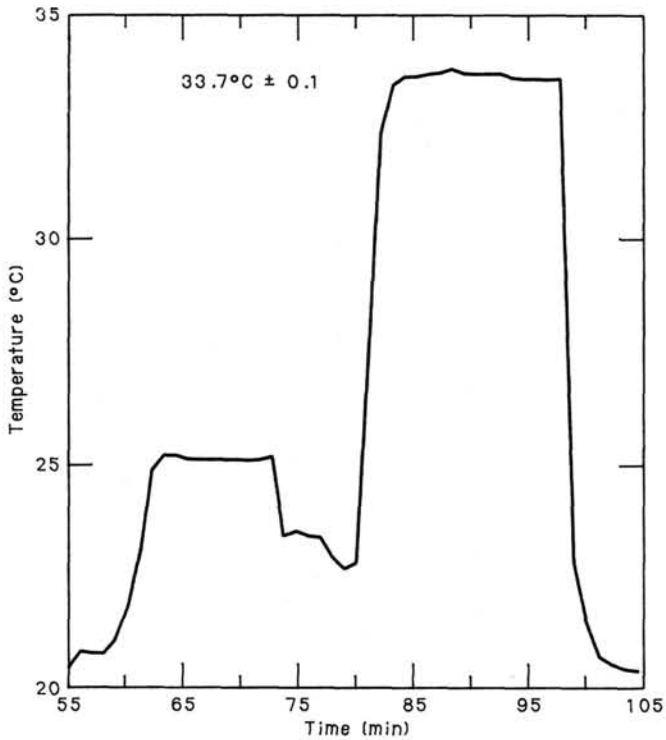

Figure 30. Downhole temperature measurement 650A HF 3 at 141.7 mbsf.

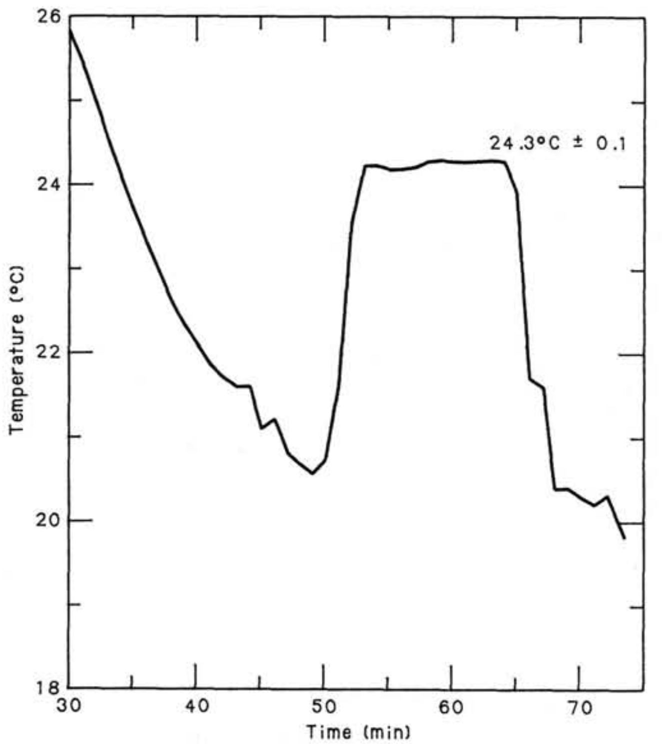

Figure 31. Downhole temperature measurement 650A HF 4 at 189.5 mbsf.

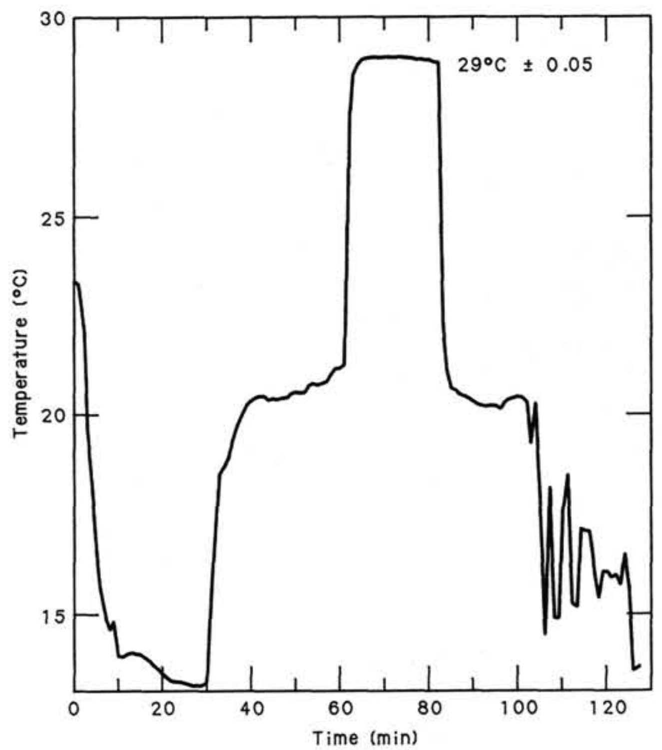

Figure 32. Downhole temperature measurement 650B HF 1 at 102.4 mbsf.

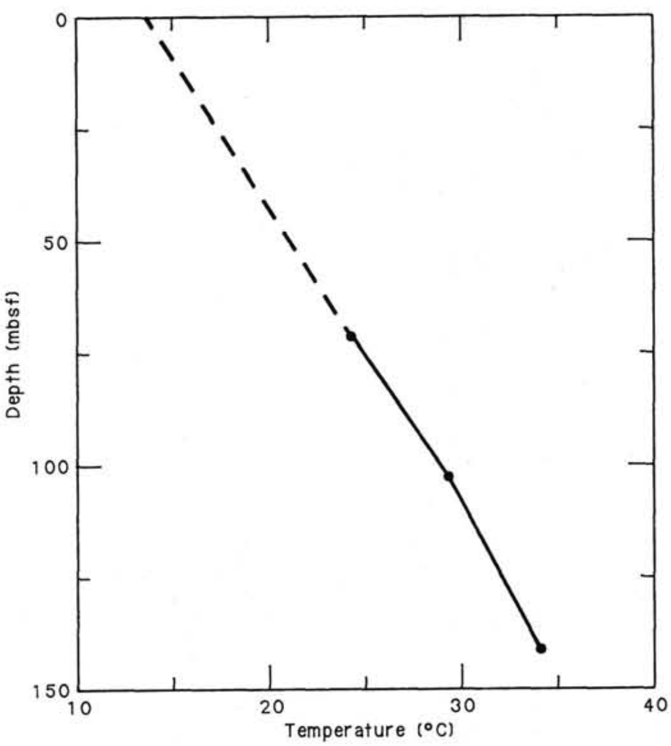

Figure 33. Downhole temperature vs. sub-bottom depth curve at Site 650.

Is This True Igneous Crustal Basement or an Intra-Sedimentary Sill?

Textural evidence within the basalt suggests that it was emplaced as a flow, rather than as a sill. Thin section observations indicate that at the top of the section and again at 145 cm down, the rock consists mostly of strongly altered glass with a few skeletal plagioclase microliths and some pseudomorphs after olivine. Elsewhere, the basalt is more crystalline. The glassy zones are interpreted as former chilled margins marking the top of flows.

A second line of evidence comes from the sediments just overlying the basalt. The reddish-brown layer of highly dolomitic sediment may be due to gradual alteration and recrystallization phenomena. There is no evidence that the sediment has been baked at magma temperatures as would be the case if this were a sill. Magnesium in interstitial waters increases downsection from 460 mbsf to the basalt contact. This observation is also taken as evidence that the interaction between basalt and overlying sediment occurred at low temperature, because at high temperature, magnesium would have been absorbed into rather than released from the basalt.

The low acoustic velocity in the uppermost basement as given from seismic analysis (2.7 km/s) is consistent with the compressional wave velocities measured on basalt samples (2.8–3.2 km/s). The relatively low velocity can be explained by the combination of vesicularity and alteration, which give the samples a high porosity, between 30% and 40%. It is not necessary to invoke interbedded sediments within the basalt pile, although their occurrence cannot be categorically excluded.

Age of the Basement

The contact between the basalt and the sediment has been recovered intact, and has been dated as uppermost Pliocene (~2.0 m.y.). Is this date representative of the age of the basin?

The position of the drill site, near the western rim of the basin, was chosen such that, if the basalt injection process is approximately symmetrical, as at an organized spreading center, the basement age would have been the oldest in the basin. Seismic stratigraphy confirms that the oldest cored sediments are correlative with the deepest organized seismic reflectors detected within the basin. The location of the site as far as possible from the Marsili Seamount, separated from the seamount by an irregular basement topography, ensures that we did not sample lateral flows from the volcano.

It can be argued that heat flow values (on the order of 150 mW/m^2) are inconsistent with an age of 2 m.y. (see "Downhole Measurements" section, this chapter). However, young crust frequently yields widely scattered heat flow values, and hydrothermal activity, nearby faulting, and/or contact with adjacent colder continental crust could easily depress conductive heat flow values below the theoretical prediction.

Depth of Emplacement of Basalt

The top of the basalt now lies at 4100 m below sea level. Given normal gas concentrations in a basaltic magma, and the pressure dependency of gas solubility in a magma, the high vesicularity of the basalt suggests it was emplaced at shallower depths. Even considering that island-arc or back-arc basin basalts contain more volatiles than mid-ocean ridge basalts, the depth of emplacement was probably shallower than 2500 m and potentially much less. Benthic foraminifer assemblages in the sediments immediately above the basalt suggest a depth of emplacement greater than 1000 m and less than 2000 m.

Implications

1. If the vesicular basalts are true basement, and the age of the overlying sediments is representative of the age of the basin, then the Marsili Basin is a very young basin (about 2 m.y. old), much younger than generally inferred by previous workers.

2. If the basin is 2 m.y. old, and the basalt was emplaced between 1000 m and 2500 m, then the basalt has subsided at a rate greater than 800 m/m.y. This rate is significantly higher than is normally observed on oceanic crust which typically subsides approximately 500 m in its first 2 m.y. due to cooling of the lithosphere (Parsons and Sclater, 1977).

Sediments

The most surprising result from the sedimentary section was its very young age and hence rapid sedimentation rate (602 m of sediment in approximately 2 m.y.).

Stratigraphy

Age control was provided by paleomagnetic stratigraphy and biostratigraphy using calcareous nannofossils and foraminifers. The rapid influx of turbidites provided an unexpected bonus for the paleomagnetic chronology because of the apparent high concentration of magnetite in the volcaniclastic fraction. The same rapid influx of sediments hindered the biostratigraphers because of the large proportion of reworked species, and the paucity of benthic foraminifers. Nonetheless it has been possible to correlate the biostratigraphic datums and the magnetostratigraphy with confidence down to the Olduvai magnetic event. Site 650 will thus provide a calibration point between western Mediterranean upper Pliocene/Pleistocene and open ocean biostratigraphic datums.

Sedimentary Cycles

Several lines of evidence can be used to deduce the timing of glacial/interglacial cycles of the late Pleistocene. The most direct line of evidence comes from the presence or absence of warm-water species of planktonic foraminifers (see "Biostratigraphy" section, this chapter). In addition, however, we found that magnetic susceptibility, carbonate content, and concentration of smectite/chlorite clay minerals in the cores fluctuate in rough harmony with each other and with the inferred warm/cold cycles. We may infer (see "Lithostratigraphy" and "Paleomagnetism" sections, respectively, this chapter) that concentration of smectite/chlorite and magnetic susceptibility could be indirect measures of the abundance of volcaniclastic turbidites, while carbonate content records the dilution or lack of dilution of the background open marine sedimentation. A correlation with climatic cycles might indicate that turbidity currents were more frequent and possibly more voluminous during eustatic lowstands associated with cold glacial stages or substages.

Since a high proportion of the terrigenous material is volcanogenic, we should consider the alternative hypothesis that the inferred cycles may indicate periods of increased and decreased volcanic activity rather than climatic/sea level fluctuations, or a mixture of volcanic and climatic cycles.

Sedimentation Rate

The sedimentation rate at Site 650 (Fig. 34) decreases drastically downsection, from more than 95 cm/1000 yr to less than 6 cm/1000 yr. This decrease is paralleled by an upsection increase in number and thickness of turbidites. Three hypotheses, which are in no way mutually exclusive, can be suggested for this increasing sedimentation rate.

First, the onset of rapid sea-level fluctuations in the Pleistocene may have facilitated the triggering of turbidites on the upper slope. This suggestion is consistent with the inference that coarse turbidites in lithostratigraphic Unit I occur preferentially during the cold swings of the paleoclimatic curve, i.e., during sea-level lowstands.

Secondly, the rate of production of source material may have increased. The coarse component of the turbidites is primarily

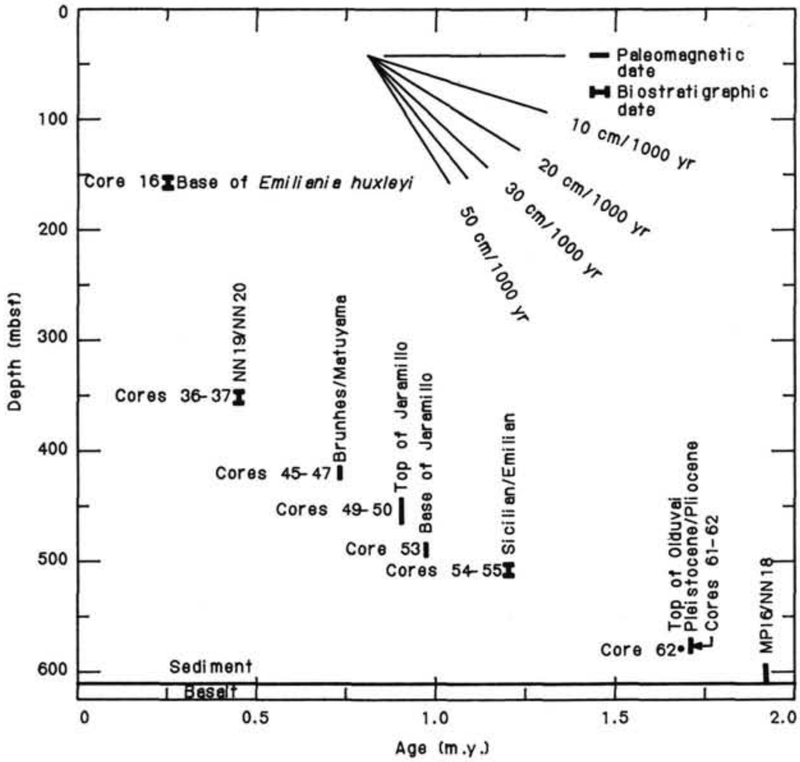

Figure 34. Sediment age vs. depth at Site 650, based on core-catcher examinations only.

pumice and volcanic glass. The occurrence of pumice suggests shallow submarine or subaerial volcanism, and preliminary determinations of glass chemistry by refractive index suggest that the Eolian Islands were a major source area. Thus the upsection increase in coarse turbidites may coincide with the birth and/or emergence of the Eolian Islands in the middle to late Pleistocene. Although the creation of a nearby unstable sediment source (the flanks of the Eolian volcanoes) is a plausible immediate cause of the upsection increase in turbidites, the full story may be more complicated. In the central Mediterranean, volcanism and tectonism are closely related; thus the birth of the Eolian Islands is likely to have been merely one aspect of a widespread volcano-tectonic phase. Other aspects of such a volcano-tectonic event could themselves have contributed to increased sedimentation rate at Site 650: Increased frequency and magnitude of earthquakes could have triggered more turbidity currents. Increased rate of mountain-building in the circum-Tyrrhenian could have lead to increased rate of erosion in the watersheds draining into the Tyrrhenian, and thus to increased input of terrigenous sediments.

Finally, as noted in the discussion of "Basement" above, the floor of Marsili Basin appears to have undergone significant subsidence. As the basin subsided, the relief, the area, and possibly the gradient of the continental slope increased. If the continental slope or continental slope canyon heads act as a temporary storage site for sediments destined to form turbidity currents, one would expect that the steeper(?), higher, continental slopes rimming the more deeply subsided late Pleistocene Marsili Basin would more efficiently transfer sediments from shallow water to the basin floor. The less steep(?), lower continental slopes rimming the shallower Pliocene Marsili Basin would transfer a lower proportion of the available sediment from shallow water to the basin floor.

"Basal" Sediments

A 10-cm-thick layer immediately above basalt is made of almost pure dolomite, and is greenish-grey in color. This thin layer is overlain by approximately 10 m of altered nannofossil ooze characterized by a reddish-brown color and the occurrence of abundant euhedral dolomite rhombs, minor authigenic feldspars, trace zeolites, and iron and manganese oxides. Post-deposition chemical interaction between sediment and basalt has undoubtedly contributed to the formation of this unit. It is not yet clear whether an initial input of precipitates from hot springs (i.e., hydrothermal sediment) contributed as well.

REFERENCES

Barberi, F., Innocenti, F., Ferra, G., Keller, J., and Villari, L. 1974. Evolution of the Eolian Arc volcanism (Southern Tyrrhenian Sea). *Earth Planet. Sci. Lett.*, 21:269–276.

Barberi, F., Bizouard, H., Capaldi, G., Ferrara, G., Innocenti, F., Joron, J. L., Lambert, B., Treuil, M., and Allegre, C., 1977. Age and nature of basalts from the Tyrrhenian abyssal plain, *In* Hsü, K. J., Montadert, L., et al., *Init. Repts. DSDP*, 42, Pt. 1: Washington (U.S. Govt. Printing Office) 509–514.

Barone, A., Fabbri, A., Rossi, S., and Sartori, R., 1982. Geological structure and evolution of the marine areas adjacent to the Calabrian Arc. *Earth Evol. Sci.*, 3:207–221.

Beccaluva, L., Rossi, P. L., and Serri, G., 1982. Neogene to recent volcanism of the Southern Tyrrhenian-Sicilian area: Implications for the geodynamic evolution of the Calabrian arc. *Earth Evol. Sci.*, 3: 222–238.

Bizon, G., and Müller, C., 1977. Remarks on some biostratigraphic problems in the Mediterranean neogene. *In* Biju-Duval, B., and Montadert, L. (Eds.) *Structural History of the Mediterranean Basins*, Paris (Technip), 381–390.

Bolis, G., Capelli, V., and Marinelli, M., 1981. Aeromagnetic data of the Italian area: instrumental to a better comprehension of the basement main characteristic in Italy, Carta Magnetica d'Italia. *AGIP—E.A.E.G. (43rd meeting). Venezia.*

Broecker, W. S., and Van Donk, J., 1970. Insolation changes, ice volume, and the ^{18}O record in deep-sea cores. *Rev. Geophys. Space Phys.*, 8:169–198.

Cifelli, R., 1974. Planktonic Foraminifera from the Mediterranean and adjacent Atlantic waters (cruise of the Atlantic II, 1969). *J. Foraminiferal Res.*, 4:171–183.

Colalongo, M. L., Pasini, G., Pelosio, G., Raffi, S., Rio, D., Ruggieri, G., Sartoni, S., Selli, R., and Sprovieri, R., 1982. The Neogene/Quaternary boundary definition: a review and a proposal. *Geogr. Fis. Din. Quat.,* 5:59-68.

Colantoni, P., Fabbri, A., Gallignani, P., Sartori, R., and Rehault, J. P., 1981. *Carta lithologica e stratigraphica del Mari Italiano.* Firenze (Litografica Artistica Cartografica).

Curray, J. R., Moore, D. G., et al., 1982. *Init. Repts. DSDP,* 64, Washington (U.S. Govt Printing Office).

Della Vedova, B., Pellis, G., Foucher, J. P., and Rehault, J. P., 1984. Geothermal structure of the Tyrrhenian Sea, *Mar. Geol.,* 55:271-289.

Dietrich, V., Emmerman, R., Puchett, H., and Keller, J., 1978. Oceanic basalt from the Tyrrhenian basin, DSDP Leg 42A, Hole 373A. *In* Hsü, K. J., Montadert, L., et al., *Init. Repts. DSDP,* 42, Pt. 1: Washington (U.S. Govt. Printing Office), 515-530.

Emiliani, C., 1978. The cause of the ice ages. *Earth Planet. Sci. Lett.,* 37:349-352.

Erickson, A. J., Simmons, G., and Ryan, W.B.F., 1977. Review of heat flow data from the Mediterranean and Aegean Seas, *In* Biju-Duval, B. and Montadert, L., (Eds.), *International Symposium on the Structural History of the Mediterranean Basins,* Paris (Technip), 263-279.

Fabbri, A., and Curzi, P. 1979. The Messinian of the Tyrrhenian Sea: seismic evidence and dynamic implications. *G. Geol.,* 42, 2:215-248.

Fabbri, A., Galligani, P., and Zitellini, N., 1981. Geologic evolution of the peri-Tyrrhenian sedimentary basins. *In* Wezel, F. C. (Ed.), *Sedimentary Basins of Mediterranean Margins.* Bologna, (Technoprint), 101-126.

Ferruci, F., Makris, J., Nicolich, R., Snoeck, M., Steinmetz, L., and Weige, W., 1982. Deep seismic sounding by OBS in Tyrrhenian Sea. *CIESM,* (28th meeting) Cannes (France) 2-6 Dec. 1982.

Finetti, I., Morelli, C., and Zarudski, E., 1970. Reflection seismic study of the Tyrrhenian Sea. *Boll. Geofis. Teor. Appl.,* 12, 48:311-346.

Garcia, M. O., Liu, N. W., and Muenow, 1979. Volatiles in submarine volcanic rocks from the Mariana Island arc and trough, *Geochim. Cosmochim. Acta,* 43, 305-312.

Gartner, S., 1977. Calcareous nannofossil biostratigraphy and revised zonation of the Pleistocene. *Mar. Micropaleontol.,* 2:1-25.

Gieskes, J. M., 1975. Chemistry of interstitial waters of marine sediments. *Ann. Rev. Earth Planet. Sci.,* 3:433-453.

Glaçon, G., 1984. La marge et les fosses héllèniques. Campagnes Ariane et Egion du programme Heat. *Résultats des Campagnes a la mer. CNEXO,* 24:1-160.

Hutchison, I., Von Herzen, R., Louden, K., Sclater, J., and Jemsek, J., 1985. Heat flow in the Balearic and Tyrrhenian basins, Western Mediterranean. *J. Geophys. Res.,* 90 (B1):685-701.

Kanamori, H., 1977. Seismic and aseismic slip along subduction zones and their tectonic implications, *In* Talwani, M. and Pitman, W. C., III (Eds.) *Island Arcs, Deep Sea Trenches and Back Arc Basins,* Washington (American Geophysical Union), 163-174.

Keller, J., Ryan, W.B.F., Ninkovitch, D., and Altherr, R., 1978, Explosive volcanic activity in the Mediterranean over the past 200,000 years as recorded in deep sea sediments. *Geol. Soc. Am. Bull.,* 89: 591-604.

Kobayashi, R., 1984. Subsidence of the Shikoku Back-Arc Basin, *Tectonophysics,* 102, 105-117.

Malinverno, A., 1981. Quantitative estimates of age and Messinian paleobathymetry of the Tyrrhenian Sea after seismic reflection, heat flow and geophysical models. *Boll. Geofis. Teor. Appl.,* 23, 90-91: 159-171.

Manheim, F. T., 1967. Evidence for submarine discharge of water on the Atlantic continental slope of the southern United States, and suggestiona for further search. *Trans. N. Y. Acad. Sci.* II, 29/7:839-853.

Martini, E., 1971. Standard Tertiary and Quaternary calcareous nannoplankton zonation. *Proc.II Planktonic Conf.,* Roma 1970:Rome (Ed. Technosciencza), 739-785.

Massiota, P., Cita, M. B., and Mancuso, M., 1976. Benthonic foraminifers from bathyal depths in the Eastern Mediterranean. *Mar. Sediments Spec. Publ.* 1:251-262.

Monechi, S., Bleil, U., and Backman, J., 1986. Magnetobiochronology of late Cretaceous-Paleogene and late Cenozoic pelagic sedimentary sequences from the Northwest Pacific (Deep Sea Drilling Project, Leg 86, Site 579). *In* Heath, G. R., Burckle, L. H., et al., *Init. Repts. DSDP,* 86: Washington (U.S. Govt. Printing Office), 787-797.

Mottl, M. J., and Holland, H. D., 1978. Chemical exchange during hydrothermal alteration of basalt by seawater-I. Experimental results for major and minor components of seawater. *Gechim. Cosmochim. Acta* 42:1103-1115.

Moussat, E., 1983. Evolution de la Mer Tyrrhénienne centrale et orientale et de ses marges séptentrionales en relation avec la néotectonique dans l'Arc Calabrais [Thesis]. Univ. Paris.

Muerdter, D. R., and Kennett, J. P., 1983. Late Quaternary planktonic foraminiferal Biostratigraphy, Strait of Sicily, Mediterranean Sea. *Mar. Micropaleontol.* 8:339-359.

Müller, C., 1978. Neogene calcareous nannofossils from the Mediterranean-Leg 42 of the Deep Sea Drilling Project. *In* Hsü, K. J., Montadert, L., et al., *Init. Repts. DSDP,* 42, Pt. 1: Washington (U.S. Govt. Printing Office), 727-752.

________, 1979. Calcareous nannoplankton from the North Atlantic (Leg 48). *In* Montadert, L., Roberts, D. G., et al., *Init. Repts. DSDP* 48: Washington (U.S. Govt. Printing Office), 589-639.

________, 1985. Biostratigraphic and paleoenvironmental interpretation of the Goban Spur region based on a study of calcareous nannoplankton. *In* Graciansky, P. C. de, Poag, C. W., et al., *Init. Repts. DSDP,* 80: Washington (U.S. Govt. Printing Office), 573-599.

Murat, A., Glaçon, G., et al., 1985. Rapport des campagnes à la mer du Marion Dufresne. *TAAF Campagne Strabon,* 82:7:1-52.

Panza, G. F., Calcagnile, G., Scandone, P., and Mueller, S., 1980. La struttura profonda dell area Mediterranea. *Le Scienze,* 141:60-69.

Parker, F. L., 1955. Distribution of planktonic foraminifera in some Mediterranean sediments. *Papers in Marine Biology and Oceanography,* London (Pergamon Press Ltd.), 204-241.

________, 1958. Eastern Mediterranean foraminifera. *Rep. Swed. Deep-Sea Exped.,* 8:219-283.

Parsons, B., and Sclater, G. J., 1977. An analysis of the variations of ocean floor bathymetry and heat flow with age. *J. Geophys. Res.,* 82:803-827.

Recq, M., Rehault, J. P., Steinmetz, L., and Fabbri, A., 1984. Amincicement de la croute et accretion au centre du bassin tyrrhénien d'aprés la sismique refraction. *Mar. Geol.,* 55:411-428.

Rio, D., Sprovieri, R., Di Stefano, I., and Raffi, I., 1984. *Globorotalia truncatulinoides* (d'Orbigny) in the Mediterranean upper Pliocene geologic record. *Micropaleontology,* 30:121-137.

Rio, D., Sprovieri, R., and Raffi, I., 1984. Calcareous plankton biostratigraphy and biochronology of the Pliocene-Lower Pleistocene succession of the Capo Rossello area, Sicily. *Mar. Micropaleontol.,* 9:135-180.

Ruggieri, G., Rio, D., and Sprovieri, R., 1984. Remarks on the chronostratigraphic classification of Lower Pleistocene. *Boll. Soc. Geol. Ital.,* 103:251-259.

Ruggieri, G., and Sprovieri, R., 1983. Recenti progressi nella stratigraffia del Pleistocene inferiore. *Boll. Soc. Paleontol. Ital.,* 22,3:315-321.

Selli, R., Lucchini, R., Rossi, P. L., Savelli, C., and Del Monte, M., 1977. Dati geologici, petrochimici e radiometrici sui vulcani centro Tirrenici, *G. Geol.,* 47:221-246.

Shackleton, N. J., and Opdyke, N. D., 1973. Oxygen-isotope and paleomagnetic stratigraphy of equatorial Pacific core V28-238: oxygen isotope temperature and ice volumes on a 10^5-year and 10^6-year scale. *Quat. Res.,* 3:39-55.

Steinmetz, L., Ferrucci, F., Hirn, A., Morelli, C., and Nicolich, R., 1983. A 550 long Moho traverse in the Tyrrhenian Sea from O.B.S. recorded P_n waves. *Geophys. Res. Lett.,* 10(6):428-431.

Tauxe, L., Opdyke, A., Pasini, G., and Elmi, C., 1983. Age of the Plio-Pleistocene boundary in the Vrica section, southern Italy. *Nature,* 304:125-129.

Thunell, R. C., 1978. Distribution of Recent planktonic foraminifera in surface sediments of the Mediterranean Sea. *Mar. Micropaleontol.,* 3:147-173.

Todd, R., 1958. Foraminifera from Western Mediterranean Deep-Sea cores. *Rep. Swed. Deep Sea Exped.,* 3:169-215.

Van Donk, J., 1976. ^{18}O record of the Atlantic Ocean for the entire Pleistocene Epoch. *In* Cine, R. M., and Hays, J. D., (Eds.), *Investigation of Late Quaternary paleoceanography and paleoclimatology.* Geol. Soc. Am. Mem. 145:147-163.

Vergnaud-Grazzini-C., and Glaçon, G., in review. Utilite du ^{14}C pour la stratigraphie du Quaternaire Récent, submitted to *C. R. Acad. Sci. Paris.*

Westrich, J. T., and Berner, R. A., 1984. The role of sedimentary organic matter in bacterial sulfate reduction: the G-model tested. *Limnol. Oceanogr.* 29/2:236-249.

SITE 650 HOLE A CORE 1 H CORED INTERVAL 3516.3-3519.3 mbsl; 0.0-3.0 mbsf

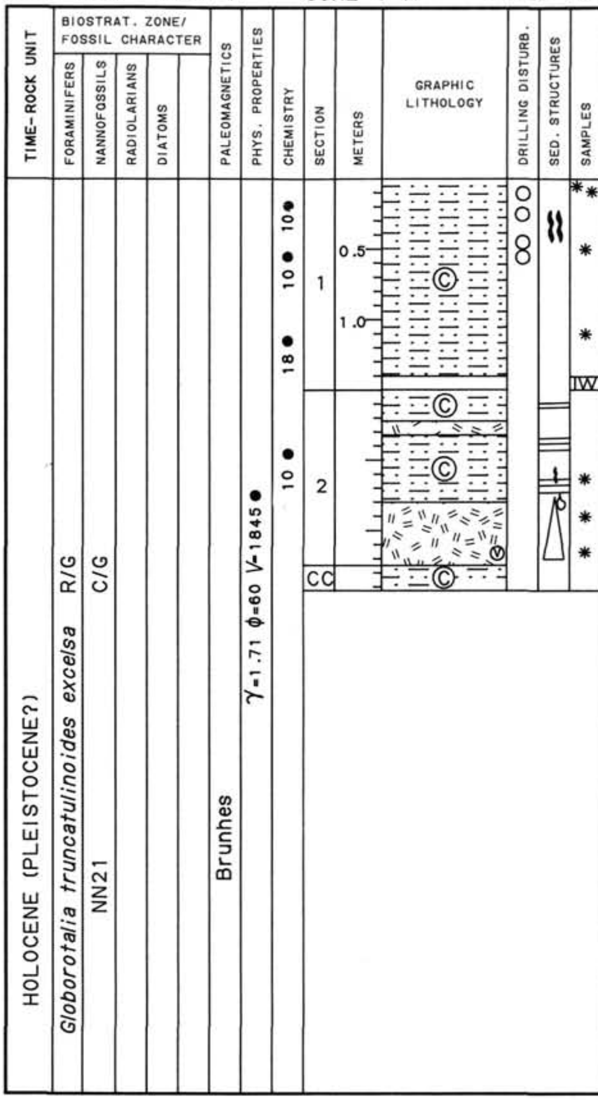

LITHOLOGIC DESCRIPTION

CALCAREOUS MUD alternating with VOLCANICLASTIC SAND

Calcareous mud, light olive-brown (2.5Y 5/4–5/6) and dark gray (5Y 4/1) to olive (5Y 5/6), homogeneous to faintly laminated, sparse minor bioturbation.

Volcaniclastic sand, black (5Y 2.5/2) to dark gray (5Y 4/1), normally graded; rounded pumice fragments in Section 2, 80–120 cm, pteropod tests in Section 2, 90–92 cm.

SMEAR SLIDE SUMMARY (%):

	1, 7 D	1, 10 D	1, 57 M	1, 114 D	2, 70 D	2, 93 M	2, 120 D
TEXTURE:							
Sand	1	2	1	—	30	80	80
Silt	3	5	4	5	50	15	15
Clay	96	93	95	95	20	5	5
COMPOSITION:							
Quartz	2	5	3	2	5	5	—
Feldspar	—	—	1	1	—	10	20
Mica	2	—	1	1	—	1	—
Clay	20	15	39	54	10	12	—
Volcanic glass	10	30	2	—	50	63	75
Calcite/dolomite	—	Tr	—	—	—	2	—
Accessory minerals	6	—	—	1	5	—	—
Zeolite	—	—	—	—	Tr	—	—
Foraminifers	3	5	1	2	Tr	2	5
Nannofossils	40	25	20	20	5	1	—
Diatoms	—	Tr	—	—	Tr	—	—
Radiolarians	1	—	—	—	—	—	—
Sponge spicules	—	5	—	—	Tr	—	—
Plant debris	—	—	—	1	—	—	—
Micrite	15	15	30	18	25	—	—
Amorphous organics	1	—	3	—	—	—	—
Pellets	—	—	—	—	—	2	—
Bioclasts	—	—	—	—	—	1	—

Information on Core Description Forms, for ALL sites, represents field notes taken aboard ship. Some of this information has been refined in accord with post-cruise findings, but production schedules prohibit definitive correlation of these forms with subsequent findings. Thus the reader should be alerted to the occasional ambiguity or discrepancy.

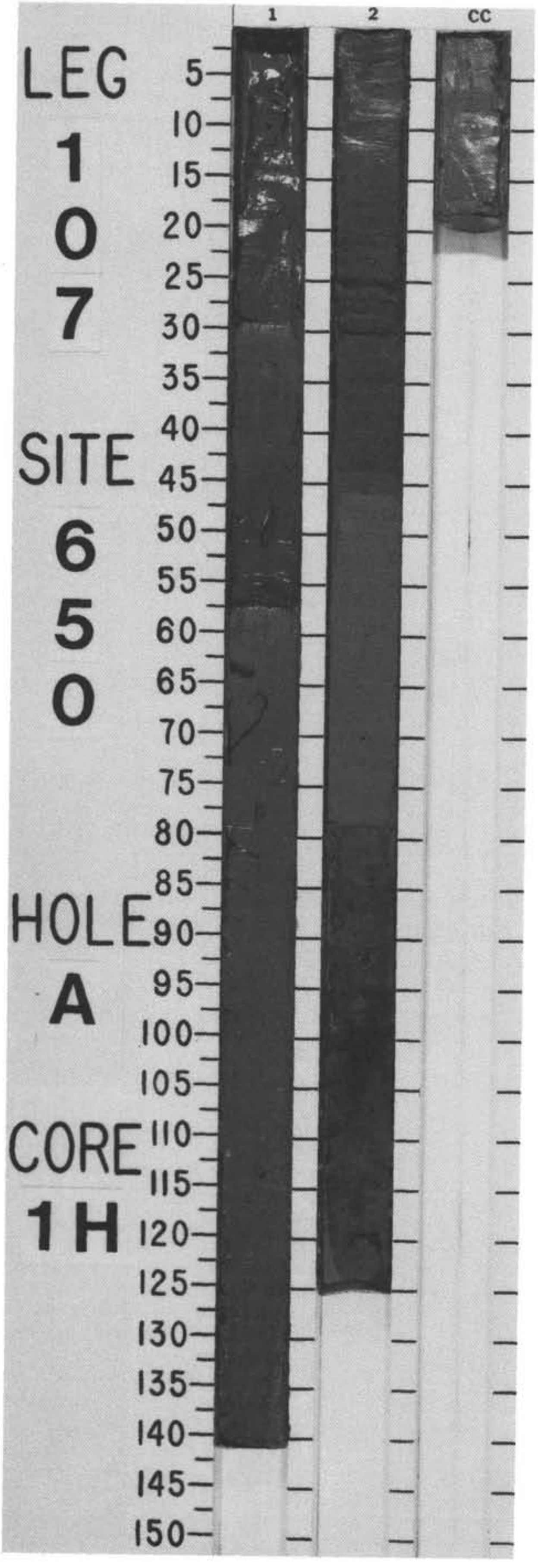
LEG
1
0
7
SITE
6
5
0
HOLE
A
CORE
1H
1
2
CC
5
10
15
20
25
30
35
40
45
50
55
60
65
70
75
80
85
90
95
100
105
110
115
120
125
130
135
140
145
150

SITE 650 HOLE A CORE 2 H CORED INTERVAL 3519.3-3529.0 mbsl; 3.0-12.7 mbsf

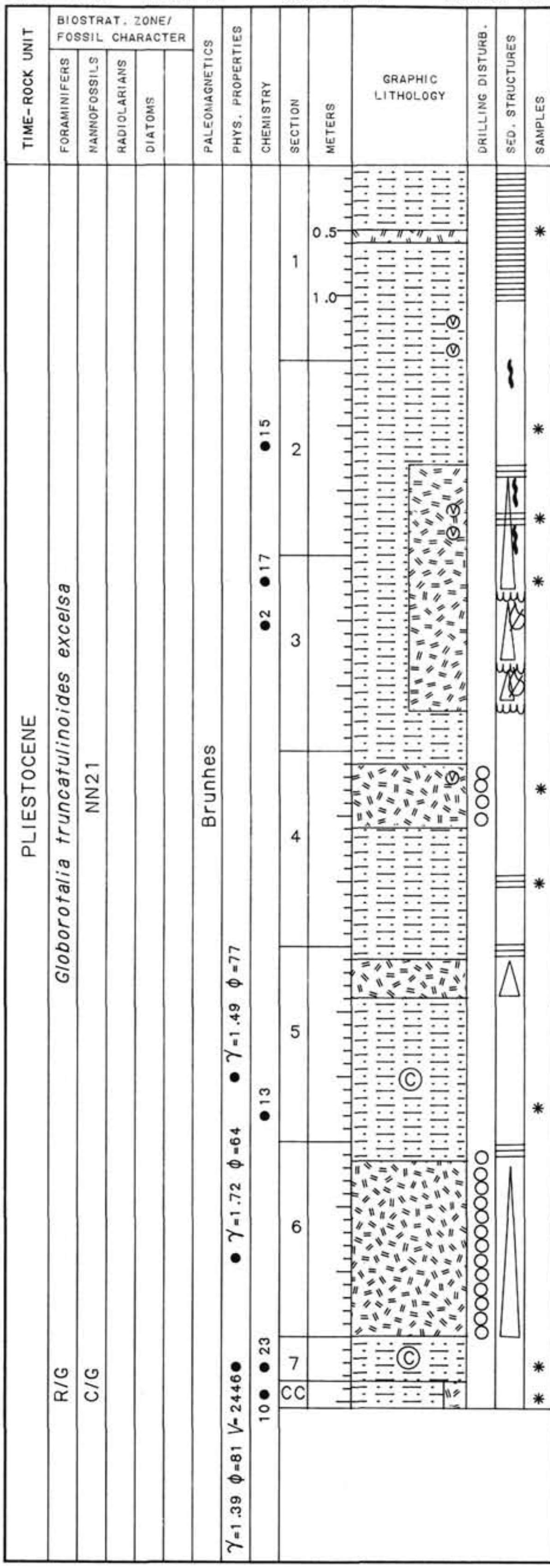

LITHOLOGIC DESCRIPTION

CALCAREOUS MUD alternating with VOLCANICLASTIC SAND and SILT

Calcareous mud, dark gray (5Y 4/1) to light olive-gray (5Y 6/2), and grayish brown (2.5Y 5/2) to pale yellow (2.5Y 7/4), homogeneous to faintly laminated.

Volcaniclastic sand and silt, black (5Y 2.5/1) to dark olive-gray (5Y 3/2), normally graded, scoured bottom contacts, discrete laminae of shell fragments and randomly scattered pumice fragments.

Interpretation: multiple turbidite sequences typically consisting of alternations of calcareous mud/volcaniclastic mud and sand/vitric ash.

SMEAR SLIDE SUMMARY (%):

	1, 58 D	2, 58 M	2, 123 D	3, 24 D	4, 36 D	4, 106 M	5, 128 D
TEXTURE:							
Sand	90	65	—	—	80	80	—
Silt	10	35	—	15	20	10	15
Clay	—	—	—	85	—	10	85
COMPOSITION:							
Quartz	10	—	—	2	12	70	—
Feldspar	15	20	15	—	5	10	—
Rock fragments	Tr	—	—	—	—	—	—
Mica	Tr	10	—	—	Tr	10	—
Clay	—	—	—	60	—	5	55
Volcanic glass	65	60	80	3	75	5	15
Calcite/dolomite	—	—	—	5	—	—	5
Accessory minerals	5	—	—	—	5	—	—
Glauconite/celadonite	—	5	5	—	—	—	—
Foraminifers	2	5	—	—	2	—	—
Nannofossils	—	—	—	30	1	—	25
Radiolarians	3	—	—	—	—	—	—
Sponge spicules	—	—	—	Tr	Tr	—	—
Plant debris	Tr	—	—	—	—	—	—

	7, 25 D	CC, 10 M
TEXTURE:		
Sand	—	70
Silt	20	30
Clay	80	—
COMPOSITION:		
Quartz	2	20
Feldspar	—	20
Mica	—	20
Clay	60	—
Volcanic glass	2	20
Calcite/dolomite	10	—
Accessory minerals	—	10
Foraminifers	Tr	5
Nannofossils	25	—
Radiolarians	—	5
Sponge spicules	1	—

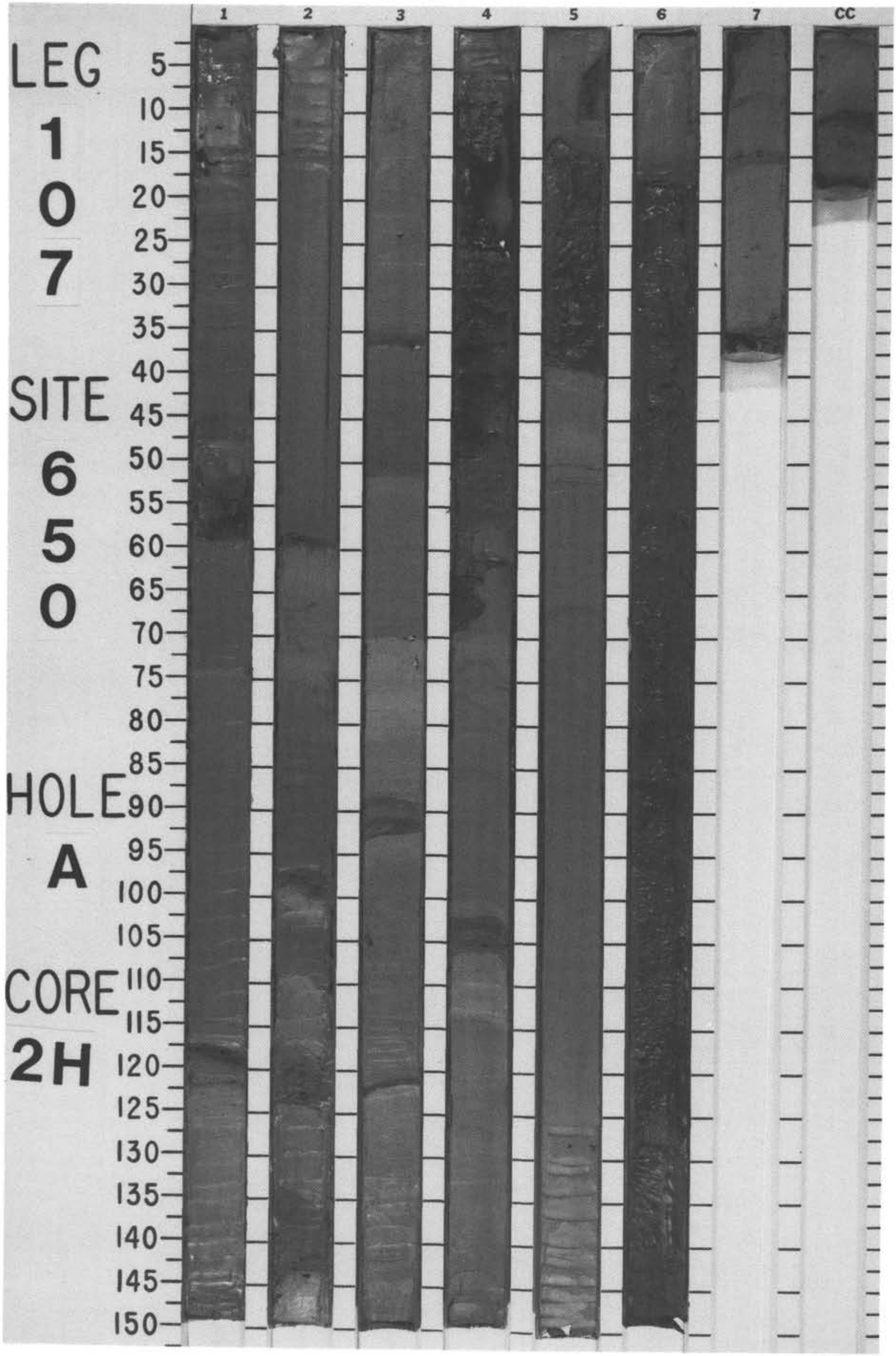
LEG
107
SITE
650
HOLE
A
CORE
2H
1
2
3
4
5
6
7
CC
5
10
15
20
25
30
35
40
45
50
55
60
65
70
75
80
85
90
95
100
105
110
115
120
125
130
135
140
145
150

SITE 650 HOLE A CORE 3 H CORED INTERVAL 3529.0-3538.7 mbsl; 12.7-22.4 mbsf

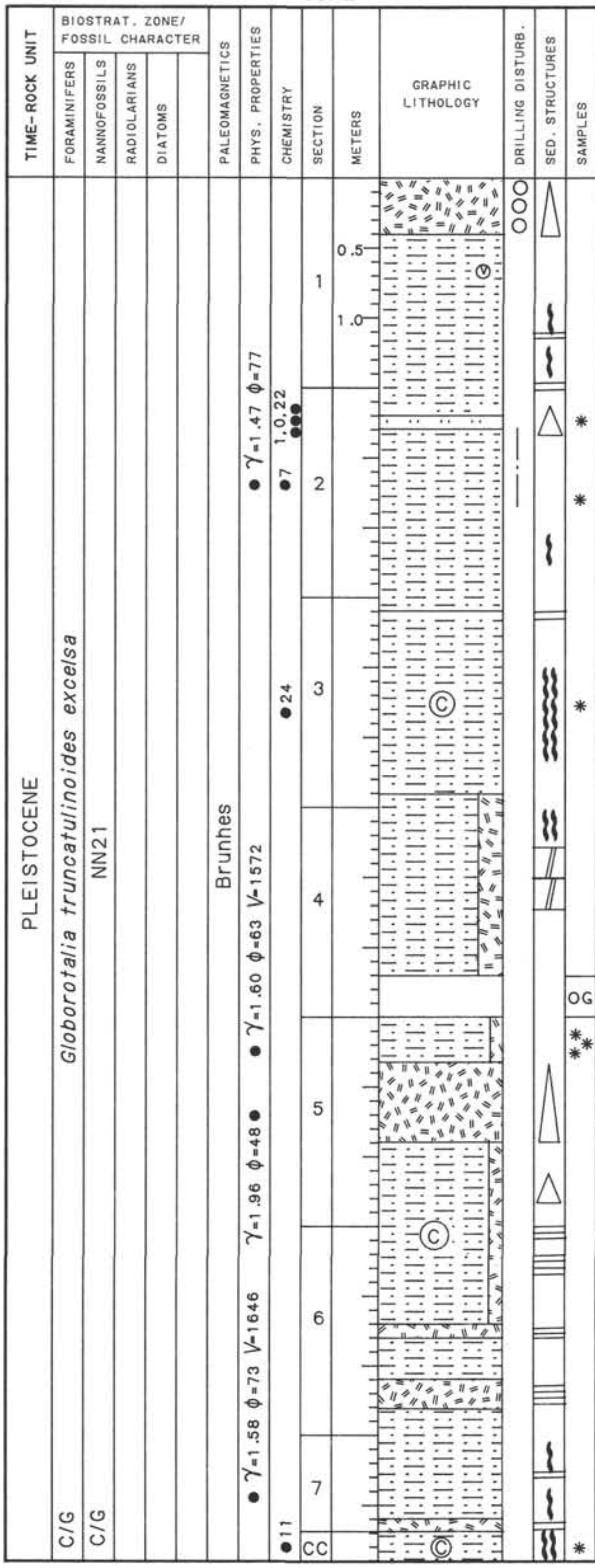

LITHOLOGIC DESCRIPTION

MUD and CALCAREOUS MUD alternating with VOLCANICLASTIC SAND

Mud and calcareous mud, grayish brown (2.5Y 5/2) to light brownish gray (2.5Y 6/2) and dark olive-gray (5Y 3/2) to pale olive (5Y 6/2), homogeneous to faintly laminated, minor bioturbation; pteropod and foraminifer silty laminae in Section 7, 10 and 20–25 cm.

Volcaniclastic sand, black (5Y 2.5/1) to light olive-gray (5Y 6/2); thin, normally graded beds to very thin (1–10 cm), cross-stratified beds in Section 3, 140 cm, to Section 5, 33 cm, and Section 5, 91 cm, to Section 6, 70 cm; pumice fragments (5 mm) in Section 1, 65 cm.

SMEAR SLIDE SUMMARY (%):

	2, 28 D	2, 79 D	3, 80 D	5, 34 D	5, 35 M	5, 40 D	7, 11 D
TEXTURE:							
Sand	1	5	—	—	10	80	—
Silt	98	20	10	—	40	10	10
Clay	1	75	90	—	50	10	90
COMPOSITION:							
Quartz	80	—	Tr	3	10	37	10
Feldspar	5	5	Tr	—	2	5	Tr
rock fragments	5	5	—	—	2	2	—
Mica	Tr	—	—	—	—	2	—
Clay	Tr	55	55	60	50	7	65
Volcanic glass	—	5	—	—	5	25	—
Calcite/dolomite	—	10	5	27	14	10	5
Accessory minerals	5	—	—	5	5	5	Tr
Foraminifers	Tr	Tr	Tr	—	2	1	—
Nannofossils	1	20	40	5	10	2	20
Radiolarians	2	—	—	—	—	1	—
Sponge spicules	1	Tr	—	—	Tr	Tr	Tr
Silicoflagellates	—	—	Tr	—	—	—	—
Plant debris	Tr	—	—	—	—	Tr	—
Pellets	1	—	—	—	—	—	—

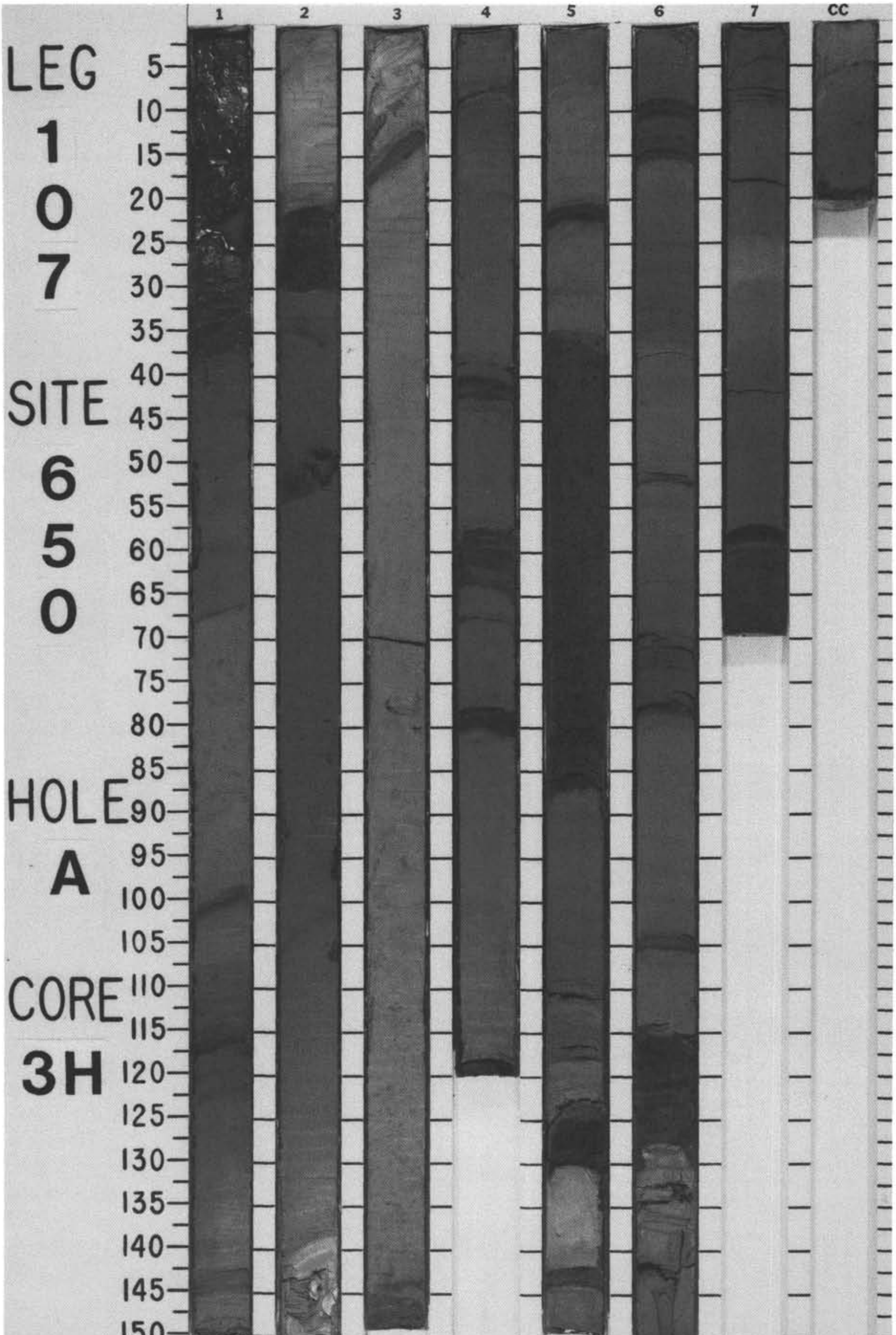
LEG
107
SITE
650
HOLE
A
CORE
3H
1
2
3
4
5
6
7
CC

SITE 650 HOLE A CORE 4 H CORED INTERVAL 3538.7-3549.1 mbsl; 22.4-32.8 mbsf

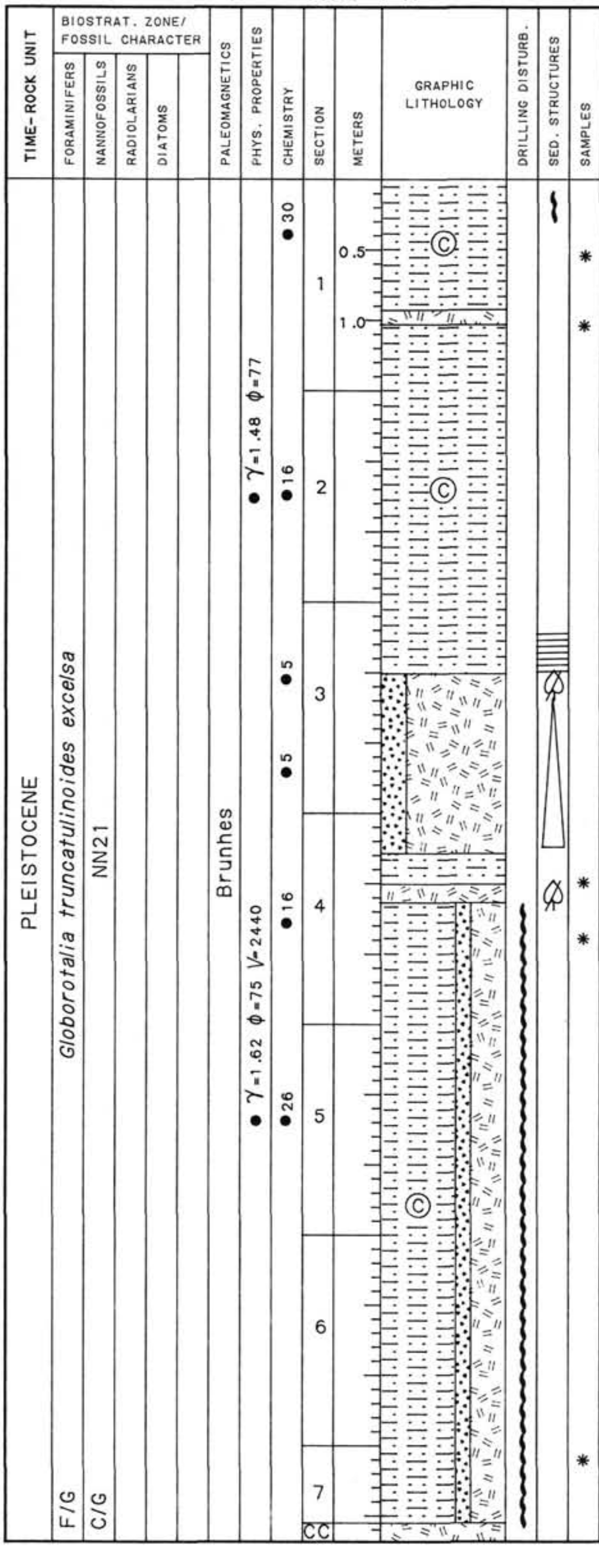

LITHOLOGIC DESCRIPTION

CALCAREOUS MUD alternating with VOLCANICLASTIC SAND

Calcareous mud, gray (5Y 5/1) to pale yellow (5Y 7/3).

Volcaniclastic sand, very dark gray (5Y 3/1) to olive (5Y 5/3); Section 3, 50 cm, to Section 4, 30 cm, normally graded with pumice and wood fragments as large as 4 cm; Section 4, 63 cm, to Section 7, 55 cm, irregular alternations ranging from cm to dm thickness, probably increased by drilling disturbance.

SMEAR SLIDE SUMMARY (%):

	1, 51 D	1, 100 M	4, 53 D	4, 78 D	7, 11 D
TEXTURE:					
Sand	—	10	80	—	30
Silt	10	70	15	5	60
Clay	90	20	5	95	10
COMPOSITION:					
Quartz	5	25	60	10	40
Feldspar	Tr	Tr	5	—	5
Rock fragments	—	—	Tr	Tr	Tr
Mica	Tr	—	—	—	Tr
Clay	55	25	16	55	25
Volcanic glass	—	25	10	5	10
Calcite/dolomite	20	—	—	7	10
Accessory minerals	5	5	5	2	5
Foraminifers	—	10	—	—	—
Nannofossils	15	5	3	20	5
Radiolarians	—	3	—	—	Tr
Sponge spicules	—	1	1	1	Tr
Plant debris	—	1	—	—	—

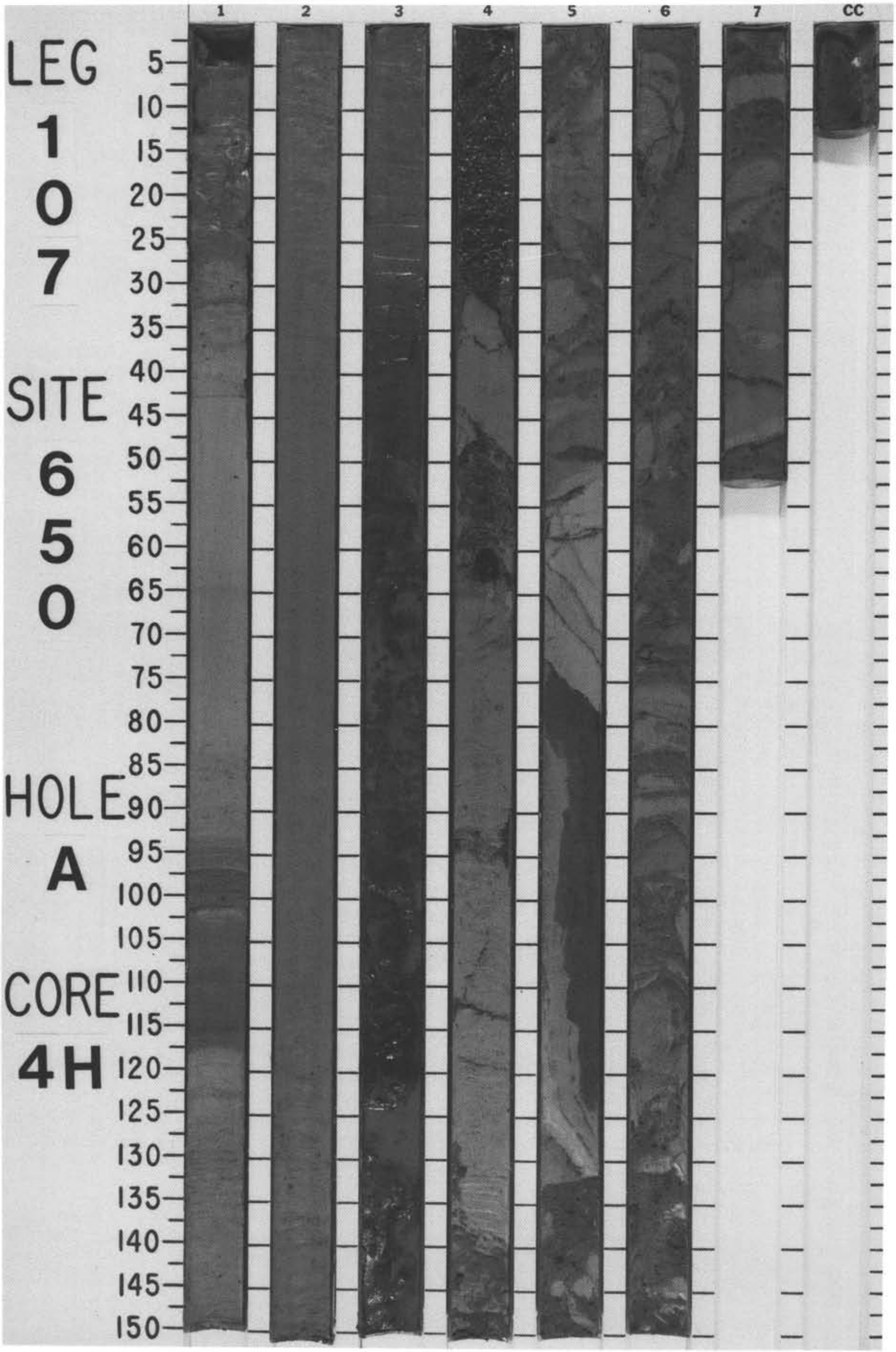
LEG 107
SITE 650
HOLE A
CORE 4H
1
2
3
4
5
6
7
CC
5
10
15
20
25
30
35
40
45
50
55
60
65
70
75
80
85
90
95
100
105
110
115
120
125
130
135
140
145
150

SITE 650 HOLE A CORE 5 H CORED INTERVAL 3549.1-3558.7 mbsl: 32.8-42.4 mbsf

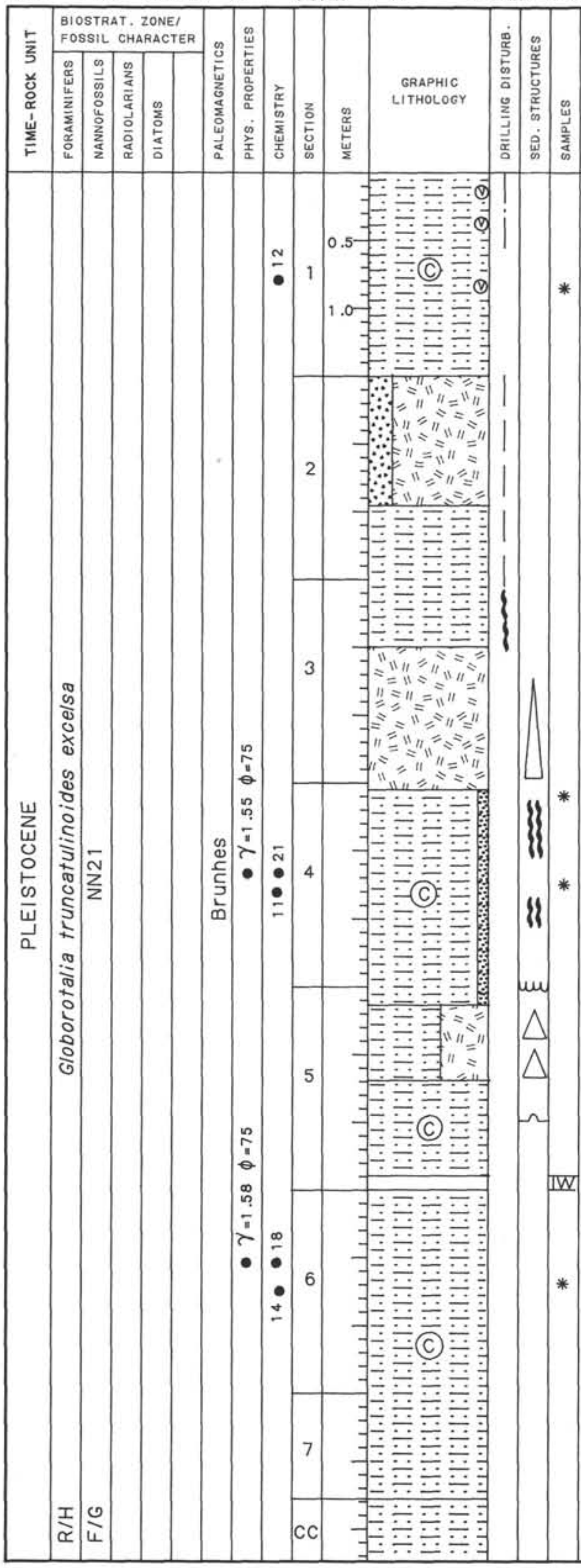

LITHOLOGIC DESCRIPTION

CALCAREOUS MUD alternating with VOLCANICLASTIC SAND and SILT

Calcareous mud, dark olive-gray (5Y 3/2) to pale olive (5Y 6/3).

Volcaniclastic sand and silt, very dark gray (5Y 3/1) to olive (5Y 5/4); thin, normally graded beds to very thin (2–5-cm) beds in Sections 4 and 5, grain size of sandy intervals in Section 2 is coarse to fine, with pumice fragments as large as 2.5 cm; grain size in Section 3 is medium to fine, and in Sections 4 and 5 is fine.

SMEAR SLIDE SUMMARY (%):

	1, 82 D	4, 12 D	4, 75 M	6, 75 D
TEXTURE:				
Sand	—	20	—	—
Silt	30	60	15	20
Clay	70	20	85	80
COMPOSITION:				
Quartz	10	5	5	10
Feldspar	—	—	—	Tr
Rock fragments	—	—	—	Tr
Clay	55	15	70	60
Volcanic glass	10	60	—	—
Calcite/dolomite	10	3	11	17
Accessory minerals	—	5	—	3
Pyrite	—	—	2	—
Foraminifers	6	2	1	—
Nannofossils	5	5	10	10
Radiolarians	3	3	—	—
Sponge spicules	1	2	1	—

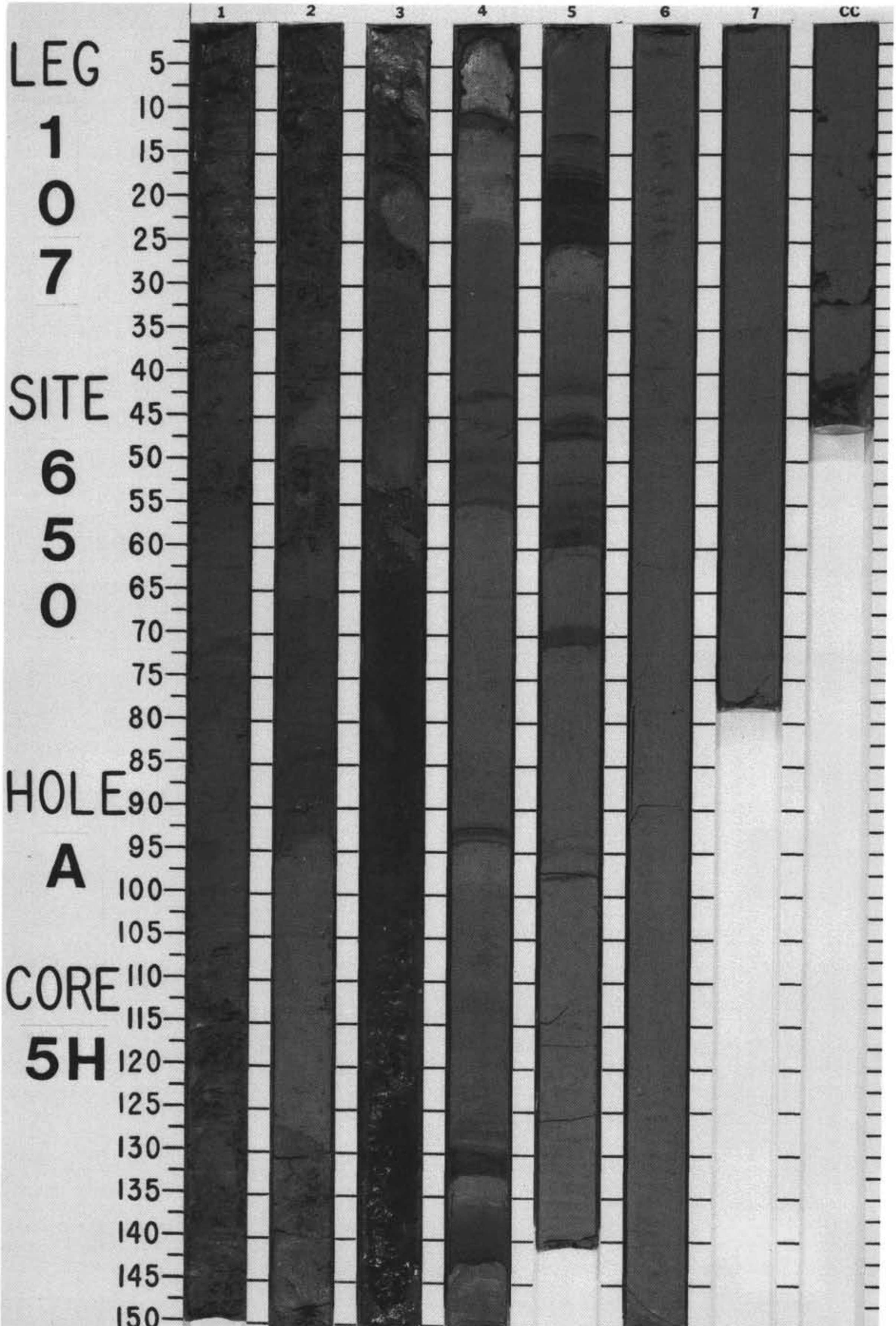
LEG
1
0
7
SITE
6
5
0
HOLE
A
CORE
5H
1
2
3
4
5
6
7
CC
5
10
15
20
25
30
35
40
45
50
55
60
65
70
75
80
85
90
95
100
105
110
115
120
125
130
135
140
145
150

SITE 650 HOLE A CORE 6 H CORED INTERVAL 3558.7-3568.4 mbsl; 42.4-52.1 mbsf

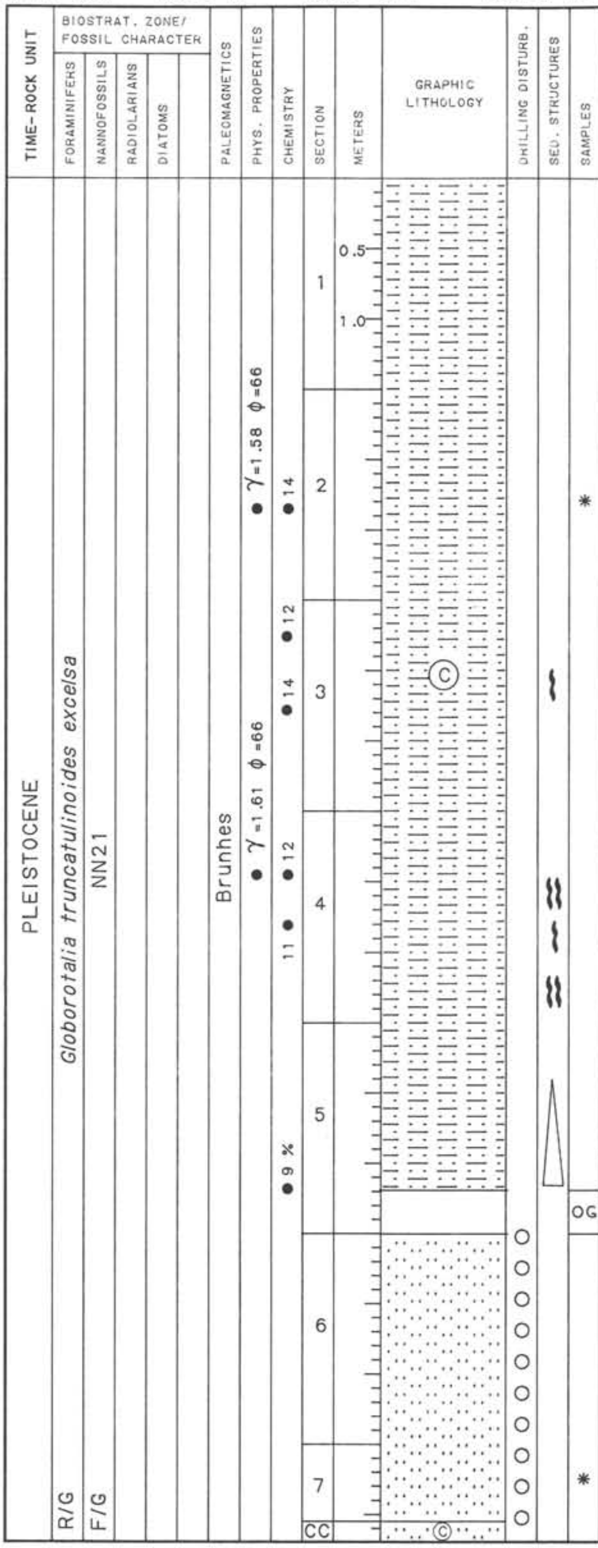

LITHOLOGIC DESCRIPTION

VOLCANICLASTIC SILT grading upward into CALCAREOUS MUD

Calcareous mud, gray (5Y 5/1) to olive (5Y 5/3), homogeneous.

Volcaniclastic silt, dark gray (5Y 4/1), homogeneous, soupy appearance.

SMEAR SLIDE SUMMARY (%):

	2, 80 D	7, 25 D
TEXTURE:		
Sand	—	5
Silt	15	75
Clay	85	20
COMPOSITION:		
Quartz	Tr	10
Feldspar	Tr	5
Rock fragments	—	3
Clay	60	20
Volcanic glass	—	15
Calcite/dolomite	15	30
Accessory minerals	—	2
Pyrite	5	—
Foraminifers	Tr	8
Nannofossils	20	5
Radiolarians	—	2
Sponge spicules	Tr	—

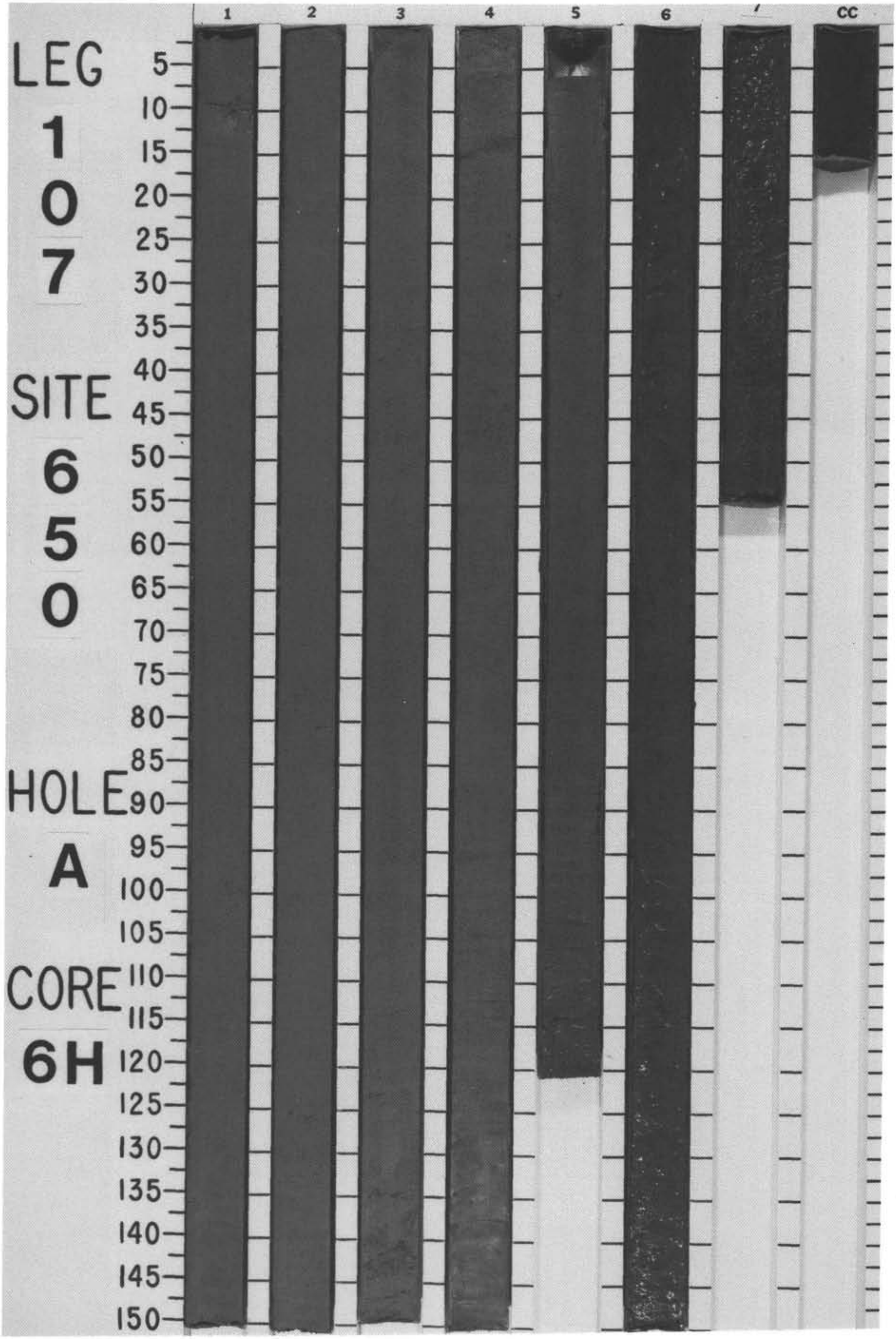
1
2
3
4
5
6
7
CC
LEG
107
SITE
650
HOLE
A
CORE
6H
5
10
15
20
25
30
35
40
45
50
55
60
65
70
75
80
85
90
95
100
105
110
115
120
125
130
135
140
145
150

SITE 650 HOLE A CORE 7 H CORED INTERVAL 3568.4-3578.1 mbsl; 52.1-61.8 mbsf

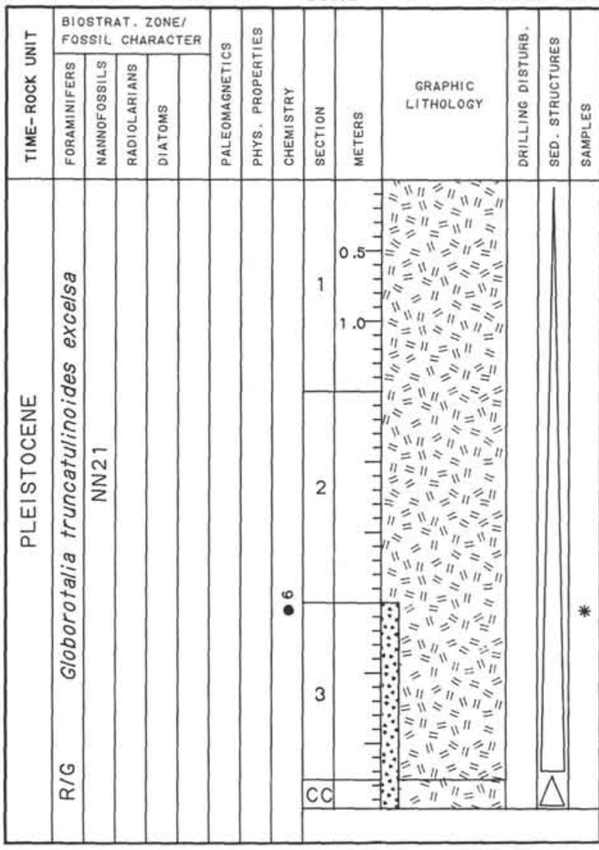

LITHOLOGIC DESCRIPTION

VOLCANICLASTIC SAND and SILT

Volcaniclastic sand and silt, dark gray (5Y 4/1), normally graded; grain size in Section 1 is fine sand to silt, in Section 2 is fine, in Section 3 is medium to fine, and in CC is coarse sand with pumice fragments as large as 5 mm.

SMEAR SLIDE SUMMARY (%):

	3, 5
	D
TEXTURE:	
Sand	50
Silt	30
Clay	20
COMPOSITION:	
Quartz	20
Feldspar	5
Mica	5
Clay	15
Volcanic glass	30
Calcite/dolomite	15
Accessory minerals	5
Foraminifers	2
Nannofossils	2
Radiolarians	1

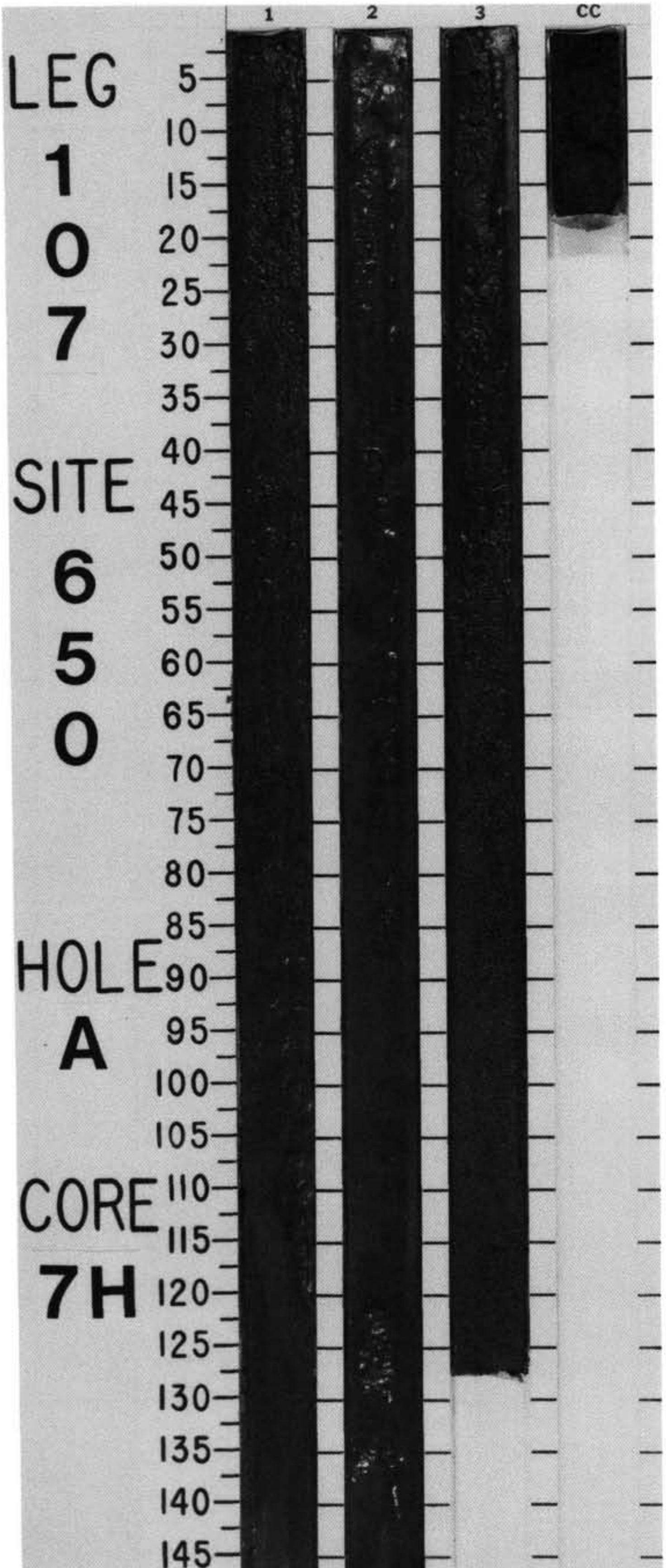
LEG
107
SITE
650
HOLE
A
CORE
7H
1
2
3
CC
5
10
15
20
25
30
35
40
45
50
55
60
65
70
75
80
85
90
95
100
105
110
115
120
125
130
135
140
145
150

SITE 650 HOLE A CORE 8 H CORED INTERVAL 3578.1-3587.6 mbsl; 61.8-71.3 mbsf

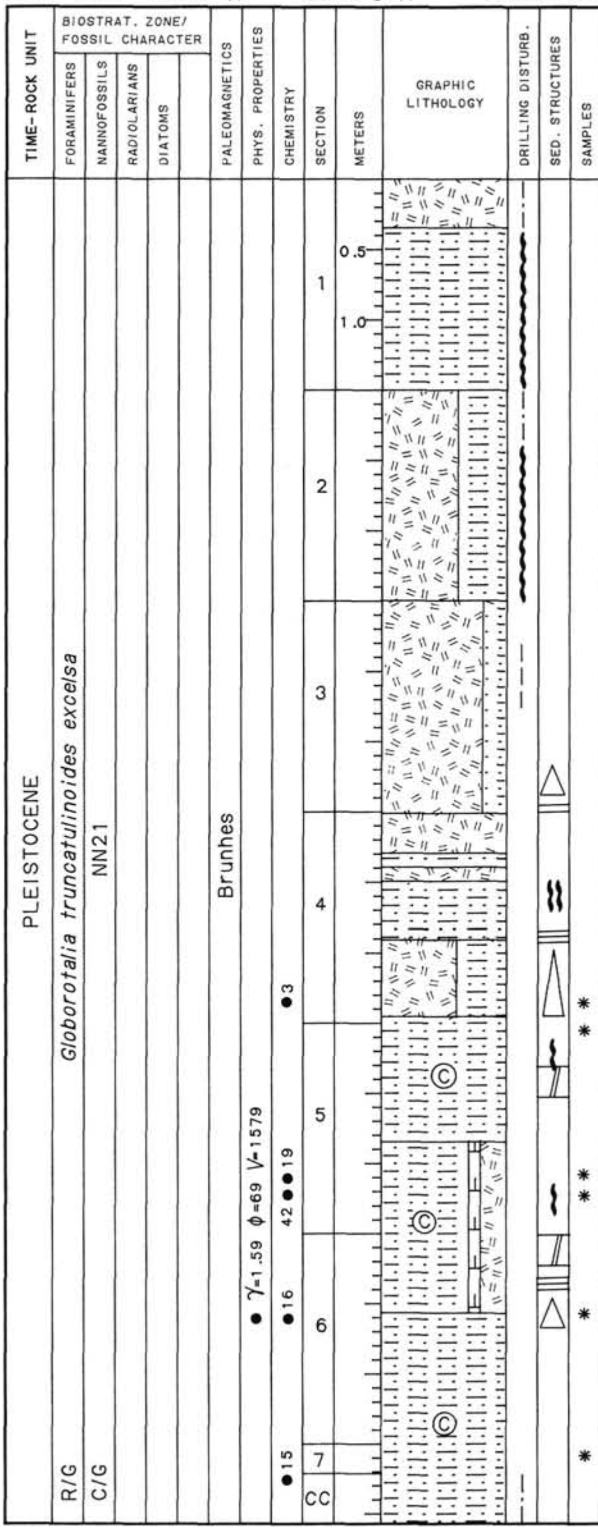

LITHOLOGIC DESCRIPTION

CALCAREOUS MUD alternating with VOLCANICLASTIC SAND and SILT

Calcareous mud, gray (5Y 5/1) to olive-gray (5Y 5/2), thick to very thin beds, thickness in Section 3 is 2–5 cm, grading upward into very thin beds (2–3 cm) of nannofossil ooze, gray (5Y 6/1) to light olive-gray (5Y 6/2), particularly in Section 5.

Volcaniclastic sand and silt, dark olive-gray (5Y 3/2) to olive (5Y 5/3), normally graded, thin to very thin beds; thickness in Section 3 is 8–15 cm, in Sections 5 and 6 is 5–10 cm; grain size is generally fine, but in Section 4, 140–150 cm, is coarse.

SMEAR SLIDE SUMMARY (%):

	4, 139 D	5, 5 D	5, 111 D	5, 117 M	6, 52 M	7, 5 D
TEXTURE:						
Sand	50	—	50	10	—	5
Silt	40	20	35	5	15	15
Clay	10	80	15	85	85	80
COMPOSITION:						
Quartz	20	3	15	—	2	3
Feldspar	3	2	2	—	2	—
Rock fragments	—	—	2	—	—	—
Mica	—	Tr	—	—	—	—
Clay	5	52	17	61	70	60
Volcanic glass	45	10	30	Tr	—	7
Calcite/dolomite	8	10	15	Tr	3	4
Accessory minerals	5	—	6	—	—	—
Glauconite/Celadonite	—	—	—	—	8	—
Foraminifers	3	2	10	10	Tr	5
Nannofossils	10	20	2	25	15	20
Radiolarians	1	1	1	4	—	1

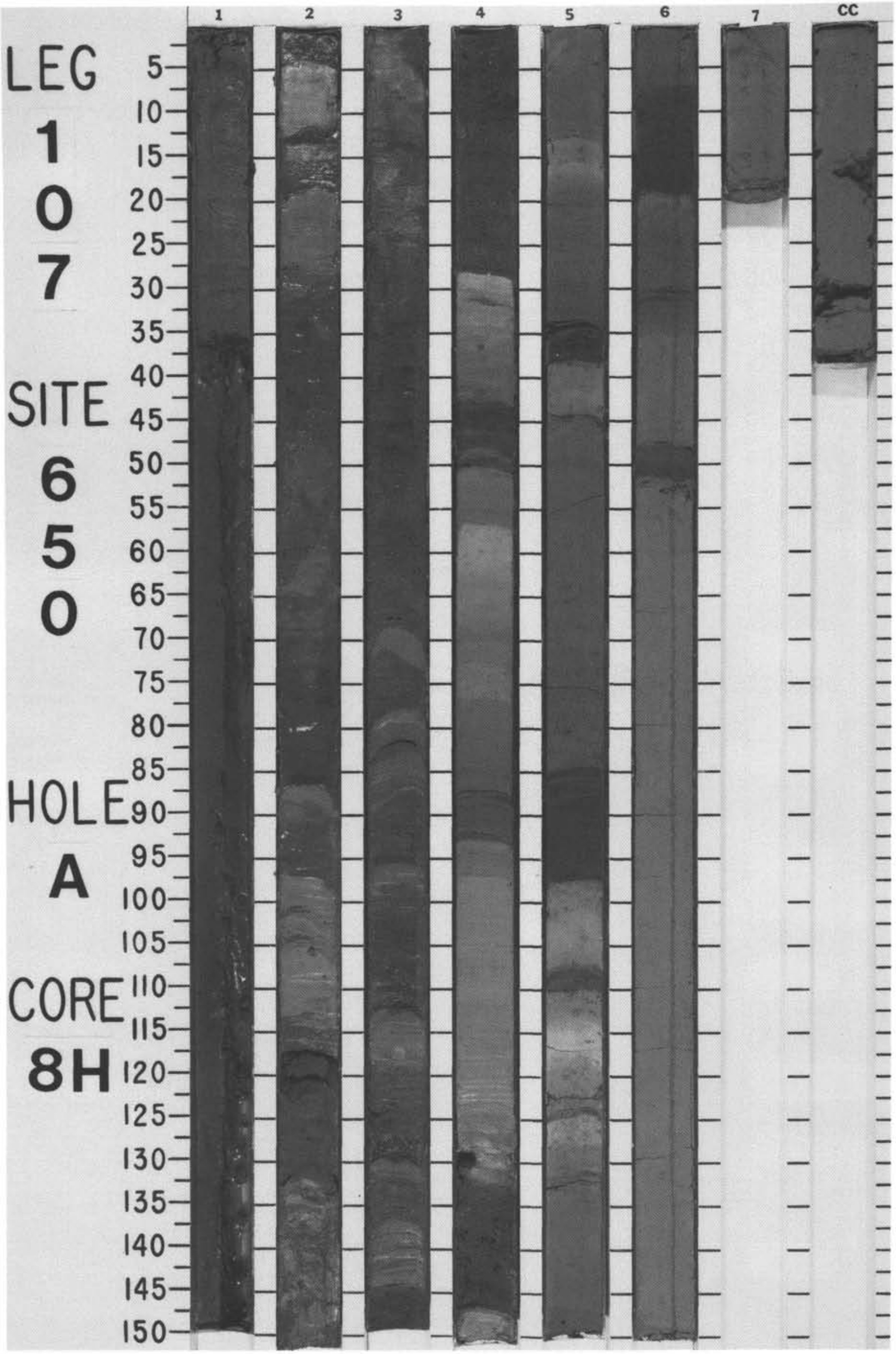
LEG
107
SITE
650
HOLE
A
CORE
8H
1
2
3
4
5
6
7
CC
5
10
15
20
25
30
35
40
45
50
55
60
65
70
75
80
85
90
95
100
105
110
115
120
125
130
135
140
145
150

SITE 650 HOLE A CORE 9 H CORED INTERVAL 3587.6-3597.3 mbsl; 71.3-81.0 mbsf

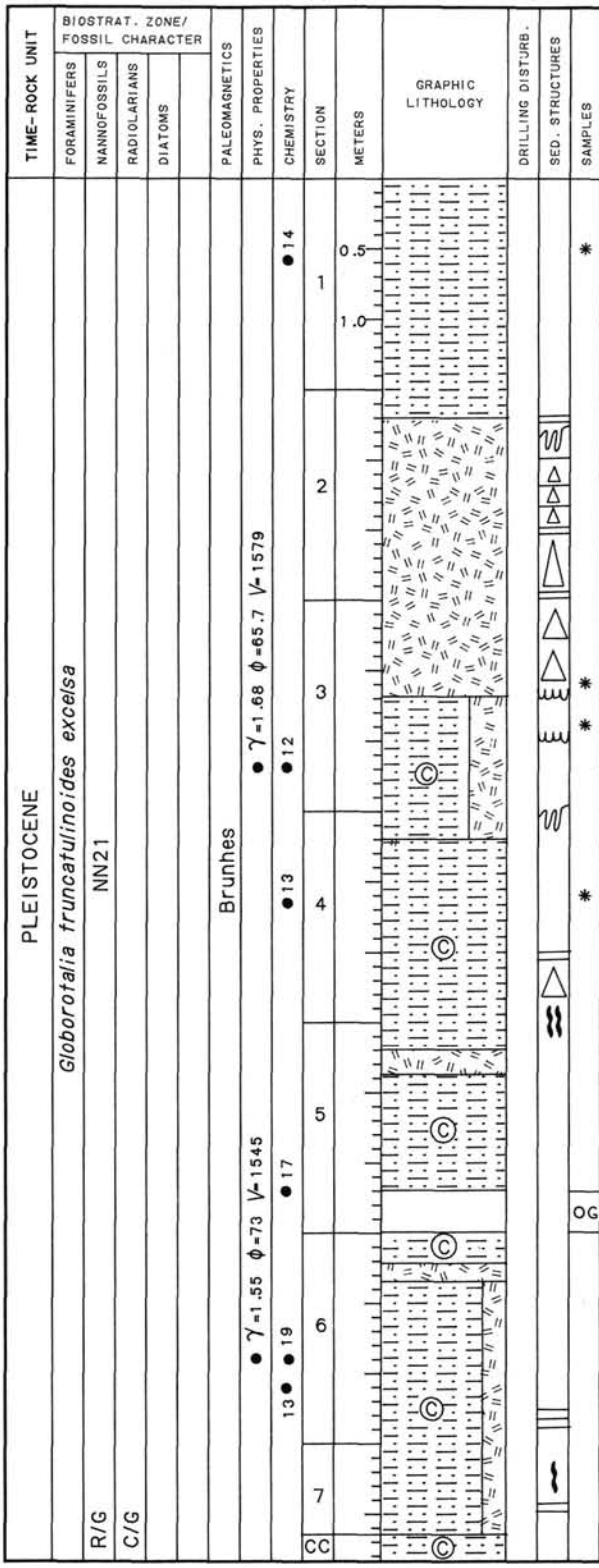

LITHOLOGIC DESCRIPTION

CALCAREOUS MUD alternating with VOLCANICLASTIC SAND

Calcareous mud, dark gray (5Y 4/1) to pale olive (5Y 6/3); dark, possibly diagenetic laminations near base of overlying sandy beds, numerous silty laminae in Section 7.

Volcaniclastic sand, very dark gray (5Y 3/1) to olive-gray (5Y 4/2); in Section 2, 70 cm, to Section 3, 70 cm, is a very thick, normally graded bed (coarse grained at base); otherwise fine-grained are beds 3–8 cm thick.

SMEAR SLIDE SUMMARY (%):

	1, 59 D	3, 63 D	3, 93 D	4, 66 M
TEXTURE:				
Sand	5	60	90	—
Silt	20	20	10	—
Clay	75	20	—	—
COMPOSITION:				
Quartz	—	20	20	5
Feldspar	—	2	—	3
Mica	—	10	—	—
Clay	60	18	—	56
Volcanic glass	10	25	75	10
Calcite/dolomite	20	—	—	10
Pyrox./Amph.	—	10	—	—
Pyrite	—	—	—	5
Foraminifers	—	10	2	Tr
Nannofossils	10	5	—	10
Radiolarians	Tr	—	3	1
Sponge spicules	Tr	—	—	—

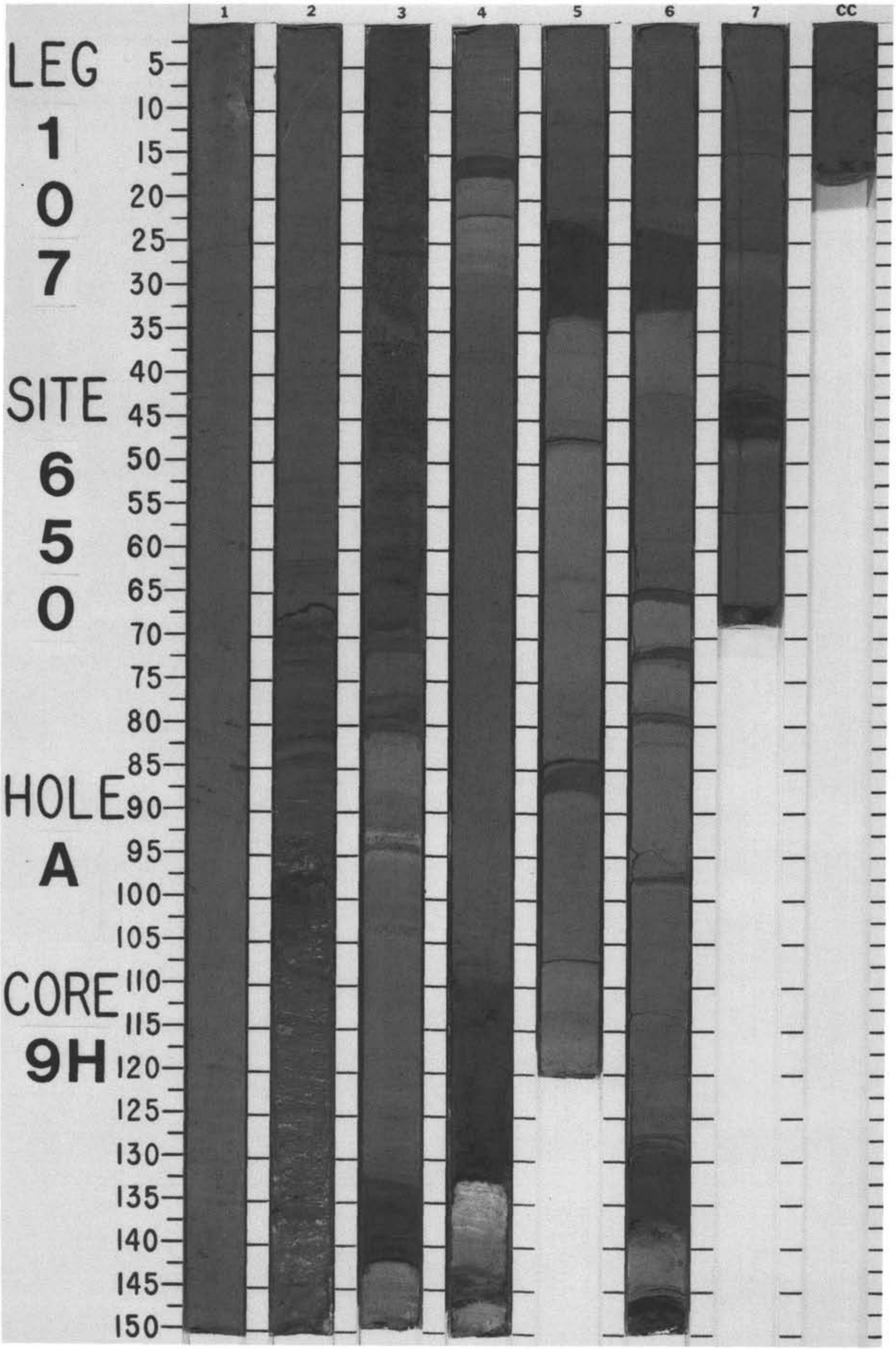
LEG
1
0
7
SITE
6
5
0
HOLE
A
CORE
9H
1
2
3
4
5
6
7
CC
5
10
15
20
25
30
35
40
45
50
55
60
65
70
75
80
85
90
95
100
105
110
115
120
125
130
135
140
145
150

SITE 650 HOLE A CORE 10 H CORED INTERVAL 3597.3-3607.0 mbsl; 81.0-90.7 mbsf

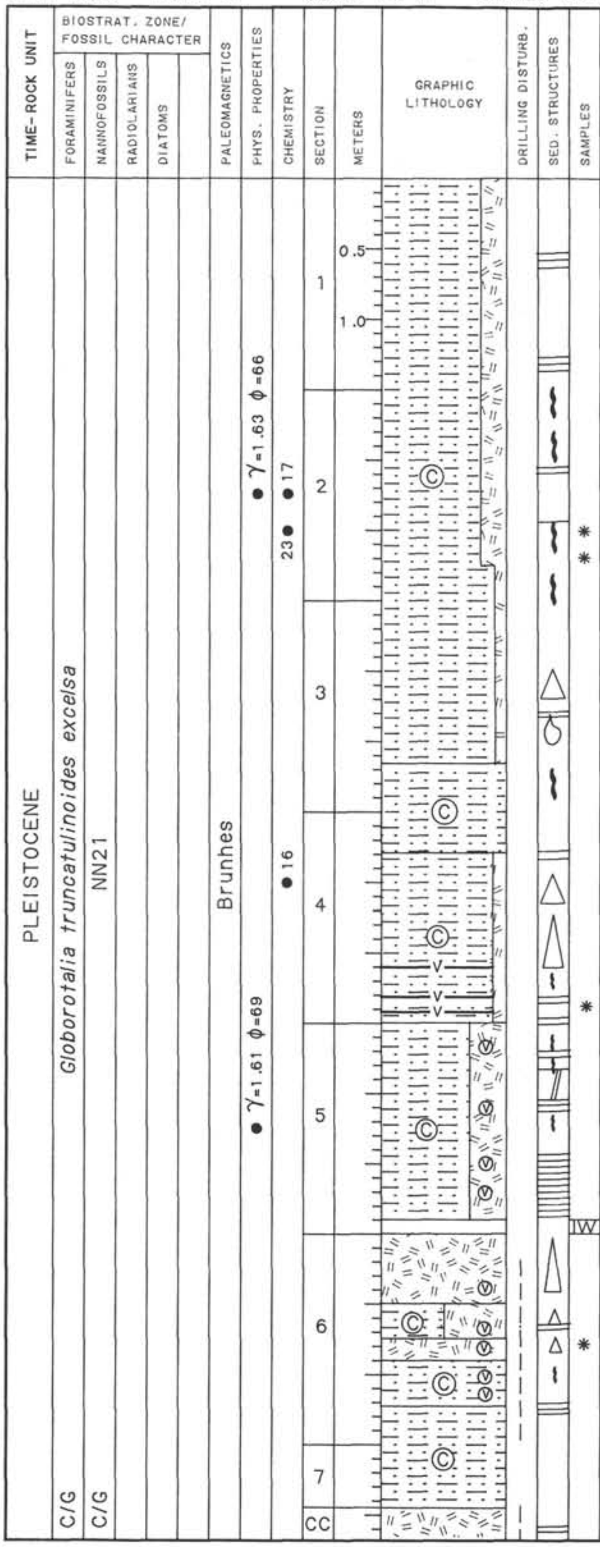

LITHOLOGIC DESCRIPTION

CALCAREOUS MUD alternating with VOLCANICLASTIC SAND and SILT

Calcareous mud, olive-gray (5Y 5/2) to light gray (5Y 7/2), thin to thick beds (5–70 cm).

Volcaniclastic sand and silt: sand, dark olive-gray (5Y 3/2) to olive-gray (5Y 4/2); silt, dark gray (5Y 4/1) to olive-gray (5Y 5/2), very thin, fine-grained to thin, normally graded beds (1–10 cm); ash laminae at the base of Section 4; numerous pumice fragments in Sections 5 and 6; silty laminae with pteropods in Section 3, 98 cm.

SMEAR SLIDE SUMMARY (%):

	2, 100 M	2, 124 M	4, 138 D	6, 87 D
TEXTURE:				
Sand	—	55	—	—
Silt	5	40	90	80
Clay	95	5	10	20
COMPOSITION:				
Feldspar	—	5	5	4
Mica	—	—	—	4
Clay	10	—	—	—
Volcanic glass	—	95	90	80
Calcite/dolomite	Tr	—	—	—
Accessory minerals	—	—	5	2
Pyroxene	—	—	—	10
Foraminifers	5	—	—	—
Nannofossils	—	Tr	—	—
Diatoms	70	—	—	—
Micrite	15	—	—	—

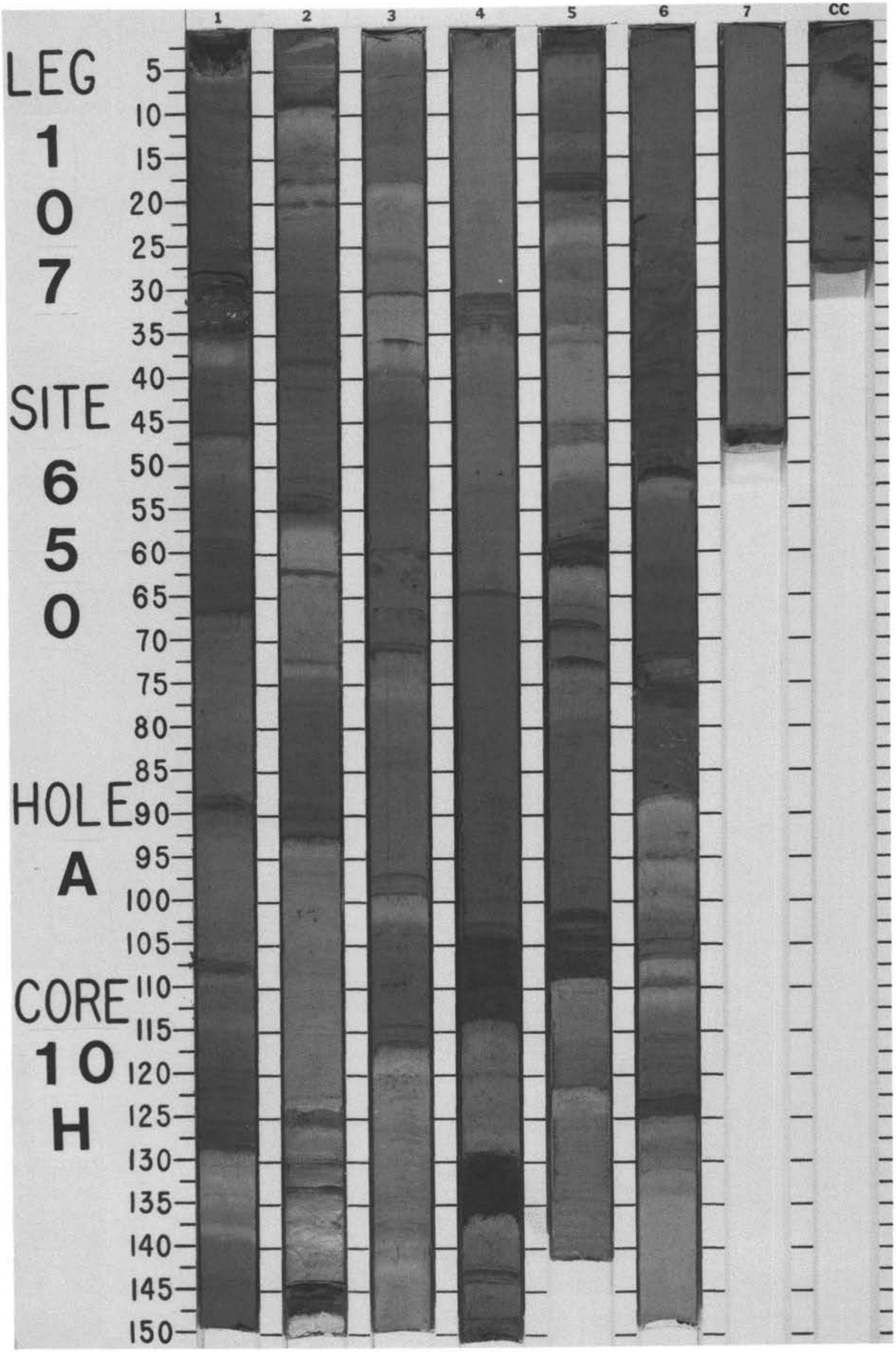
LEG
1
0
7
SITE
6
5
0
HOLE
A
CORE
10
H
1
2
3
4
5
6
7
CC

SITE 650 HOLE A CORE 11 H CORED INTERVAL 3607.0-3616.6 mbsl; 90.7-100.3 mbsf

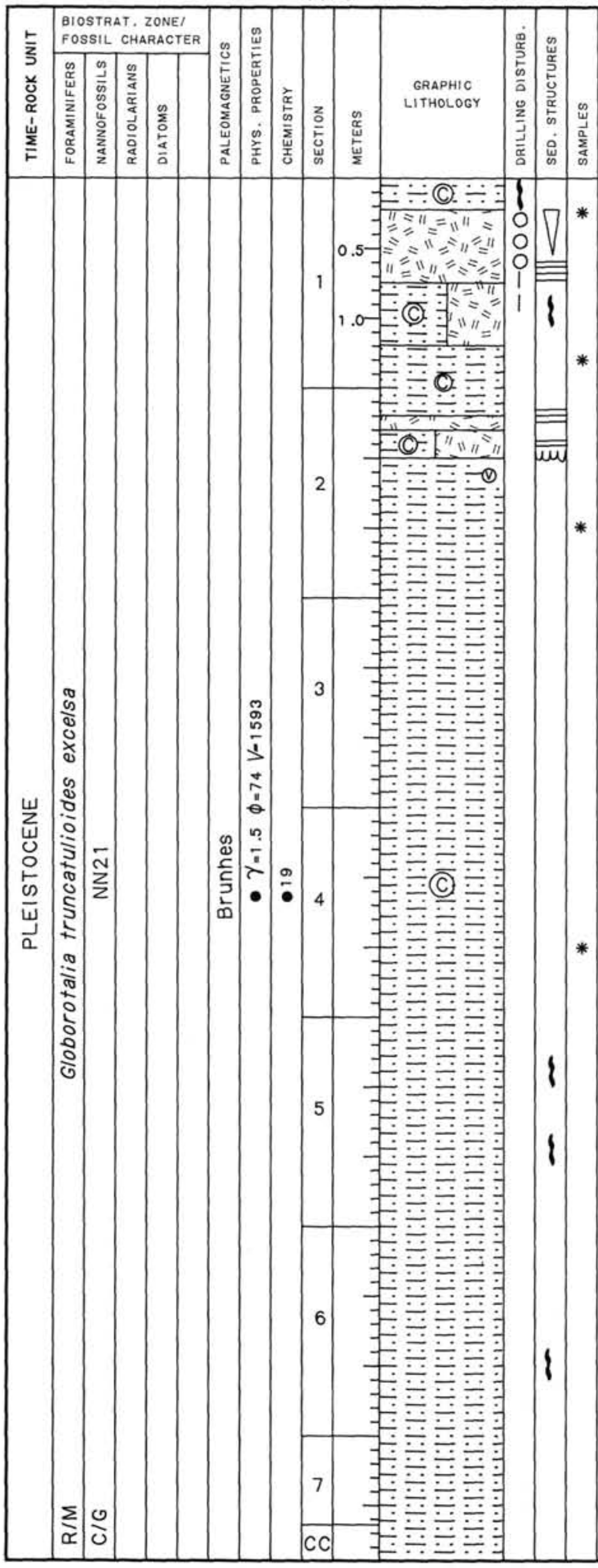

LITHOLOGIC DESCRIPTION

CALCAREOUS MUD alternating with VOLCANICLASTIC SAND and SILT, and a thick sequence of homogeneous CALCAREOUS MUD

Calcareous mud (mudstone), gray (5Y 5/1) to light olive-gray (5Y 6/2); faintly laminated above Section 2, 48 cm; scoured surface in Section 2, 48 cm; homogeneous mudstone below.

Volcaniclastic sand and silt: sand, dark olive-gray (5Y 3/2); silt, dark gray (5Y 4/1) to olive-gray (5Y 4/2); thick, reversely graded bed in Section 1, 25–75 cm, with a soupy, disturbed appearance, otherwise thin beds (5–10 cm).

SMEAR SLIDE SUMMARY (%):

	1, 30 D	1, 120 D	2, 100 D	4, 100 D
TEXTURE:				
Sand	70	40	—	—
Silt	30	60	10	15
Clay	—	—	90	85
COMPOSITION:				
Quartz	30	5	—	Tr
Feldspar	40	—	—	—
Mica	5	—	—	Tr
Clay	—	60	10	10
Volcanic glass	20	30	15	15
Calcite/dolomite	—	5	Tr	—
Accessory minerals	5	—	Tr	Tr
Zeolite	—	—	—	Tr
Foraminifers	—	—	—	Tr
Nannofossils	—	—	60	55
Diatoms	—	—	—	Tr
Sponge spicules	—	—	Tr	—
Micrite	—	—	15	20

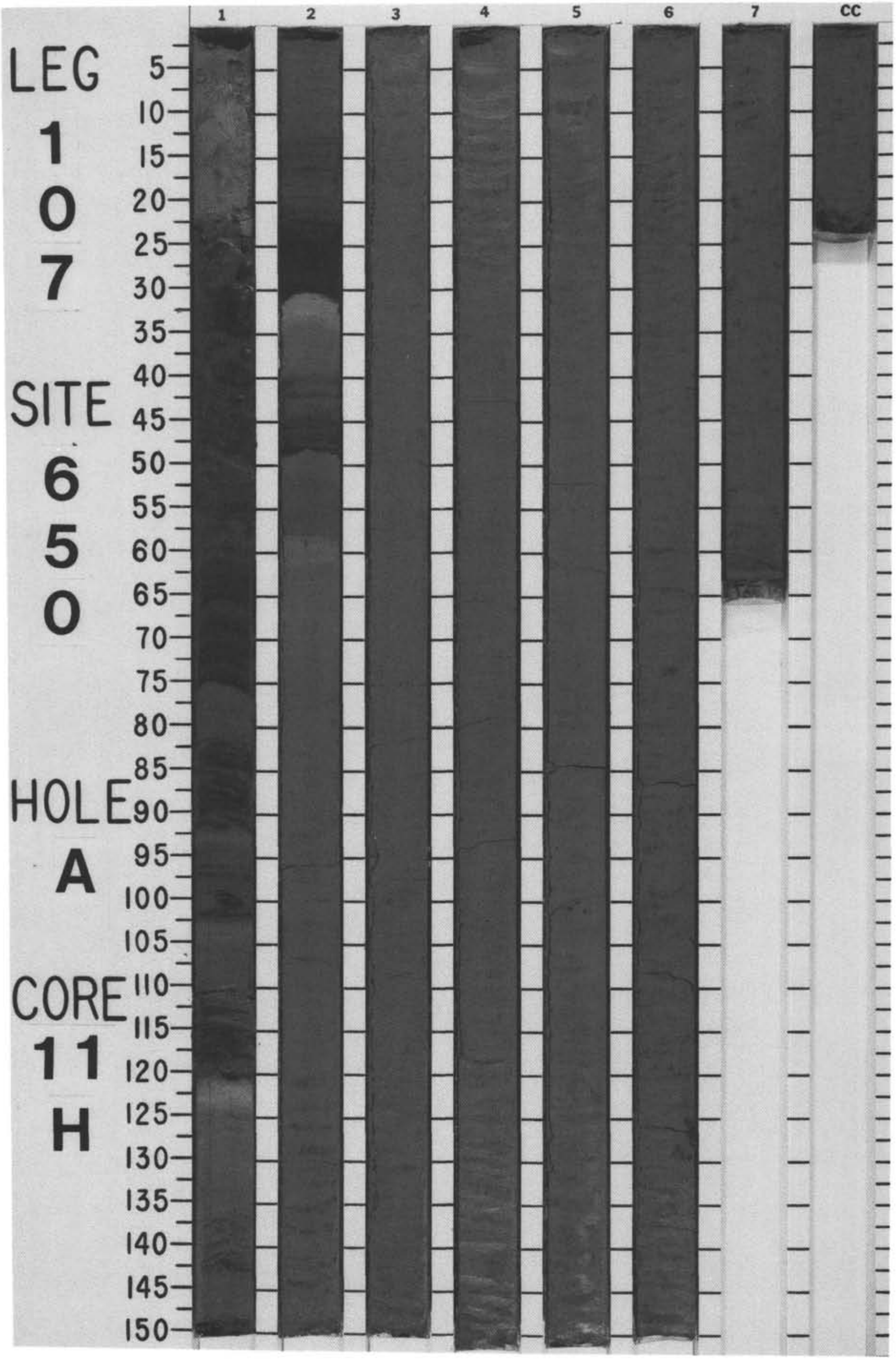
LEG
1
0
7
SITE
6
5
0
HOLE
A
CORE
11
H
1
2
3
4
5
6
7
CC
5
10
15
20
25
30
35
40
45
50
55
60
65
70
75
80
85
90
95
100
105
110
115
120
125
130
135
140
145
150

SITE 650 HOLE A CORE 12 H CORED INTERVAL 3616.6-3626.0 mbsl; 100.3-109.7 mbsf

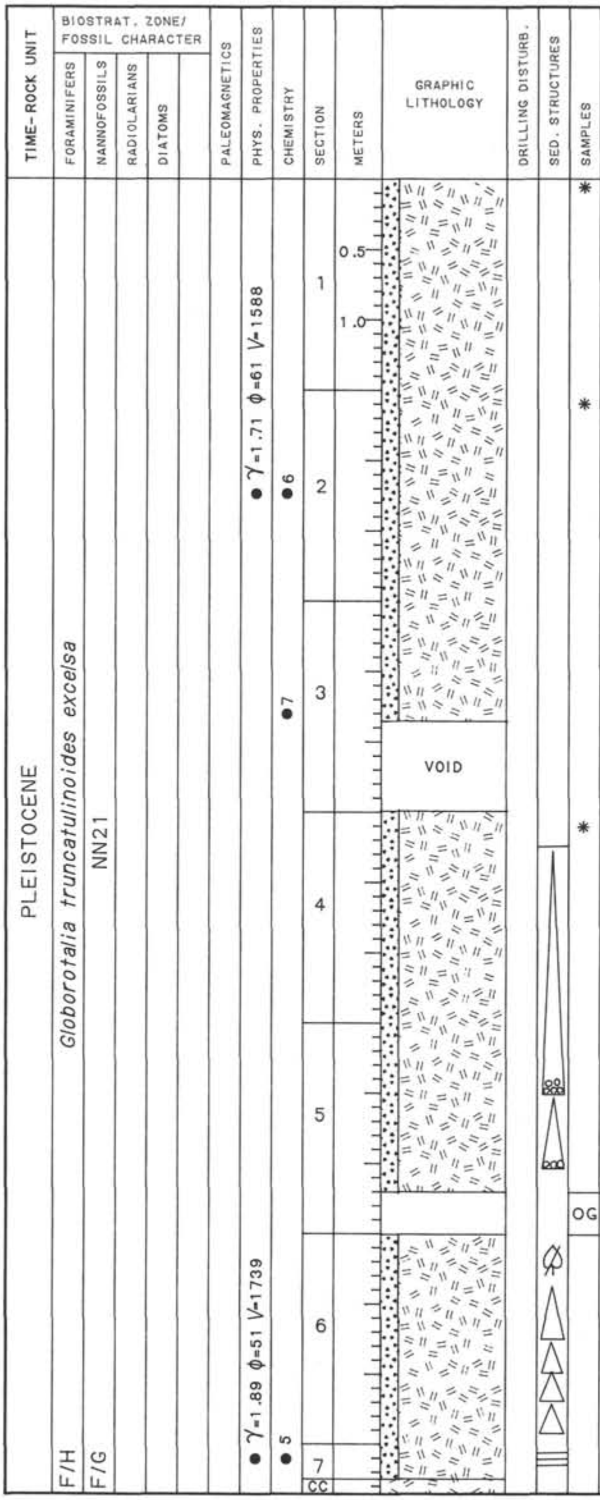

LITHOLOGIC DESCRIPTION

VOLCANICLASTIC SAND and SILT

Volcaniclastic sand and silt, dark olive-gray (5Y 3/2) to olive-gray (5Y 5/2), fining upward sequence; Sections 1–3, homogeneous fine sand and silt, Sections 4–6, thin to very thick (20–150 cm) normally graded beds, pumice fragments as large as 9 mm, grading upward into fine sand; wood fragment in Section 6, 20 cm.

SMEAR SLIDE SUMMARY (%):

	1, 10 D	2, 10 D	4, 10 D
TEXTURE:			
Sand	10	50	50
Silt	80	40	40
Clay	10	10	10
COMPOSITION:			
Quartz	Tr	10	10
Feldspar	Tr	5	10
Mica	Tr	5	5
Clay	20	—	5
Volcanic glass	40	45	50
Calcite/dolomite	—	Tr	—
Pyroxene (orth.)	10	10	—
Zeolite	5	Tr	Tr
Foraminifers	5	10	5
Nannofossils	20	5	10
Sponge spicules	—	5	Tr
Micrite	Tr	5	5

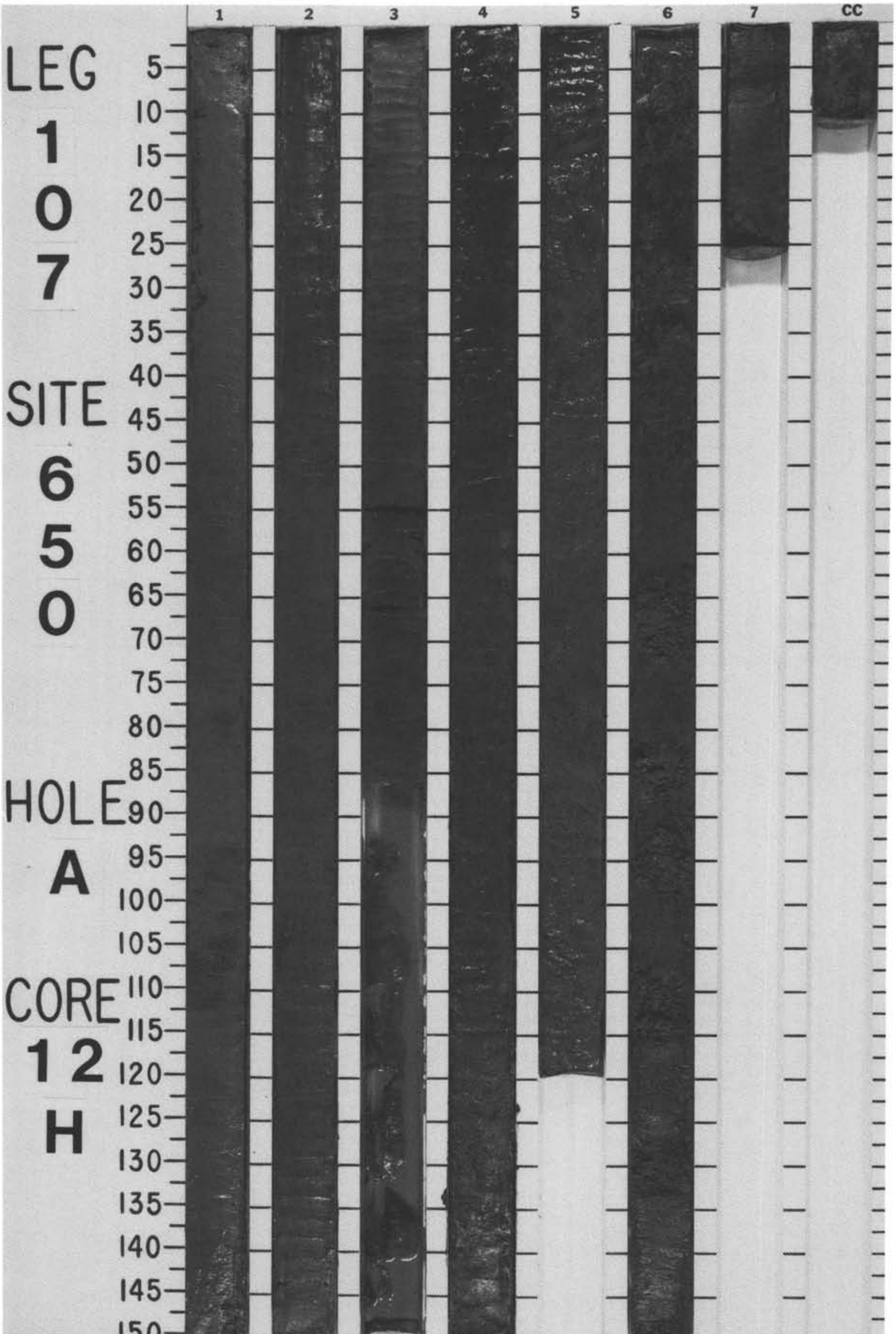
LEG
1
0
7
SITE
6
5
0
HOLE
A
CORE
12
H
1
2
3
4
5
6
7
CC
5
10
15
20
25
30
35
40
45
50
55
60
65
70
75
80
85
90
95
100
105
110
115
120
125
130
135
140
145
150

SITE 650 HOLE A CORE 13 H CORED INTERVAL 3626.0-3635.7 mbsl; 109.7-119.4 mbsf

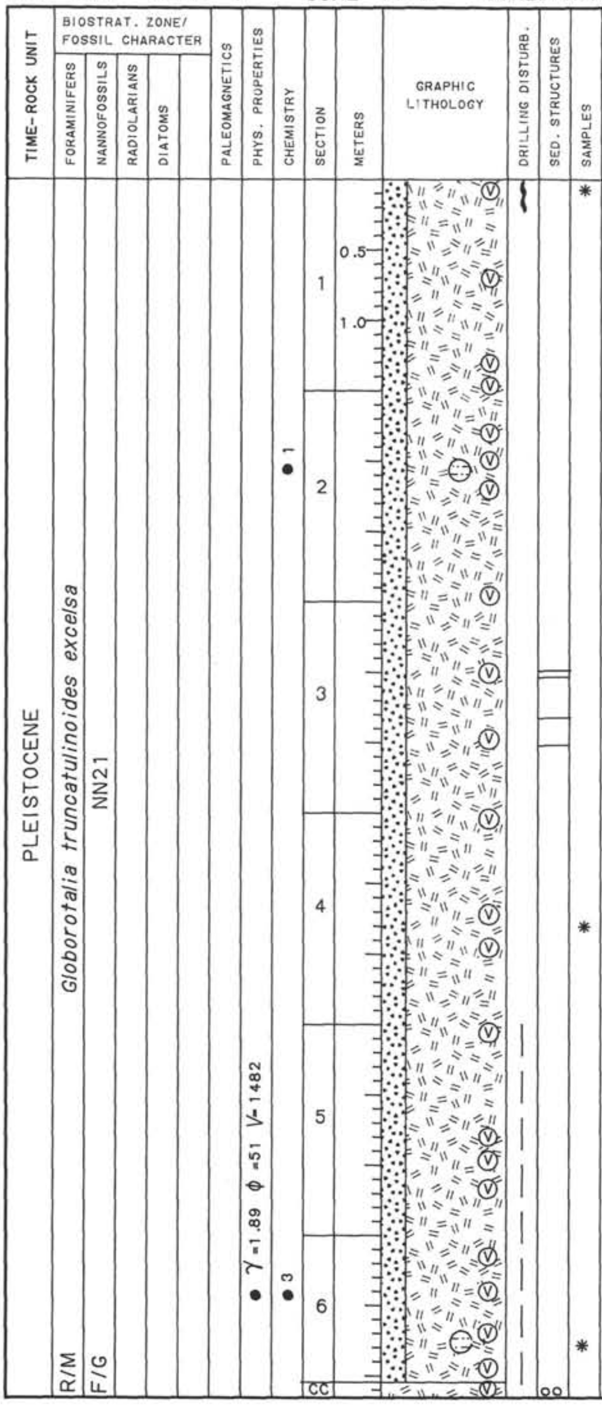

LITHOLOGIC DESCRIPTION

VOLCANICLASTIC SAND

Volcaniclastic sand, dark gray (5Y 4/1) to olive-gray (5Y 5/2), poorly bedded to homogeneous, numerous pumice fragments as large as 2 cm; mud pebbles in Section 4, 72 cm, and in Section 6, 80 cm.

SMEAR SLIDE SUMMARY (%):

	1, 10 D	4, 80 D	6, 80 D
TEXTURE:			
Sand	50	70	60
Silt	15	10	10
Clay	35	20	30
COMPOSITION:			
Quartz	5	10	5
Feldspar	10	10	10
Mica	5	5	5
Clay	10	—	5
Volcanic glass	25	30	30
Accessory minerals	20	—	25
Pyroxene	—	35	—
Zeolite	—	—	Tr
Foraminifers	5	5	5
Nannofossils	10	5	10
Micrite	10	—	5

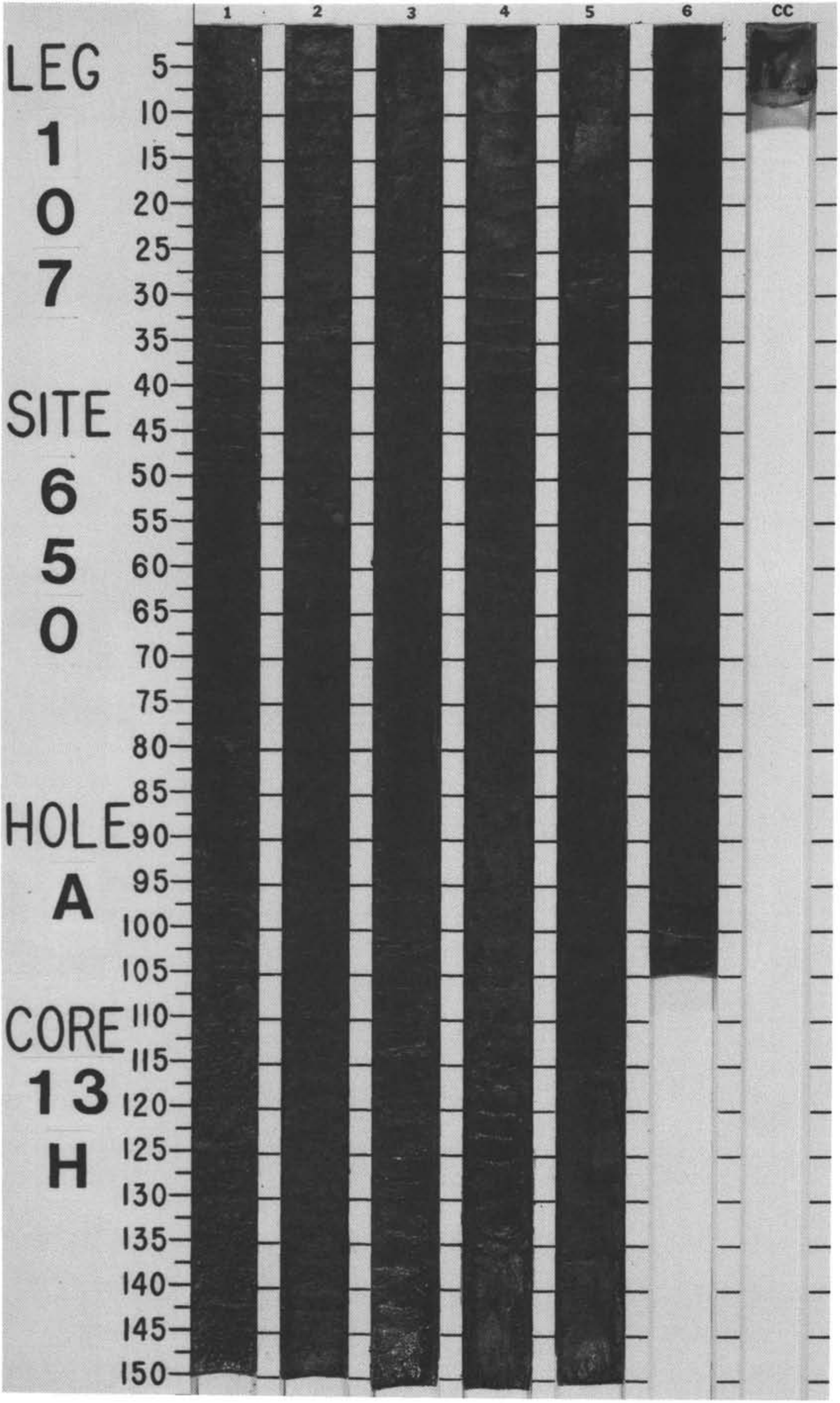
LEG
1
0
7
SITE
6
5
0
HOLE
A
CORE
13
H
1
2
3
4
5
6
CC

SITE 650 HOLE A CORE 14 X CORED INTERVAL 3635.7-3648.4 mbsl; 119.4-132.1 mbsf

TIME-ROCK UNIT	FORAMINIFERS	NANNOFOSSILS	RADIOLARIANS	DIATOMS	PALEOMAGNETICS	PHYS. PROPERTIES	CHEMISTRY	SECTION	METERS	GRAPHIC LITHOLOGY	DRILLING DISTURB.	SED. STRUCTURES	SAMPLES
PLEISTOCENE	R/G *Globorotalia truncatulinoides excelsa*	F/G NN21						CC		V			*

LITHOLOGIC DESCRIPTION

VOLCANICLASTIC SAND

Volcaniclastic sand, very dark gray (5Y 3/1), homogeneous, coarse-grained.

SMEAR SLIDE SUMMARY (%):

	CC, 0 D
TEXTURE:	
Sand	65
Silt	5
Clay	30
COMPOSITION:	
Quartz	10
Feldspar	15
Clay	10
Volcanic glass	25
Accessory minerals	30
Foraminifers	Tr
Nannofossils	5
Micrite	5

SITE 650 HOLE A CORE 15X CORED INTERVAL 3648.4-3658.0 mbsl; 132.1-141.7 mbsf

TIME-ROCK UNIT	FORAMINIFERS	NANNOFOSSILS	RADIOLARIANS	DIATOMS	PALEOMAGNETICS	PHYS. PROPERTIES	CHEMISTRY	SECTION	METERS	GRAPHIC LITHOLOGY	DRILLING DISTURB.	SED. STRUCTURES	SAMPLES
PLEISTOCENE	*Globorotalia truncatulinoides excelsa*	NN21			Brunhes	• γ=1.60 ϕ=68	•14 •15 14 •	1, 2, 3, CC	0.5, 1.0	C, VOID, C, VOID, C			*, IW

LITHOLOGIC DESCRIPTION

CALCAREOUS MUD

Calcareous mud, olive-gray (5Y 4/2–5/2), homogeneous to faintly laminated.

SMEAR SLIDE SUMMARY (%):

	2, 50 D
TEXTURE:	
Sand	—
Silt	5
Clay	95
COMPOSITION:	
Quartz	5
Clay	35
Accessory minerals	5
Zeolite	Tr
Foraminifers	Tr
Nannofossils	25
Sponge spicules	Tr
Micrite	30

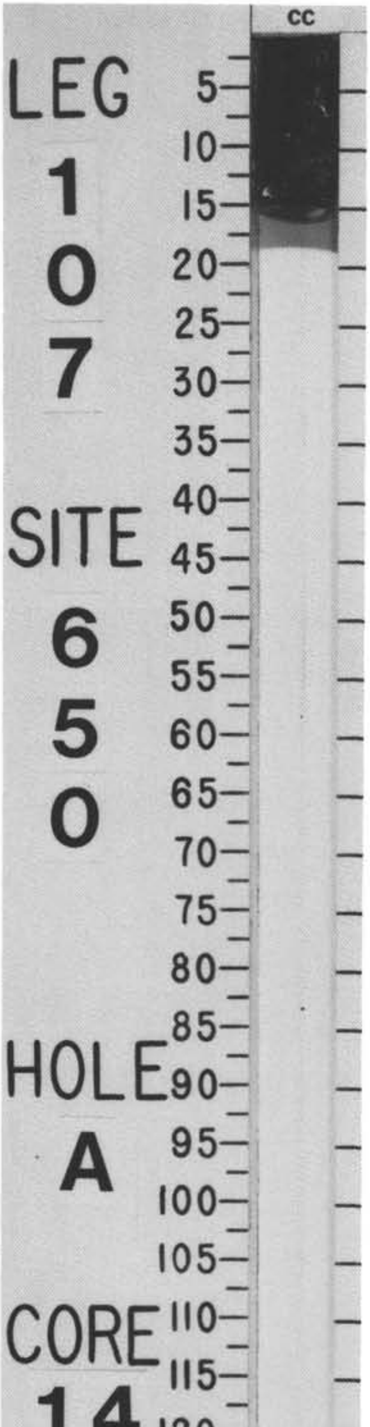
CC
LEG
1
0
7
SITE
6
5
0
HOLE
A
CORE
14
X

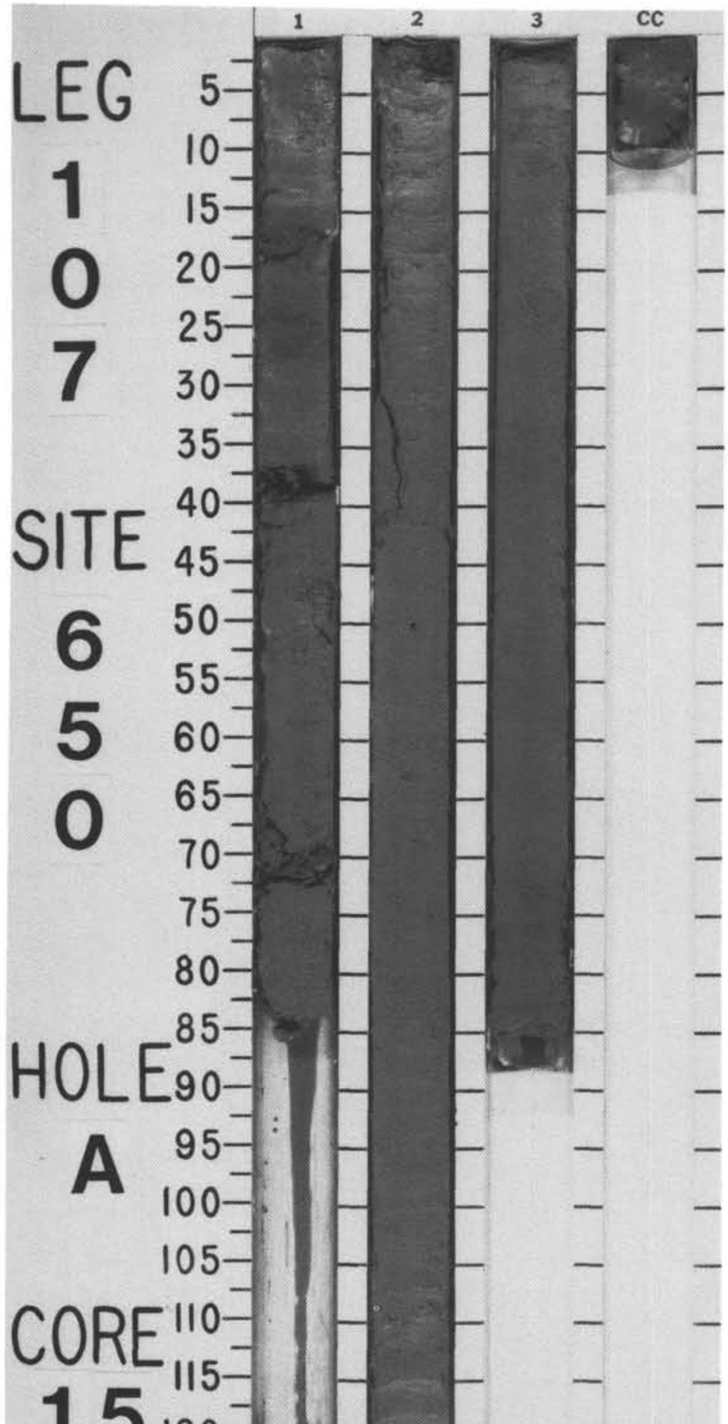
1
2
3
CC
LEG
1
0
7
SITE
6
5
0
HOLE
A
CORE
15
X

SITE 650 HOLE A CORE 16 X CORED INTERVAL 3658.0-3667.6 mbsl; 141.7-151.3 mbsf

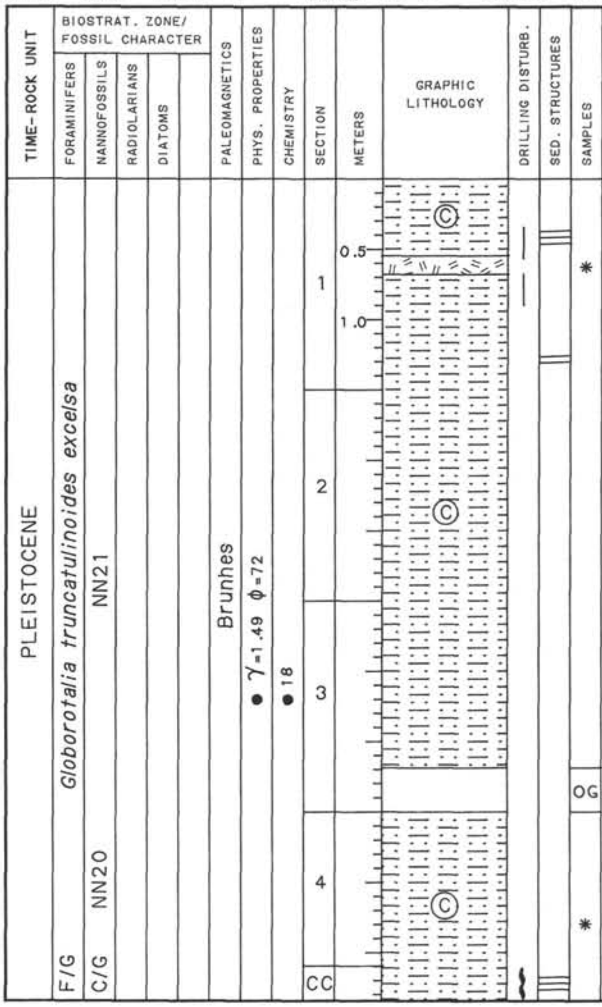

LITHOLOGIC DESCRIPTION

CALCAREOUS MUD and VOLCANICLASTIC SILT

Calcareous mud, olive-gray (5Y 4/2–5/2), homogeneous to faintly laminated.

Volcaniclastic silt, olive (5Y 4/3) in Section 1, 55–70 cm.

SMEAR SLIDE SUMMARY (%):

	1, 60 M	4, 85 D
TEXTURE:		
Sand	10	5
Silt	50	20
Clay	40	75
COMPOSITION:		
Quartz	10	5
Feldspar	1	—
Rock fragments	1	—
Mica	1	1
Clay	57	33
Volcanic glass	5	5
Accessory minerals	5	5
Zeolite	—	1
Foraminifers	1	1
Nannofossils	5	25
Diatoms	—	1
Micrite	14	23

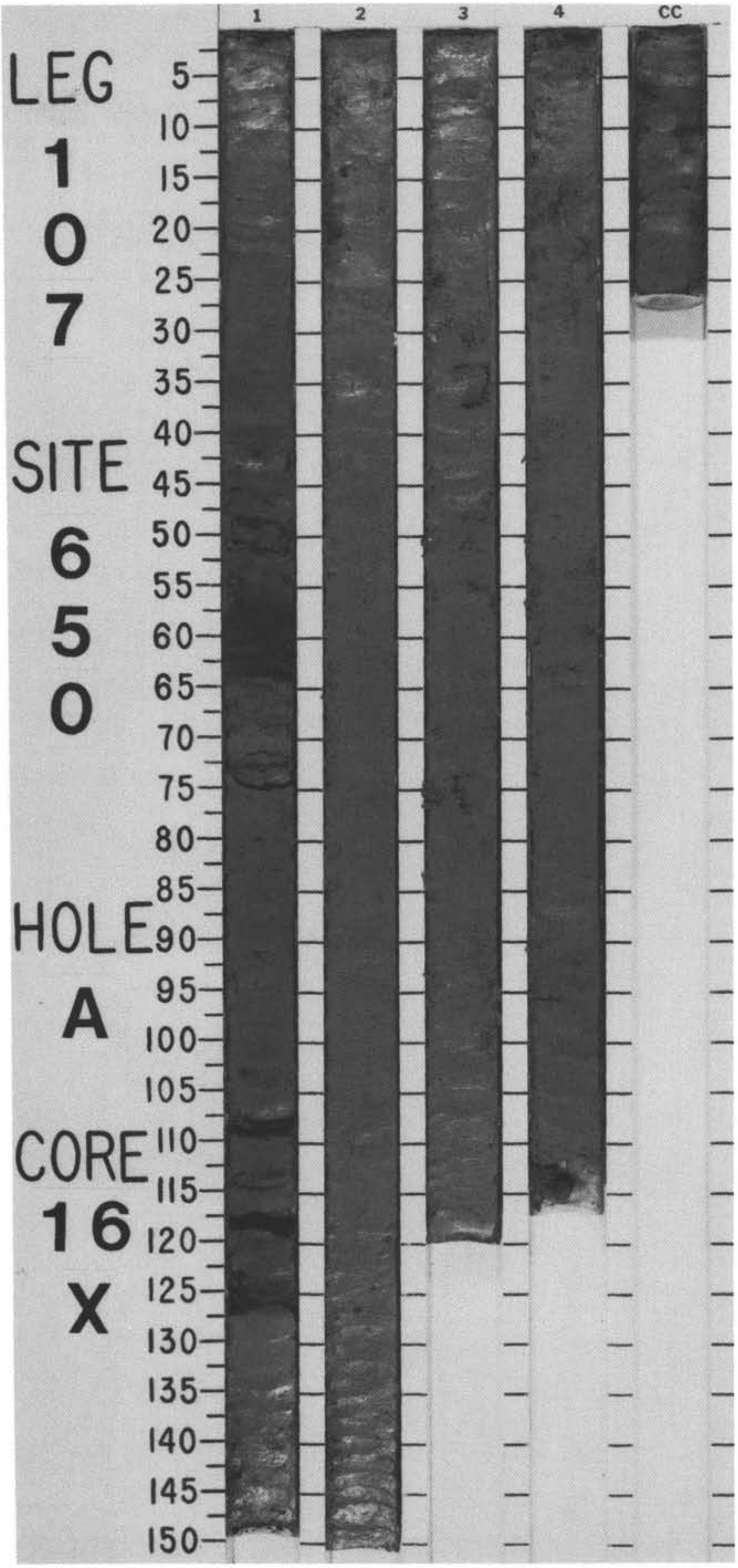
LEG 107
SITE 650
HOLE A
CORE 16 X
1
2
3
4
CC
5
10
15
20
25
30
35
40
45
50
55
60
65
70
75
80
85
90
95
100
105
110
115
120
125
130
135
140
145
150

SITE 650 HOLE A CORE 17 X CORED INTERVAL 3667.6-3676.8 mbsl; 151.3-160.5 mbsf

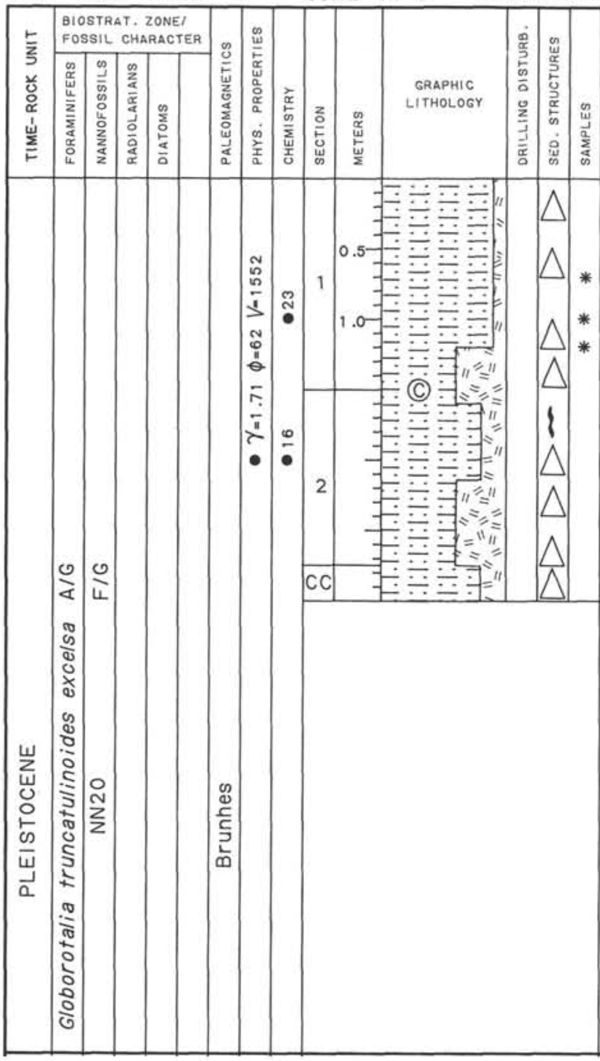

LITHOLOGIC DESCRIPTION

CALCAREOUS MUD alternating with VOLCANICLASTIC SAND

Calcareous mud, gray (5Y 5/1–6/1), thin beds (5–40 cm), homogeneous to faintly laminated.

Volcaniclastic sand, dark gray (5Y 4/1), very thin to thin (3–15 cm) normally graded beds, numerous pumice fragments.

SMEAR SLIDE SUMMARY (%):

	1, 72 M	1, 100 D	1, 121 D
TEXTURE:			
Sand	60	—	3
Silt	15	15	57
Clay	25	85	40
COMPOSITION:			
Quartz	20	1	5
Feldspar	5	—	5
Rock fragments	1	—	—
Mica	1	—	—
Clay	35	20	60
Volcanic glass	5	5	10
Calcite/dolomite	—	—	20
Accessory minerals	5	1	—
Foraminifers	5	1	—
Nannofossils	10	31	—
Diatoms	2	1	—
Micrite	11	40	—

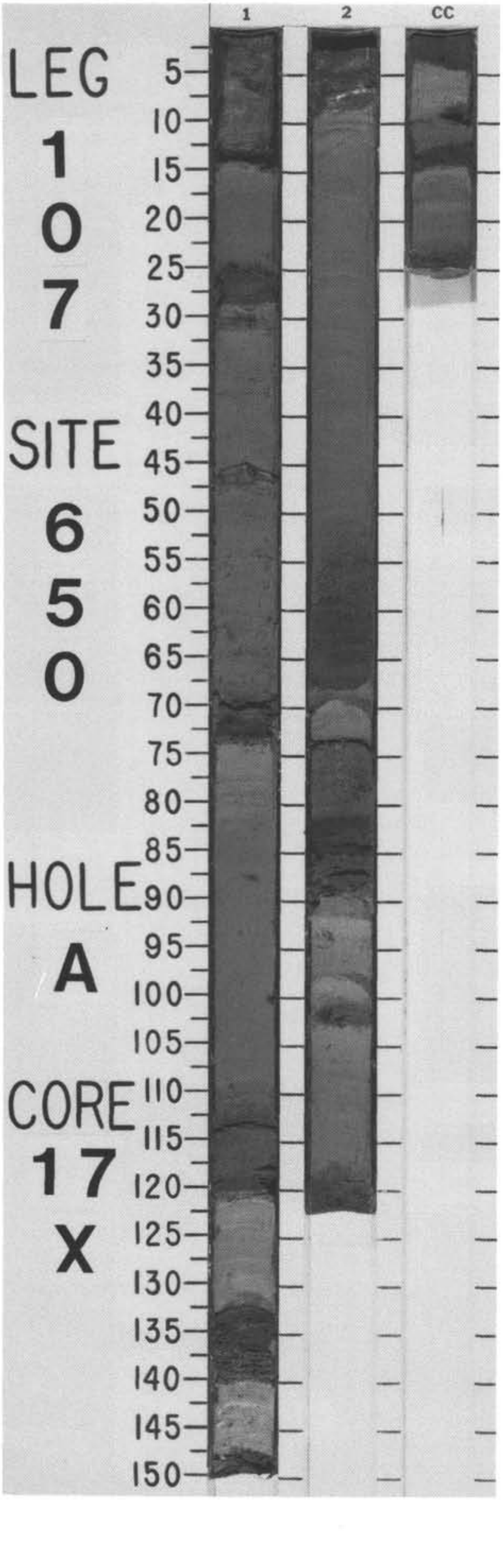
LEG
107
SITE
650
HOLE
A
CORE
17
X
1
2
CC

SITE 650 HOLE A CORE 18 X CORED INTERVAL 3676.8-3686.5 mbsl; 160.5-170.2 mbsf

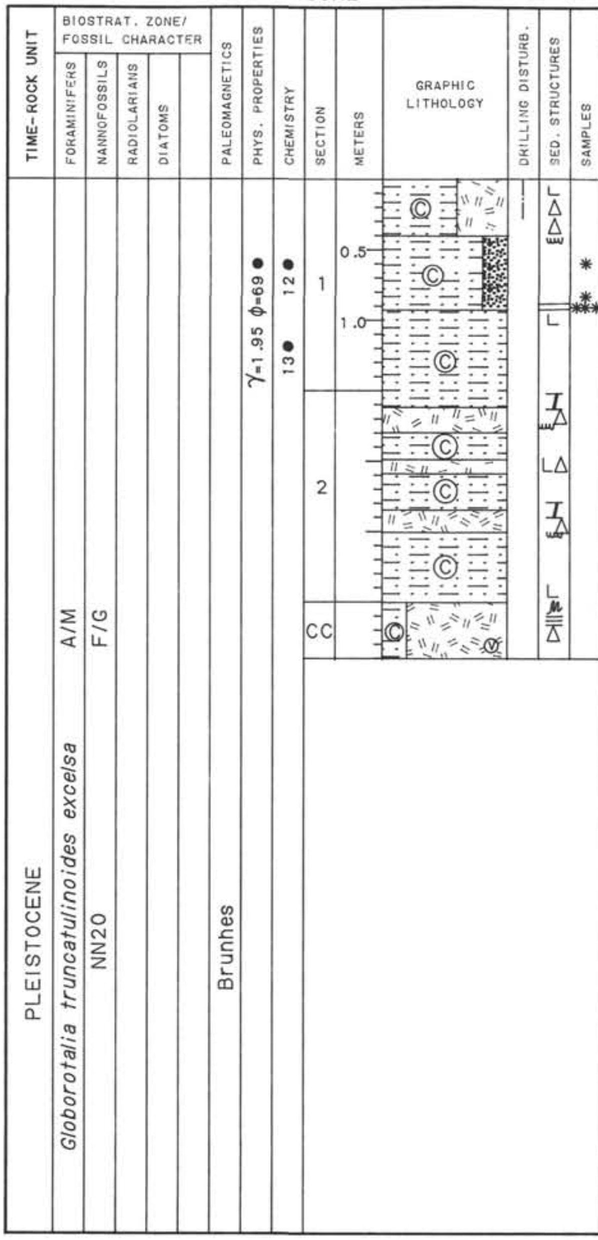

LITHOLOGIC DESCRIPTION

CALCAREOUS MUD alternating with VOLCANICLASTIC SAND

Calcareous mud, dark gray (5Y 4/1) to gray (5Y 5/1), thin beds (15–60 cm).

Volcaniclastic sand, black (5Y 2.5/1) to dark olive-gray (5Y 3/2), thin (5–15 cm) normally graded beds, commonly overlying scoured surfaces, parallel to micro-cross-laminations; pumice fragments as large as 2 cm in CC, 35–40 cm.

Minor lithology: calcareous mudstone, indurated calcareous mud (possibly hardgrounds) at the top of mud/sand depositional packages in Section 1, 10–13, 92–93, and 97–97.5 cm, and in Section 2, 49–51 and 148–150 cm.

SMEAR SLIDE SUMMARY (%):

	1, 63 D	1, 90 M	1, 94 M	1, 96.5 M	1, 98 M
TEXTURE:					
Sand	5	40	5	15	5
Silt	20	60	15	40	10
Clay	75	—	80	45	85
COMPOSITION:					
Quartz	3	20	5	10	2
Feldspar	5	30	5	15	2
Rock fragments	Tr	10	—	—	—
Mica	2	10	—	6	—
Clay	62	—	55	37	11
Volcanic glass	5	5	—	—	—
Calcite/dolomite	10	5	15	10	—
Accessory minerals	Tr	5	—	10	—
Opaques	—	10	—	—	—
Foraminifers	2	5	5	1	5
Nannofossils	10	—	15	10	50
Radiolarians	1	—	Tr	1	—
Sponge spicules	—	—	Tr	—	—
Micrite	—	—	—	—	30

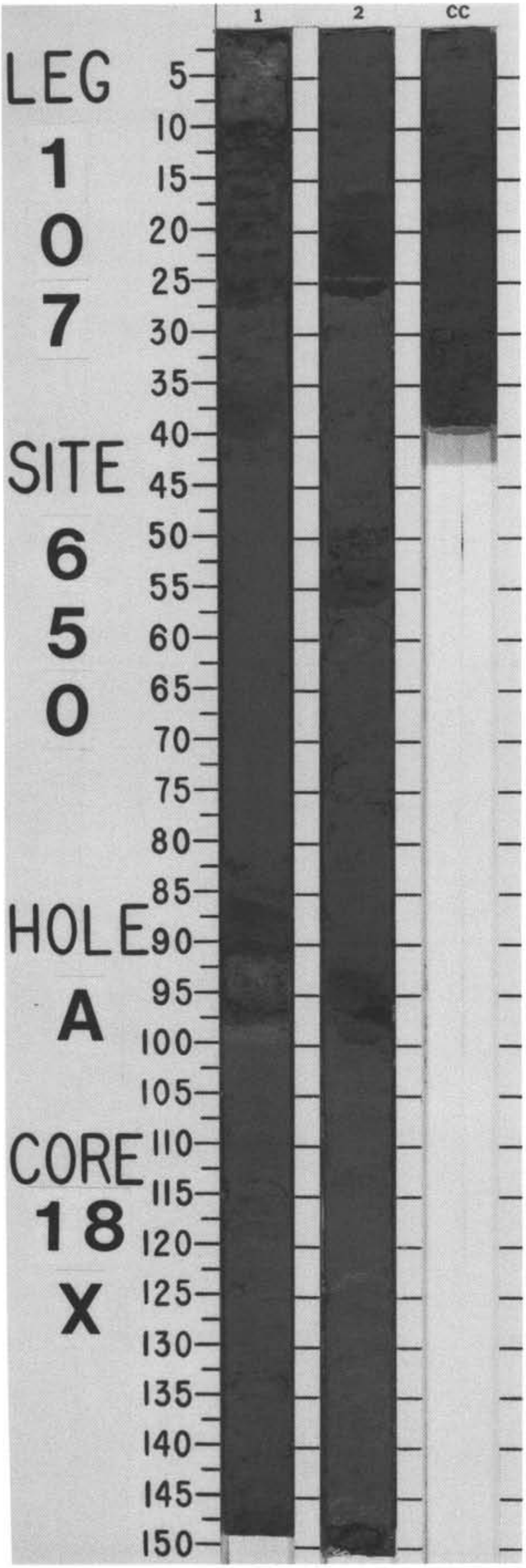
LEG
1
0
7
SITE
6
5
0
HOLE
A
CORE
18
X
1
2
CC

SITE 650 HOLE A CORE 19 X CORED INTERVAL 3686.5-3696.1 mbsl; 170.2-179.8 mbsf

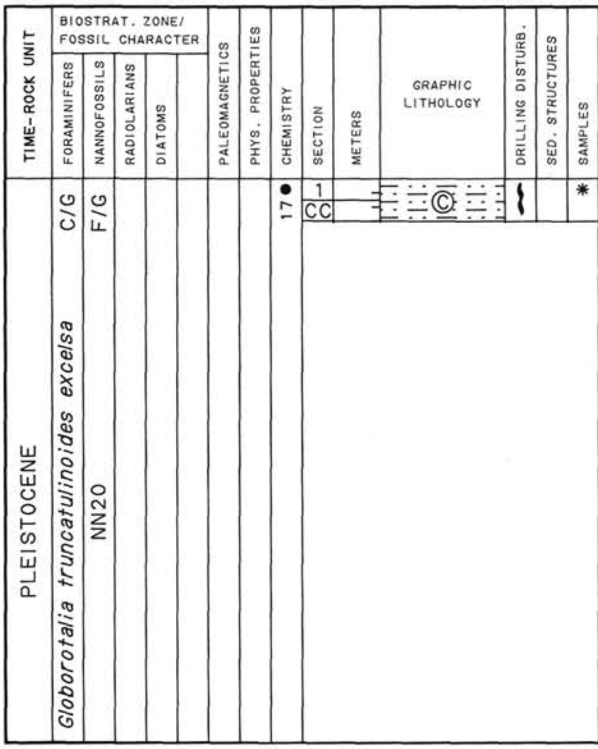

LITHOLOGIC DESCRIPTION

CALCAREOUS MUD

Calcareous mud, dark gray (5Y 4/1) to gray (5Y 5/1).

SMEAR SLIDE SUMMARY (%):

	1, 14
	D
TEXTURE:	
Sand	5
Silt	25
Clay	70
COMPOSITION:	
Quartz	5
Feldspar	5
Rock fragments	Tr
Mica	2
Clay	48
Volcanic glass	5
Calcite/dolomite	10
Foraminifers	8
Nannofossils	15
Radiolarians	2

SITE 650 HOLE A CORE 20 X CORED INTERVAL 3696.1-3705.8 mbsl; 179.8-189.5 mbsf

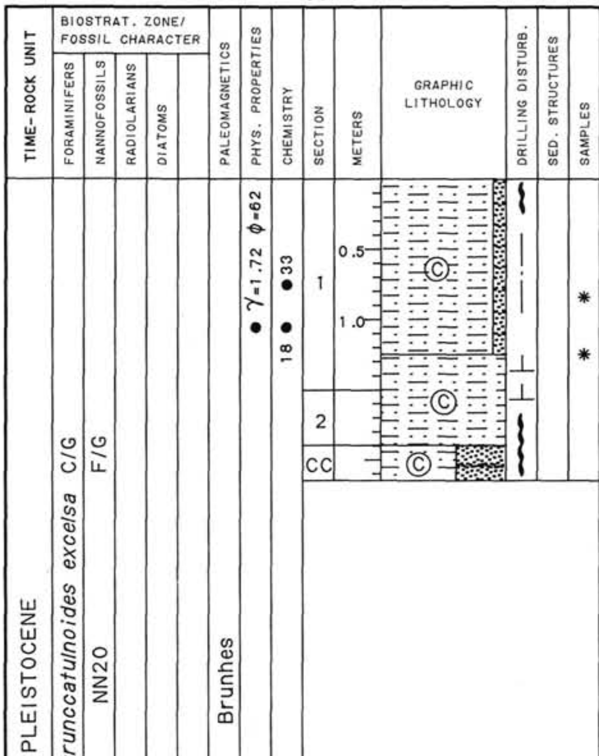

LITHOLOGIC DESCRIPTION

CALCAREOUS MUD (MUDSTONE), SAND, and SILT

Calcareous mud (mudstone), dark gray (5Y 4/1–5/2); degree of induration increases below Section 1, 128 cm.

Sand and silt, very dark gray (5Y 3/1) to dark gray (5Y 4/1), very thin beds (2–5 cm), very fine grained, feldspathic in Section 1, 62–65 and 119–124 cm, and in CC, 17–21 cm.

SMEAR SLIDE SUMMARY (%):

	1, 81	1, 124
	D	M
TEXTURE:		
Sand	10	70
Silt	10	20
Clay	80	10
COMPOSITION:		
Quartz	4	30
Feldspar	3	40
Rock fragments	3	2
Mica	Tr	3
Clay	49	—
Calcite/dolomite	5	5
Accessory minerals	—	5
Glauconite/celadonite	Tr	—
Opaques	—	5
Foraminifers	10	7
Nannofossils	25	—
Radiolarians	1	3

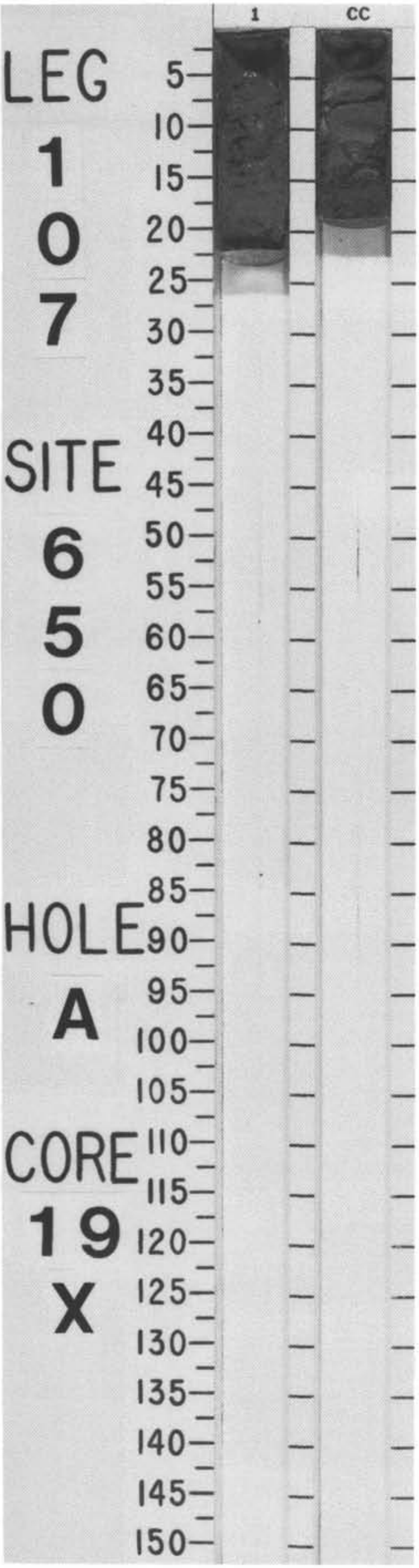
1
CC
LEG 107
SITE 650
HOLE A
CORE 19 X

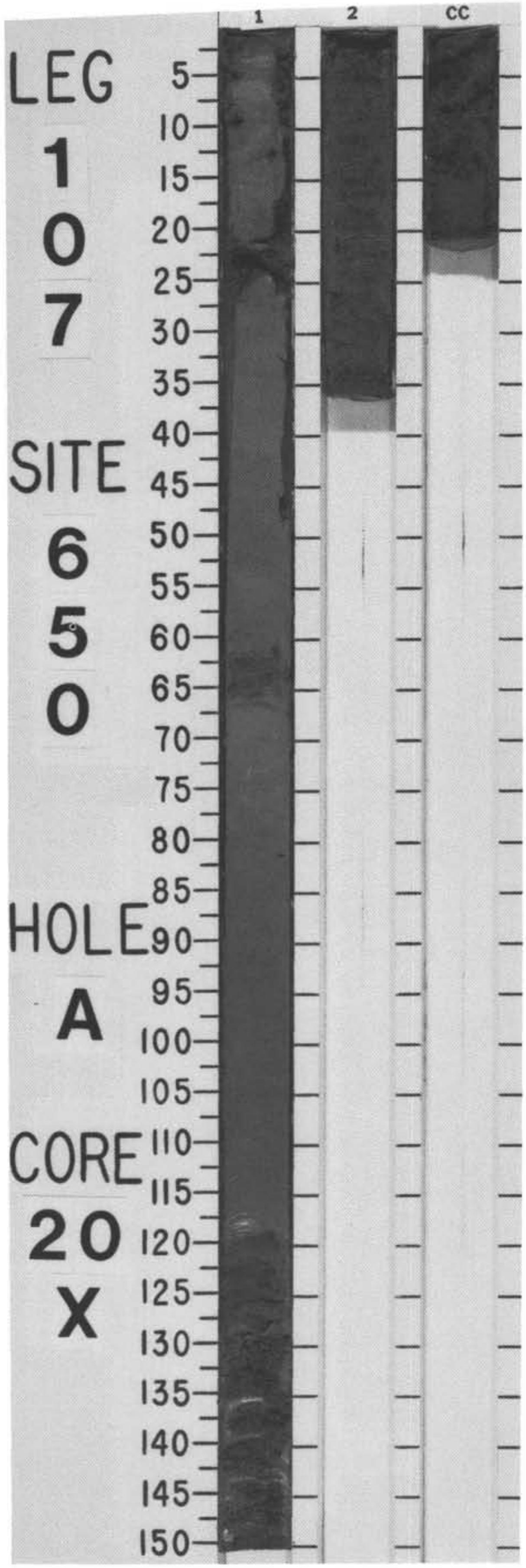
1
2
CC
LEG 107
SITE 650
HOLE A
CORE 20 X

SITE 650 HOLE A CORE 21 X CORED INTERVAL 3705.8-3715.5 mbsl; 189.5-199.2 mbsf

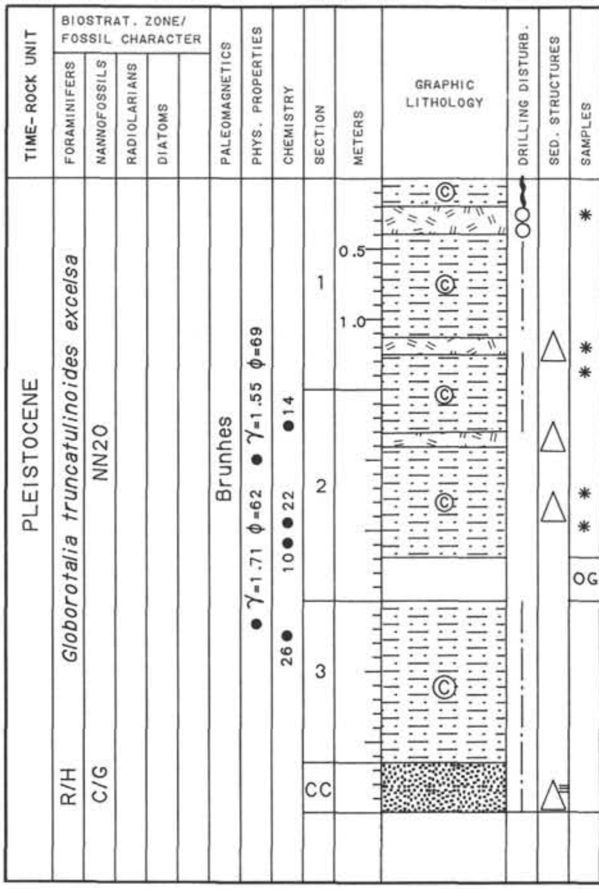

LITHOLOGIC DESCRIPTION

CALCARL OUS MUD alternating with SILT and SAND representing several mud/sand depositional packages

Calcareous mud, dark gray (5Y 4/1) to olive (5Y 5/3), thin to thick beds (50–120 cm), generally disturbed by drilling.

Silt and sand, black (5Y 2.5/1) to olive-gray (5Y 5/2); thin (10–20 cm), normally graded beds overlying sharp scoured surfaces, upper part commonly cross-bedded.

SMEAR SLIDE SUMMARY (%):

	1, 29 D	1, 122 D	1, 140 D	2, 79 D	2, 99 D
TEXTURE:					
Sand	30	50	5	8	—
Silt	50	35	20	25	10
Clay	20	15	75	67	90
COMPOSITION:					
Quartz	20	8	6	6	3
Feldspar	5	5	3	4	3
Rock fragments	20	—	—	—	—
Mica	—	3	—	—	—
Clay	16	10	67	69	52
Volcanic glass	20	45	—	—	—
Calcite/dolomite	10	5	10	10	10
Accessory minerals	3	5	—	—	—
Opaques	—	10	2	—	—
Foraminifers	Tr	3	2	6	2
Nannofossils	5	5	10	5	30
Radiolarians	—	1	Tr	Tr	Tr
Sponge spicules	1	—	—	—	—

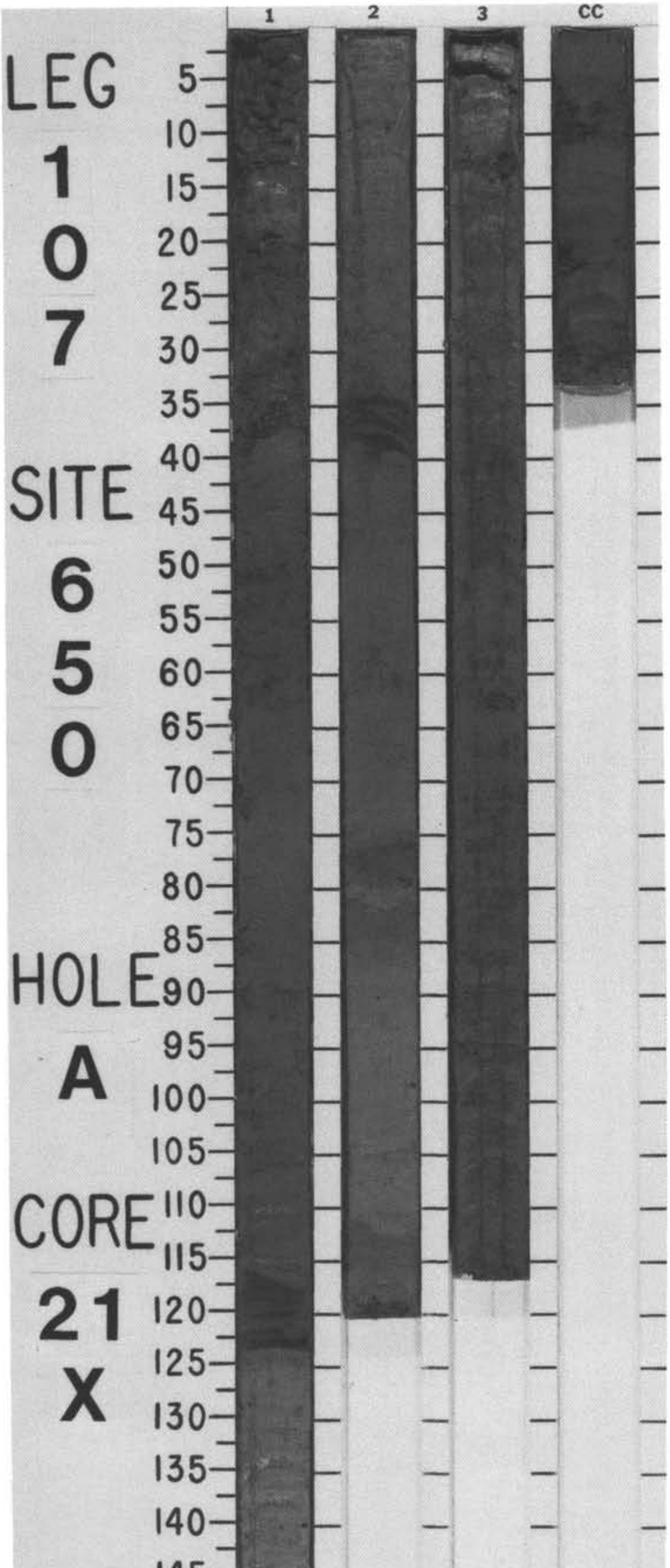
LEG 1 0 7
SITE 6 5 0
HOLE A
CORE 21 X
1
2
3
CC
5
10
15
20
25
30
35
40
45
50
55
60
65
70
75
80
85
90
95
100
105
110
115
120
125
130
135
140
145
150

SITE 650 HOLE A CORE 22 X CORED INTERVAL 3715.5-3725.2 mbsl; 199.2-208.9 mbsf

TIME-ROCK UNIT: PLEISTOCENE

BIOSTRAT. ZONE/FOSSIL CHARACTER: Foraminifers: *Globorotalia truncatulinoides excelsa*, R/P; Nannofossils: NN20, F/G

PALEOMAGNETICS: Brunhes

PHYS. PROPERTIES: γ=1.64 ϕ=64 V=1504●

CHEMISTRY: 32●, 10●

SECTION: 1, 2, CC

METERS: 0.5, 1.0

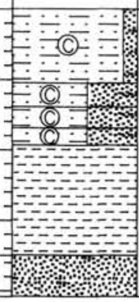

LITHOLOGIC DESCRIPTION

CALCAREOUS CLAY and MUD alternating with SILT and SAND

Calcareous clay and mud, dark gray (5Y 4/1) to olive (5Y 5/3); upper part contains angular clasts (apparently broken by drilling) of indurated mud (possibly hardgrounds).

Silt and sand, black (5Y 2.5/1) to olive-gray (5Y 5/2), normally graded, very fine grained sand to silt.

SMEAR SLIDE SUMMARY (%):

	1, 69 M	1, 115 D
TEXTURE:		
Sand	60	—
Silt	30	10
Clay	10	90
COMPOSITION:		
Quartz	35	4
Feldspar	25	2
Rock fragments	2	—
Mica	6	—
Clay	Tr	50
Volcanic glass	6	—
Calcite/dolomite	6	7
Accessory minerals	3	Tr
Glauconite/celadonite	3	—
Opaques	6	—
Foraminifers	8	5
Nannofossils	Tr	32
Radiolarians	Tr	Tr

SITE 650 HOLE A CORE 23 X CORED INTERVAL 3725.2-3734.9 mbsl; 208.9-218.6 mbsf

TIME-ROCK UNIT: PLEISTOCENE

BIOSTRAT. ZONE/FOSSIL CHARACTER: Foraminifers: *Globorotalia truncatulinoides excelsa*, F/P; Nannofossils: NN20, F/G

PHYS. PROPERTIES: γ=1.73 ϕ=58 V=2239●

CHEMISTRY: 9●

SECTION: 1, CC

LITHOLOGIC DESCRIPTION

CLAYSTONE

Claystone, olive-gray (5Y 4/2) to gray (5Y 5/1), angular clasts floating in a homogeneous matrix (drilling disturbance).

SMEAR SLIDE SUMMARY (%):

	1, 10 D	CC, 26 M
TEXTURE:		
Sand	—	5
Silt	10	5
Clay	90	90
COMPOSITION:		
Quartz	10	6
Feldspar	5	5
Clay	76	76
Volcanic glass	—	4
Calcite/dolomite	4	—
Accessory minerals	—	3
Foraminifers	1	3
Nannofossils	4	3

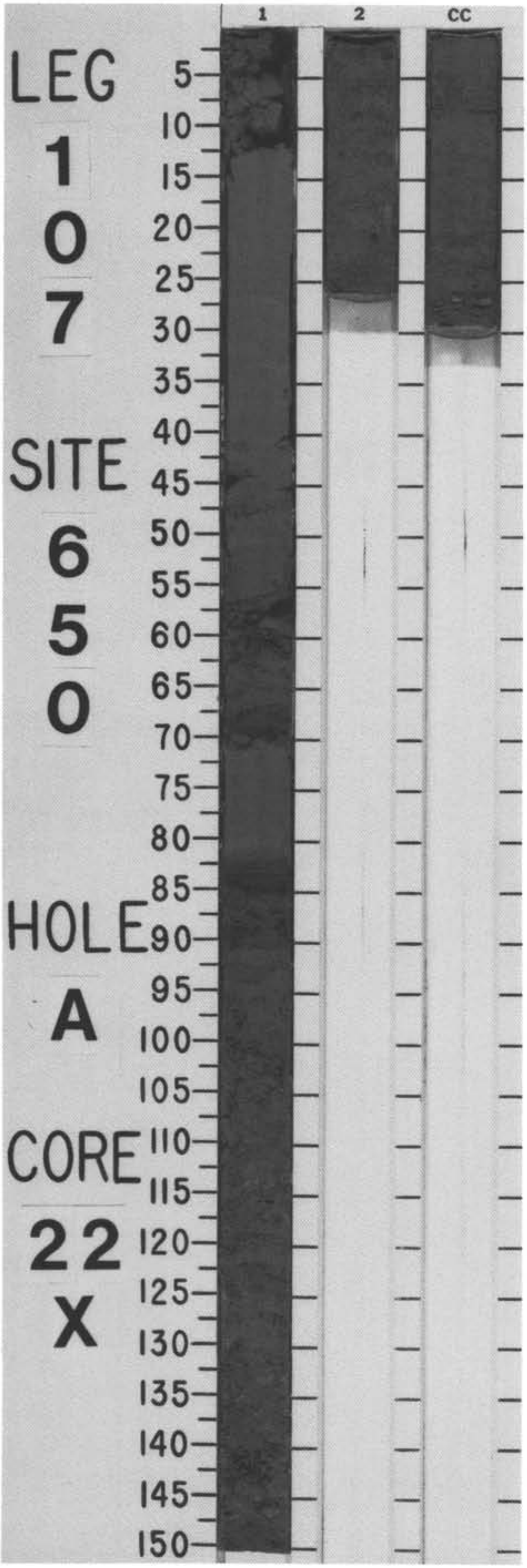
LEG
1
0
7
SITE
6
5
0
HOLE
A
CORE
22
X
1
2
CC

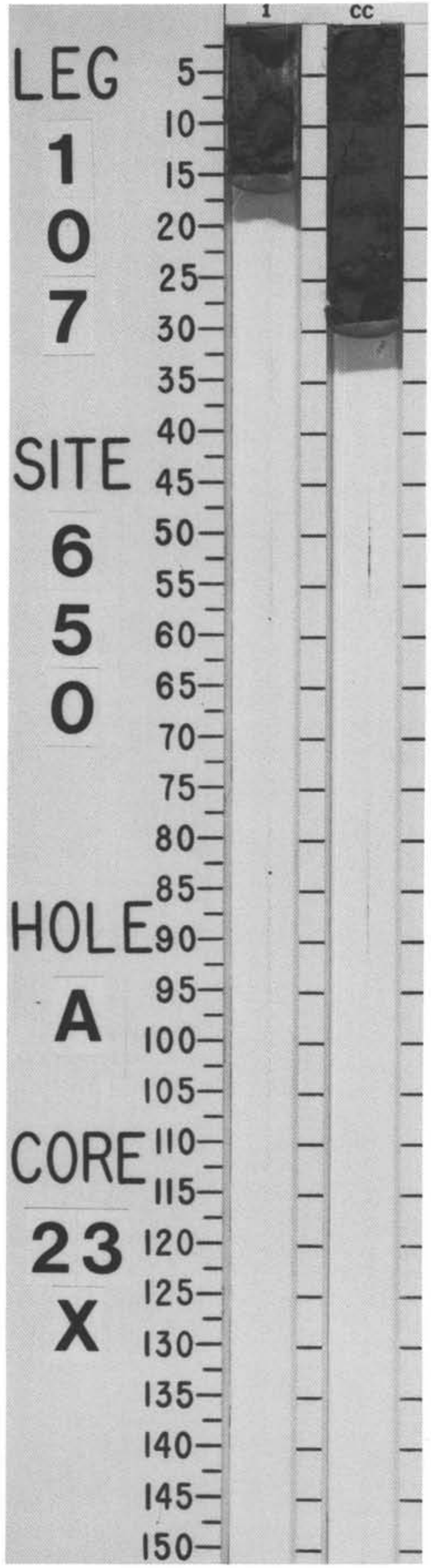
LEG
1
0
7
SITE
6
5
0
HOLE
A
CORE
23
X
1
CC

SITE 650 HOLE A CORE 24 X CORED INTERVAL 3734.9-3744.5 mbsl; 218.6-228.2 mbsf

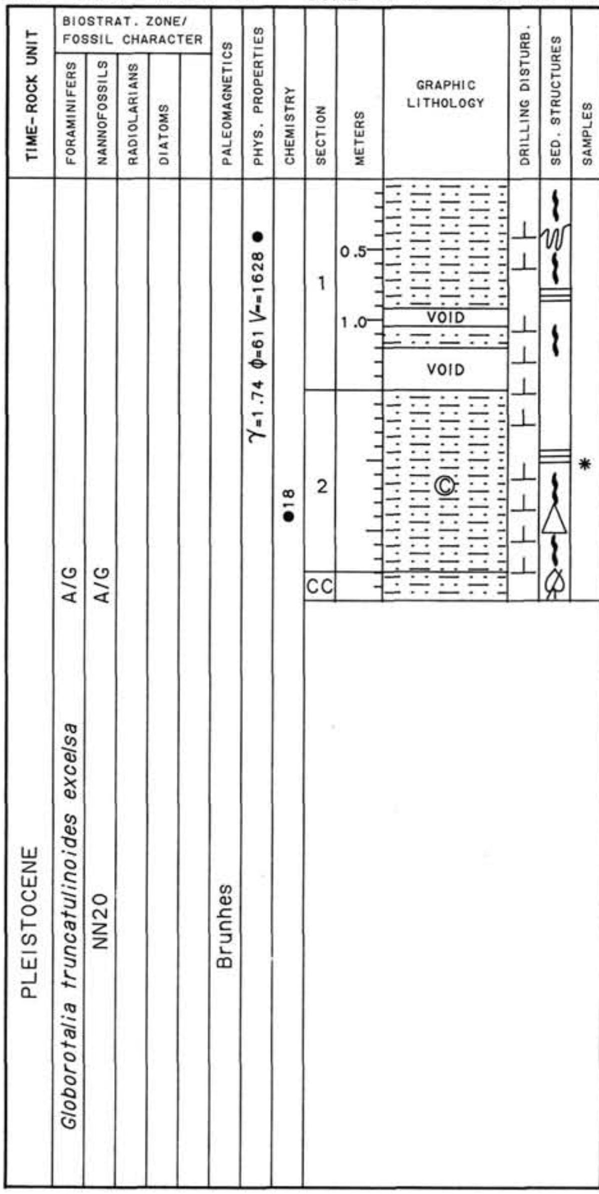

LITHOLOGIC DESCRIPTION

CALCAREOUS MUDSTONE

Calcareous mudstone, olive-gray (5Y 4/2) to gray (5Y 6/1), indurated pieces disturbed into drilling biscuits; coal fragment (centimeter-sized) in CC, 14 cm.

Minor lithology: silt, laminae with sharp upper and lower contacts in Section 2, 43, 90, and 117 cm.

SMEAR SLIDE SUMMARY (%):

	2, 50
	D
TEXTURE:	
Sand	—
Silt	5
Clay	95
COMPOSITION:	
Clay	10
Volcanic glass	5
Calcite/dolomite	Tr
Zeolite	Tr
Foraminifers	5
Nannofossils	40
Micrite	40

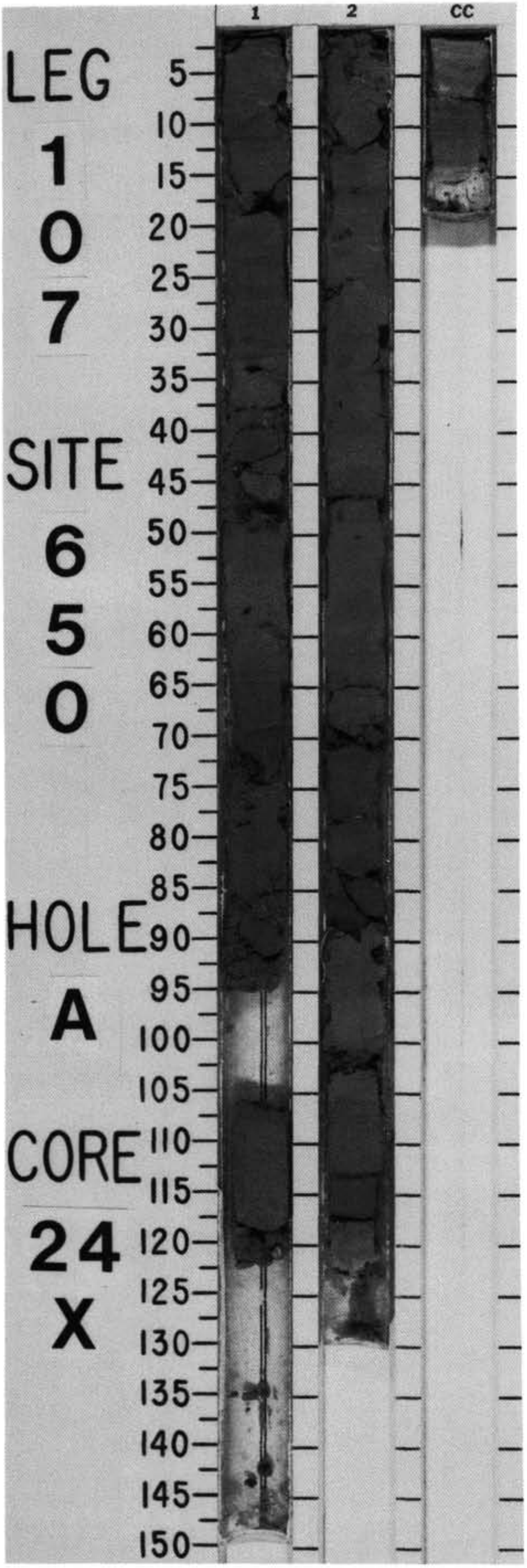
LEG
1
0
7
SITE
6
5
0
HOLE
A
CORE
24
X
1
2
CC

SITE 650 HOLE A CORE 25 X CORED INTERVAL 3744.5-3754.1 mbsl; 228.2-237.8 mbsf

TIME-ROCK UNIT	FORAMINIFERS	NANNOFOSSILS	RADIOLARIANS	DIATOMS	PALEOMAGNETICS	PHYS. PROPERTIES	CHEMISTRY	SECTION	METERS	GRAPHIC LITHOLOGY	DRILLING DISTURB.	SED. STRUCTURES	SAMPLES
PLEISTOCENE	R/M *Globorotalia truncatulinoides excelsa*	F/G NN20			Brunhes	● γ=1.78 φ=68	17●	1, 2, CC	0.5, 1.0	VOID			*, *, IW

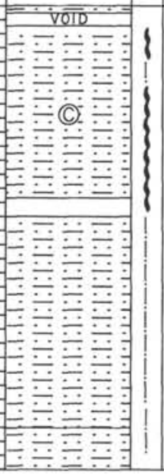

LITHOLOGIC DESCRIPTION

CALCAREOUS MUD

Calcareous mud, dark gray (5Y 4/1) to gray (5Y 6/1), homogeneous.

Minor lithology: wacke, quartzose, arkosic; metasedimentary clast (2.5 x 4.5 x 0.5 cm) in Section 1, 17–19 cm; shear marks in a tectonic fabric (observed in thin section); mechanical grooves from drilling.

SMEAR SLIDE SUMMARY (%):

	1, 6 M	1, 60 D
TEXTURE:		
Sand	1	—
Silt	14	5
Clay	85	95
COMPOSITION:		
Quartz	10	1
Feldspar	1	—
Mica	1	—
Clay	38	29
Volcanic glass	3	—
Accessory minerals	1	—
Foraminifers	1	1
Nannofossils	25	50
Micrite	20	19

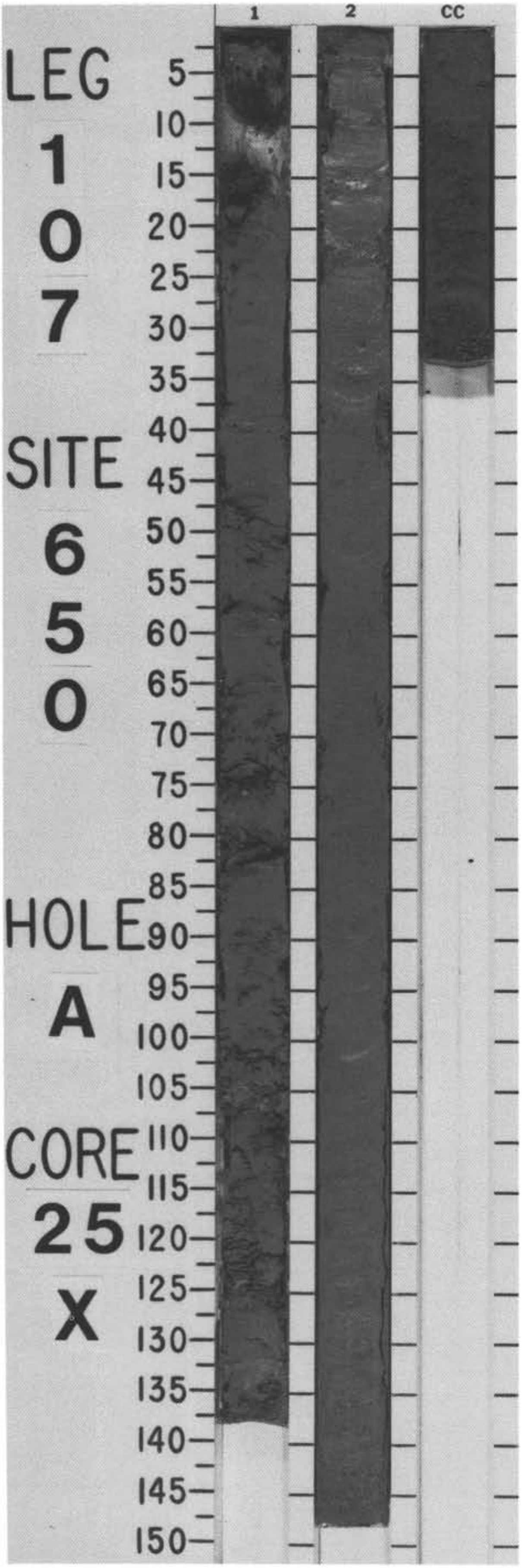
LEG
1
0
7
SITE
6
5
0
HOLE
A
CORE
25
X
1
2
CC
5
10
15
20
25
30
35
40
45
50
55
60
65
70
75
80
85
90
95
100
105
110
115
120
125
130
135
140
145
150

SITE 650 HOLE A CORE 26 X CORED INTERVAL 3754.1-3763.8 mbsl; 237.8-247.5 mbsf

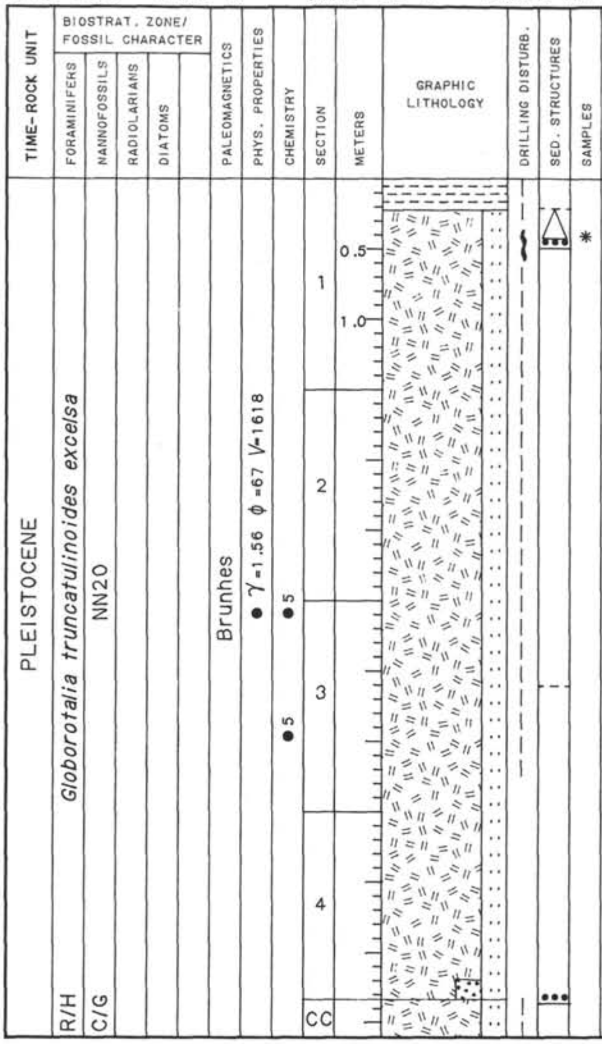

LITHOLOGIC DESCRIPTION

MUD and SANDY MUD

Mud and sandy mud, dark gray (5Y 4/1) to olive-gray (5Y 5/2), very thick, homogeneous sequence, with the exception of two graded units in Section 1, 20–40 cm, and Section 4, 60–130 cm, which are volcaniclastic.

SMEAR SLIDE SUMMARY (%):

	1, 40 M
TEXTURE:	
Sand	30
Silt	60
Clay	10
COMPOSITION:	
Feldspar	10
Volcanic glass	80
Foraminifers	10

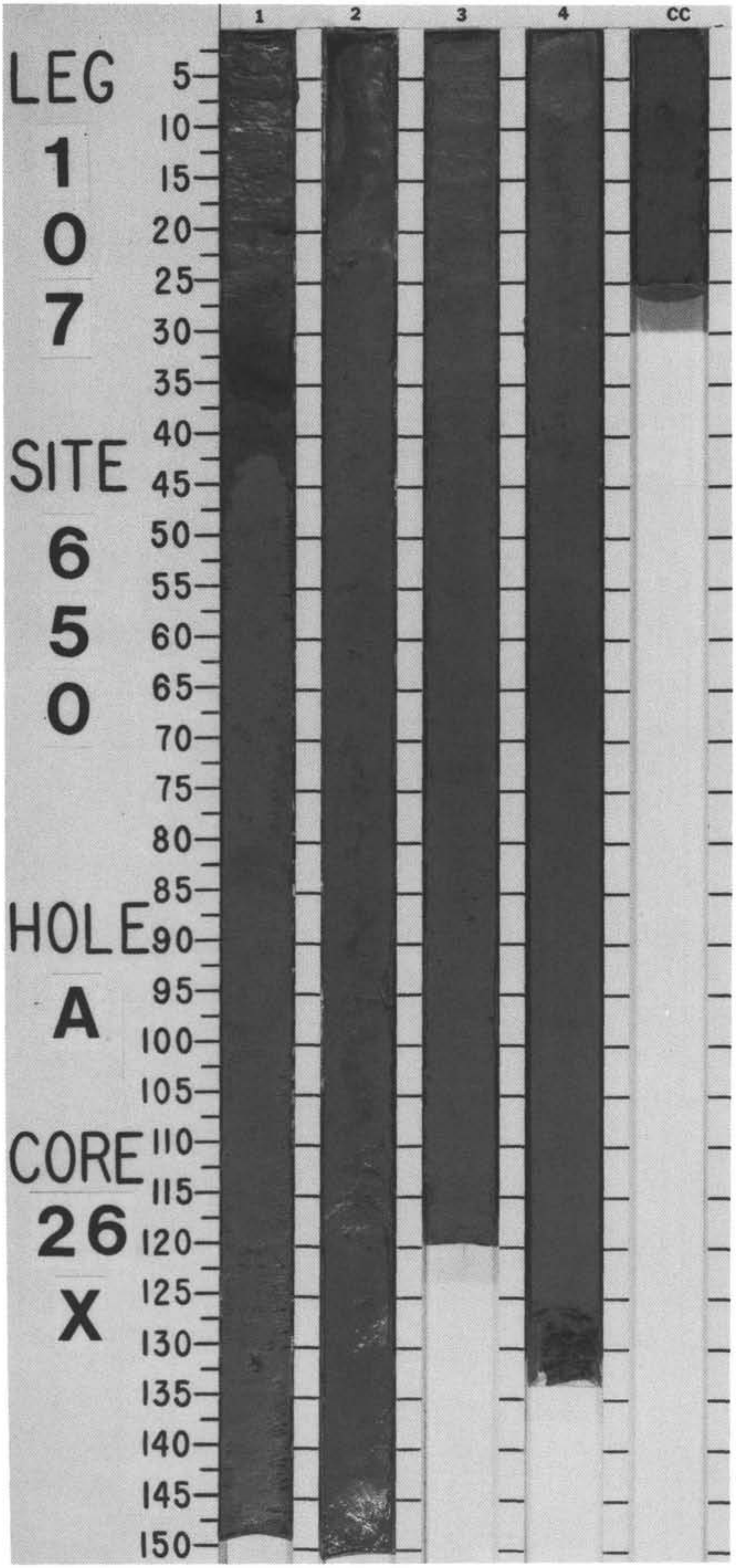
LEG
1
0
7
SITE
6
5
0
HOLE
A
CORE
26
X
1
2
3
4
CC

SITE 650 HOLE A CORE 27 X CORED INTERVAL 3763.8-3773.5 mbsl; 247.5-257.2 mbsf

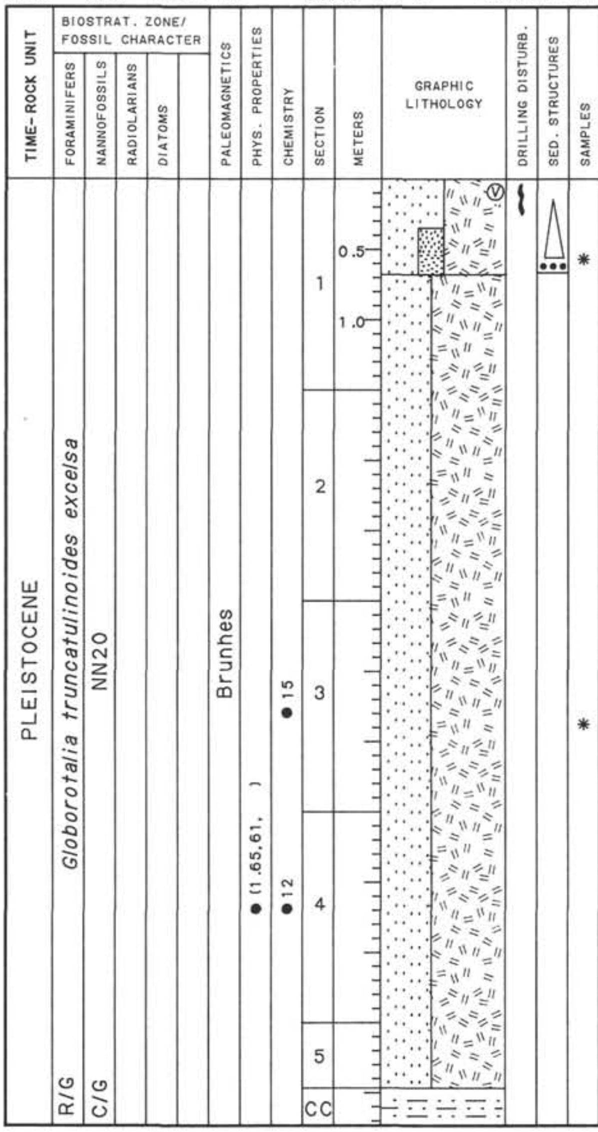

LITHOLOGIC DESCRIPTION

MUD

Mud, gray (5Y 5/1) to light olive-gray (5Y 6/2), homogeneous with exception of normally graded bed in Section 1; high volcanic glass admixture throughout.

SMEAR SLIDE SUMMARY (%):

	1, 65 D	3, 80 D
TEXTURE:		
Sand	50	—
Silt	10	45
Clay	40	55
COMPOSITION:		
Quartz	2	—
Feldspar	3	—
Clay	—	5
Volcanic glass	40	40
Accessory minerals	5	—
Nannofossils	35	40
Diatoms	—	Tr
Micrite	15	15

28X-NO RECOVERY

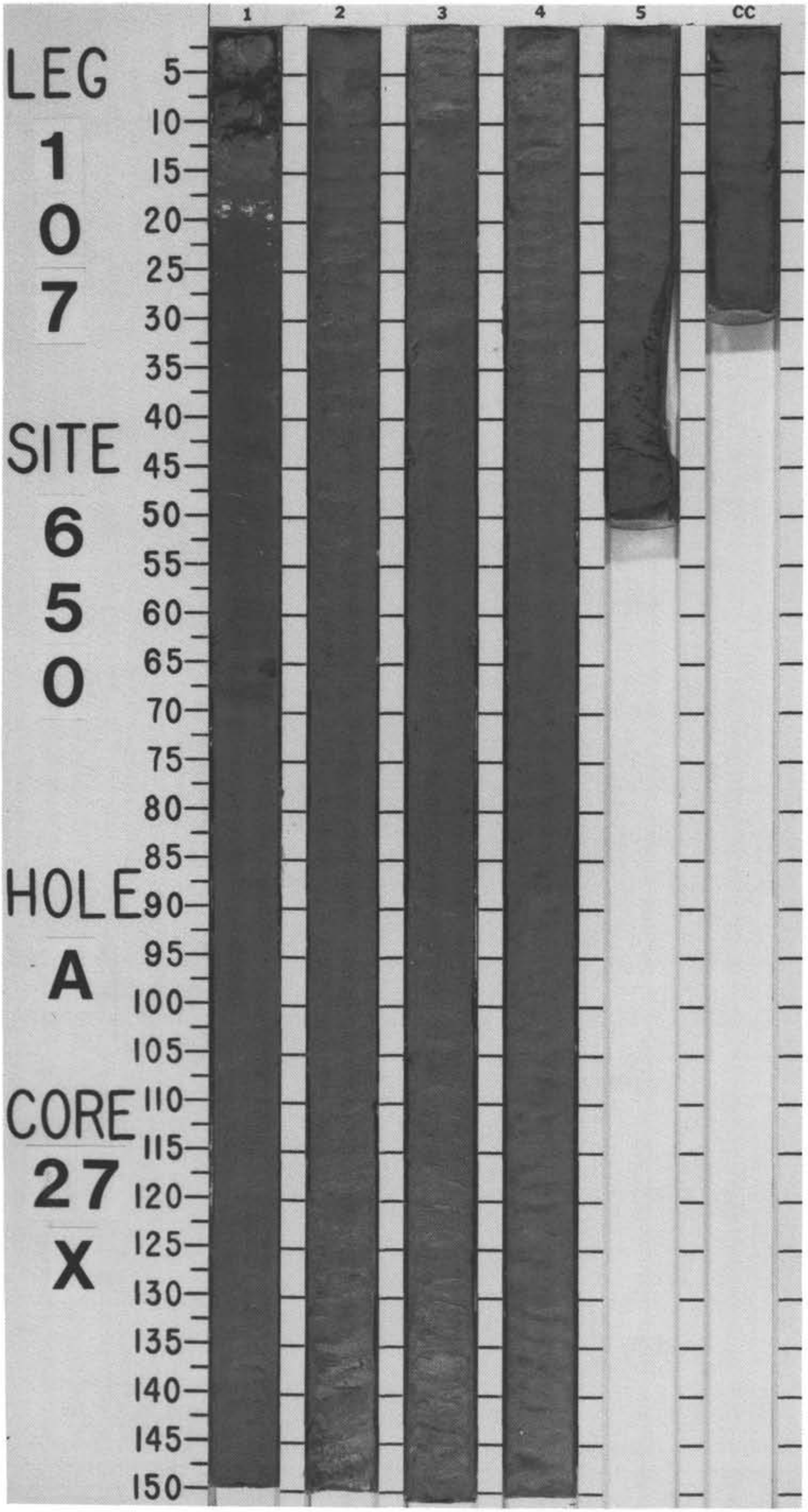
LEG
1
0
7
SITE
6
5
0
HOLE
A
CORE
27
X
1
2
3
4
5
CC
5
10
15
20
25
30
35
40
45
50
55
60
65
70
75
80
85
90
95
100
105
110
115
120
125
130
135
140
145
150

SITE 650 HOLE A CORE 29 X CORED INTERVAL 3783.1-3792.8 mbsl; 266.8-276.5 mbsf

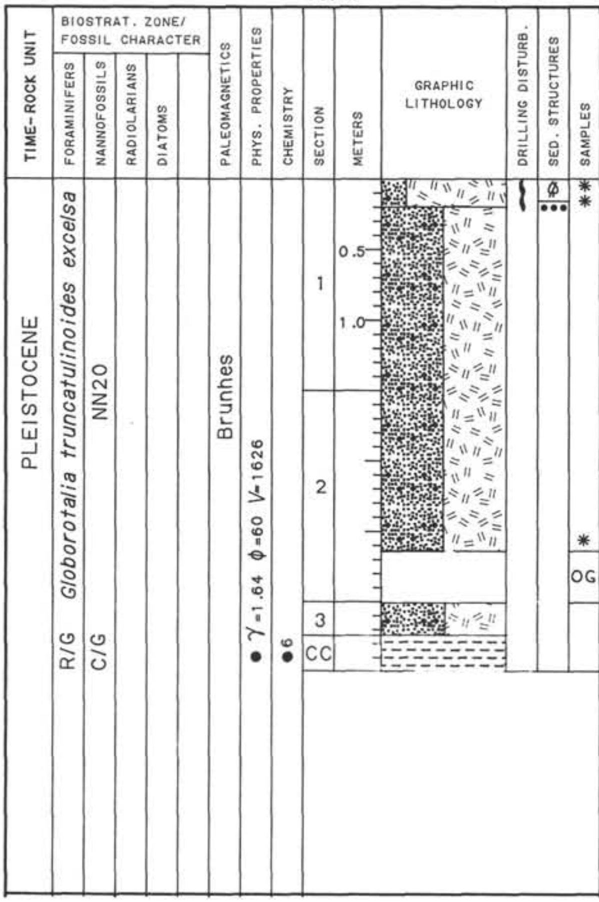

LITHOLOGIC DESCRIPTION

SANDY MUD

Sandy mud, olive-gray (5Y 5/2), homogeneous except for Section 1, 0–20 cm which is very disturbed by drilling; coarsening-upward sequence; shell fragments at Section 1, 20 cm; "peppery" appearance due to obsidian component throughout.

SMEAR SLIDE SUMMARY (%):

	1, 1 M	1, 21 D	2, 100 D
TEXTURE:			
Sand	10	20	—
Silt	20	20	40
Clay	70	60	60
COMPOSITION:			
Quartz	—	5	—
Feldspar	Tr	Tr	Tr
Rock fragments/tuff	—	Tr	—
Clay	30	10	—
Volcanic glass	40	40	50
Accessory minerals	Tr	5	Tr
Zeolite	—	—	Tr
Foraminifers	—	Tr	—
Nannofossils	30	30	30
Micrite	—	10	20

30X-NO RECOVERY

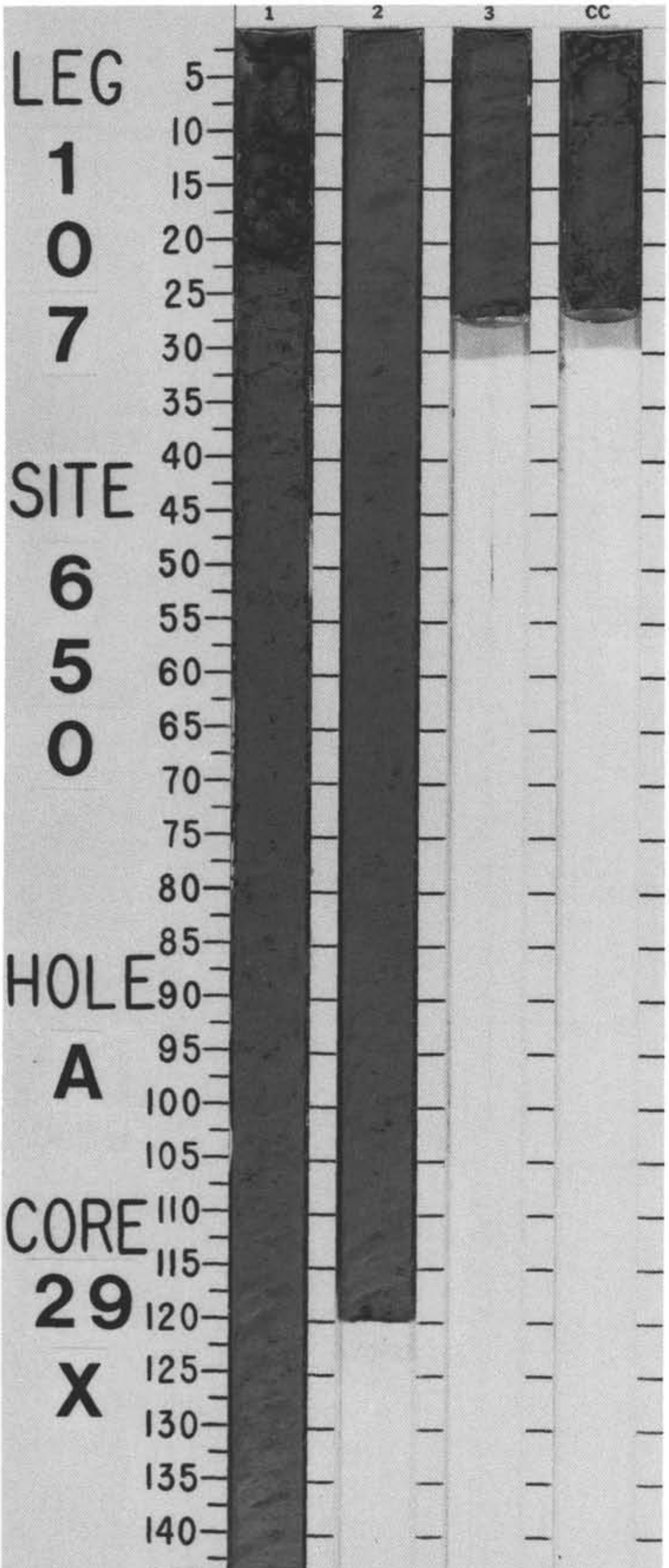
1
2
3
CC
LEG
107
SITE
650
HOLE
A
CORE
29X
5
10
15
20
25
30
35
40
45
50
55
60
65
70
75
80
85
90
95
100
105
110
115
120
125
130
135
140
145
150

SITE 650 HOLE A CORE 31 X CORED INTERVAL 3802.5-3812.1 mbsl; 286.2-295.8 mbsf

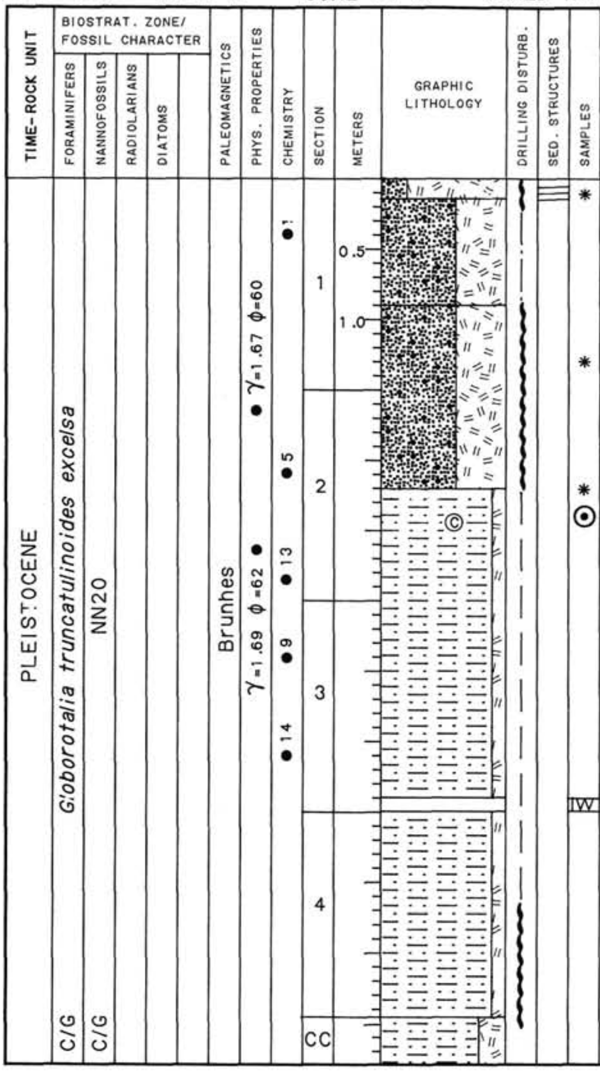

LITHOLOGIC DESCRIPTION

MUD

Mud, dark gray (5Y 4/1) to pale olive (5Y 6/4), darker colors associated with more indurated sections of the core, homogeneous, "argille scagliose" appearance in lower part of core.

SMEAR SLIDE SUMMARY (%):

	1, 10 M	1, 130 D	2, 70 D
TEXTURE:			
Sand	65	15	—
Silt	30	15	—
Clay	5	70	100
COMPOSITION:			
Quartz	5	5	1
Feldspar	10	5	5
Rock fragments/tuff	Tr	—	—
Clay	5	25	30
Volcanic glass	55	15	10
Accessory minerals	15	10	4
Foraminifers	—	15	—
Nannofossils	10	20	15
Silicoflagellates	—	—	Tr
Micrite	—	5	30
Ostracods?	—	—	5

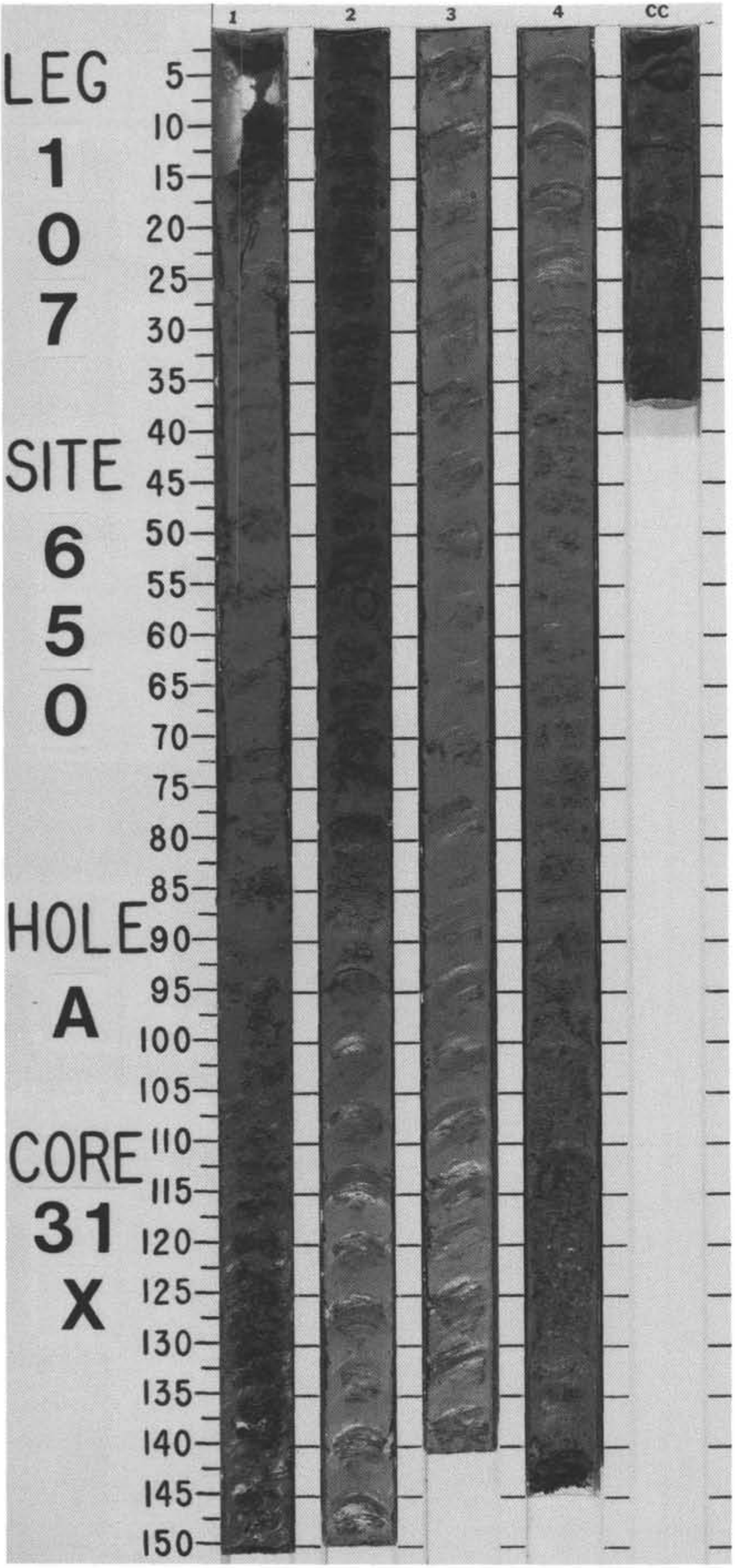
LEG 1 0 7
SITE 6 5 0
HOLE A
CORE 31 X
1
2
3
4
CC
5
10
15
20
25
30
35
40
45
50
55
60
65
70
75
80
85
90
95
100
105
110
115
120
125
130
135
140
145
150

SITE 650 HOLE A CORE 32 X CORED INTERVAL 3812.1-3821.8 mbsl; 295.8-305.5 mbsf

TIME-ROCK UNIT	BIOSTRAT. ZONE/FOSSIL CHARACTER: FORAMINIFERS	NANNOFOSSILS	RADIOLARIANS	DIATOMS	PALEOMAGNETICS	PHYS. PROPERTIES	CHEMISTRY	SECTION	METERS	GRAPHIC LITHOLOGY	DRILLING DISTURB.	SED. STRUCTURES	SAMPLES
PLEISTOCENE	*Globorotalia truncatulinoides excelsa* C/G	NN20 C/G			Brunhes		● 55, ● 13, ● 3	1, 2, CC	0.5, 1.0	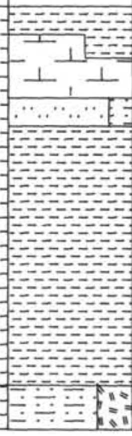			* * *

LITHOLOGIC DESCRIPTION

CLAYSTONE and NANNOFOSSIL OOZE

Claystone and mudstone, gray (5Y 5/1) to light gray (5Y 7/2), alternating with very thin beds of nannofossil ooze and sandy silt down to Section 1, 85 cm; thick homogeneous sequence below that.

Nannofossil ooze, light gray (5Y 7/2) to white (5Y 8/2), very thin beds, burrowed in Section 1, 26–27 and 30–33 cm.

Minor lithology: sandy silt, dark gray (5Y 4/1) to gray (5Y 5/1), very thin beds in Section 1, 65–69, 71–72, and 77–86 cm.

SMEAR SLIDE SUMMARY (%):

	1, 31 M	1, 107 D	CC, 22 D
TEXTURE:			
Sand	—	—	—
Silt	—	1	25
Clay	100	99	75
COMPOSITION:			
Quartz	Tr	1	10
Feldspar	Tr	—	2
Mica	Tr	—	1
Clay	6	62	53
Volcanic glass	—	—	20
Calcite/dolomite	1	4	—
Accessory minerals	1	1	2
Foraminifers	2	1	2
Nannofossils	90	30	10
Sponge spicules	—	1	—

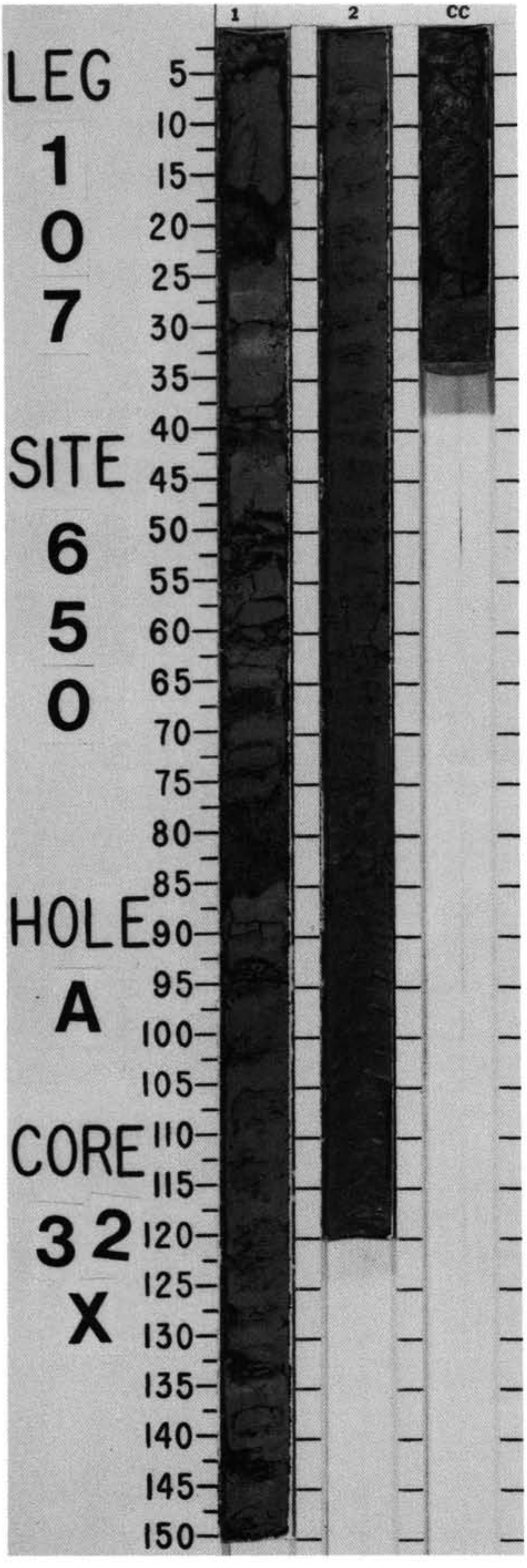
LEG 107
SITE 650
HOLE A
CORE 32X
1
2
CC

SITE 650 HOLE A CORE 33 X CORED INTERVAL 3821.8-3831.4 mbsl; 305.5-315.1 mbsf

TIME-ROCK UNIT	FORAMINIFERS	NANNOFOSSILS	RADIOLARIANS	DIATOMS	PALEOMAGNETICS	PHYS. PROPERTIES	CHEMISTRY	SECTION	METERS	GRAPHIC LITHOLOGY	DRILLING DISTURB.	SED. STRUCTURES	SAMPLES
PLEISTOCENE	*Globorotalia truncatulinoides excelsa* R/P R/H R/G	NN20 C/M					● 6 ● 3	CC			ooo		* **

LITHOLOGIC DESCRIPTION

VOLCANICLASTIC MUD

Volcaniclastic mud, black (5Y 2.5/1) to olive-gray (5Y 5/2).

SMEAR SLIDE SUMMARY (%):

	CC, 4 D	CC, 24 M	CC, 24.5 M
TEXTURE:			
Sand	—	—	20
Silt	30	20	20
Clay	70	80	60
COMPOSITION:			
Quartz	10	10	12
Feldspar	5	Tr	4
Mica	2	—	1
Clay	25	60	43
Volcanic glass	20	25	30
Accessory minerals	5	3	8
Micronodules	—	2	1
Foraminifers	10	—	1
Nannofossils	20	—	—
Diatoms	3	—	—
Radiolarians	Tr	—	—

SITE 650 HOLE A CORE 34 X CORED INTERVAL 3831.4-3841.1 mbsl; 315.1-324.8 mbsf

TIME-ROCK UNIT	FORAMINIFERS	NANNOFOSSILS	RADIOLARIANS	DIATOMS	PALEOMAGNETICS	PHYS. PROPERTIES	CHEMISTRY	SECTION	METERS	GRAPHIC LITHOLOGY	DRILLING DISTURB.	SED. STRUCTURES	SAMPLES
PLEISTOCENE	*Globorotalia truncatulinoides excelsa* A/P	NN20 A/G				● γ=1.63 φ=65; ● γ=1.89 φ=55	●6; ●6 6●; ●51; 24●	1; CC	0.5; 1.0				*; *; * *

LITHOLOGIC DESCRIPTION

Homogeneous VOLCANICLASTIC MUDSTONE overlying thin-bedded alternations of CALCAREOUS MUD and CALCAREOUS OOZE.

Volcaniclastic mudstone, dark gray (5Y 4/1), homogeneous, indurated.

Calcareous mud, olive-gray (5Y 5/2) to gray (5Y 6/1), parallel to wavy laminations in Section 1, 80 cm, to CC, 7 and 15–22 cm.

Minor lithology: calcareous ooze, light gray (5Y 7/1) in Section 1, 70–80 cm, and CC, 7–15 cm.

SMEAR SLIDE SUMMARY (%):

	1, 35 D	1, 126 D	CC, 4.5 M	CC, 20 M
TEXTURE:				
Sand	10	10	5	—
Silt	10	20	20	10
Clay	80	70	75	90
COMPOSITION:				
Quartz	8	2	8	5
Feldspar	Tr	1	6	3
Mica	—	—	2	Tr
Clay	61	72	58	67
Volcanic glass	15	1	Tr	2
Calcite/dolomite	7	6	6	8
Accessory minerals	Tr	—	—	Tr
Opaques	3	—	—	—
Foraminifers	Tr	10	10	8
Nannofossils	6	6	10	6
Diatoms	—	2	Tr	1
Radiolarians	—	Tr	—	Tr
Sponge spicules	—	Tr	Tr	—

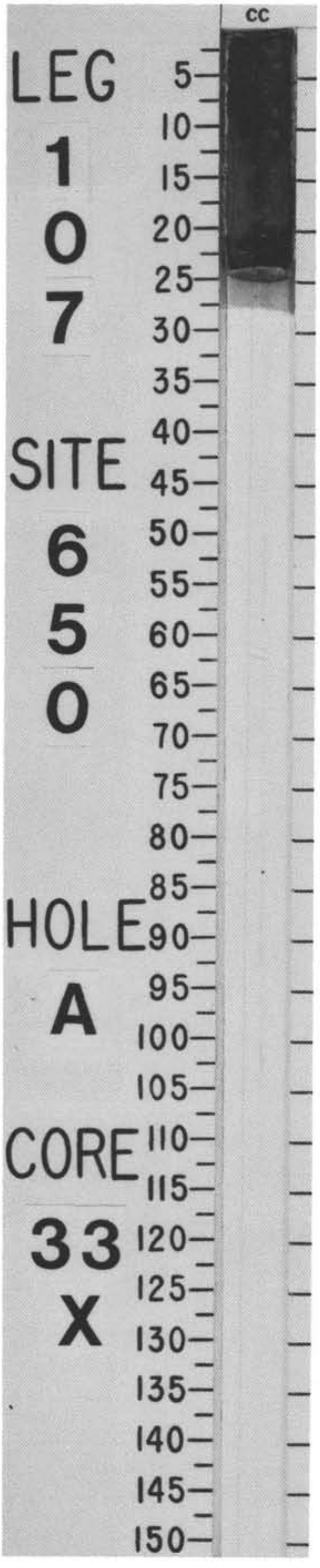
CC
LEG 107
SITE 650
HOLE A
CORE 33 X
5
10
15
20
25
30
35
40
45
50
55
60
65
70
75
80
85
90
95
100
105
110
115
120
125
130
135
140
145
150

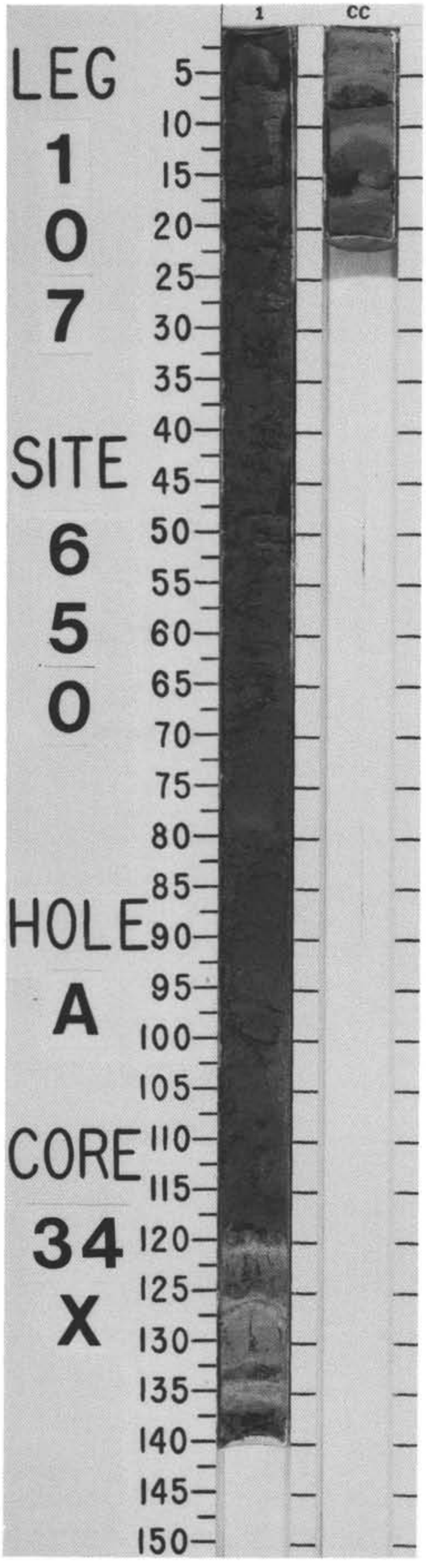
1
CC
LEG 107
SITE 650
HOLE A
CORE 34 X
5
10
15
20
25
30
35
40
45
50
55
60
65
70
75
80
85
90
95
100
105
110
115
120
125
130
135
140
145
150

SITE 650 HOLE A CORE 35 X CORED INTERVAL 3841.1-3850.8 mbsl; 324.8-334.5 mbsf

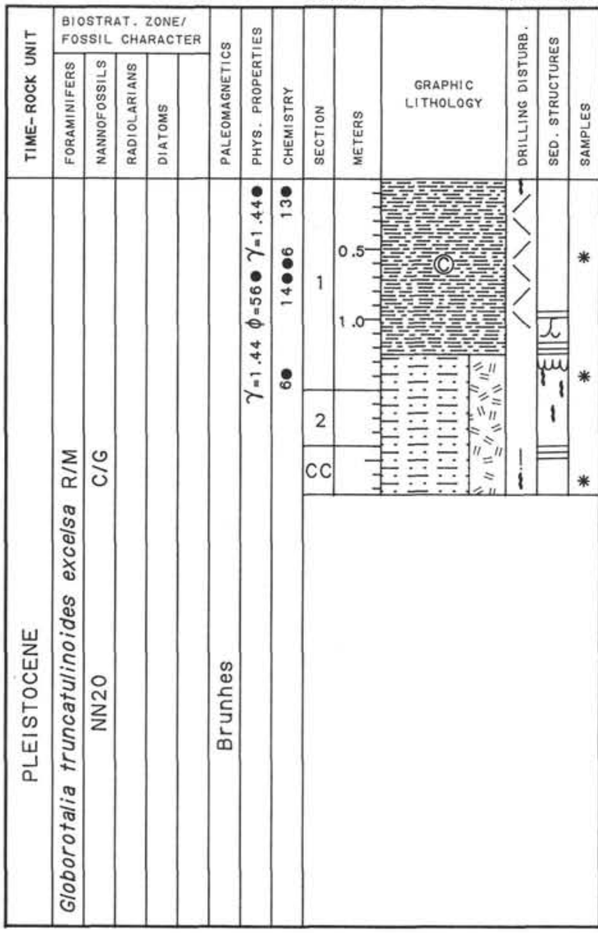

LITHOLOGIC DESCRIPTION

CALCAREOUS MUD and VOLCANICLASTIC MUD

Calcareous mud, dark gray (5Y 4/1) to olive-gray (5Y 5/2), homogeneous to parallel and flaser bedded, foraminifers filled with pyrite.

Volcaniclastic mud, very dark gray (5Y 3/1) to dark olive-gray (5Y 3/2), homogeneous, burrowed.

SMEAR SLIDE SUMMARY (%):

	1, 60 D	1, 140 D	CC, 22 D
TEXTURE:			
Sand	—	—	20
Silt	20	40	30
Clay	80	60	50
COMPOSITION:			
Quartz	1	7	7
Feldspar	—	—	1
Rock fragments	—	Tr	—
Mica	2	—	—
Clay	57	60	50
Volcanic glass	10	25	30
Calcite/dolomite	Tr	1	—
Accessory minerals	2	3	3
Pyrite	—	1	1
Foraminifers	—	Tr	3
Nannofossils	15	2	5
Sponge spicules	1	1	—
Pellets	2	—	—
Unspecified carb's.	10	—	—

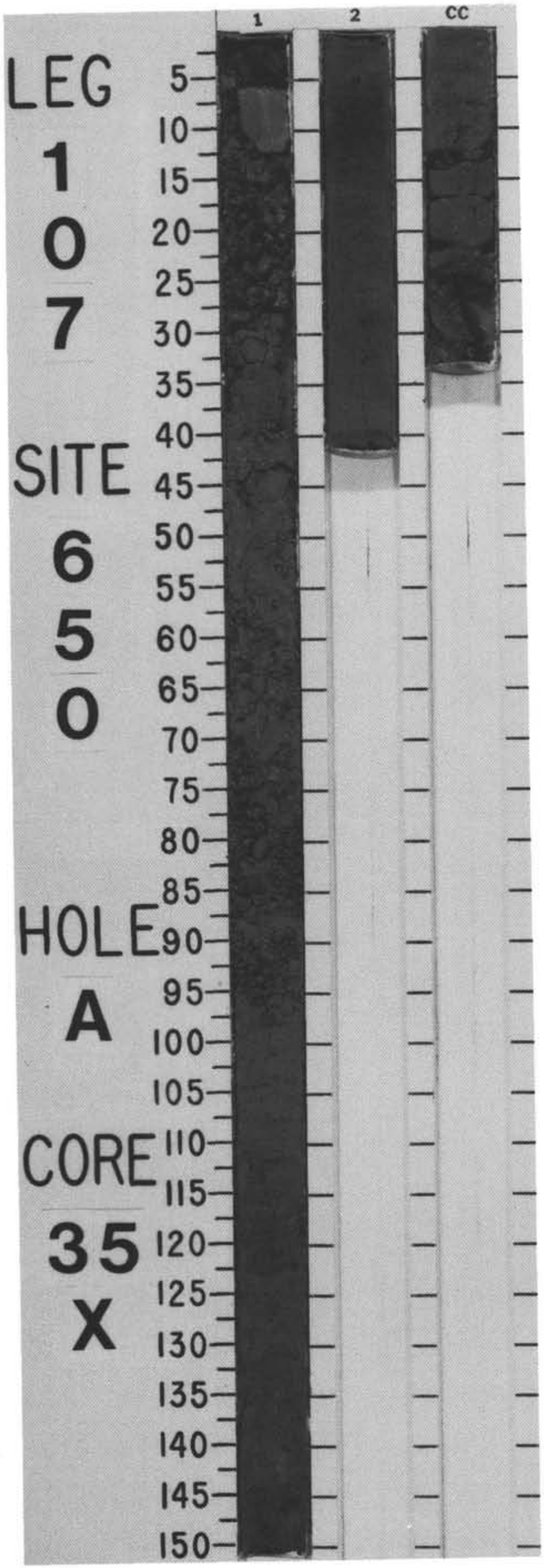
1
2
CC
LEG
107
SITE
650
HOLE
A
CORE
35
X
5
10
15
20
25
30
35
40
45
50
55
60
65
70
75
80
85
90
95
100
105
110
115
120
125
130
135
140
145
150

SITE 650 HOLE A CORE 36 X CORED INTERVAL 3850.8-3860.5 mbsl; 334.5-344.2 mbsf

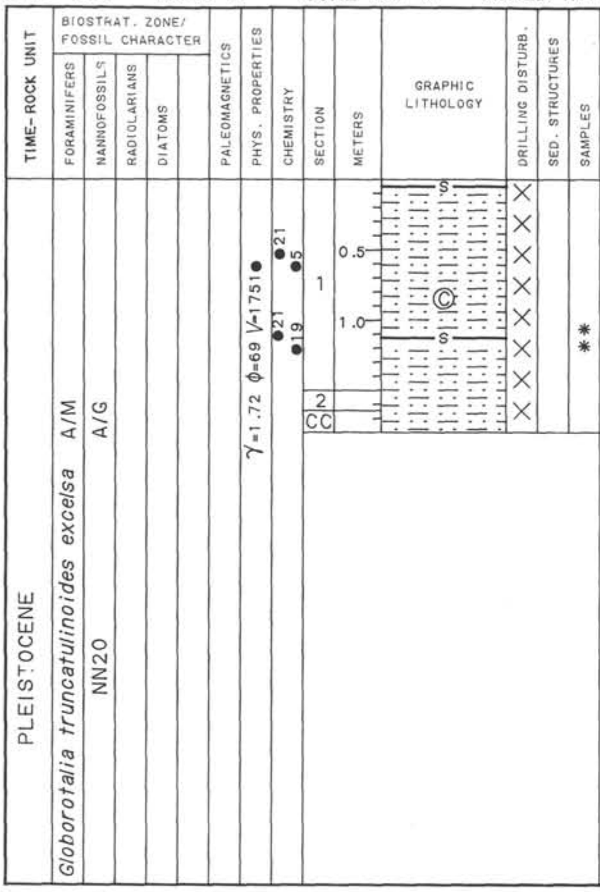

LITHOLOGIC DESCRIPTION

CALCAREOUS MUDSTONE

Calcareous mudstone, olive-gray (5Y 5/2) to gray (5Y 6/1), homogeneous and brecciated throughout, petroliferous odor at base.

Minor lithology: dark mudstone (possibly sapropelic), black (5Y 2.5/1), laminae in Section 1, 7 and 116 cm.

SMEAR SLIDE SUMMARY (%):

	1, 110 M	1, 116 D
TEXTURE:		
Sand	—	—
Silt	20	—
Clay	80	—
COMPOSITION:		
Quartz	8	6
Feldspar	5	3
Mica	1	Tr
Clay	18	64
Volcanic glass	20	Tr
Calcite/dolomite	5	9
Accessory minerals	—	3
Zeolite (Analcime?)	3	—
Opaques	40	—
Foraminifers	Tr	10
Nannofossils	Tr	5
Diatoms	Tr	—
Radiolarians	—	Tr
Ostracods	—	Tr

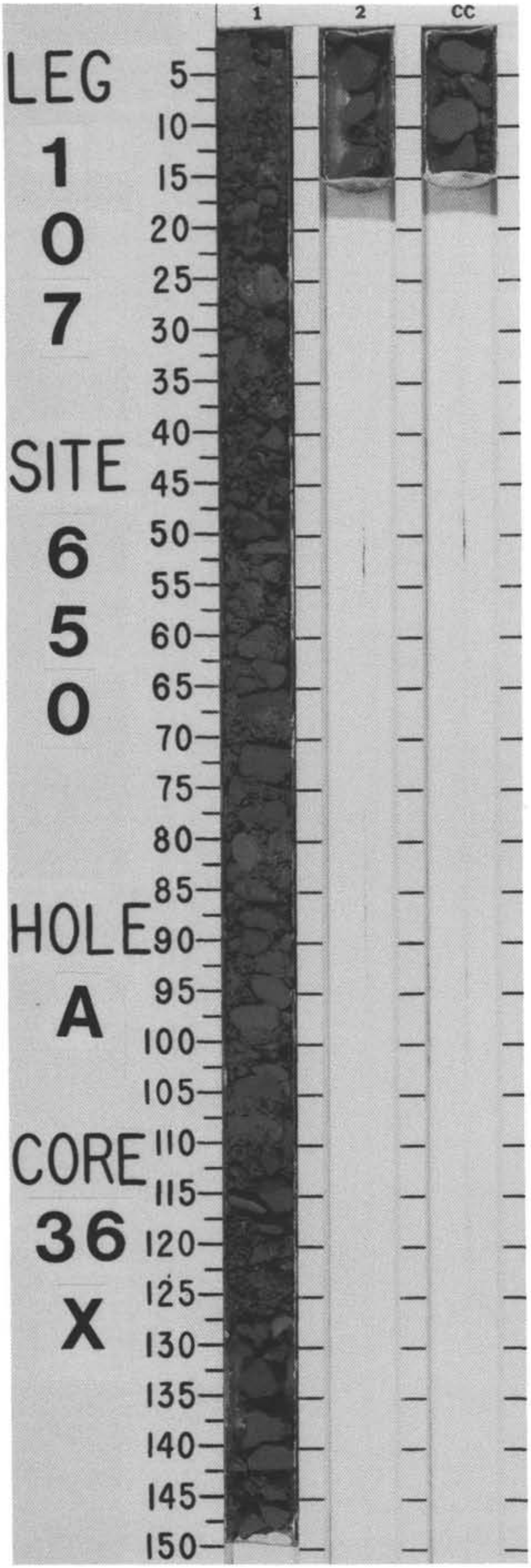
LEG
1
0
7
SITE
6
5
0
HOLE
A
CORE
36
X
1
2
CC
5
10
15
20
25
30
35
40
45
50
55
60
65
70
75
80
85
90
95
100
105
110
115
120
125
130
135
140
145
150

SITE 650 HOLE A CORE 37 X CORED INTERVAL 3860.5-3870.2 mbsl; 344.2-353.9 mbsf

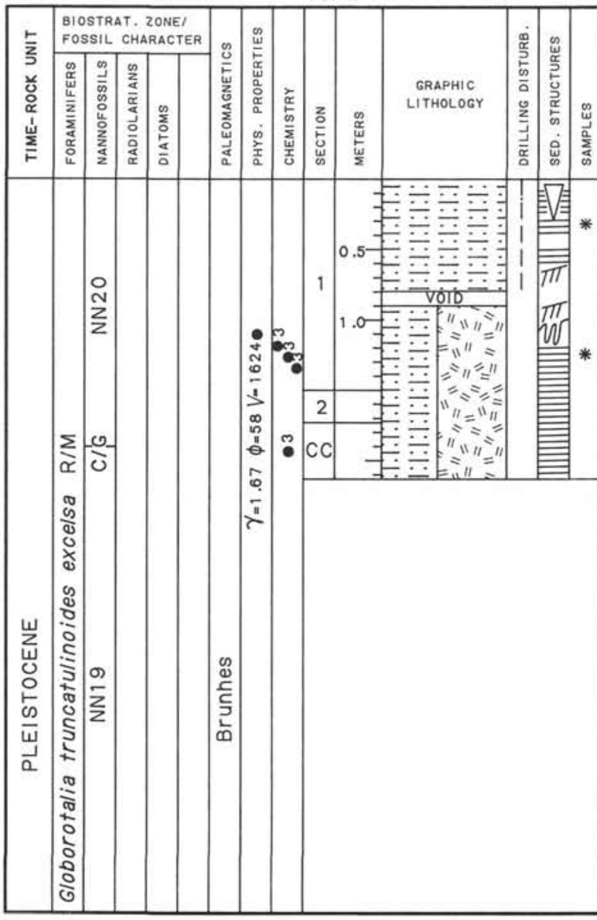

LITHOLOGIC DESCRIPTION

VOLCANICLASTIC MUDSTONE

Volcaniclastic mud, dark olive-gray (5Y 3/2) to olive-gray (5Y 4/2), dark vitric grain component creating a "salt and pepper" appearance, volcanic component increasing downcore; synsedimentary disturbance in Section 1, 90–115 cm.

SMEAR SLIDE SUMMARY (%):

	1, 36 D	1, 127 D
TEXTURE:		
Sand	5	15
Silt	45	65
Clay	50	20
COMPOSITION:		
Quartz	5	10
Feldspar	1	1
Clay	52	30
Volcanic glass	25	50
Accessory minerals	5	2
Foraminifers	2	2
Nannofossils	10	4
Diatoms	—	1

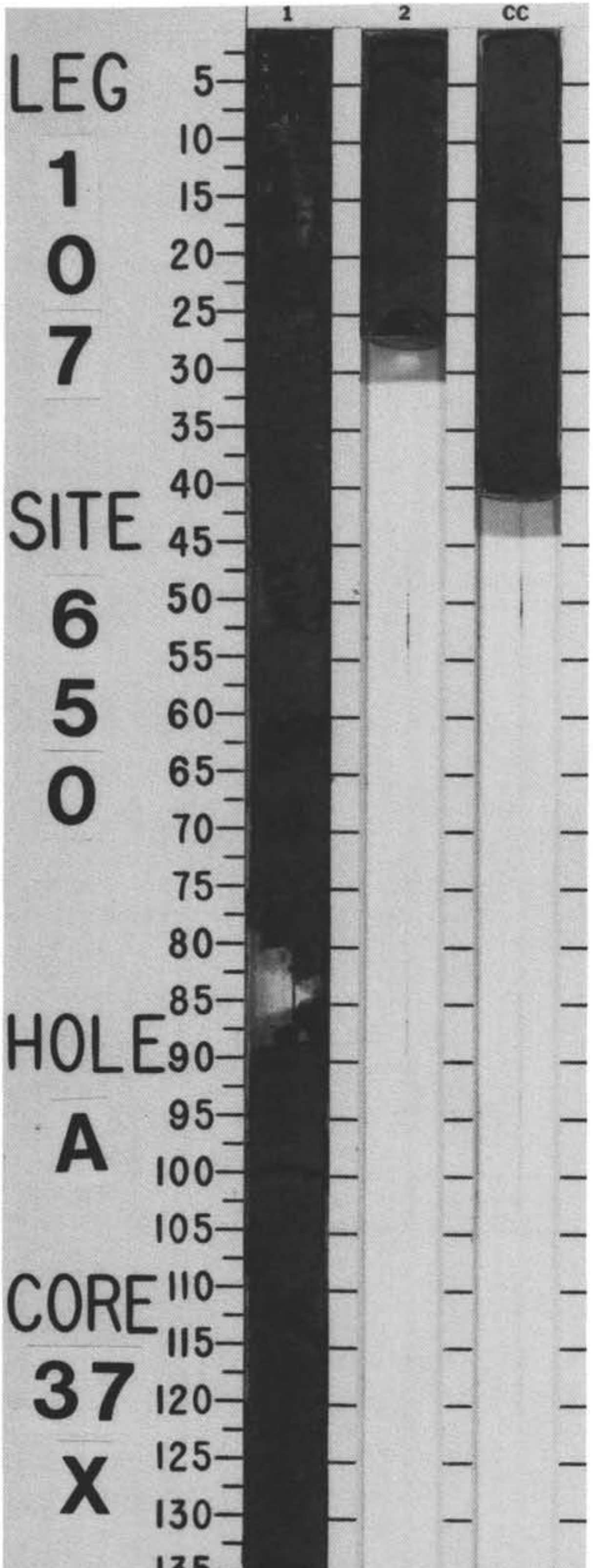
LEG
107
SITE
650
HOLE
A
CORE
37
X
1
2
CC
5
10
15
20
25
30
35
40
45
50
55
60
65
70
75
80
85
90
95
100
105
110
115
120
125
130
135
140
145
150

SITE 650 HOLE A CORE 38 X CORED INTERVAL 3870.2-3879.8 mbsl; 353.9-363.5 mbsf

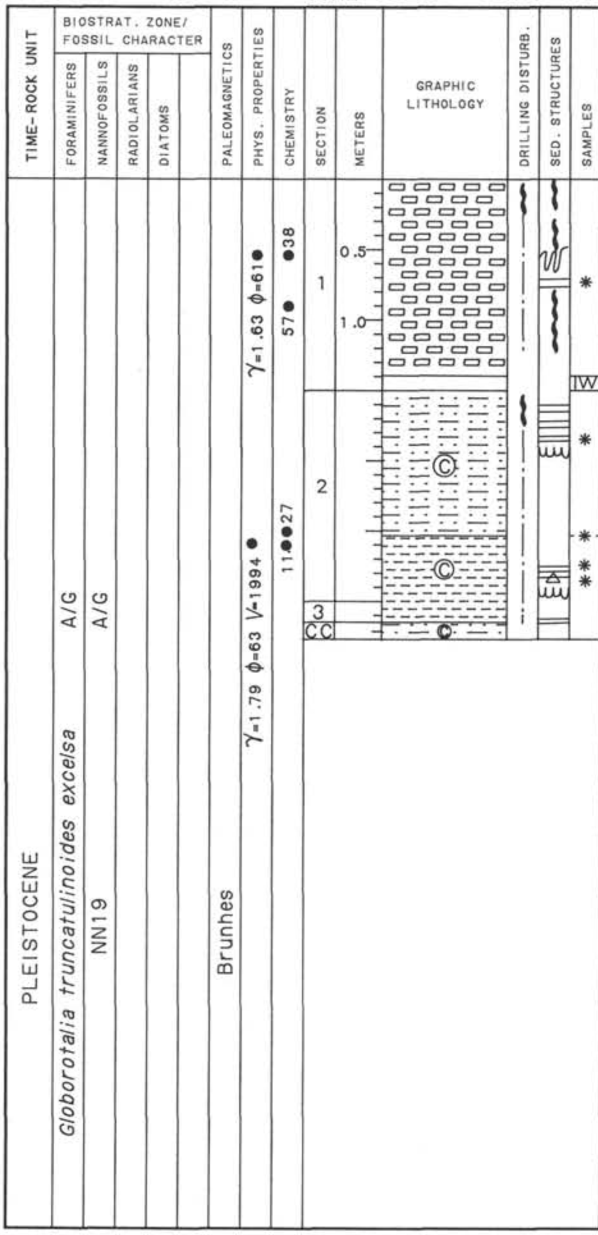

LITHOLOGIC DESCRIPTION

Thin-bedded alternations of MARLY CALCAREOUS OOZE, CALCAREOUS MUDSTONE, and CALCAREOUS CLAYSTONE

Marly calcareous ooze, olive-gray (5Y 4/2) to light gray (5Y 7/2), burrowed.

Calcareous mudstone, dark gray (5Y 4/1) to pale olive (5Y 6/3), faintly laminated, framboidal pyrite infilling foraminifer tests.

Calcareous claystone, olive-gray (5Y 5/2) to light olive-gray (5Y 6/2), faintly laminated, burrowed.

Minor lithology: silt, very dark gray (5Y 3/1), laminae generally overlying scoured surfaces, normally graded in Section 1, 71 and 119 cm, and in Section 2, 15, 35, and 129 cm.

Minor tensional fault in Section 2, 40 cm.

SMEAR SLIDE SUMMARY (%):

	1, 72 M	2, 36 M	2, 110 D	2, 130 M	2, 140 D
TEXTURE:					
Sand	—	20	2	—	—
Silt	80	20	8	80	80
Clay	20	60	90	20	20
COMPOSITION:					
Quartz	5	—	Tr	1	5
Feldspar	10	5	2	10	5
	—	—	1	—	—
Mica	5	—	—	—	—
Clay	—	25	20	—	40
Volcanic glass	—	2	Tr	—	—
Calcite/dolomite	15	—	—	10	—
Accessory minerals	—	—	—	4	—
Clay aggregates	60	—	—	35	—
Sanidine	5	—	—	25	—
Opaques	—	—	5	—	—
Foraminifers	—	20	2	—	10
Nannofossils	—	—	40	15	40
Sponge spicules	—	23	—	—	—
Micrite	—	25	30	—	—
Pyroxene	—	—	Tr	—	—

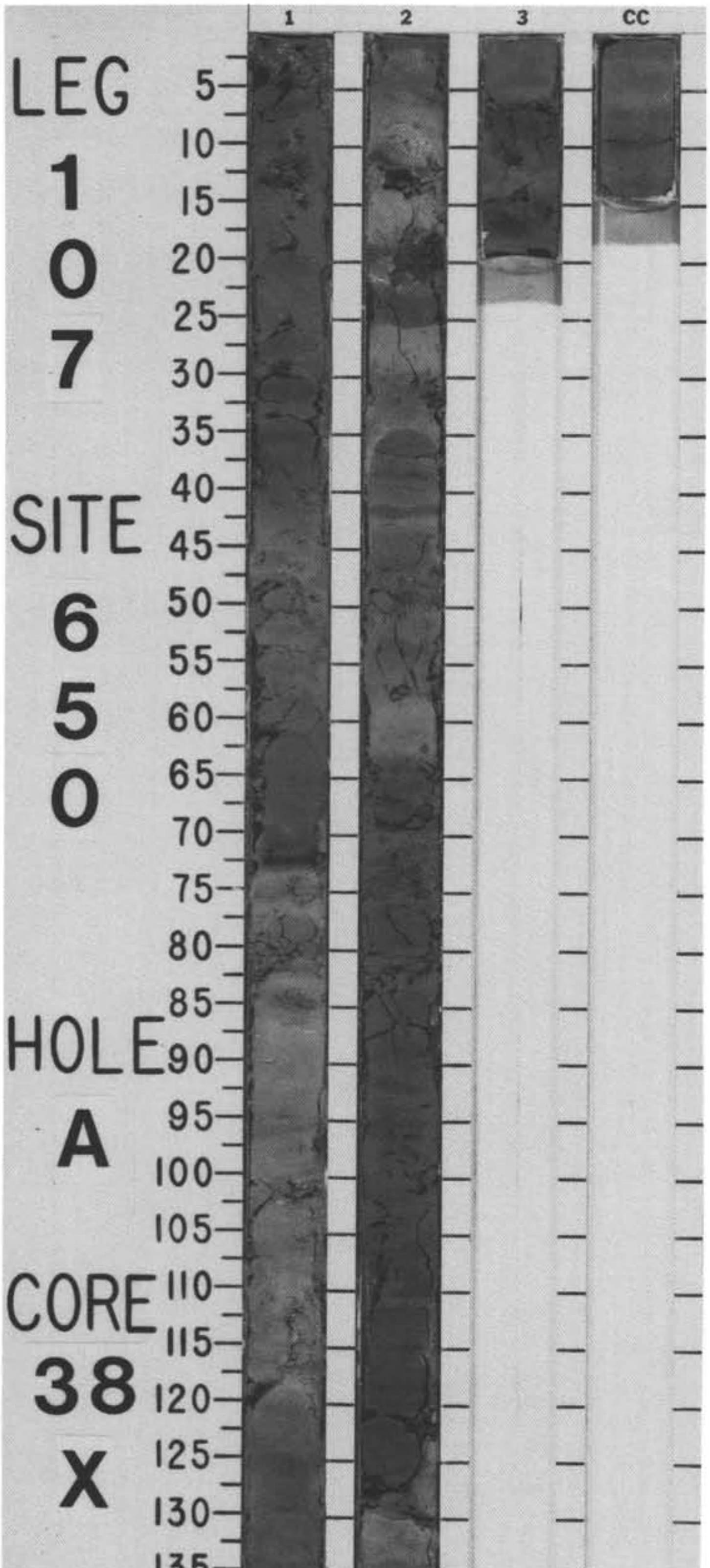
1
2
3
CC
LEG
1
0
7
SITE
6
5
0
HOLE
A
CORE
38
X
5
10
15
20
25
30
35
40
45
50
55
60
65
70
75
80
85
90
95
100
105
110
115
120
125
130
135
140
145
150

SITE 650 HOLE A CORE 39 X CORED INTERVAL 3879.8-3889.4 mbsl; 363.5-373.1 mbsf

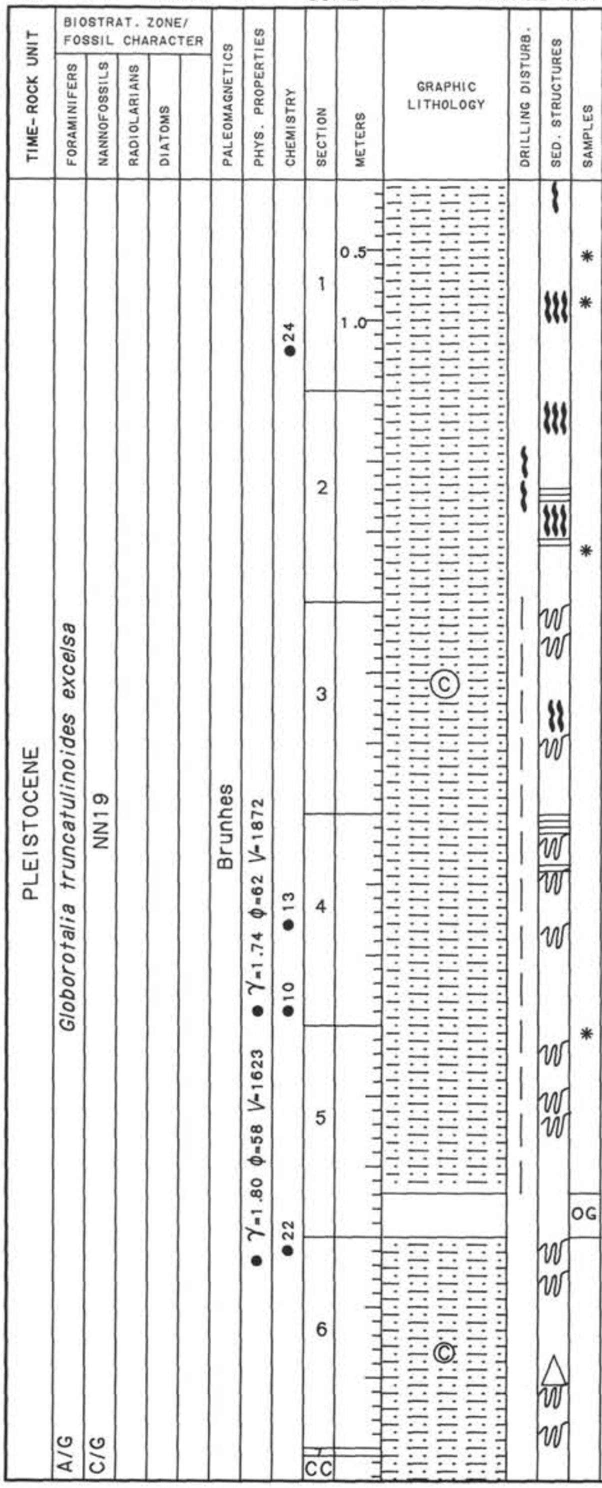

LITHOLOGIC DESCRIPTION

CALCAREOUS MUDSTONE

Calcareous mudstone, light olive-brown (2.5Y 5/4), dark olive-gray (5Y 3/2) to gray (5Y 6/1), very dark brown (10YR 2/2), weak red (2.5YR 4/2), grayish olive (5GY 3/2), and dusky yellowish green (10GY 3/2); color variations partly due to minor content of sulfides, and occurring as laminae, beds, and variegated patches.

SMEAR SLIDE SUMMARY (%):

	1, 59 D	1, 89 D	2, 113 M	5, 3 M
TEXTURE:				
Sand	—	10	—	20
Silt	30	30	15	50
Clay	70	60	85	30
COMPOSITION:				
Quartz	5	5	Tr	Tr
Feldspar	5	5	Tr	10
Mica	2	—	1	—
Clay	5	10	20	32
Volcanic glass	10	—	2	30
Calcite/dolomite	5	15	—	—
Accessory minerals	—	—	1	—
Aragonite needles	5	5	—	—
Sulfides	5	40	—	—
Pyroxene	—	—	—	10
Foraminifers	10	5	Tr	3
Nannofossils	46	15	71	15
Micrite	2	—	5	—

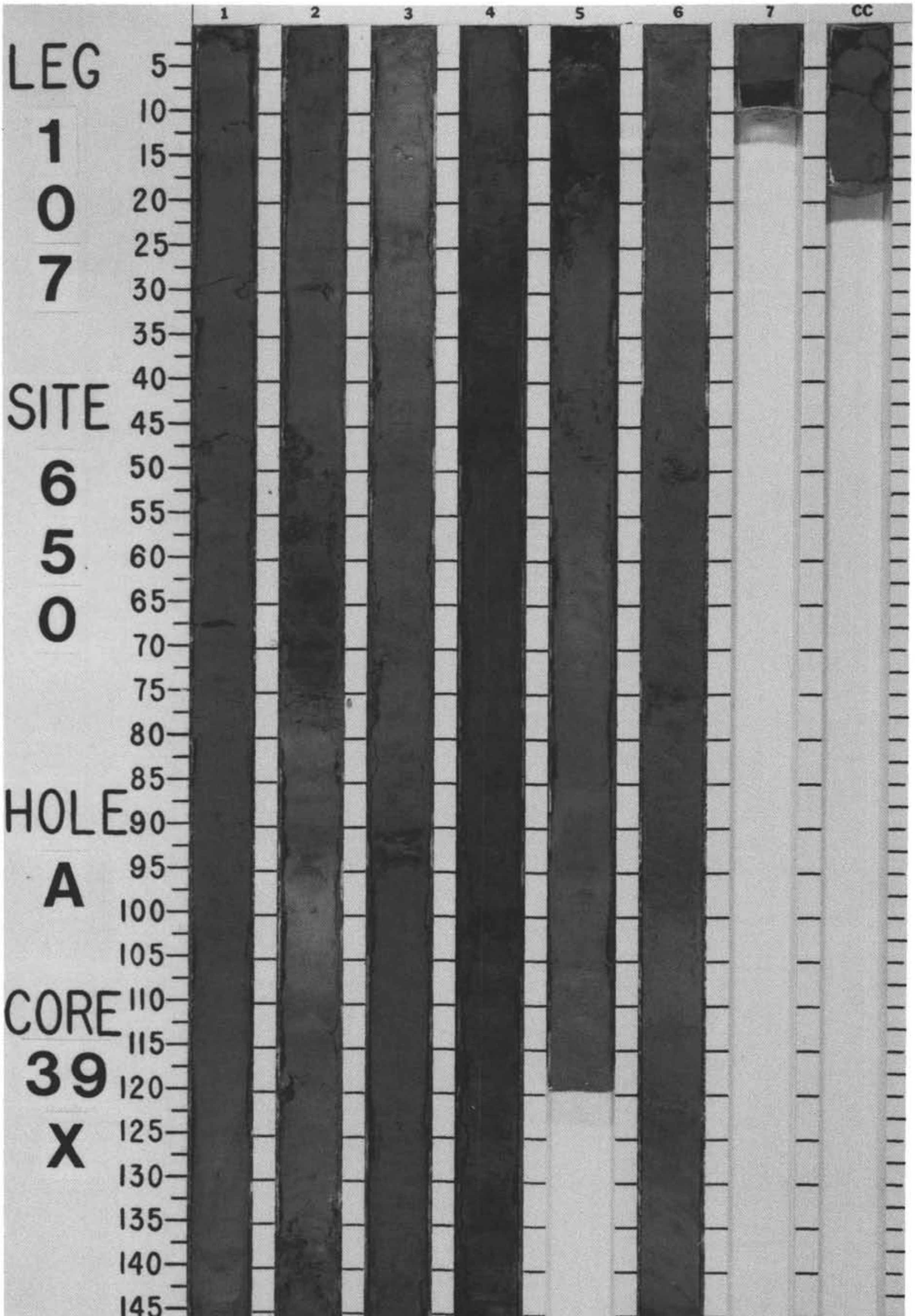
LEG
107
SITE
650
HOLE
A
CORE
39
X
1
2
3
4
5
6
7
CC

SITE 650 HOLE A CORE 40 X CORED INTERVAL 3889.4-3899.1 mbsl; 373.1-382.8 mbsf

TIME-ROCK UNIT	BIOSTRAT. ZONE/ FOSSIL CHARACTER: FORAMINIFERS	NANNOFOSSILS	RADIOLARIANS	DIATOMS	PALEOMAGNETICS	PHYS. PROPERTIES	CHEMISTRY	SECTION	METERS	GRAPHIC LITHOLOGY	DRILLING DISTURB.	SED. STRUCTURES	SAMPLES
PLEISTOCENE	*Globorotalia truncatulinoides excelsa*	NN19			Brunhes	● γ=1.9 ϕ=52 V=1771	● 17; ● 5; ● 22	1, 2, 3, 4, CC	0.5, 1.0	©			* * *

LITHOLOGIC DESCRIPTION

CLAYSTONE and CALCAREOUS CLAYSTONE

Claystone to calcareous claystone, olive-gray (5Y 5/2) to gray (5Y 6/1), homogeneous, few primary or secondary features preserved due at least partially to drilling disturbance.

SMEAR SLIDE SUMMARY (%):

	1, 100 D	3, 137 D	4, 74 M
TEXTURE:			
Sand	—	—	—
Silt	—	5	5
Clay	—	95	95
COMPOSITION:			
Quartz	—	1	1
Feldspar	—	1	1
Clay	40	40	30
Volcanic glass	Tr	—	—
Calcite/dolomite	Tr	—	2
Accessory minerals	—	5	5
Pyrite	Tr	—	—
Glauconite?	—	1	—
Pyroxene?	—	—	1
Foraminifers	—	2	5
Nannofossils	30	10	20
Micrite	30	40	35

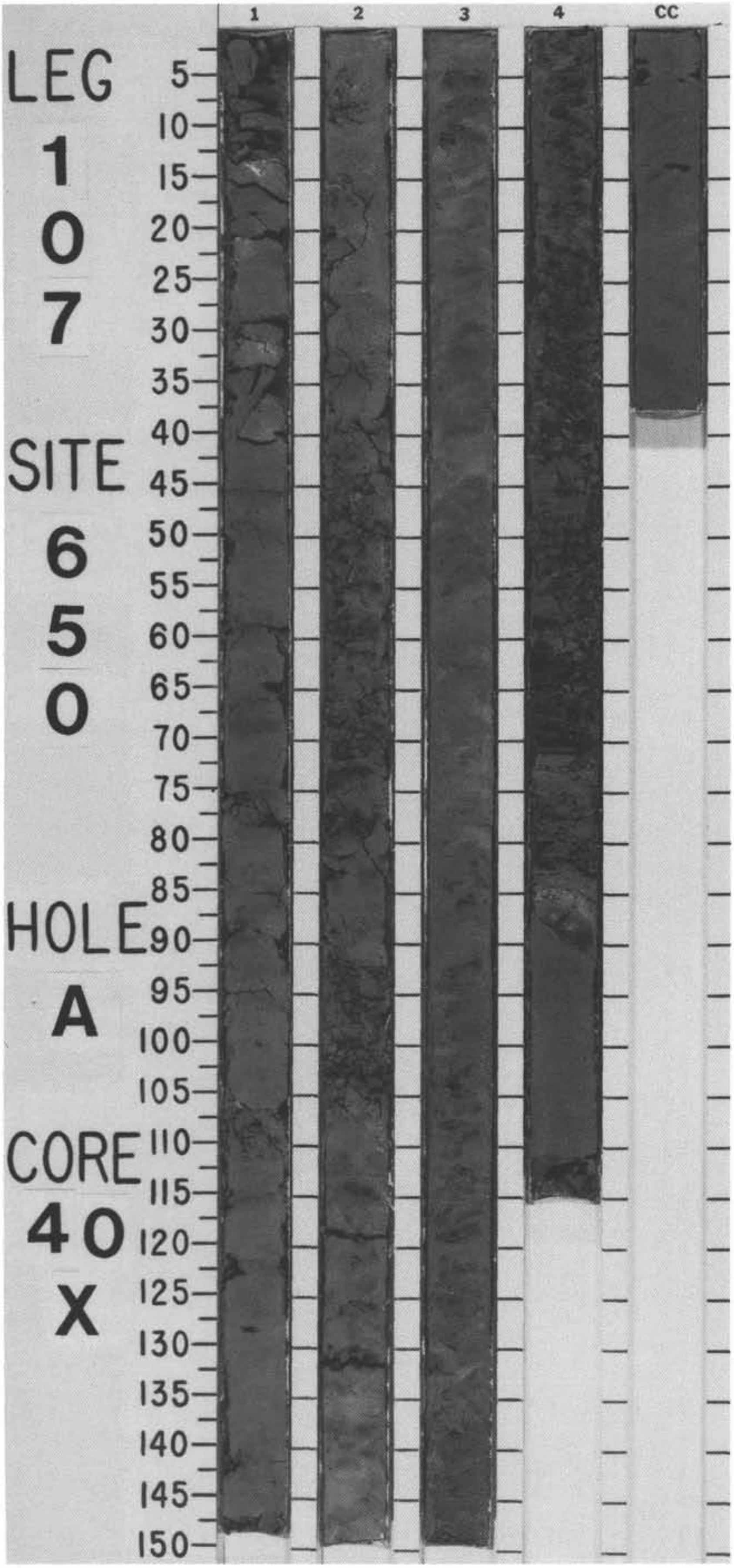
LEG 107
SITE 650
HOLE A
CORE 40 X
1
2
3
4
CC
5
10
15
20
25
30
35
40
45
50
55
60
65
70
75
80
85
90
95
100
105
110
115
120
125
130
135
140
145
150

SITE 650 HOLE A CORE 41 X CORED INTERVAL 3899.1-3908.7 mbsl; 382.8-392.4 mbsf

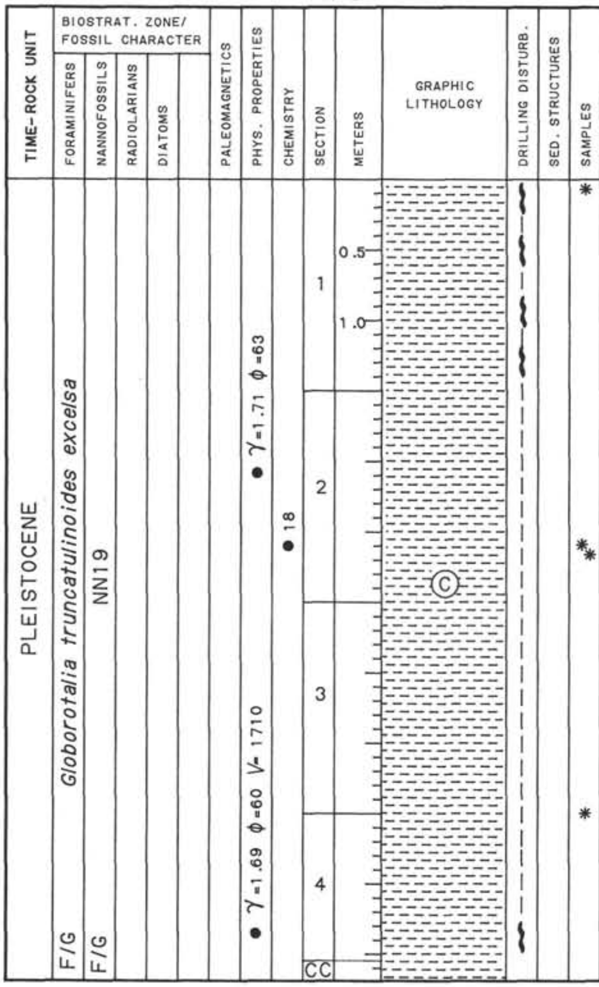

LITHOLOGIC DESCRIPTION

CALCAREOUS CLAYSTONE

Calcareous claystone, very dark gray (5Y 3/1) to olive-gray (5Y 5/2), homogeneous, drilling biscuits.

COMPOSITION:

Quartz	3	2	5	3
Feldspar	1	—	—	—
Mica	—	1	—	1
Clay	56	37	—	36
Foraminifers	10	10	10	10
Nannofossils	25	40	75	40
Diatoms	5	10	10	10
652A-38 4, 100				
652A-45				
Unidentified	—	—	33	
Organic matter plant debris(?)	—	—	3	

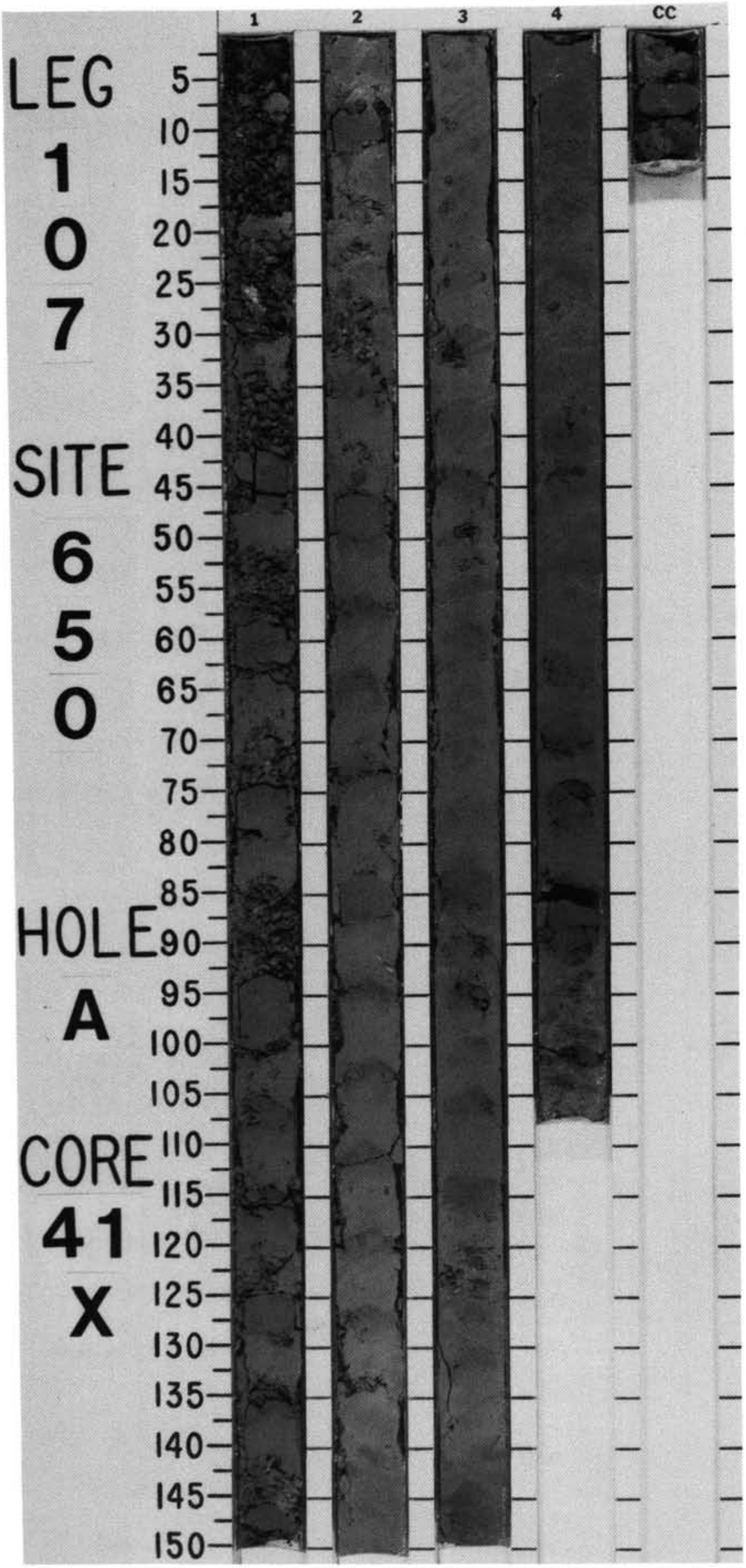
LEG 1070
SITE 650
HOLE A
CORE 41X
1
2
3
4
CC
5
10
15
20
25
30
35
40
45
50
55
60
65
70
75
80
85
90
95
100
105
110
115
120
125
130
135
140
145
150

SITE 650 HOLE A CORE 42 X CORED INTERVAL 3908.7-3913.7 mbsl; 392.4-397.4 mbsf

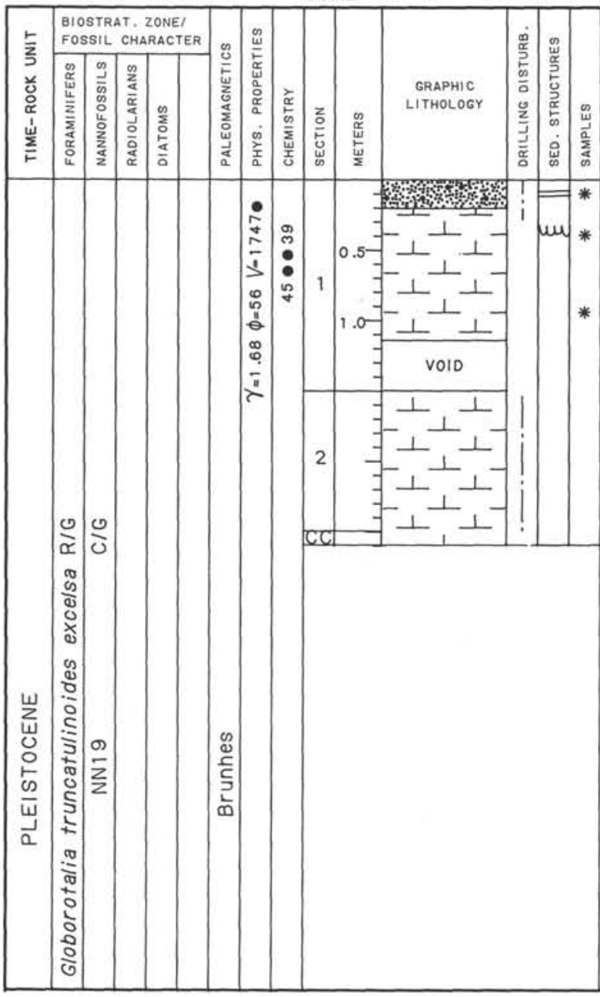

LITHOLOGIC DESCRIPTION

SILTY SAND and MARLY NANNOFOSSIL CHALK

Silty sand, dark gray (5Y 4/1), faint laminations, scoured basal contact; a very thin silty sand bed with scoured basal contact in Section 1, 31–33 cm.

Marly nannofossil chalk, gray (5Y 5/1–6/1) to olive-gray (5Y 5/2), progressively indurated downcore; dark laminae with framboidal pyrite in Section 1, 85 cm.

SMEAR SLIDE SUMMARY (%):

	1, 13 M	1, 46 D	1, 85 M
TEXTURE:			
Sand	50	—	10
Silt	20	20	30
Clay	30	80	60
COMPOSITION:			
Quartz	10	Tr	5
Feldspar	20	Tr	Tr
Clay	20	21	30
Calcite/dolomite	—	—	5
Accessory minerals	—	2	Tr
Pyroxene	20	—	—
Pyrite	Tr	—	10
Zeolites	—	—	Tr
Foraminifers	25	5	Tr
Nannofossils	5	50	25
Plant debris	—	22	25

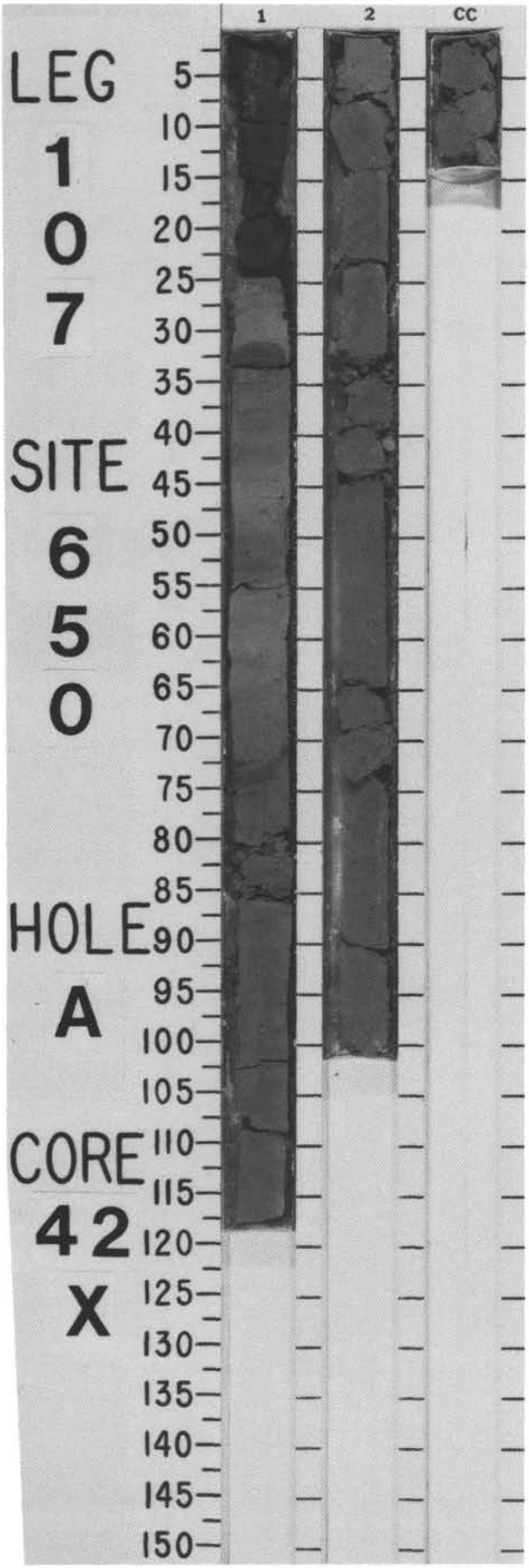
LEG
1
0
7
SITE
6
5
0
HOLE
A
CORE
42
X
1
2
CC

SITE 650 HOLE A CORE 43 X CORED INTERVAL 3913.7-3915.7 mbsl; 397.4-399.4 mbsf

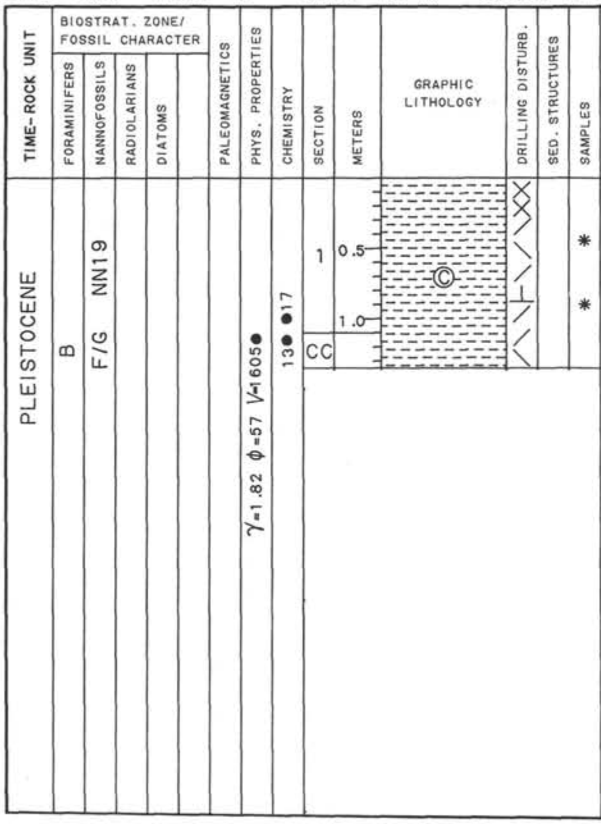

LITHOLOGIC DESCRIPTION

CALCAREOUS CLAYSTONE

Calcareous claystone, olive-gray (5Y 5/2), homogeneous; two hard pebbles in Section 1, 0–3 cm, and a nodule of disseminated pyrite in Section 1, 41–42.5 cm.

SMEAR SLIDE SUMMARY (%):

	1, 42 M	1, 95 D
TEXTURE:		
Sand	5	5
Silt	20	10
Clay	75	85
COMPOSITION:		
Quartz	6	3
Feldspar	6	2
Mica	Tr	—
Clay	30	85
Volcanic glass	5	Tr
Calcite/dolomite	—	Tr
Accessory minerals	3	Tr
Pyrite	15	—
Foraminifers	1	—
Nannofossils	1	4
Radiolarians	1	—
Sponge spicules	Tr	—
Micrite	32	6

44X-NO RECOVERY

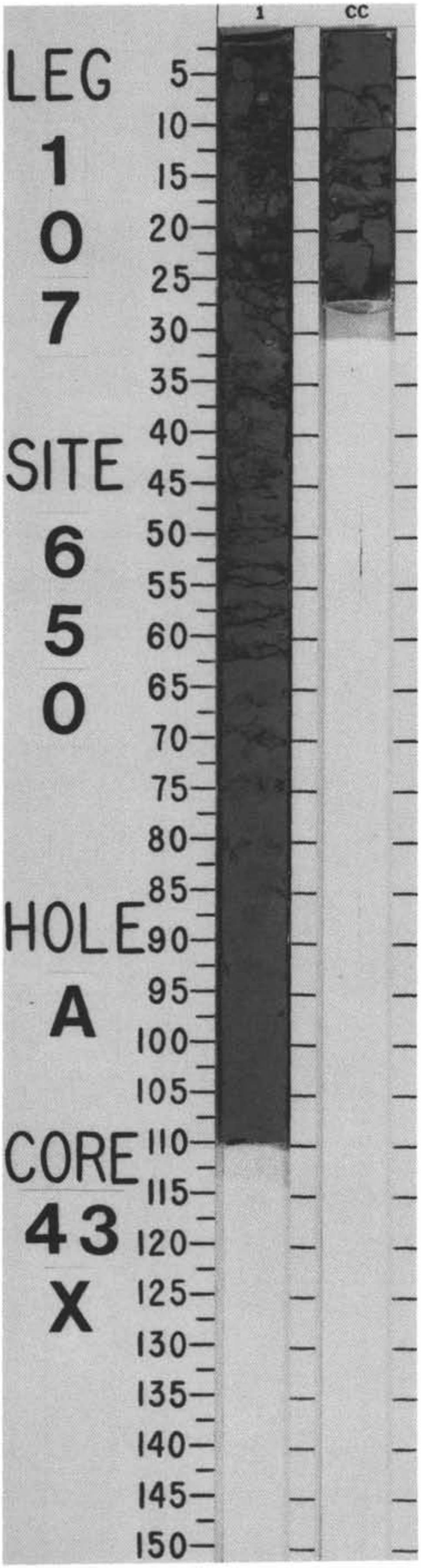
1
CC
LEG
1
0
7
SITE
6
5
0
HOLE
A
CORE
43
X
5
10
15
20
25
30
35
40
45
50
55
60
65
70
75
80
85
90
95
100
105
110
115
120
125
130
135
140
145
150

SITE 650 HOLE A CORE 45 X CORED INTERVAL 3922.4-3928.1 mbsl; 406.1-411.8 mbsf

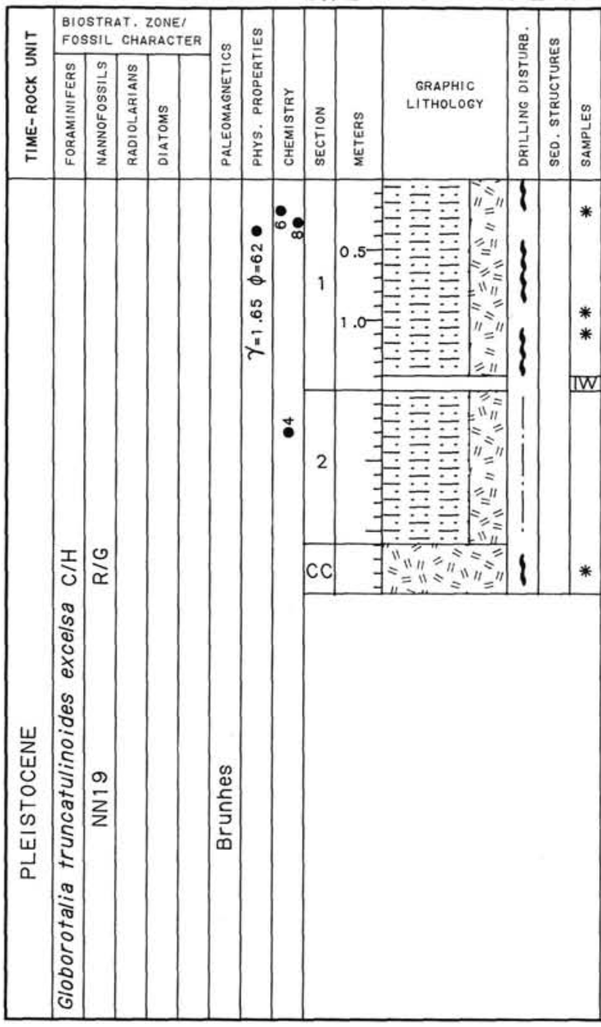

LITHOLOGIC DESCRIPTION

VOLCANICLASTIC MUDSTONE

Volcaniclastic mudstone, very dark gray (5Y 3/1) to gray (5Y 5/1), generally homogeneous to alternating laminae of mudstone and claystone; distinct laminae offset by small normal faults in Section 1, 90–110 cm, and calcareous fragment in Section 1, 52 cm.

SMEAR SLIDE SUMMARY (%):

	1, 27 D	1, 96 D	1, 111 D	CC, 15 D
TEXTURE:				
Sand	5	5	5	5
Silt	15	20	15	15
Clay	80	75	80	80
COMPOSITION:				
Quartz	5	6	5	3
Feldspar	5		3	5
Clay	60	65	54	35
Volcanic glass	23	15	30	50
Calcite/dolomite	2	2	Tr	Tr
Foraminifers	5	5	5	5
Diatoms	Tr	Tr	Tr	—
Radiolarians	Tr	3	3	2

SITE 650 HOLE A CORE 46 X CORED INTERVAL 3928.1-3937.8 mbsl; 411.8-421.5 mbsf

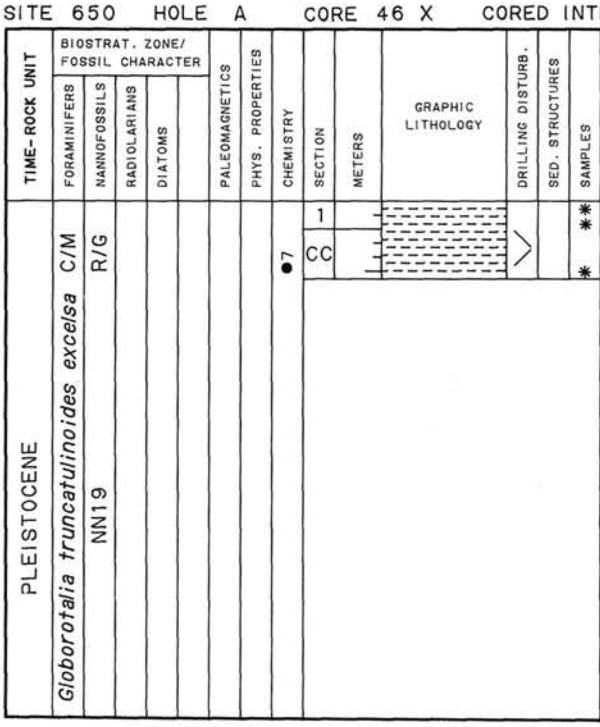

LITHOLOGIC DESCRIPTION

CLAYSTONE

Claystone, dark gray (5Y 4/1) to gray (5Y 5/1), homogeneous; putrid claystone lamina (possibly sapropellic) in CC, 30 cm.

SMEAR SLIDE SUMMARY (%):

	1, 8 D	1, 12 D	CC, 33 D
TEXTURE:			
Sand	5	5	—
Silt	15	35	—
Clay	80	60	—
COMPOSITION:			
Quartz	6	6	8
Feldspar	4	4	8
Clay	78	66	68
Volcanic glass	4	8	1
Calcite/dolomite	2	7	1
Accessory minerals	Tr	3	2
Foraminifers	5	5	4
Diatoms	—	—	1
Radiolarians	1	1	1
Silicoflagellates	—	Tr	—
Micrite	—	—	6

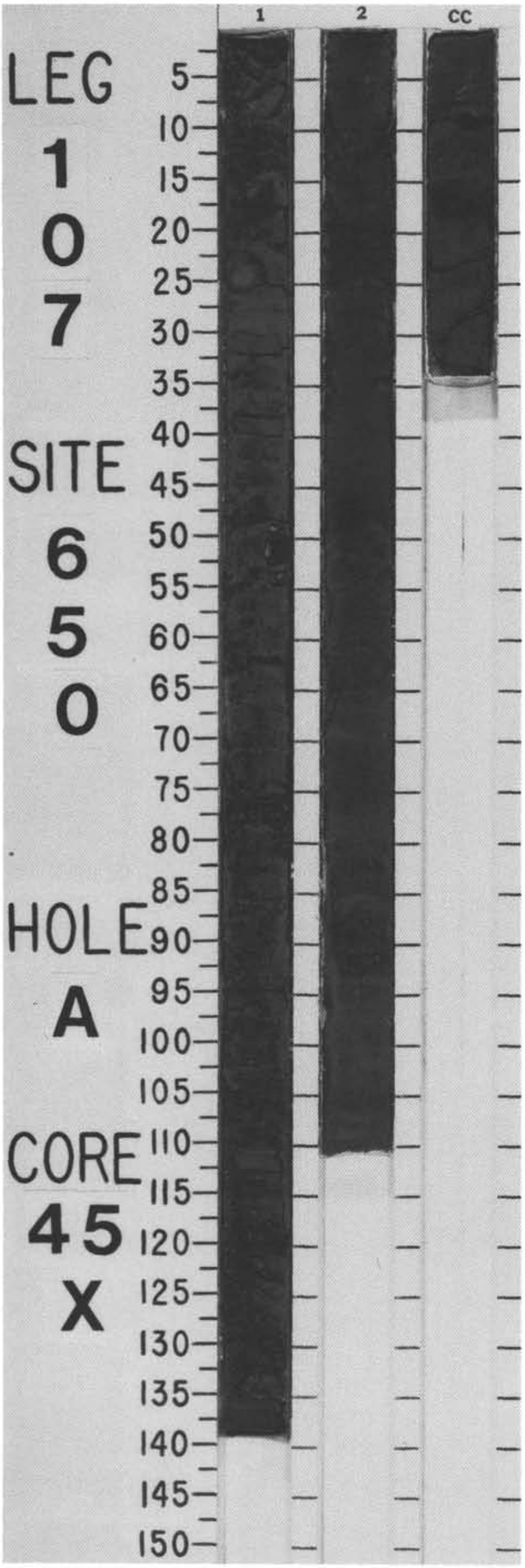
1
2
CC
LEG
1
0
7
SITE
6
5
0
HOLE
A
CORE
45
X
5
10
15
20
25
30
35
40
45
50
55
60
65
70
75
80
85
90
95
100
105
110
115
120
125
130
135
140
145
150

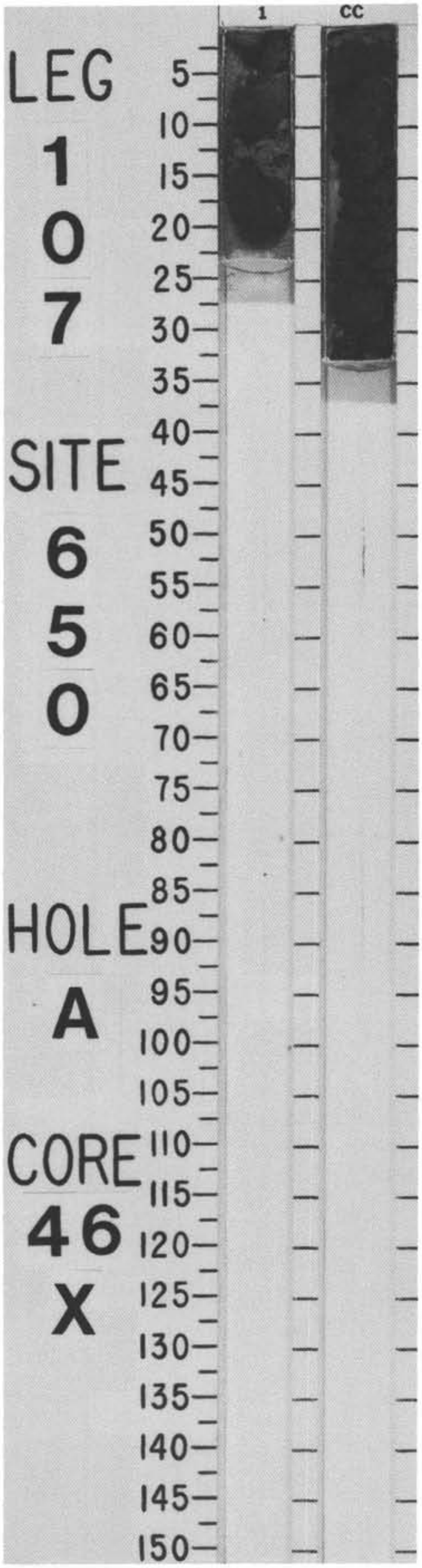
1
CC
LEG
1
0
7
SITE
6
5
0
HOLE
A
CORE
46
X
5
10
15
20
25
30
35
40
45
50
55
60
65
70
75
80
85
90
95
100
105
110
115
120
125
130
135
140
145
150

SITE 650 HOLE A CORE 47 X CORED INTERVAL 3937.8-3947.4 mbsl, 421.5-431.1 mbsf

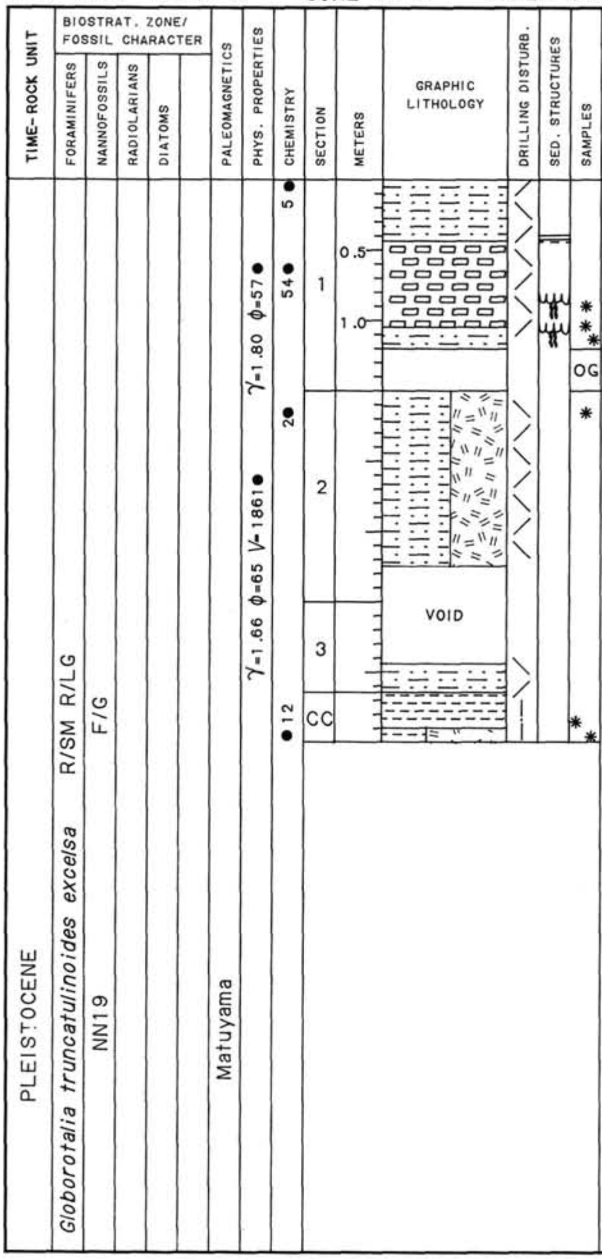

LITHOLOGIC DESCRIPTION

CLAYSTONE, CALCAROUS OOZE, and VOLCANICLASTIC MUDSTONE

Claystone, gray (5Y 5/1–6/1) to olive-gray (5Y 5/2), homogeneous to faintly laminated.

Calcareous ooze (chalk), dark gray (5Y 4/1) to light gray (5Y 7/1), sharp color changes (light over dark) defining scoured contact.

Volcaniclastic mudstone, dark gray (5Y 4/1) to gray (5Y 5/1), homogeneous.

SMEAR SLIDE SUMMARY (%):

	1, 92 D	1, 109 D	1, 115 D	2, 20 D	CC, 28 D	CC, 29 D
TEXTURE:						
Sand	10	—	—	5	10	5
Silt	20	10	10	10	10	10
Clay	70	90	90	85	80	85
COMPOSITION:						
Quartz	7	4	4	5	5	6
Feldspar	5	6	6	7	2	5
Clay	72	85	80	47	75	31
Volcanic glass	Tr	Tr	Tr	35	10	50
Calcite/dolomite	—	—	2	—	Tr	—
Accessory minerals	Tr	Tr	—	1	Tr	Tr
Foraminifers	8	3	5	3	7	5
Nannofossils	Tr	—	Tr	—	—	—
Diatoms	3	Tr	3	2	—	—
Radiolarians	2	—	Tr	Tr	1	3
Sponge spicules	Tr	—	—	—	—	—
Silicoflagellates	Tr	—	Tr	Tr	—	—
Micrite	3	2	Tr	—	Tr	—

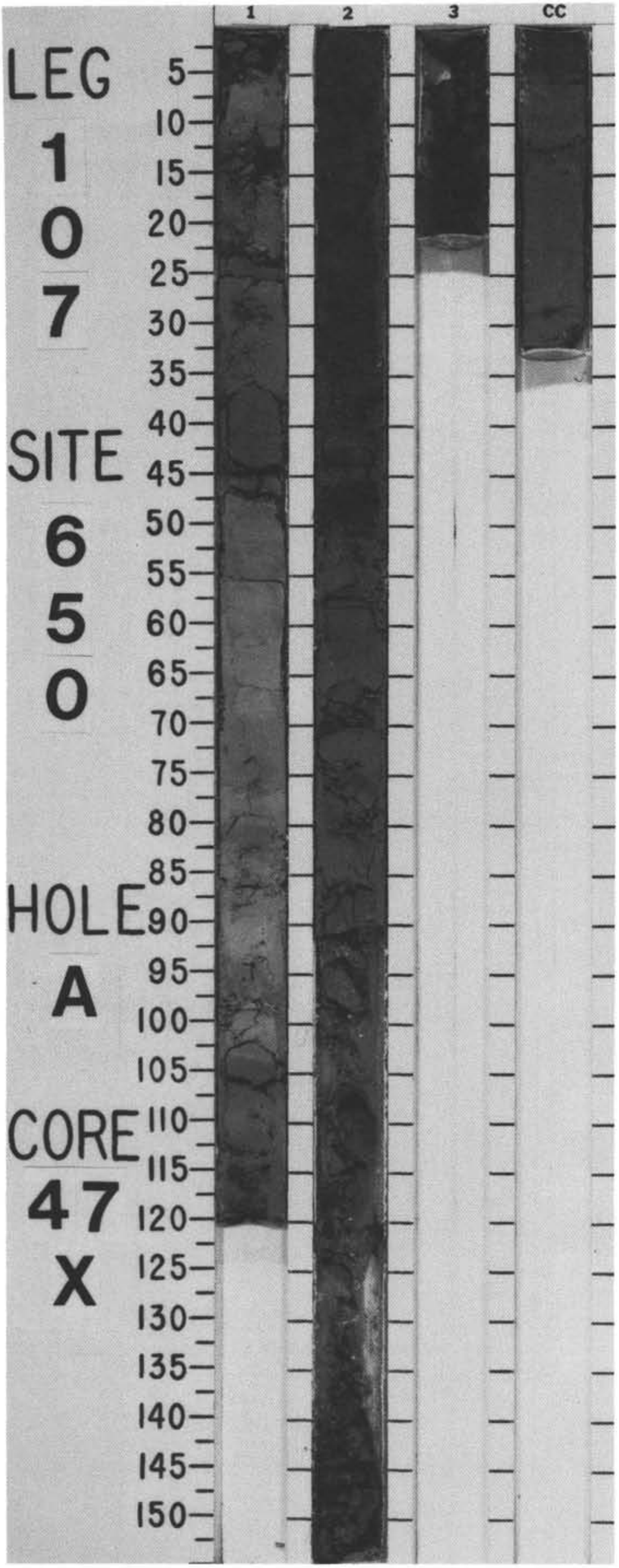
LEG
107
SITE
650
HOLE
A
CORE
47
X
1
2
3
CC
5
10
15
20
25
30
35
40
45
50
55
60
65
70
75
80
85
90
95
100
105
110
115
120
125
130
135
140
145
150

SITE 650 HOLE A CORE 48 X CORED INTERVAL 3947.4-3957.1 mbsl; 431.1-440.8 mbsf

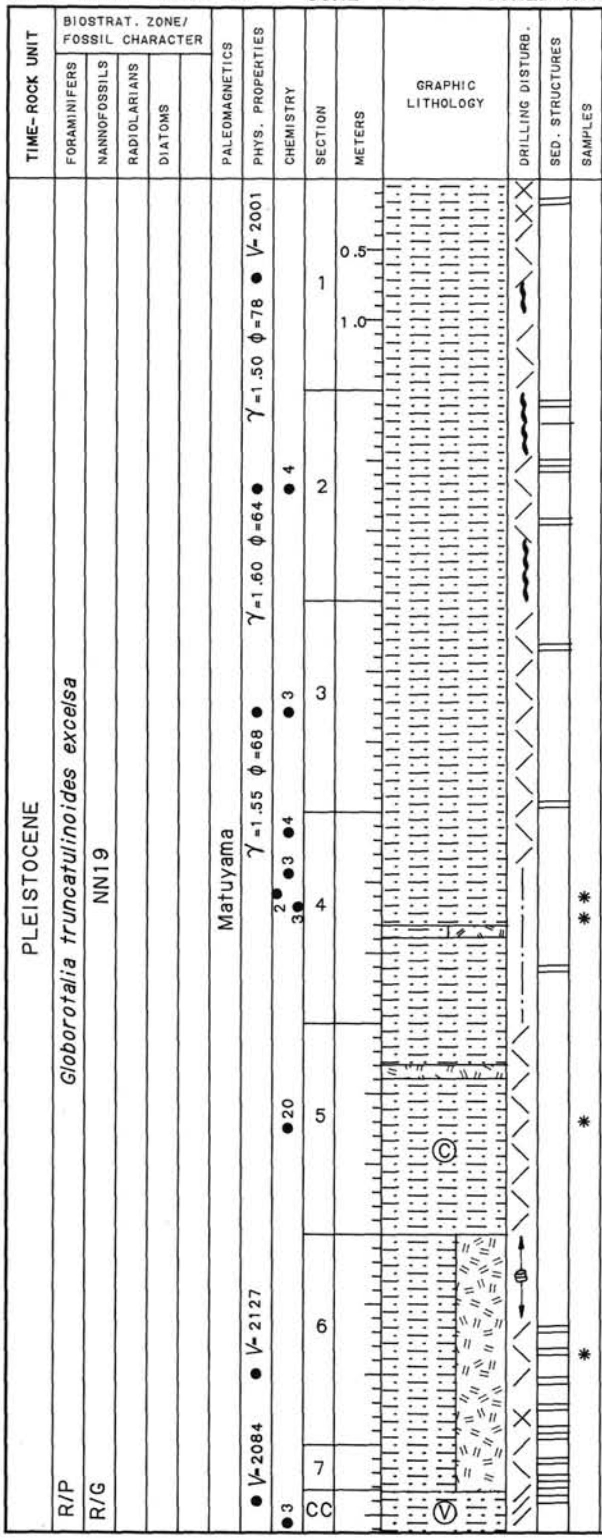

LITHOLOGIC DESCRIPTION

Thin to very thick bedded alternations of MUDSTONE, CALCAREOUS MUDSTONE, and VOLCANICLASTIC MUDSTONE

Mudstone and calcareous mudstone, olive-gray (5Y 4/2–5/2), generally homogeneous and disturbed by drilling, but undisturbed pieces (drilling biscuits) are finely laminated; black (5Y 2.5/1) laminations and broken pieces (possibly sapropelic) found in Section 3, 37 cm, 147–150 cm, and in Section 4, 35–63 cm, foraminiferal tests infilled with pyrite.

Volcaniclastic mudstone, greenish gray (5BG 5/1), dark greenish gray (5GY 4/1) to light greenish gray (5GY 7/1), and gray (5Y 6/1) to light gray (5Y 7/1); color change downcore from gray and olive-gray to greenish gray corresponds to an increase in volcanic material.

SMEAR SLIDE SUMMARY (%):

	4, 60 M	4, 78 M	5, 70.5 D	6, 84 D
TEXTURE:				
Sand	—	3	—	—
Silt	10	12	10	—
Clay	90	85	90	—
COMPOSITION:				
Quartz	2	3	2	2
Rock fragments	—	Tr	—	—
Mica	Tr	—	—	—
Clay	90	50	78	40
Volcanic glass	5	40	—	50
Calcite/dolomite	—	3	10	2
Accessory minerals	2	2	2	2
Opaques	Tr	—	—	—
Foraminifers	1	2	—	1
Nannofossils	—	—	8	3
Sponge spicules	—	Tr	—	Tr
Silicoflagellates	Tr	—	—	—

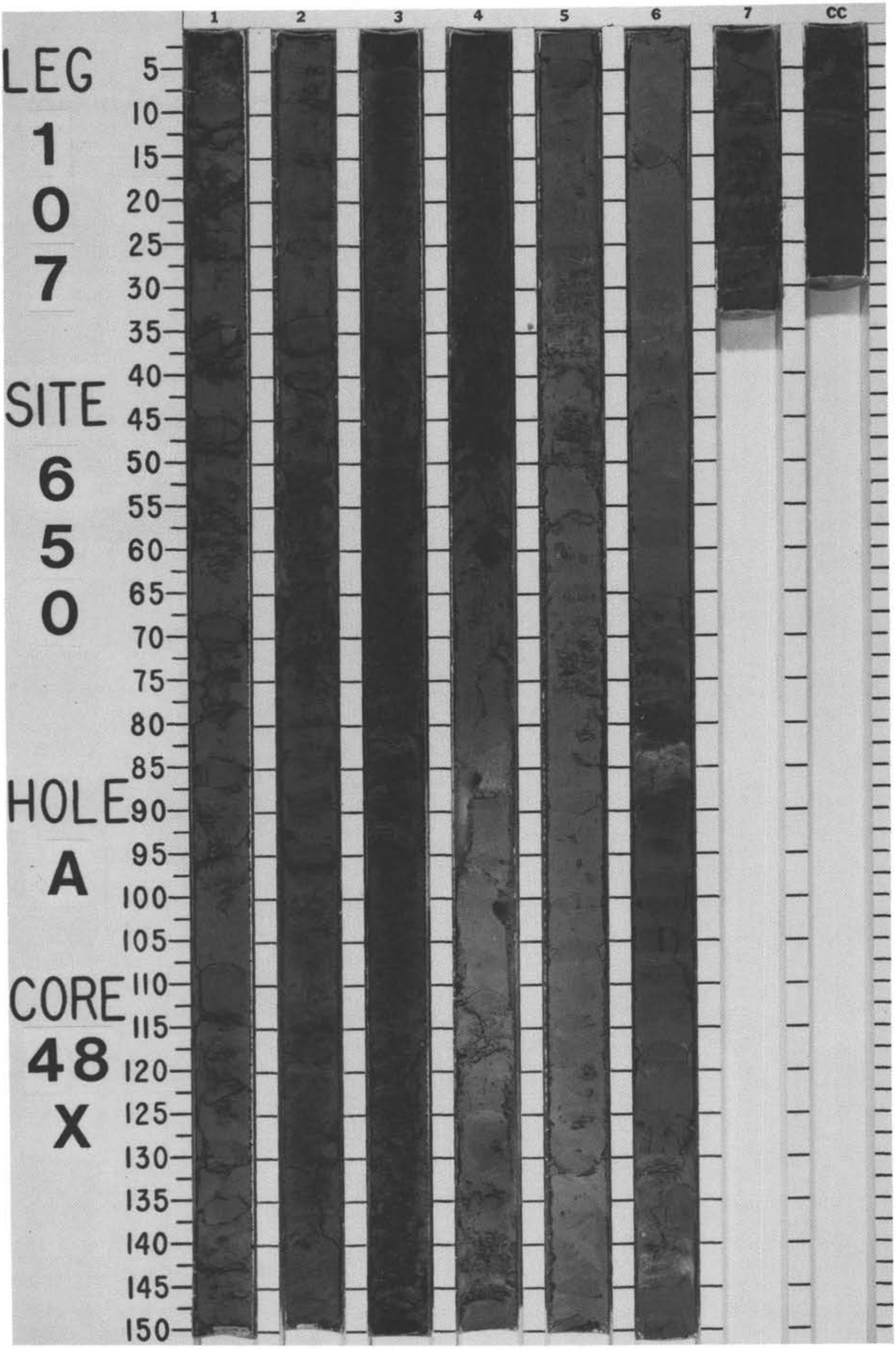
LEG
1
0
7
SITE
6
5
0
HOLE
A
CORE
48
X
1
2
3
4
5
6
7
CC
5
10
15
20
25
30
35
40
45
50
55
60
65
70
75
80
85
90
95
100
105
110
115
120
125
130
135
140
145
150

SITE 650 HOLE A CORE 49 X CORED INTERVAL 3957.1-3966.7 mbsl; 440.8-450.4 mbsf

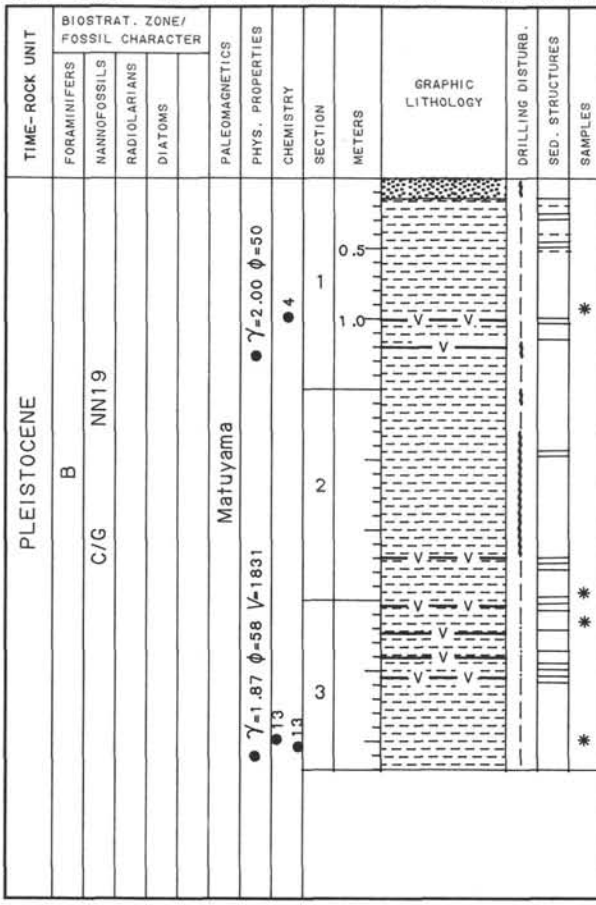

LITHOLOGIC DESCRIPTION

SANDY SILTSTONE, CLAYSTONE, and CALCAREOUS CLAYSTONE

Sandy siltstone, light olive-gray (5Y 6/2), brecciated, "salt and pepper" appearance.

Claystone and calcareous claystone, dark gray (5Y 4/1) to olive-gray (5Y 5/3), homogeneous to faintly laminated; pyrite infilling foraminiferal tests in Section 2.

Minor lithology: silty ash, light olive-gray (5Y 6/2) and olive-gray (5Y 5/2–10Y 6/3); laminae in Section 1, 104–117 cm, Section 2, 120–130 cm, and Section 3, 0–62 cm.

SMEAR SLIDE SUMMARY (%):

	1, 100 D	2, 147 M	3, 20 M	3, 100 D
TEXTURE:				
Sand	—	5	—	—
Silt	10	75	10	5
Clay	90	20	90	95
COMPOSITION:				
Quartz	2	5	15	2
Feldspar	1	10	5	10
Rock fragments	—	Tr	—	—
Clay	40	10	45	20
Volcanic glass	2	40	15	17
Calcite/dolomite	—	—	5	2
Accessory minerals	—	10	—	—
Opaques	—	10	—	—
Foraminifers	5	10	—	2
Nannofossils	45	5	10	42
Micrite	5	—	5	5

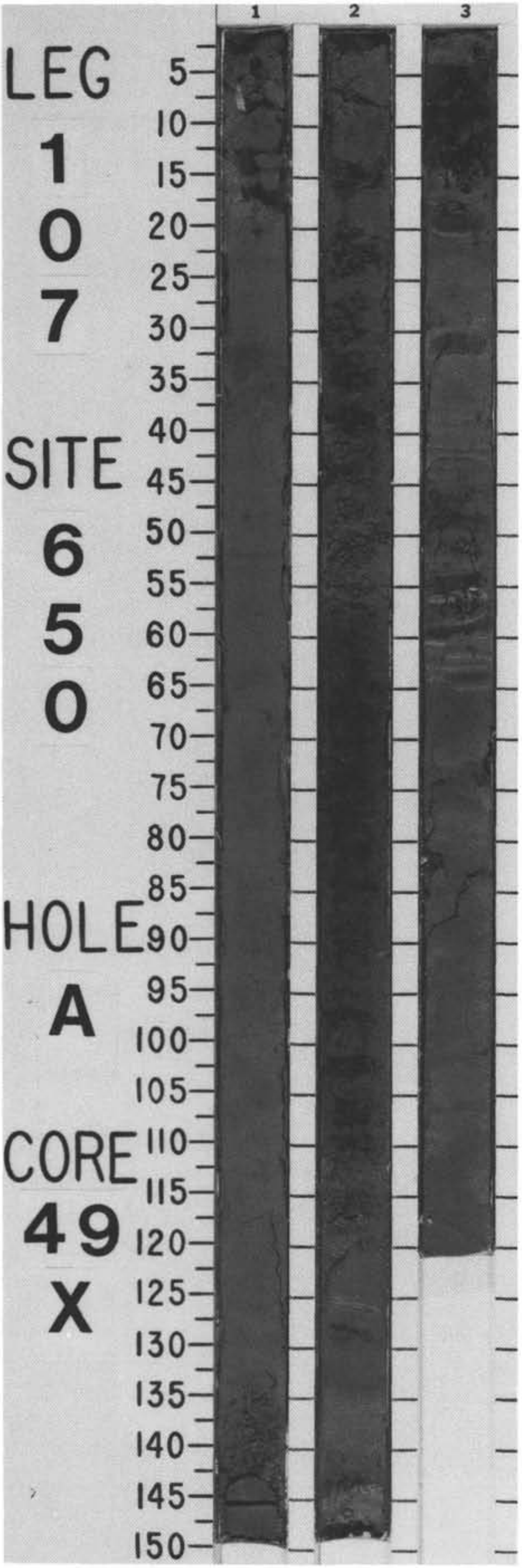
LEG
1
0
7
SITE
6
5
0
HOLE
A
CORE
49
X
1
2
3
5
10
15
20
25
30
35
40
45
50
55
60
65
70
75
80
85
90
95
100
105
110
115
120
125
130
135
140
145
150

SITE 650 HOLE A CORE 50 X CORED INTERVAL 3966.7-3976.4 mbsl 450.4-460.1 mbsf

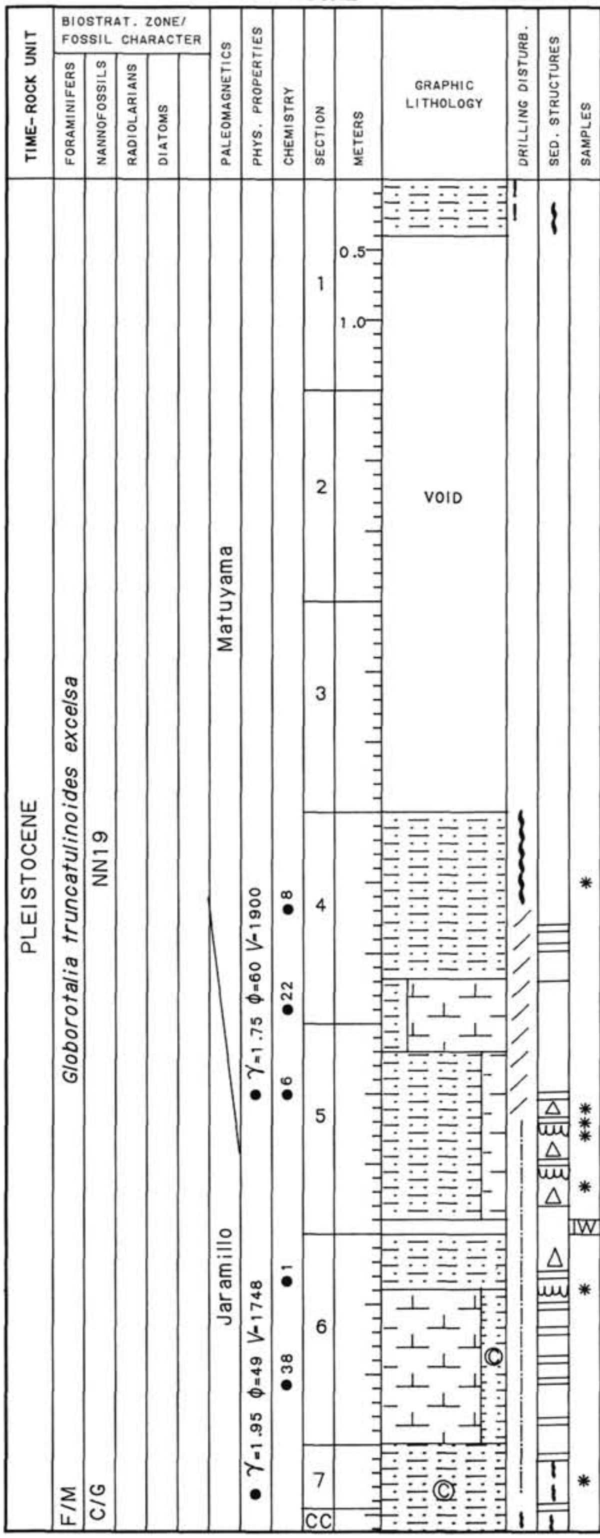

LITHOLOGIC DESCRIPTION

Very thin- to thick-bedded alternations of MUDSTONE, CALCAREOUS MUDSTONE, and NANNOFOSSIL OOZE (CHALK)

Mudstone and calcareous mudstone, dark olive-gray (5Y 3/2) to gray (5Y 5/1) and dusky yellowish green (5GY 5/1) to light olive-gray (5GY 5/2), homogeneous to faintly laminated and mottled, diffuse black sulfide(?) halo in Section 7.

Marly nannofossil ooze (chalk), gray (5Y 6/1) to light gray (5Y 7/2), homogeneous.

Minor lithology: silty tuff, dark olive-gray (5Y 3/2), laminae to very thin beds; generally has a scoured lower contact and grades normally into faintly laminated mudstone in Section 5, 61, 73, 100–102, and 129 cm, and Section 6, 30–36 cm.

SMEAR SLIDE SUMMARY (%):

	4, 50 D	5, 61 M	5, 70 D	5, 86 M	5, 118 D	6, 36 M	7, 25 D
TEXTURE:							
Sand	—	—	—	—	—	10	—
Silt	20	40	10	20	20	40	15
Clay	80	60	90	80	80	50	85
COMPOSITION:							
Quartz	—	2	1	2	1	5	1
Feldspar	—	—	1	2	1	10	1
Clay	20	20	14	24	12	35	15
Volcanic glass	10	2	—	—	5	20	2
Calcite/dolomite	5	6	3	7	4	—	5
Accessory minerals	5	5	—	—	1	—	—
Opaques	—	—	—	15	—	10	1
Pyroxene	—	—	—	—	Tr	1	—
Foraminifers	—	30	—	—	—	—	5
Nannofossils	30	20	30	30	50	5	50
Sponge spicules	—	—	1	—	—	—	—
Micrite	30	15	50	20	26	14	20

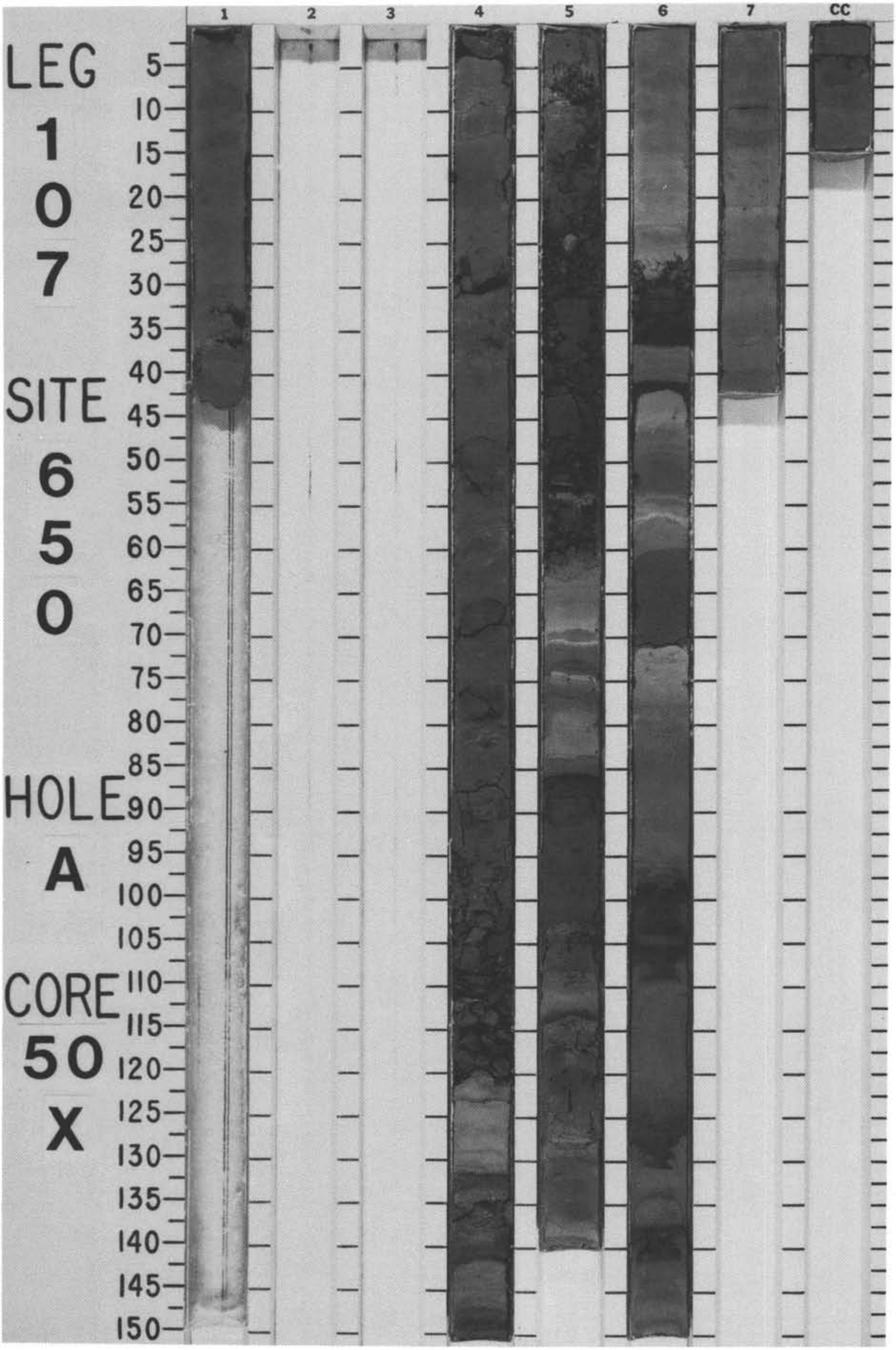
LEG 107
SITE 650
HOLE A
CORE 50X
1 2 3 4 5 6 7 CC
5 10 15 20 25 30 35 40 45 50 55 60 65 70 75 80 85 90 95 100 105 110 115 120 125 130 135 140 145 150

SITE 650 HOLE A CORE 51 X CORED INTERVAL 3976.4-3985.4 mbsl; 460.1-469.1 mbsf

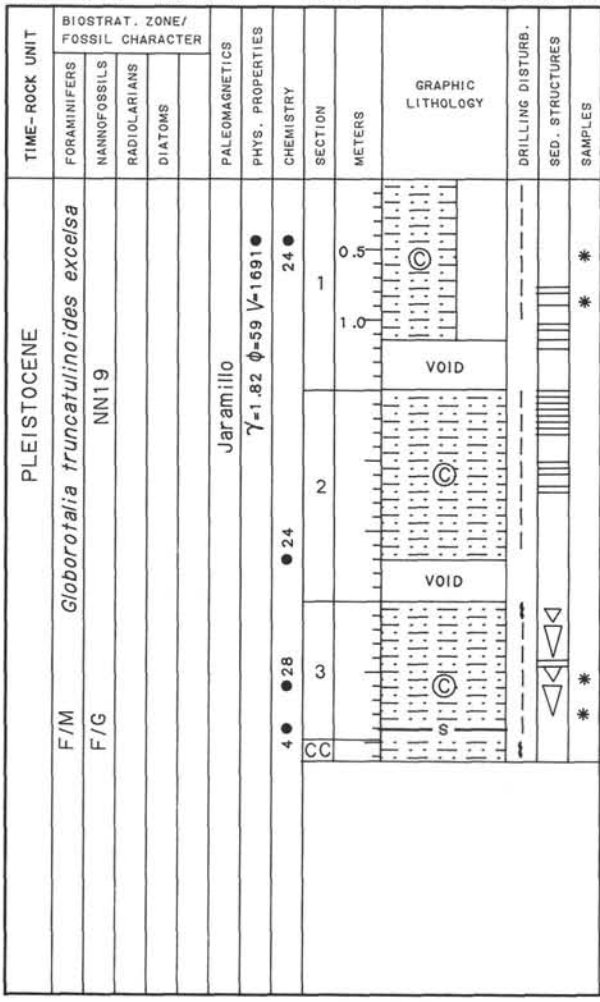

LITHOLOGIC DESCRIPTION

CALCAREOUS MUDSTONE

Calcareous mudstone, dark gray (5Y 4/1) to gray (5Y 6/1), homogeneous to faintly laminated in Section 1, faintly laminated in Section 2, and has coarsening-upward sequences in Section 3.

Minor lithology: silt, black (5Y 2.5/2) to dark olive-gray (5Y 3/2), high-angle (15–30°) cross-stratification, commonly foraminiferal in Section 1, 83–88 cm, in Section 2, 106–107 and 114–116 cm, and in Section 3, 54–55 cm. Sapropel, black (5Y 2.5/1) in Section 3, 80–81, 84–86, and 90–92 cm.

SMEAR SLIDE SUMMARY (%):

	1, 58 D	1, 86 D	3, 59 D	3, 89 M
TEXTURE:				
Sand	—	5	—	—
Silt	15	50	25	40
Clay	85	45	75	60
COMPOSITION:				
Quartz	5	20	5	25
Feldspar	1	5	2	5
Mica	—	—	—	2
Clay	59	20	48	53
Volcanic glass	5	5	—	—
Foraminifers	1	30	10	2
Nannofossils	24	15	30	10
Sponge spicules	—	—	—	1
Micrite	5	5	5	2

SITE 650 HOLE A CORE 52 X CORED INTERVAL 3985.4-3995.6 mbsl; 469.7-479.3 mbsf

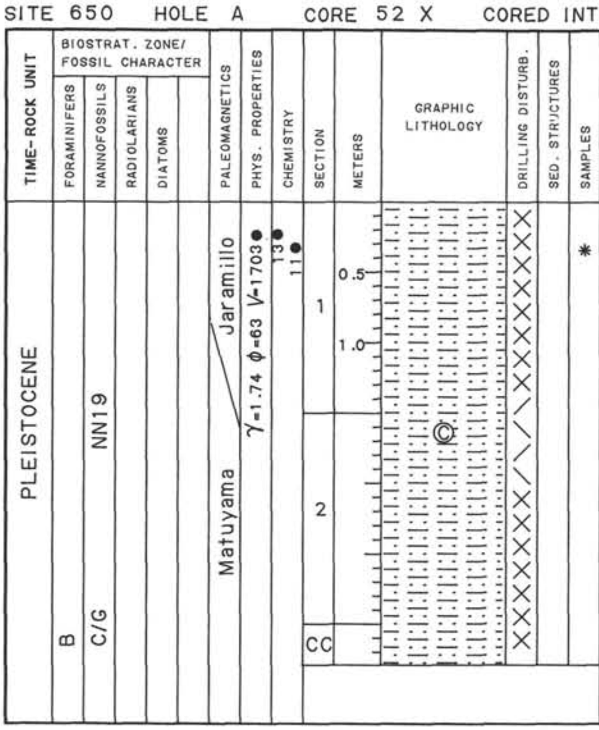

LITHOLOGIC DESCRIPTION

CALCAREOUS MUDSTONE

Calcareous mudstone, dusky yellowish green (5GY 5/2), homogeneous drilling breccia.

SMEAR SLIDE SUMMARY (%):

	1, 30 D
TEXTURE:	
Sand	—
Silt	15
Clay	85
COMPOSITION:	
Quartz	15
Feldspar	2
Clay	40
Volcanic glass	5
Accessory minerals	2
Foraminifers	1
Nannofossils	30
Sponge spicules	5

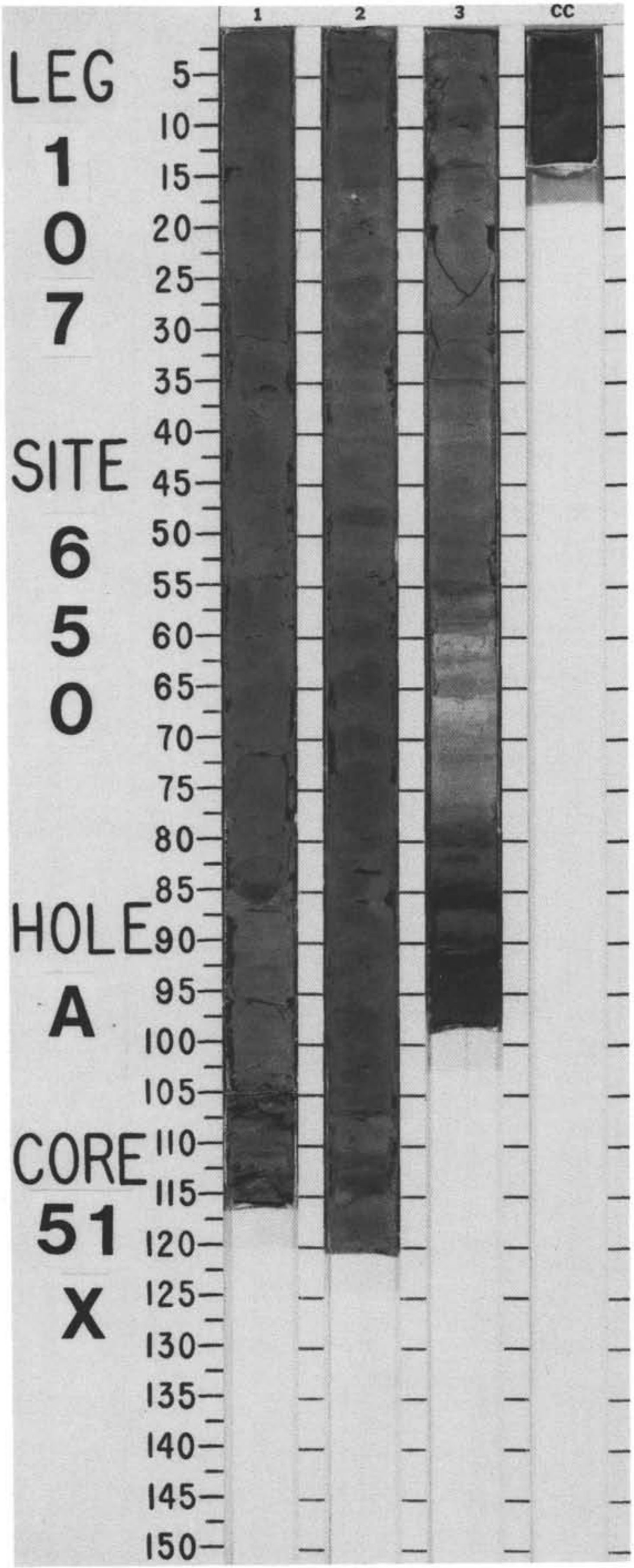
1
2
3
CC
LEG
107
SITE
650
HOLE
A
CORE
51
X

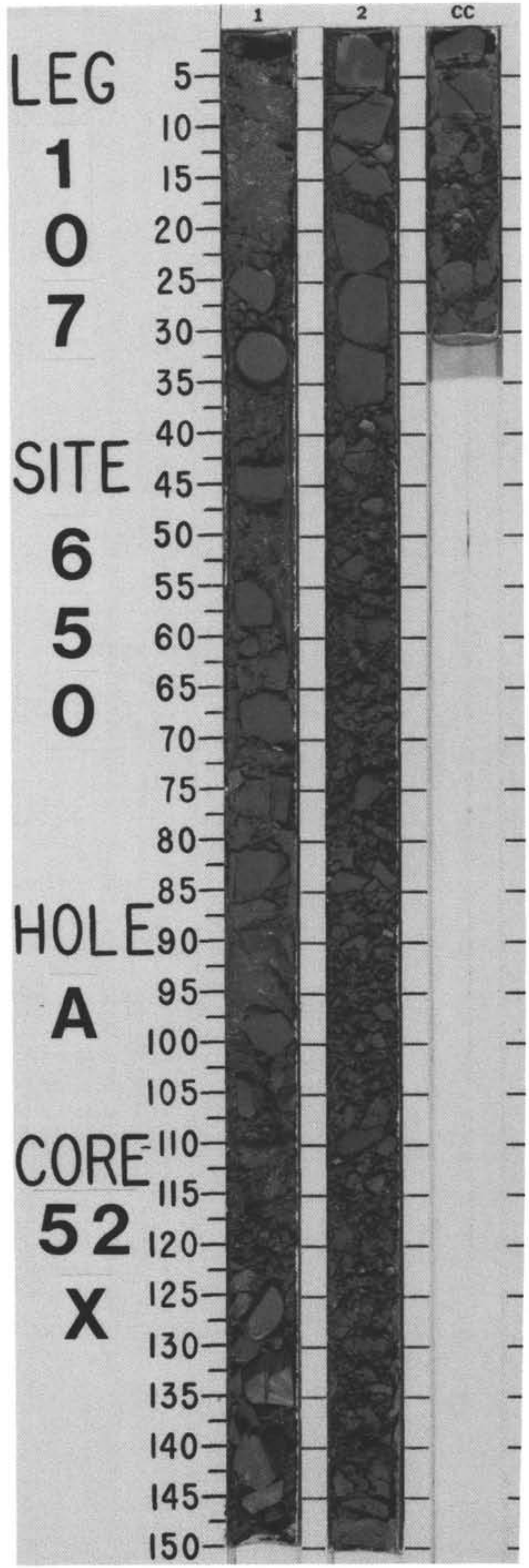
1
2
CC
LEG
107
SITE
650
HOLE
A
CORE
52
X

SITE 650 HOLE A CORE 53 X CORED INTERVAL 3995.6-4005.2 mbsl; 479.3-488.9 mbsf

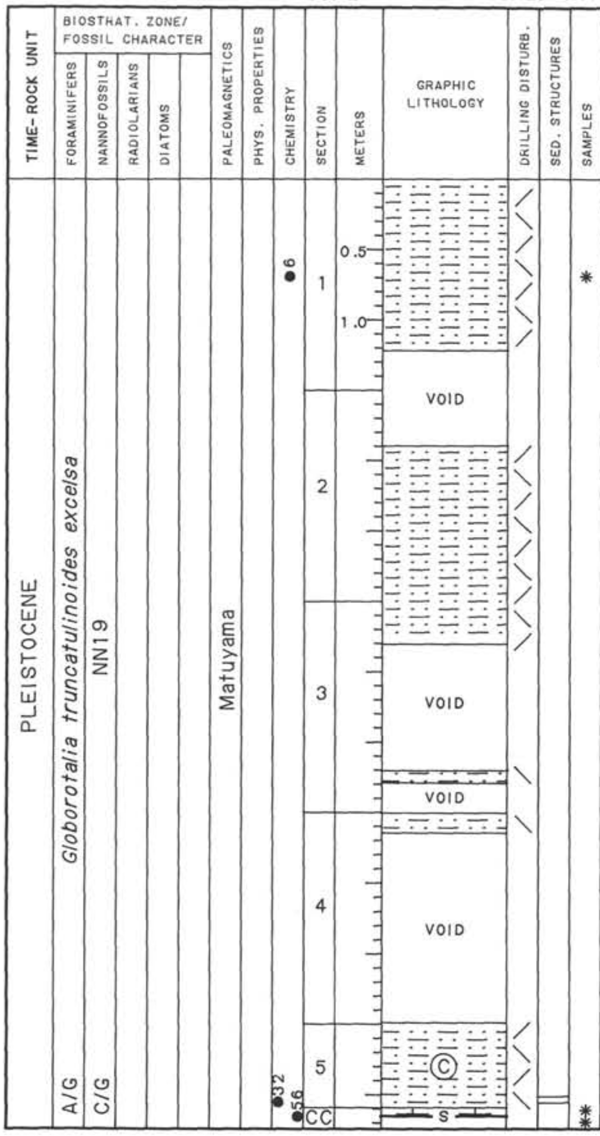

LITHOLOGIC DESCRIPTION

MUDSTONE and CALCAREOUS MUDSTONE

Mudstone and calcareous mudstone, dusky yellowish green (5GY 5/2) and gray (5Y 5/1), homogeneous drilling breccia.

Minor lithology: dark mudstone (possibly sapropelic), black (5Y 2.5/1) in Section 5, 59 cm, and in CC, 4 cm.

SMEAR SLIDE SUMMARY (%):

	1, 65 D	CC, 4 D	CC, 8 D
TEXTURE:			
Sand	—	—	—
Silt	50	40	20
Clay	50	60	80
COMPOSITION:			
Feldspar	—	10	2
Mica	—	—	25
Clay	35	15	—
Volcanic glass	10	15	—
Calcite/dolomite	Tr	Tr	1
Cement	—	—	1
Accessory minerals	—	20	2
Foraminifers	—	—	10
Nannofossils	10	20	30
Sponge spicules	5	Tr	—
Micrite	40	20	30

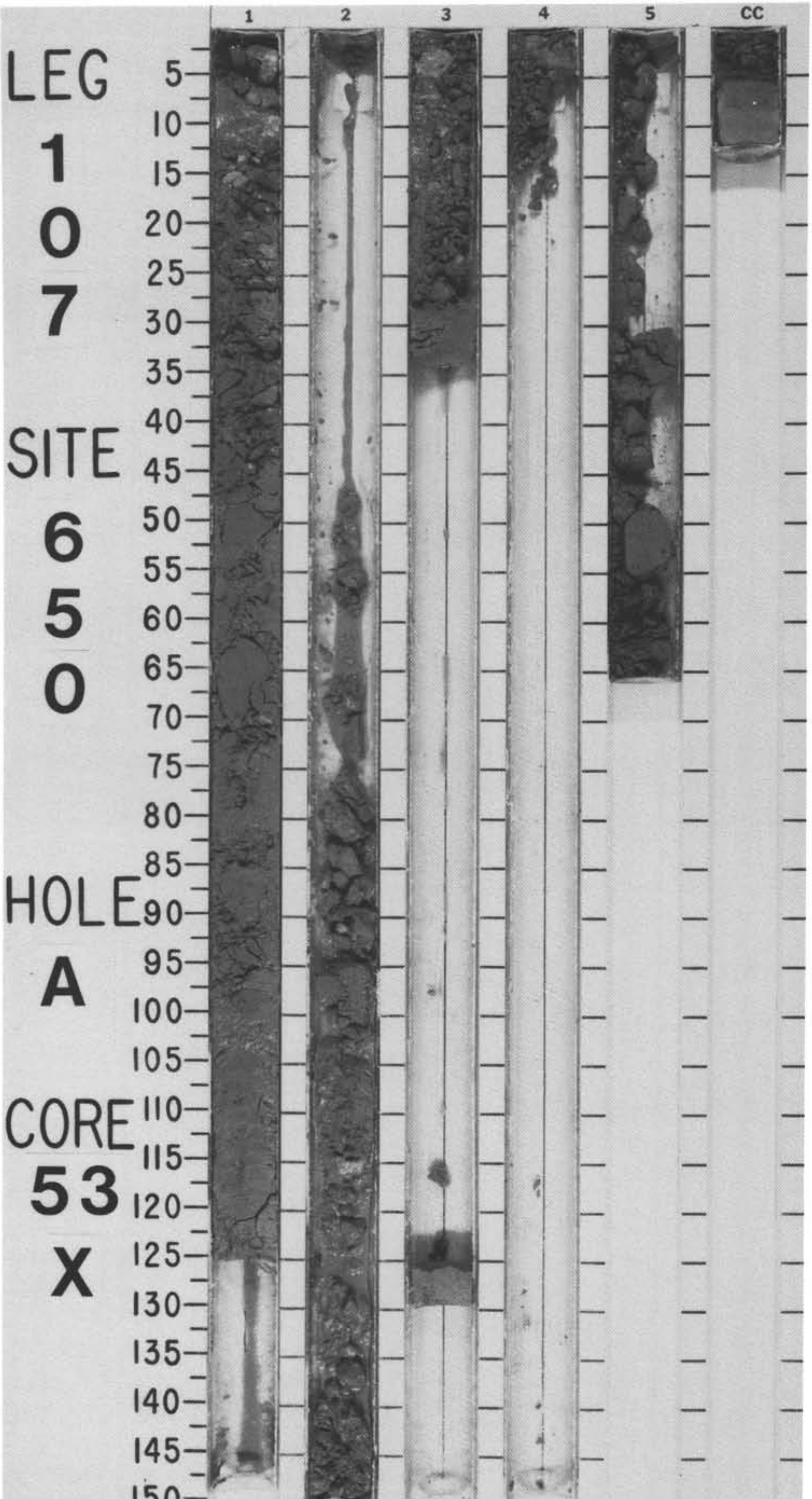
LEG
1
0
7
SITE
6
5
0
HOLE
A
CORE
53
X
1
2
3
4
5
CC
5
10
15
20
25
30
35
40
45
50
55
60
65
70
75
80
85
90
95
100
105
110
115
120
125
130
135
140
145
150

SITE 650 HOLE A CORE 54 X CORED INTERVAL 4005.2-4014.9 mbsl; 488.9-498.6 mbsf

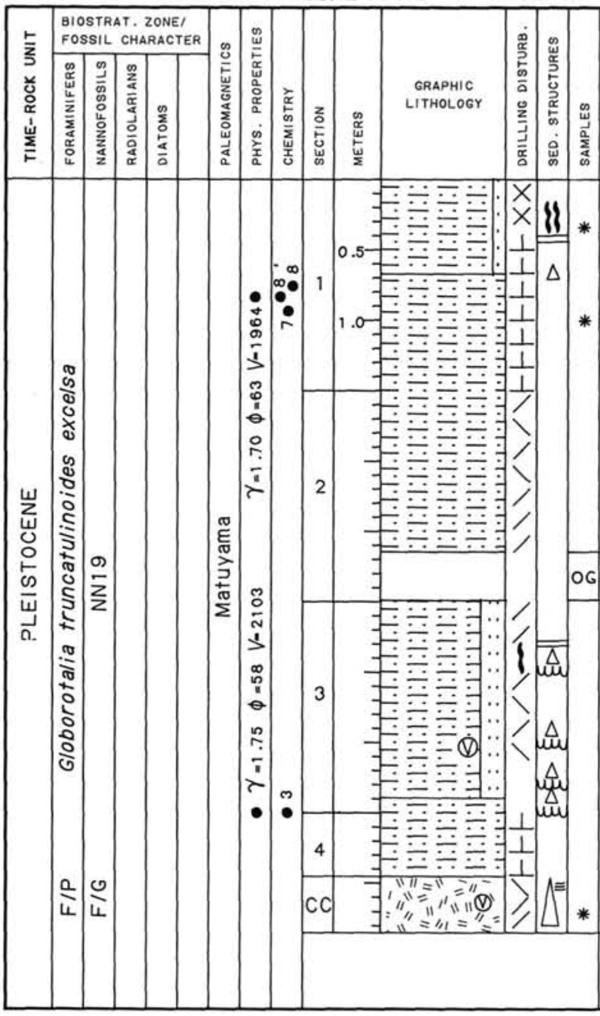

LITHOLOGIC DESCRIPTION

MUDSTONE

Mudstone, grayish green (5G 5/2) and olive-gray (5Y 5/2) to light olive-gray (5Y 6/2), homogeneous, volcaniclastic; pumice fragments in Section 3, 122 cm, and CC, 27 cm.

Minor lithology: siltstone, gray (5Y 6/1), laminae to very thin beds overlying scoured contacts, normally graded, micro-cross-laminated in Section 1, 68 and 75 cm, and in Section 3, 50, 103, 130, and 136–137 cm.

SMEAR SLIDE SUMMARY (%):

	1, 36 D	1, 93 D	CC, 24 D
TEXTURE:			
Sand	—	—	—
Silt	20	25	25
Clay	80	75	75
COMPOSITION:			
Feldspar	2	—	10
Rock fragments	—	2	—
Clay	30	30	50
Volcanic glass	2	10	10
Calcite/dolomite	1	3	2
Accessory minerals	—	—	2
Opaques	5	—	5
Nannofossils	30	30	—
Sponge spicules	—	2	1
Micrite	30	23	20

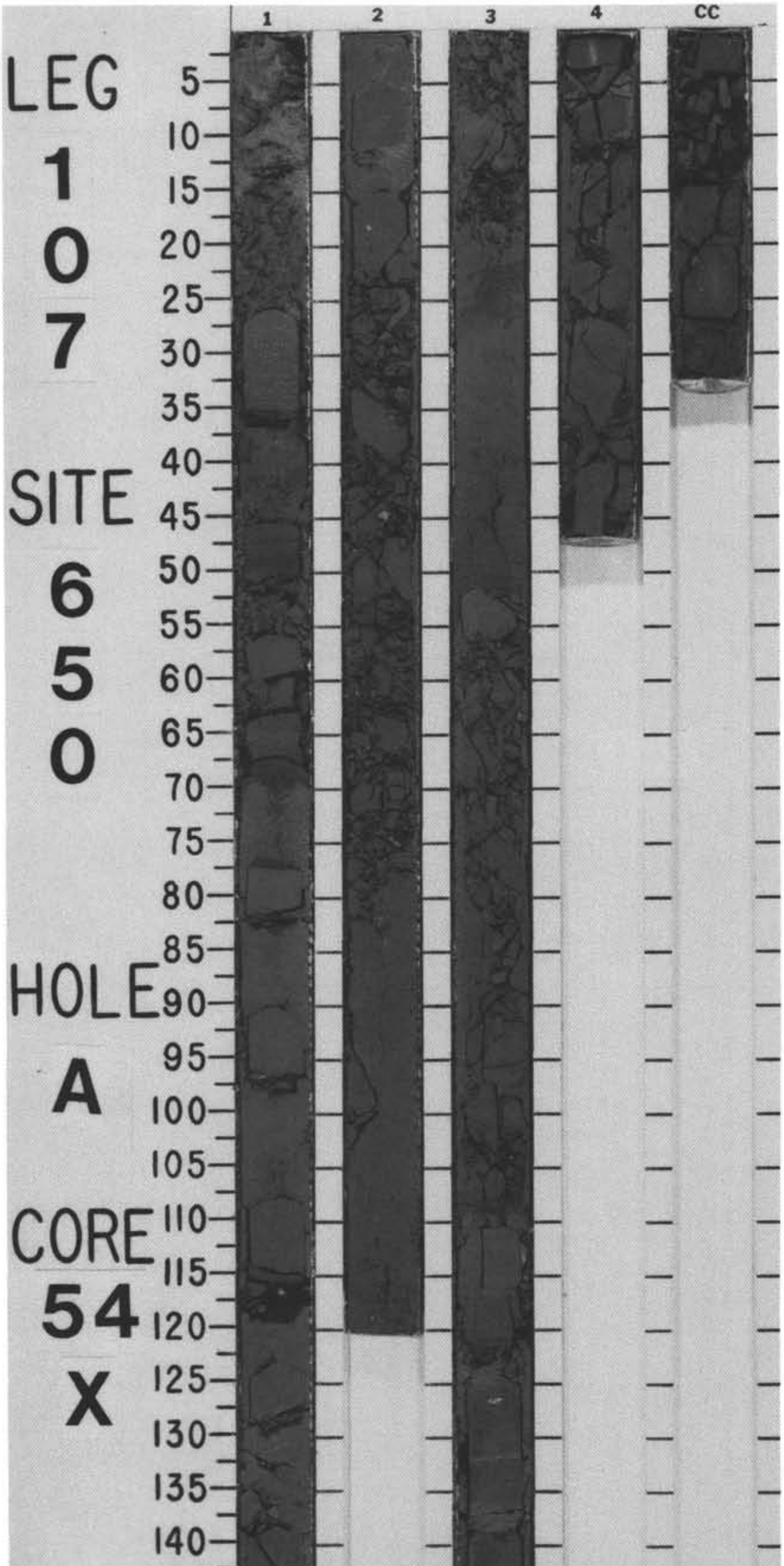
LEG
1
0
7
SITE
6
5
0
HOLE
A
CORE
54
X
1
2
3
4
CC

SITE 650 HOLE A CORE 55 X CORED INTERVAL 4014.9-4024.5 mbsl; 498.2-508.2 mbsf

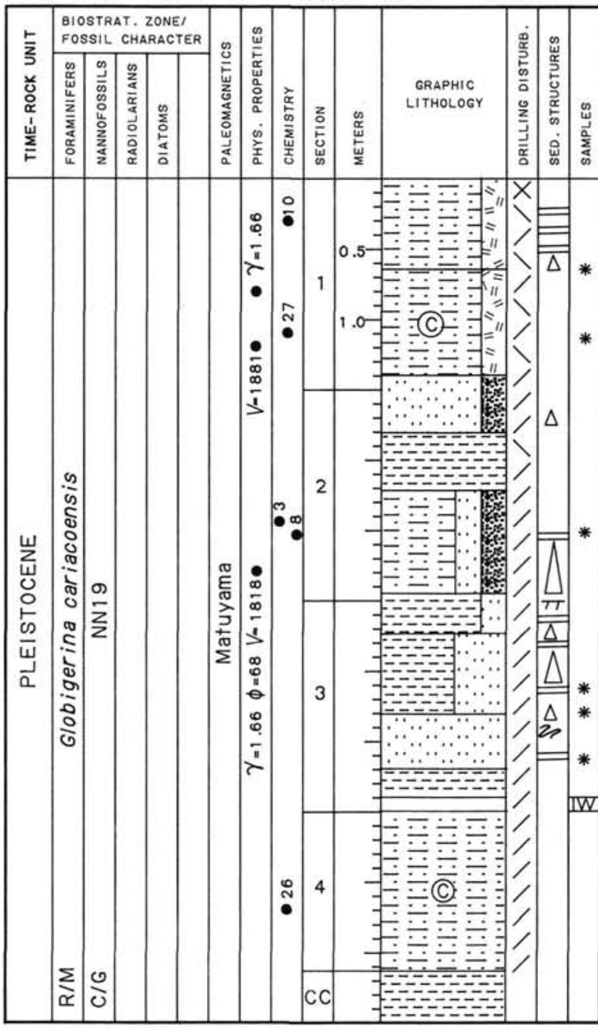

LITHOLOGIC DESCRIPTION

Multiple sequences of SANDSTONE and SILTSTONE fining upward into MUDSTONE and CLAYSTONE

Claystone and mudstone, dark greenish gray (5G 4/1) to greenish gray (5G 6/1, 5GY 5/1–6/1, and 5BG 5/1), homogeneous to faintly laminated, generally calcareous.

Siltstone and sandstone, dark gray (5Y 4/1) to gray (5Y 5/1), generally volcaniclastic and cross-laminated with a scoured basal contact.

SMEAR SLIDE SUMMARY (%):

	1, 62 M	1, 112 D	2, 103 D	3, 69 D	3, 86 M	3, 118 M
TEXTURE:						
Sand	10	—	—	—	—	—
Silt	60	20	15	15	15	15
Clay	30	80	85	85	85	85
COMPOSITION:						
Quartz	20	5	2	2	2	2
Feldspar	Tr	—	1	—	—	—
Mica	2	—	Tr	Tr	—	1
Clay	13	60	60	67	61	80
Volcanic glass	40	20	15	5	5	7
Calcite	12	5	5	11	25	3
Accessory minerals	20	2	1	2	—	—
Pyrite? (micronodules)fl—	—	—	—	Tr	—	
Foraminifers	2	Tr	1	3	5	1
Nannofossils	—	6	15	10	—	5
Diatoms	1	—	—	—	—	—
Radiolarians	—	1	—	—	2	—
Sponge spicules	—	1	—	—	Tr	1
Plant debris	—	—	—	—	Tr	—

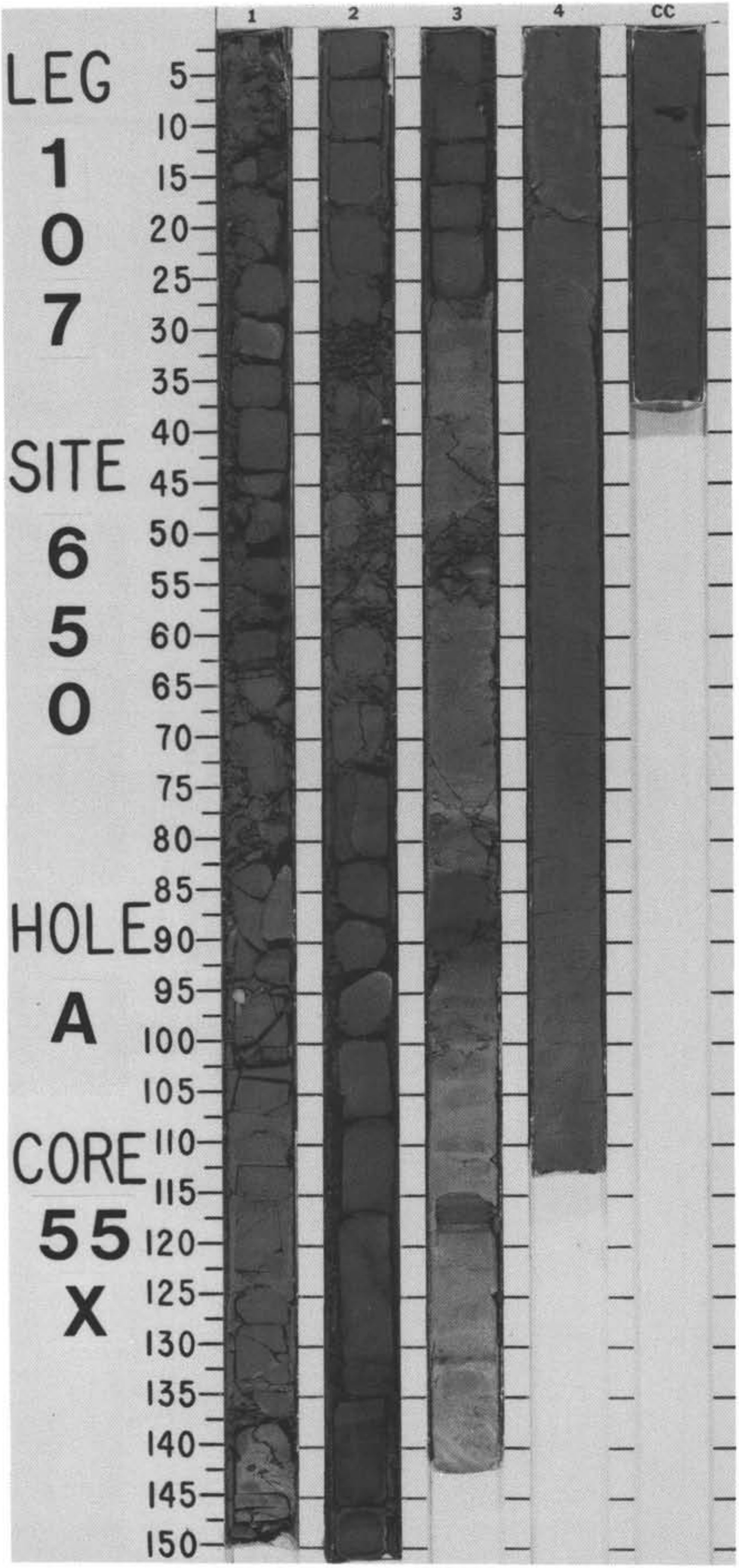
LEG 107
SITE 650
HOLE A
CORE 55 X
1
2
3
4
CC
5
10
15
20
25
30
35
40
45
50
55
60
65
70
75
80
85
90
95
100
105
110
115
120
125
130
135
140
145
150

SITE 650 HOLE A CORE 56 X CORED INTERVAL 4024.5-4034.2 mbsl; 508.2-517.9 mbsf

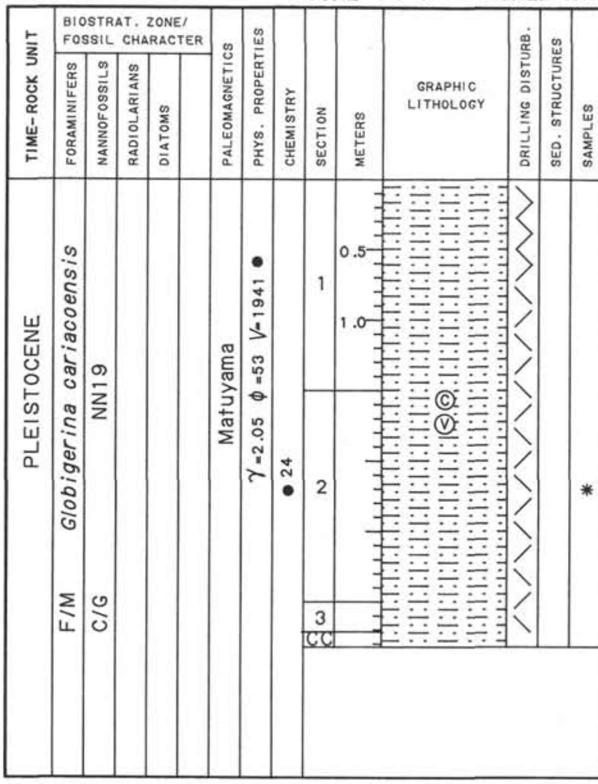

LITHOLOGIC DESCRIPTION

TUFFACEOUS CALCAREOUS MUDSTONE

Tuffaceous calcareous mudstone, greenish gray (5GY 5/1), homogeneous brecciated mudstone alternating with homogeneous undisturbed mudstone (drilling biscuits).

SMEAR SLIDE SUMMARY (%):

	2, 75
	D
TEXTURE:	
Sand	—
Silt	20
Clay	80
COMPOSITION:	
Quartz	3
Feldspar	4
Clay	58
Volcanic glass	30
Calcite/dolomite	1
Foraminifers	Tr
Nannofossils	Tr
Diatoms	Tr
Radiolarians	Tr
Silicoflagellates	Tr
Micrite	4

SITE 650 HOLE A CORE 57 X CORED INTERVAL 4034.2-4043.8 mbsl; 517.9-527.5 mbsf

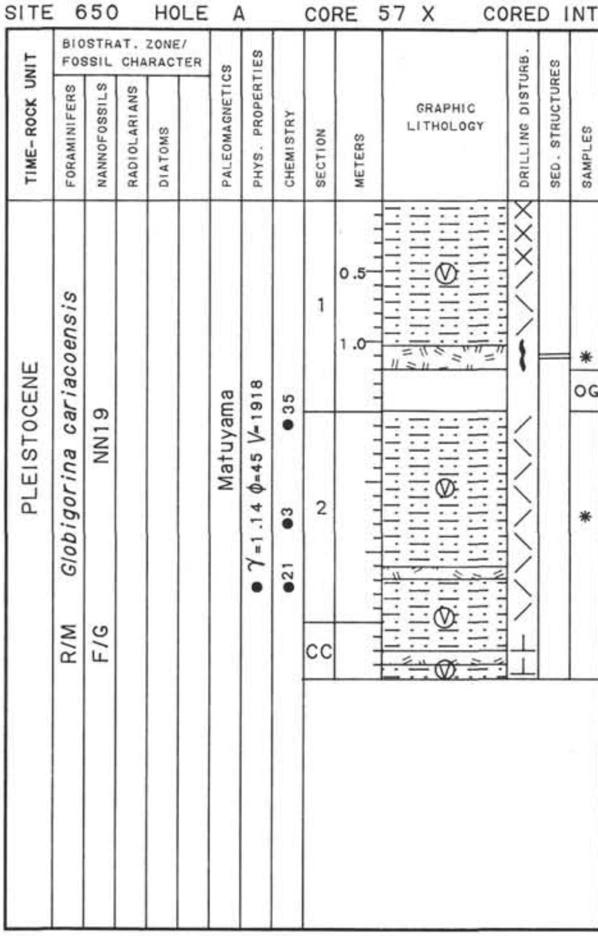

LITHOLOGIC DESCRIPTION

TUFFACEOUS MUDSTONE and CLAYEY VOLCANICLASTIC SILT

Tuffaceous mudstone, gray (5Y 5/1), homogeneous; calcareous and very indurated in Section 1, 6–10 cm.

Clayey volcaniclastic silt, laminated, coarsening into minor sandy intervals in Section 1, 108–111 cm, in Section 2, 116–120 cm, and in CC, 16–17 and 23–29 cm.

SMEAR SLIDE SUMMARY (%):

	1, 111	2, 75
	M	D
TEXTURE:		
Sand	15	5
Silt	45	50
Clay	40	45
COMPOSITION:		
Quartz	2	2
Feldspar	8	4
Mica	—	1
Clay	33	35
Volcanic glass	40	50
Accessory minerals	2	2
Foraminifers	5	3
Nannofossils	2	Tr
Radiolarians	2	—
Sponge spicules	3	3
Fish remains	—	Tr
Spar cement	3	—

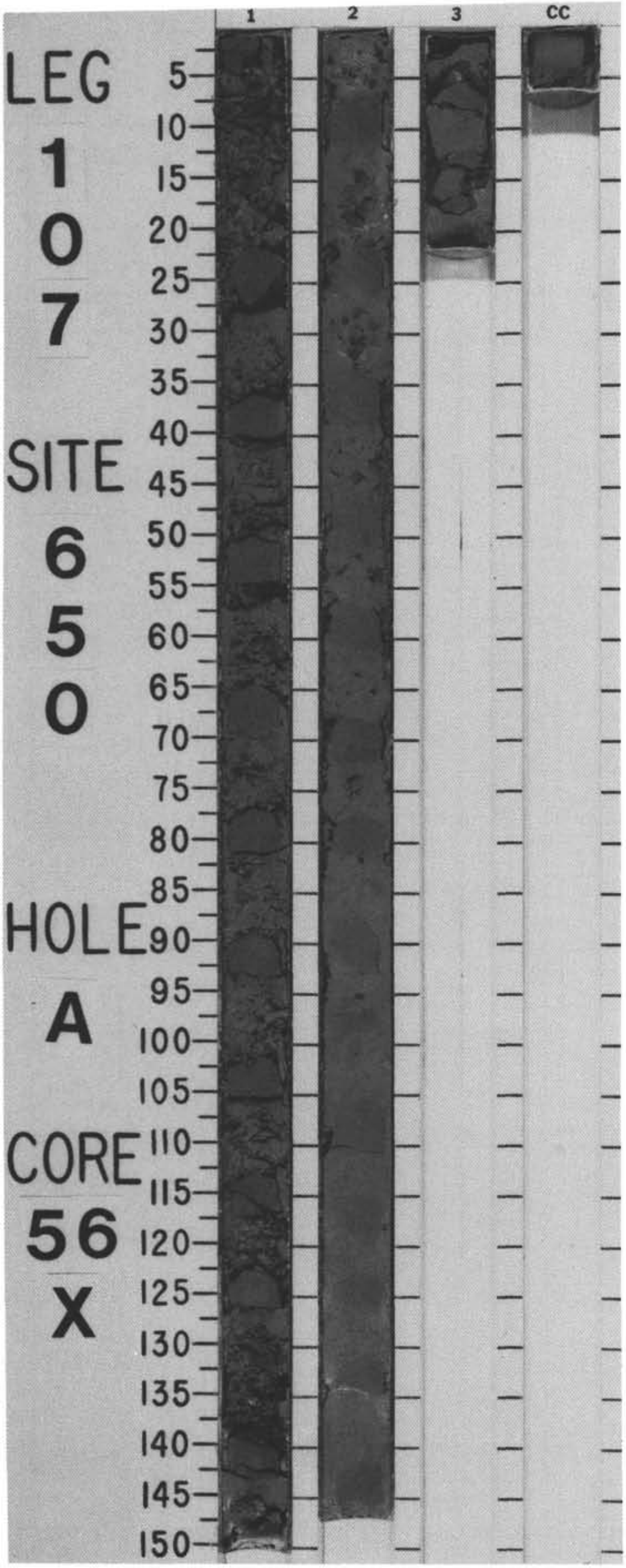
1
2
3
CC
LEG
1
0
7
SITE
6
5
0
HOLE
A
CORE
56
X
5
10
15
20
25
30
35
40
45
50
55
60
65
70
75
80
85
90
95
100
105
110
115
120
125
130
135
140
145
150

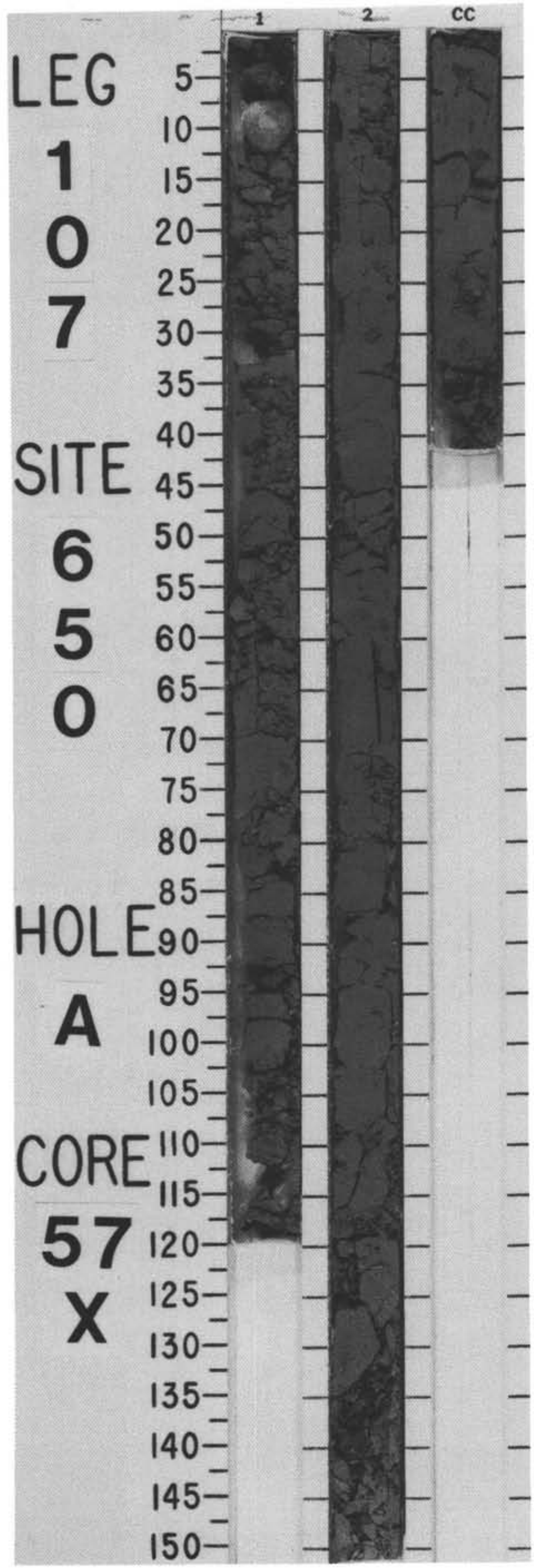
1
2
CC
LEG
1
0
7
SITE
6
5
0
HOLE
A
CORE
57
X
5
10
15
20
25
30
35
40
45
50
55
60
65
70
75
80
85
90
95
100
105
110
115
120
125
130
135
140
145
150

SITE 650 HOLE A CORE 58 X CORED INTERVAL 4043.8-4043.5 mbsl; 527.5-537.2 mbsf

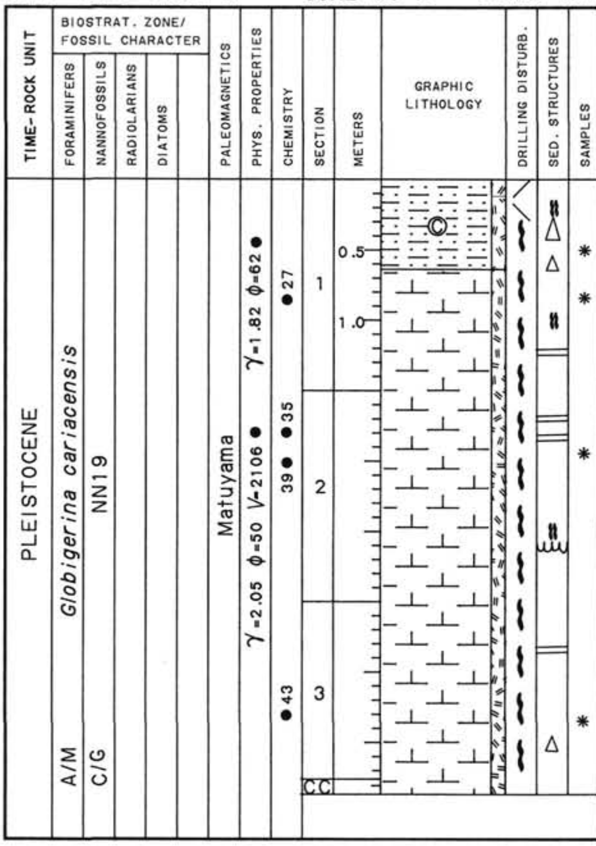

LITHOLOGIC DESCRIPTION

CALCAREOUS MUD and NANNOFOSSIL OOZE

Calcareous mud, dark bluish gray (5B 4/1) and dark greenish gray (5G 4/1) to greenish gray (5G 6/1), thin (15–20 cm), fining-upward sequences.

Nannofossil ooze, bluish gray (5B 5/1–6/1), greenish gray (5GY 6/1), and dark gray (5Y 4/1) to gray (5Y 6/1), common sandy foraminiferal laminae throughout (possibly basal part of indistinct graded units); volcanic glass is a common constituent.

SMEAR SLIDE SUMMARY (%):

	1, 54 D	1, 84 D	2, 50 D	3, 82 D
TEXTURE:				
Sand	—	—	—	—
Silt	10	30	20	—
Clay	90	70	80	—
COMPOSITION:				
Quartz	3	2	2	1
Clay	68	43	35	33
Volcanic glass	10	10	25	10
Calcite/dolomite	6	5	5	5
Accessory minerals	3	5	2	—
Micronodules	—	5	1	1
Nannofossils	10	30	30	50

SITE 650 HOLE A CORE 59 X CORED INTERVAL 4053.5-4063.1 mbsl; 537.2-546.8 mbsf

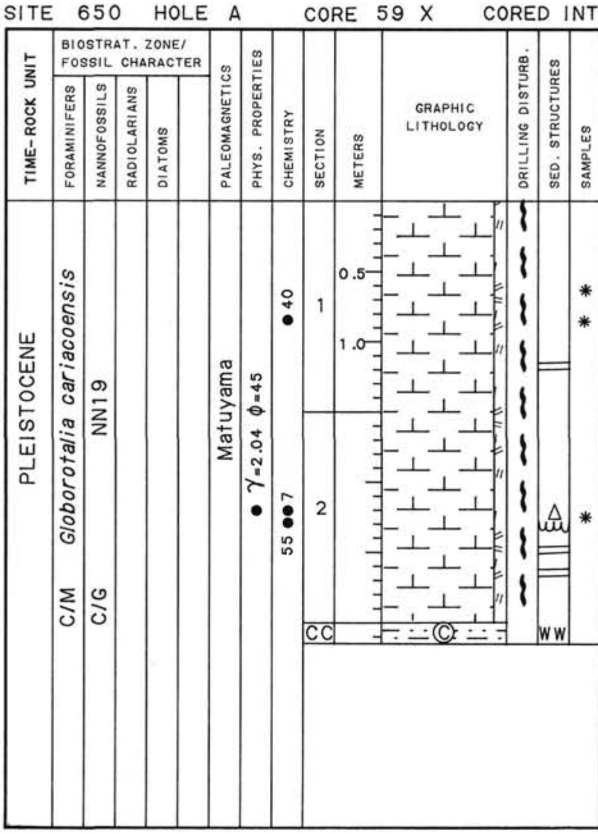

LITHOLOGIC DESCRIPTION

NANNOFOSSIL OOZE and CALCAREOUS MUD

Nannofossil ooze, dark greenish gray (5G 4/1) to greenish gray (5G 5/1 and 5GY 6/1) and dark gray (5Y 4/1) to light olive-gray (5Y 6/2); volcaniclastic and foraminiferal in Section 2, 75–80 cm.

Calcareous mud, olive (5Y 4/3), wavy laminae.

SMEAR SLIDE SUMMARY (%):

	1, 69 M	1, 84 D	2, 78 D
TEXTURE:			
Sand	30	—	—
Silt	30	5	40
Clay	40	95	60
COMPOSITION:			
Quartz	Tr	2	5
Feldspar	20	—	—
Clay	10	18	29
Volcanic glass	30	5	20
Calcite/dolomite	2	3	5
Accessory minerals	26	1	—
Pyroxene	5	—	—
Micronodules	—	1	—
Foraminifers	2	—	10
Nannofossils	5	70	30
Sponge spicules	—	—	1

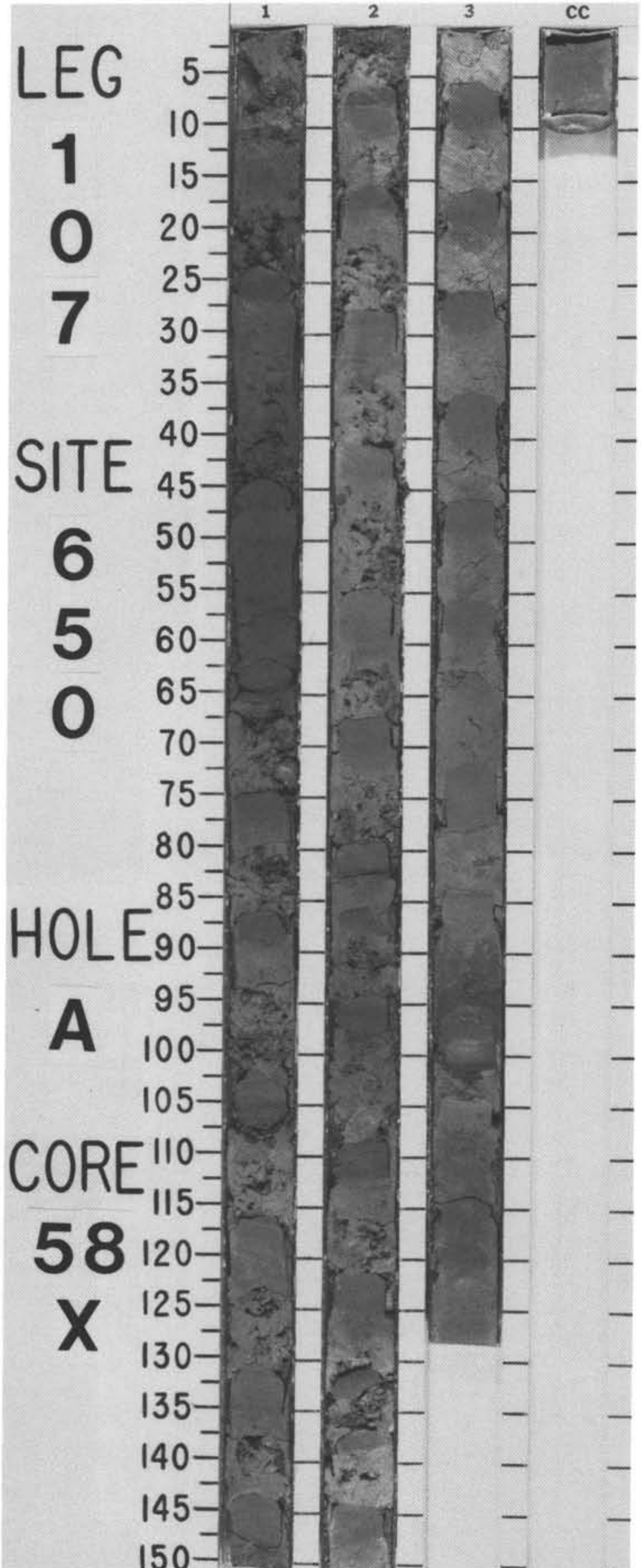
LEG
107
SITE
650
HOLE
A
CORE
58
X
1
2
3
CC

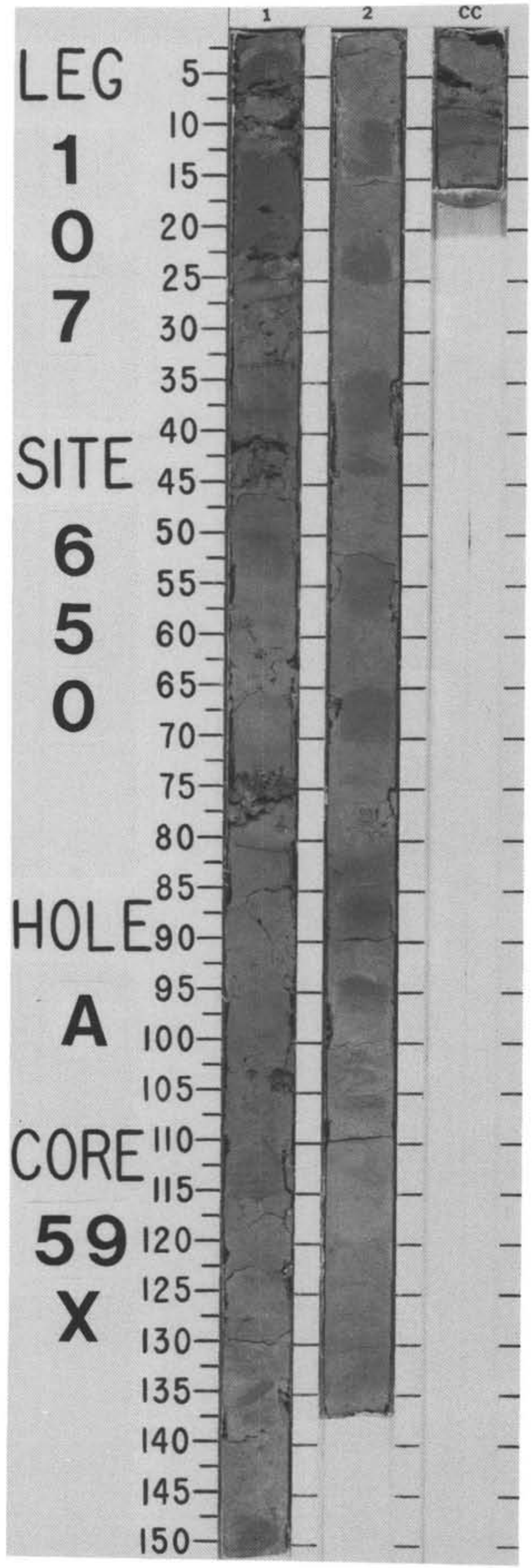
LEG
107
SITE
650
HOLE
A
CORE
59
X
1
2
CC

SITE 650 HOLE A CORE 60 X CORED INTERVAL 4063.1-4072.8 mbsl; 546.8-556.5 mbsf

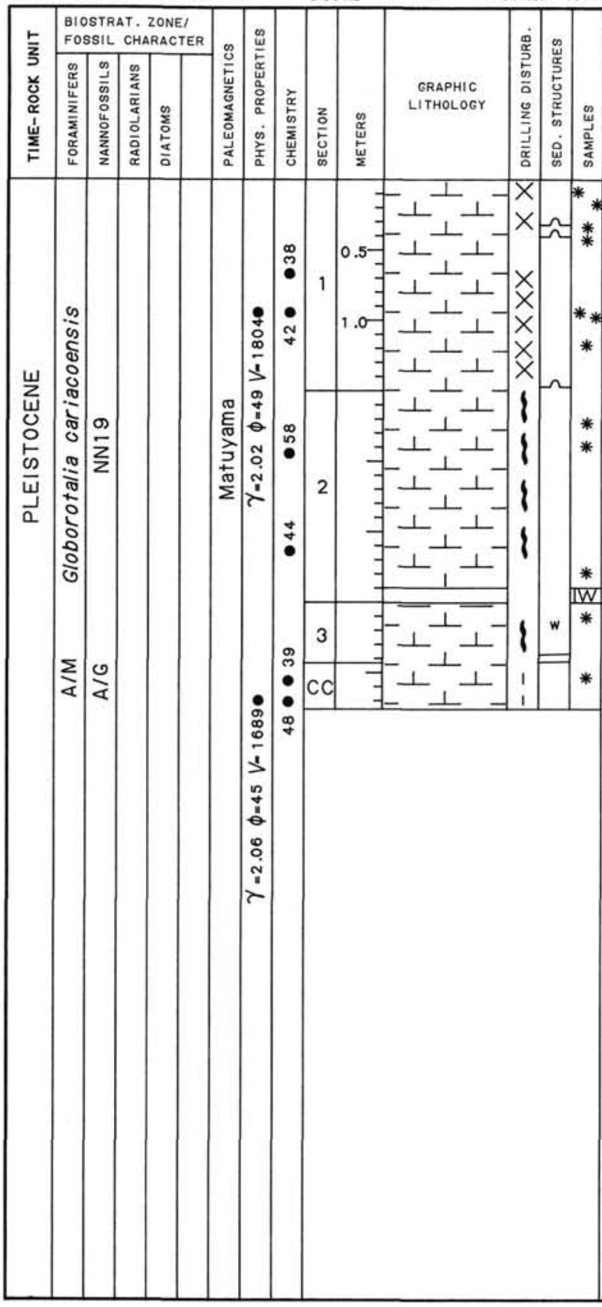

LITHOLOGIC DESCRIPTION

NANNOFOSSIL OOZE

Nannofossil ooze, olive-brown (2.5Y 4/4) to grayish brown (2.5Y 5/2) and olive-gray (5Y 4/2–5/2) to gray (5Y 5/1), alternating with intervals of pebbly mudstone or intraformational conglomerate in Section 1, 10–26, 42–50, 93–111, 116–122, 125–130, and 140–145 cm; in Section 2, 45 cm, pebble color is gray (5Y 5/1) to light gray (5Y 7/1); pebble lithology is nannofossil ooze with the exception of Section 2, 45 cm, which is a foraminifer-nannofossil ooze.

SMEAR SLIDE SUMMARY (%):

	1, 15 M	1, 19 M	1, 35 M	1, 46 M	1, 97 M	1, 97.5 M	1, 118 M
TEXTURE:							
Sand	—	—	—	—	—	—	—
Silt	30	10	15	10	5	25	10
Clay	70	90	85	90	95	75	90
COMPOSITION:							
Quartz	1	—	—	—	—	—	Tr
Feldspar	1	1	1	1	2	2	—
Clay	20	19	25	10	10	20	40
Volcanic glass	5	2	2	5	2	5	—
Calcite/dolomite	7	2	—	2	6	2	Tr
Accessory minerals	1	—	—	—	—	1	—
Opaques	—	5	—	—	—	—	—
Foraminifers	5	1	5	—	—	5	Tr
Nannofossils	40	50	40	60	50	40	50
Silicoflagellates	—	—	—	2	—	—	—
Micrite	20	20	27	20	20	25	10
Braarudosphaera	—	—	—	—	—	Tr	—

	2, 24 D	2, 45 D	2, 132 D	3, 17 D	CC, 14 D
TEXTURE:					
Sand	—	—	—	—	—
Silt	10	10	10	10	10
Clay	90	90	90	90	90
COMPOSITION:					
Quartz	—	—	5	—	Tr
Feldspar	3	—	Tr	2	—
Mica	—	—	5	—	Tr
Clay	17	20	30	22	40
Volcanic glass	5	—	—	5	Tr
Calcite/dolomite	—	Tr	—	—	5
Foraminifers	5	10	5	1	5
Nannofossils	50	50	40	50	35
Micrite	20	10	5	20	—
Unpecified carbonate	—	10	10	—	15

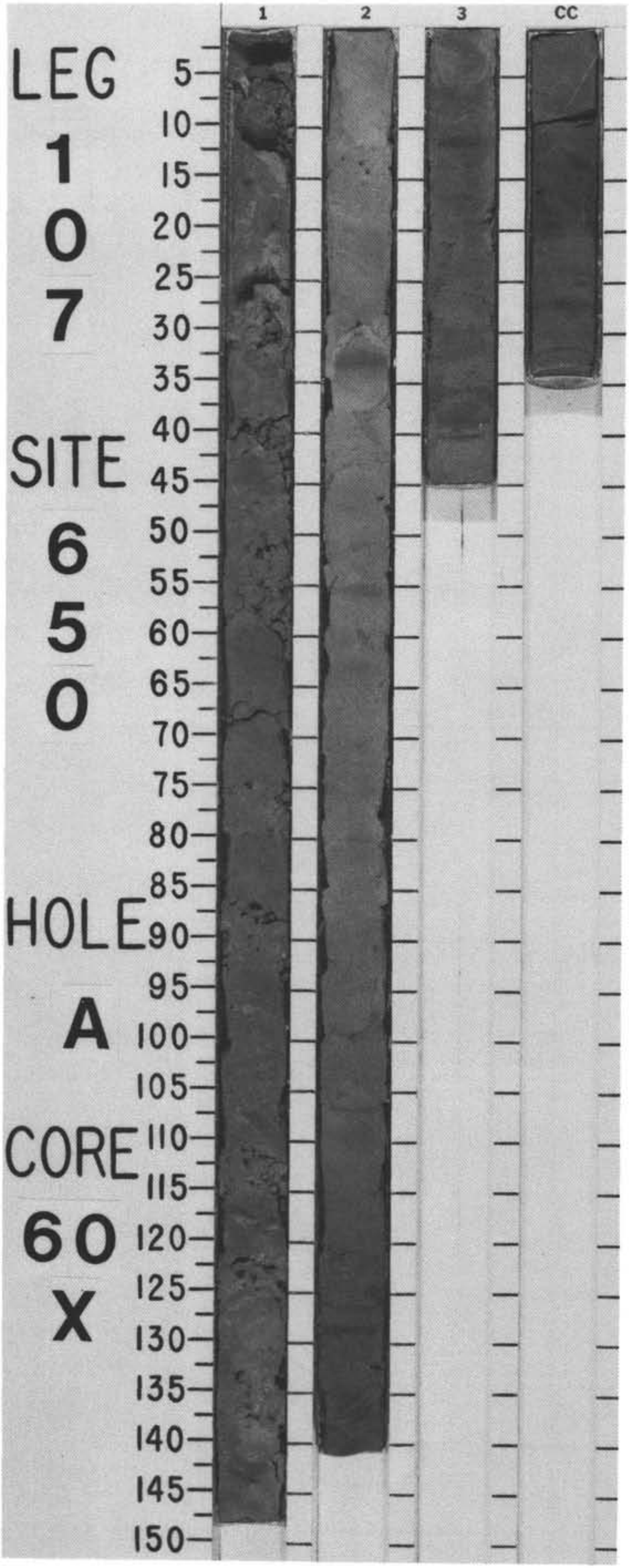
1
2
3
CC
LEG
107
SITE
650
HOLE
A
CORE
60
X
5
10
15
20
25
30
35
40
45
50
55
60
65
70
75
80
85
90
95
100
105
110
115
120
125
130
135
140
145
150

SITE 650 HOLE A CORE 61 X CORED INTERVAL 4072.8-4082.4 mbsl; 556.5-566.1 mbsf

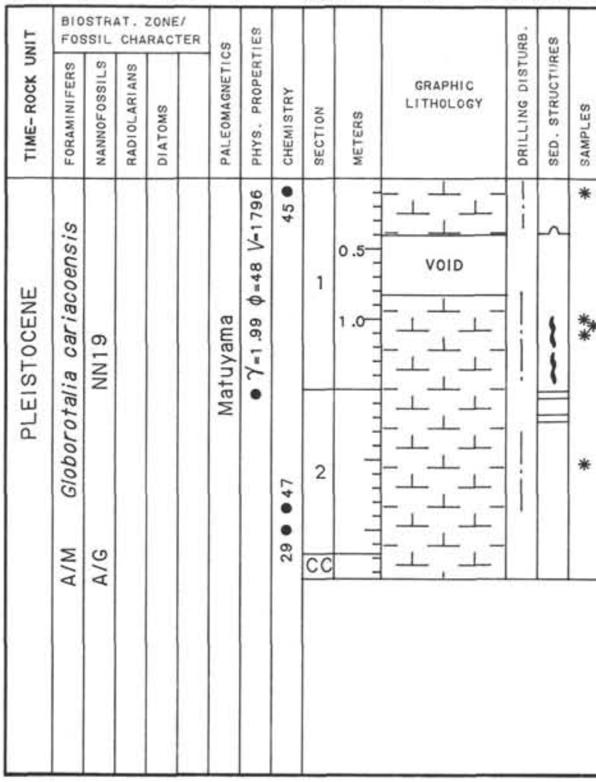

LITHOLOGIC DESCRIPTION

NANNOFOSSIL OOZE

Nannofossil ooze, light brownish gray (2.5Y 6/2) with very thin intervals of dark grayish brown (2.5Y 4/2), grayish brown (2.5Y 5/2), light yellowish brown (2.5Y 6/4) and gray (N 5) calcareous claystone, mottled to very finely laminated, small-scale convolute laminations in Section 1, 36–40 cm.

SMEAR SLIDE SUMMARY (%):

	1, 12 D	1, 99 D	1, 103 D	1, 112 D	2, 51 D
TEXTURE:					
Sand	—	—	—	—	—
Silt	5	5	25	5	5
Clay	95	95	75	95	95
COMPOSITION:					
Quartz	—	—	—	Tr	—
Feldspar	—	—	1	—	—
Mica	—	Tr	—	—	Tr
Clay	20	5	20	20	20
Volcanic glass	5	—	5	—	—
Calcite/dolomite	—	40	1	—	Tr
Foraminifers	5	Tr	8	20	20
Nannofossils	50	20	50	40	50
Micrite	20	20	15	10	5
Unspecified carbonate	—	15	—	10	5

SITE 650 HOLE A CORE 62 X CORED INTERVAL 4082.4-4092.1 mbsl; 566.1-575.8 mbsf

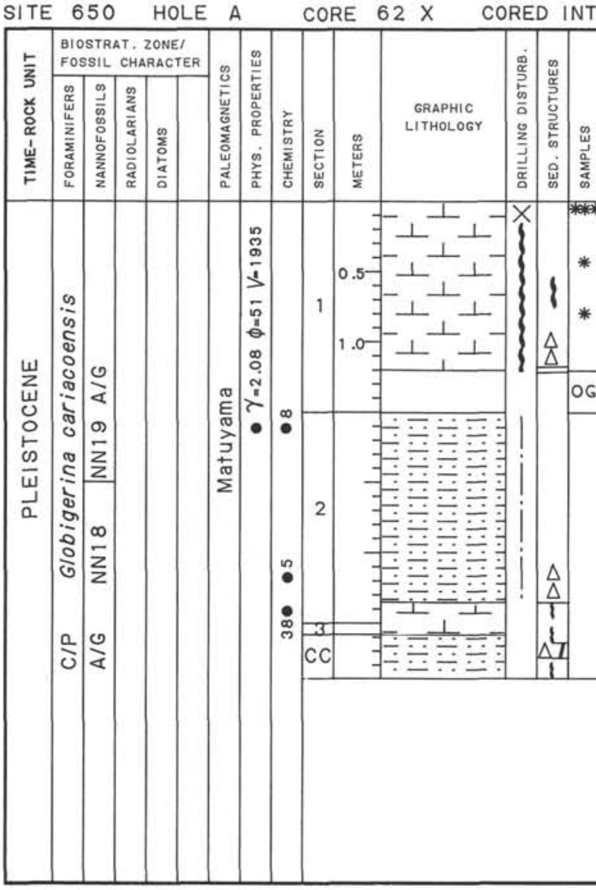

LITHOLOGIC DESCRIPTION

NANNOFOSSIL OOZE and MUDSTONE

Nannofossil ooze, dark gray (5Y 4/1) to gray (5Y 6/1), with enrichment of foraminifers in Section 1, 43–47 cm.

Mudstone, dusky yellowish green (5GY 5/2, 10GY 3/2), homogeneous.

Minor lithology: siltstone, laminae to very thin, normally graded beds in Section 1, 95 and 112 cm, and in Section 2, 120–126 and 126–131 cm; micro-cross-lamination.

SMEAR SLIDE SUMMARY (%):

	1, 1 M	1, 5 M	1, 5 M	1, 50 D	1, 83 D
TEXTURE:					
Sand	—	5	—	—	—
Silt	5	10	5	15	5
Clay	95	85	95	85	95
COMPOSITION:					
Quartz	—	—	—	Tr	Tr
Feldspar	1	1	1	Tr	—
Clay	20	25	22	10	15
Volcanic glass	2	2	2	—	—
Calcite/dolomite	1	2	1	30	—
Accessory minerals	1	—	—	—	—
Opaques	—	—	2	—	—
Foraminifers	5	5	—	10	40
Nannofossils	50	40	50	25	20
Micrite	20	25	22	20	15
Unspecified carbonate	—	—	—	5	10

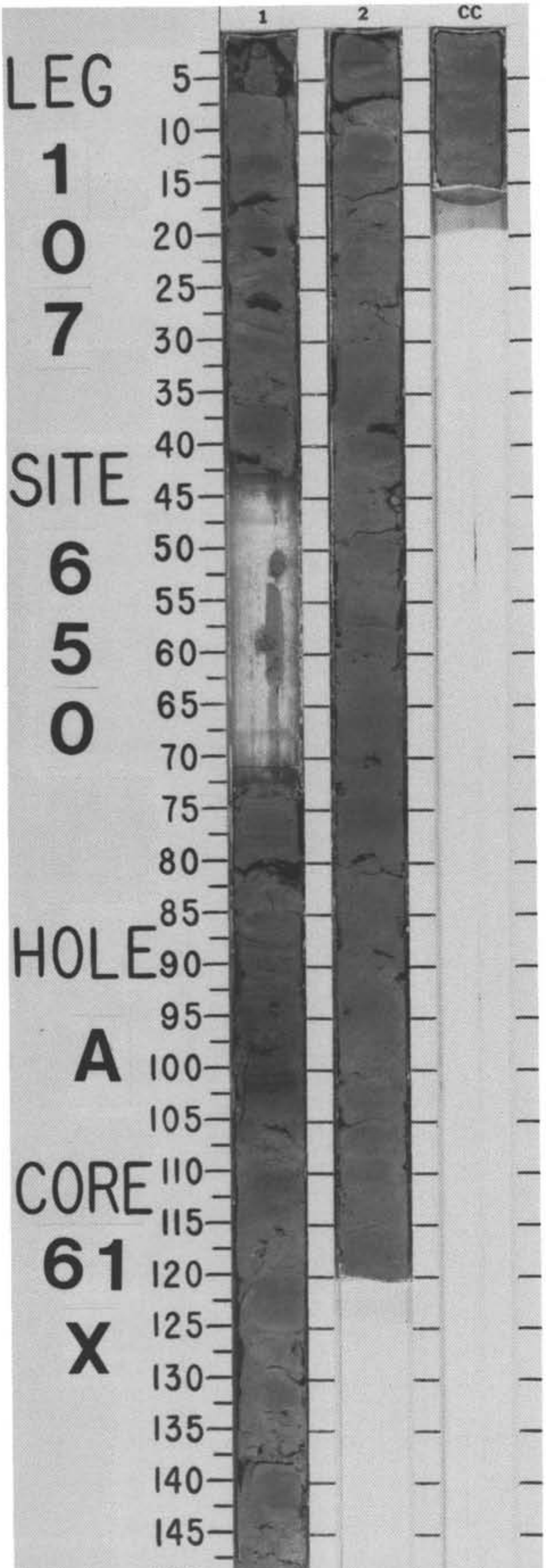
1
2
CC
LEG
1
0
7
SITE
6
5
0
HOLE
A
CORE
61
X
5
10
15
20
25
30
35
40
45
50
55
60
65
70
75
80
85
90
95
100
105
110
115
120
125
130
135
140
145
150

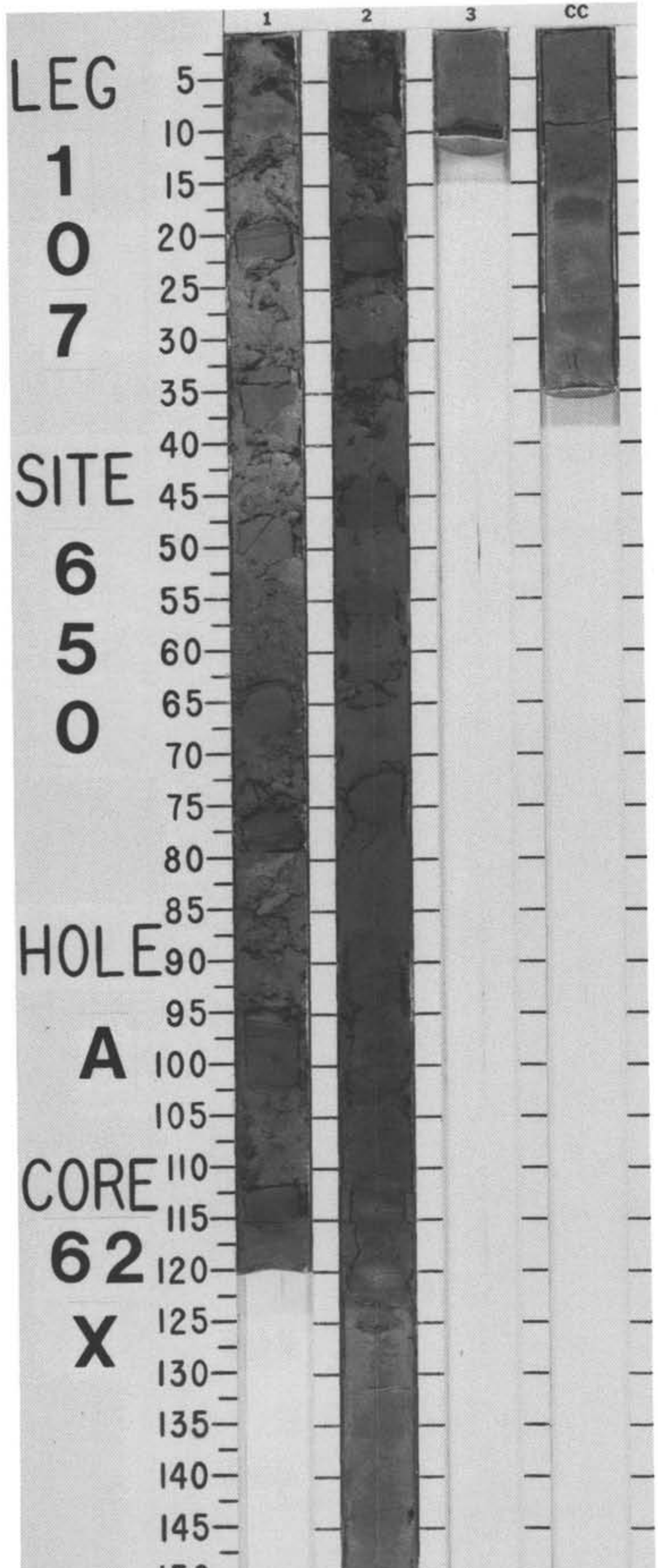
1
2
3
CC
LEG
1
0
7
SITE
6
5
0
HOLE
A
CORE
62
X
5
10
15
20
25
30
35
40
45
50
55
60
65
70
75
80
85
90
95
100
105
110
115
120
125
130
135
140
145
150

SITE 650 HOLE A CORE 63 X CORED INTERVAL 4092.1-4100.7 mbsl; 575.8-584.4 mbsf

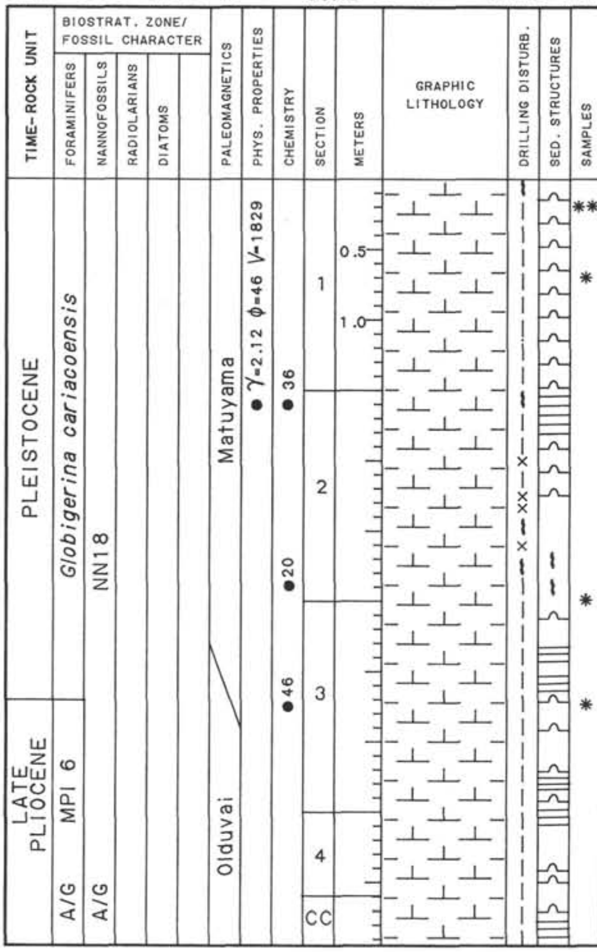

LITHOLOGIC DESCRIPTION

NANNOFOSSIL OOZE (CHALK)

Nannofossil ooze (chalk), dark gray (5Y 4/1) to gray (5Y 6/1), slumps and intraformational conglomerates, mud pebbles in brecciated intervals varying slightly in color (greenish to pinkish).

SMEAR SLIDE SUMMARY (%):

	1, 21 M	1, 21 D	1, 74 D	2, 149 M	3, 76 D
TEXTURE:					
Sand	—	—	—	5	—
Silt	20	15	15	15	15
Clay	80	85	85	80	85
COMPOSITION:					
Quartz	—	1	—	5	—
Clay	30	44	30	55	60
Calcite/dolomite	—	—	5	5	5
Foraminifers	10	10	10	5	10
Nannofossils	60	30	30	25	25
Pellets	—	5	—	—	—
Bioclasts	—	5	25	5	—
Micrite	—	5	—	—	—

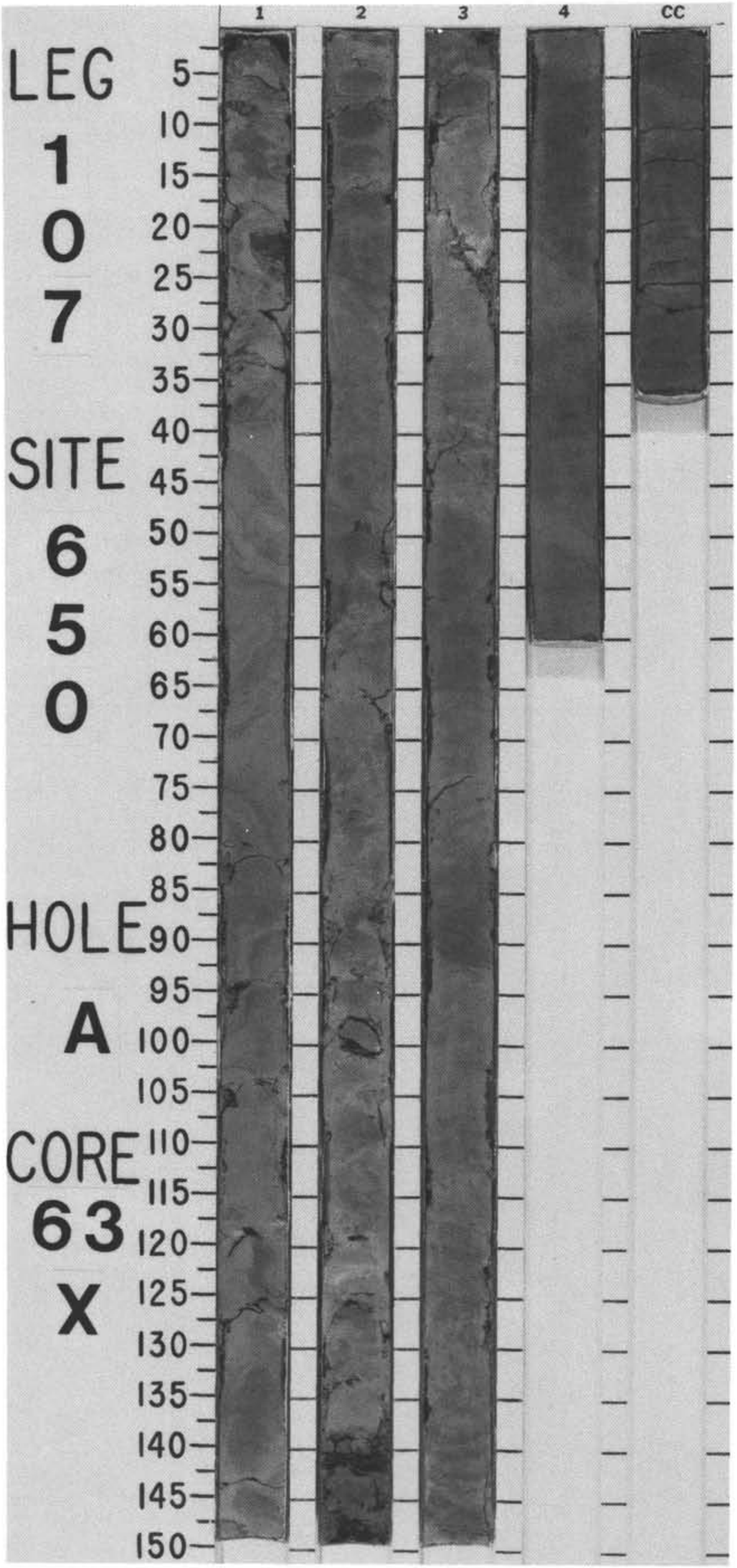
LEG
1
0
7
SITE
6
5
0
HOLE
A
CORE
63
X
1
2
3
4
CC

SITE 650 HOLE A CORE 64 X CORED INTERVAL 4100.7-4110.4 mbsl; 584.4-594.1 mbsf

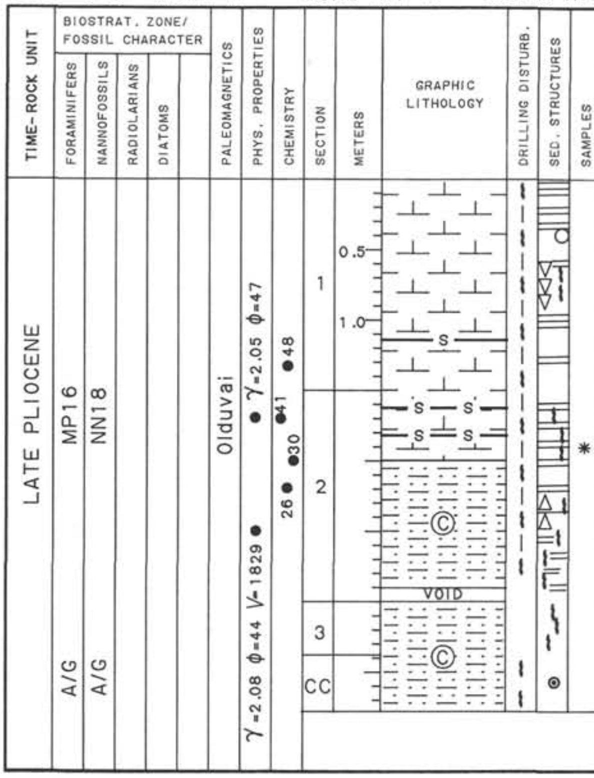

LITHOLOGIC DESCRIPTION

NANNOFOSSIL OOZE and CALCAREOUS MUDSTONE

Nannofossil ooze, dark gray (5Y 4/1) to gray (5Y 6/1).

Calcareous mudstone, dark olive-gray (5Y 3/2) to olive-gray (5Y 5/2), black foraminifers (pyritized?) in Section 2.

Minor lithology: dark mudstone (possibly sapropelic), very dark grayish brown (2.5Y 3/2) to dark grayish brown (2.5Y 4/2) and dark olive-gray (5Y 3/2) in Section 1, 116 and 144 cm, and in Section 2, 7, 15, 26, 39, and 50 cm, alternating with millimeter-thin laminae containing *Braarudosphaera*.

SMEAR SLIDE SUMMARY (%):

	2, 40
	M
TEXTURE:	
Sand	—
Silt	5
Clay	95
COMPOSITION:	
Calcite/dolomite	15
Accessory minerals	5
Foraminifers	20
Nannofossils	60

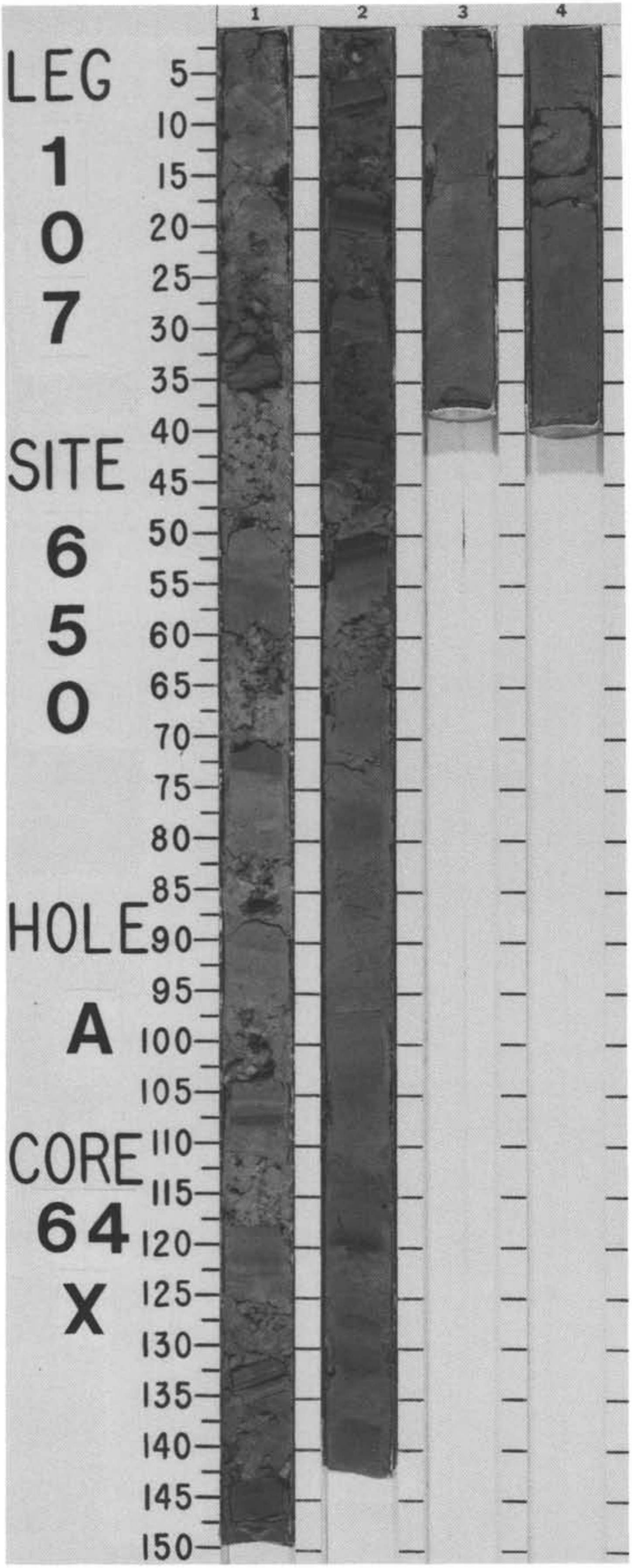
LEG
107
SITE
650
HOLE
A
CORE
64X
1
2
3
4

SITE 650 HOLE A CORE 65 X CORED INTERVAL 4110.4-4016 mbsl 394-599.8 mbsf

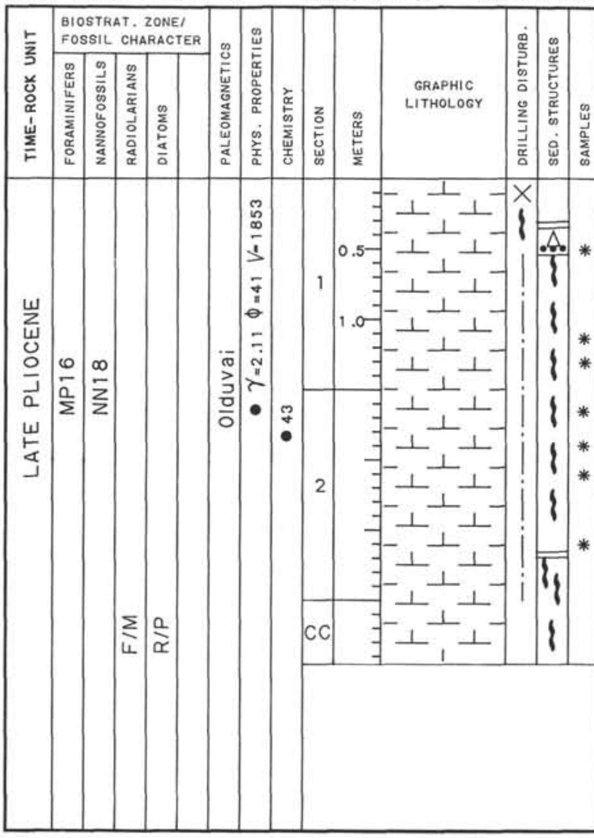

LITHOLOGIC DESCRIPTION

NANNOFOSSIL OOZE

Nannofossil ooze, pale green graded sequence (10G 6/2), olive-gray (5Y 5/2) to light olive-gray (5Y 6/2), and brown (7.5YR 5/2–10YR 5/3) to light yellowish brown (10YR 6/4); the cored interval is dominantly brownish in color with thin zones of green in Section 2, 6 and 112 cm, and in CC, 35 cm; CC, 38–39 cm, is metalliferous.

SMEAR SLIDE SUMMARY (%):

	1, 56 D	1, 116 D	1, 133 M	2, 18 D	2, 40 M	2, 68 M	2, 112 M
TEXTURE:							
Sand	10	5	—	—	—	—	10
Silt	30	20	15	15	10	15	10
Clay	60	75	85	85	90	85	80
COMPOSITION:							
Feldspar	—	1	—	—	—	—	Tr
Rock fragments	—	1	—	—	—	—	—
Clay	30	40	35	45	45	45	23
Calcite/dolomite	2	1	5	10	5	10	1
Accessory minerals	—	1	—	5	5	5	—
Opaques	3	—	—	—	—	—	—
Zeolite	—	—	5	—	—	—	—
Foraminifers	15	10	15	5	10	5	10
Nannofossils	25	35	30	30	30	30	45
Sponge spicules	—	1	—	—	—	—	1
Micrite	25	10	—	—	—	—	—
Bioclasts	—	—	10	5	5	5	—
Spar cement	—	—	—	—	—	—	20

SITE 650 HOLE A CORE 66 X CORED INTERVAL 4016.1-4121.1 mbsl; 599.8-604.8 mbsf

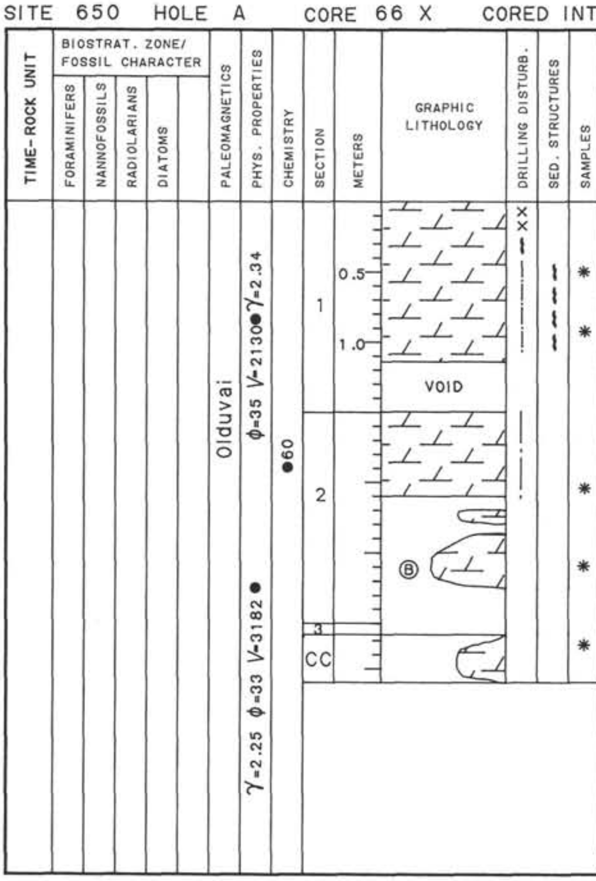

LITHOLOGIC DESCRIPTION

DOLOMITE (DOLOMITIC MUDSTONE)

Dolomite (dolomitic mudstone), dark yellowish brown (10YR 4/4) to brownish yellow (10YR 6/6) above sediment/basalt contact and light gray (5Y 7/2) intercalated within the basalt in Section 2, 107–111 cm, 9-mm crust of volcanic glass at sediment/basalt contact.

SMEAR SLIDE SUMMARY (%):

	1, 47 D	1, 95 D	2, 56 D	2, 110 M	CC, 5 D	CC, 65 D
TEXTURE:						
Sand	—	—	—	—	—	—
Silt	15	60	—	10	10	10
Clay	85	40	—	90	90	90
COMPOSITION:						
Feldspar	5	5	20	7	Tr	1
Clay	21	25	5	43	40	60
Volcanic glass	—	—	5	—	—	—
Calcite/dolomite	65	70	70	50	30	36
Accessory minerals	—	—	—	—	Tr	2
Zeolites	6	Tr	—	—	—	—
Nannofossils	3	—	—	Tr	—	1
Fish remains	—	Tr	—	—	—	—
Micrite	—	—	—	—	30	—

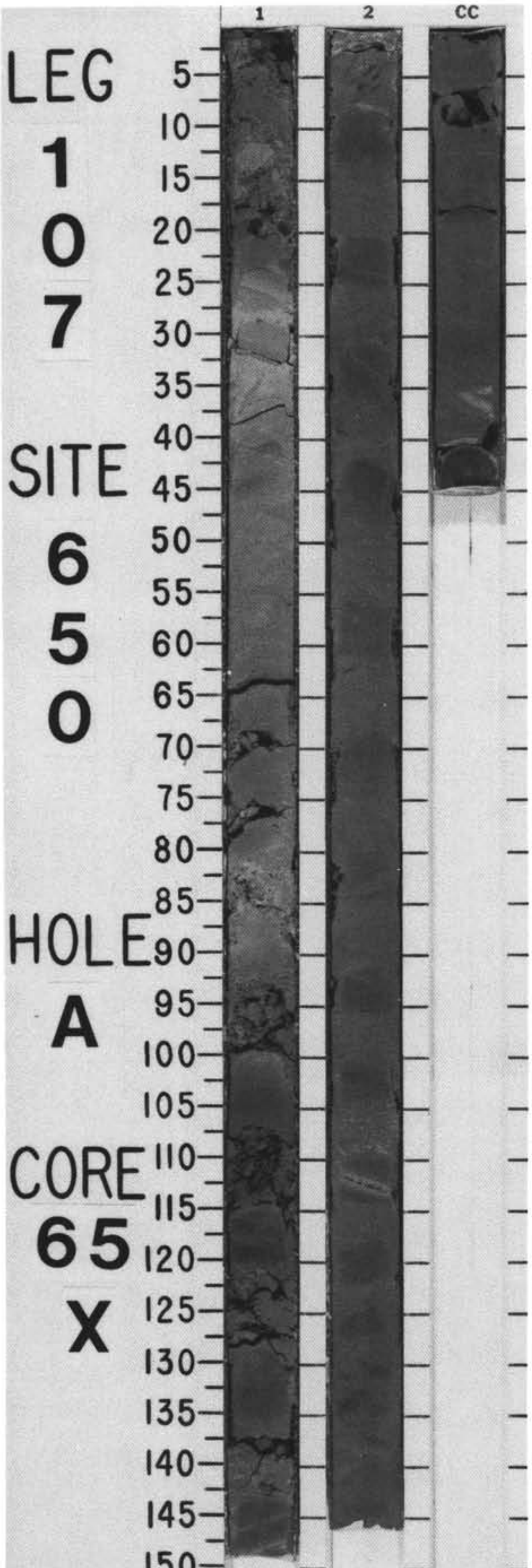
LEG
107
SITE
650
HOLE
A
CORE
65
X
1
2
CC

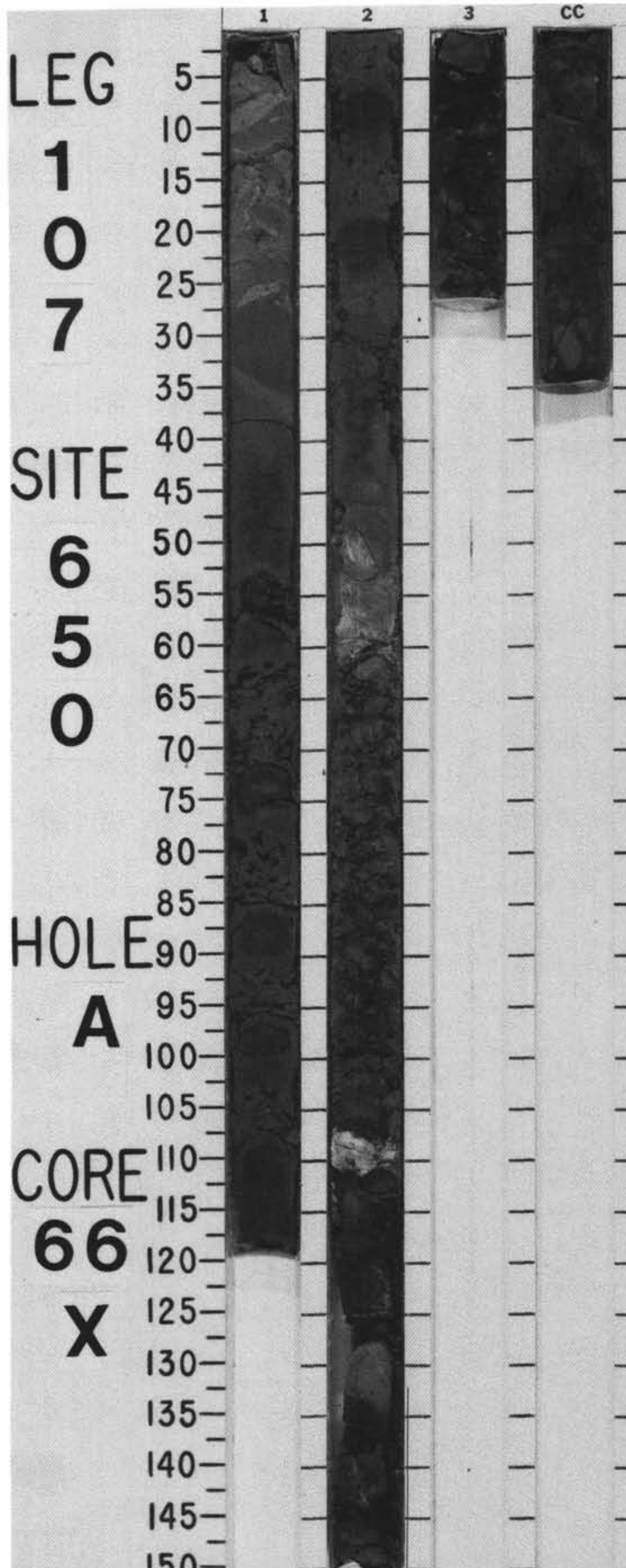
LEG
107
SITE
650
HOLE
A
CORE
66
X
1
2
3
CC

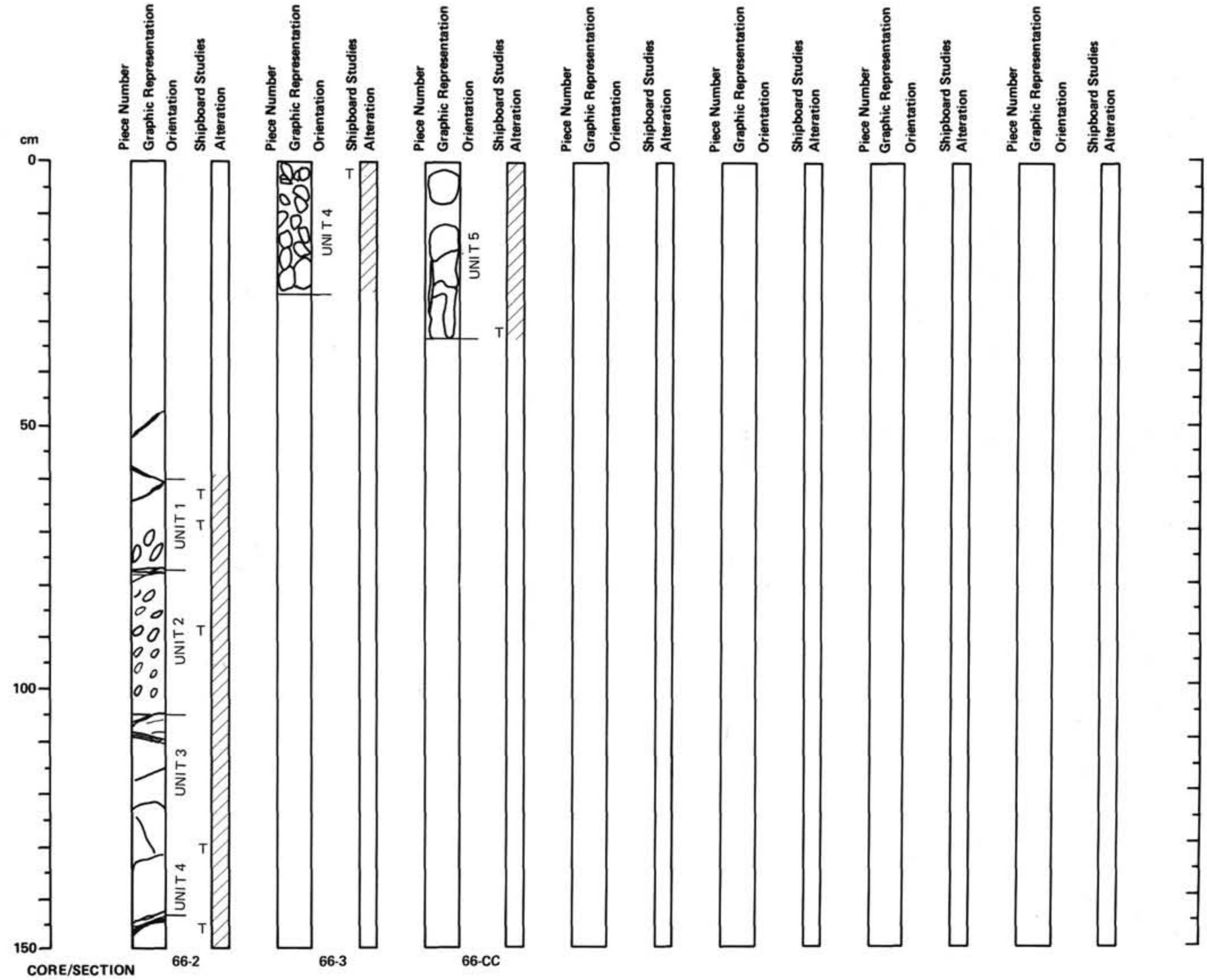

UNIT 1 AND 2

Fragmented altered vesicular basalt, close to the contact with the sediment. The basalt is made of highly altered, brownish glass. A few skeletal Ca-plagioclase crystals are scattered in the groundmass. Relict euhedral olivine pseudomorphs can be recognized. No pyroxenes can be recognized. Vesicles range up to 2-3 mm in diameter. Crystallinity increases downward. Intersertal to intergranular texture. Pale green dolomite-rich mud intercalated in the dolerite is observed in Interval 650A-66X-2, 105-110cm.

UNIT 3

Dark gray vesicular basalt. Ca-plagioclase laths (grain size larger than in section above) in altered matrix. Texture is intersertal to intergranular.

UNIT 4

Top of unit 4 is probably an altered chilled glass margin marking the top of a flow. Euhedral olivine and skeletal plagioclase crystals in altered glass.

UNIT 5

Fragmented altered vesicular basalt. Intersertal to intergranular texture. Laths of plagioclase in altered groundmass. Rare clinopyroxene crystals are present. Pseudomorphs after olivine.

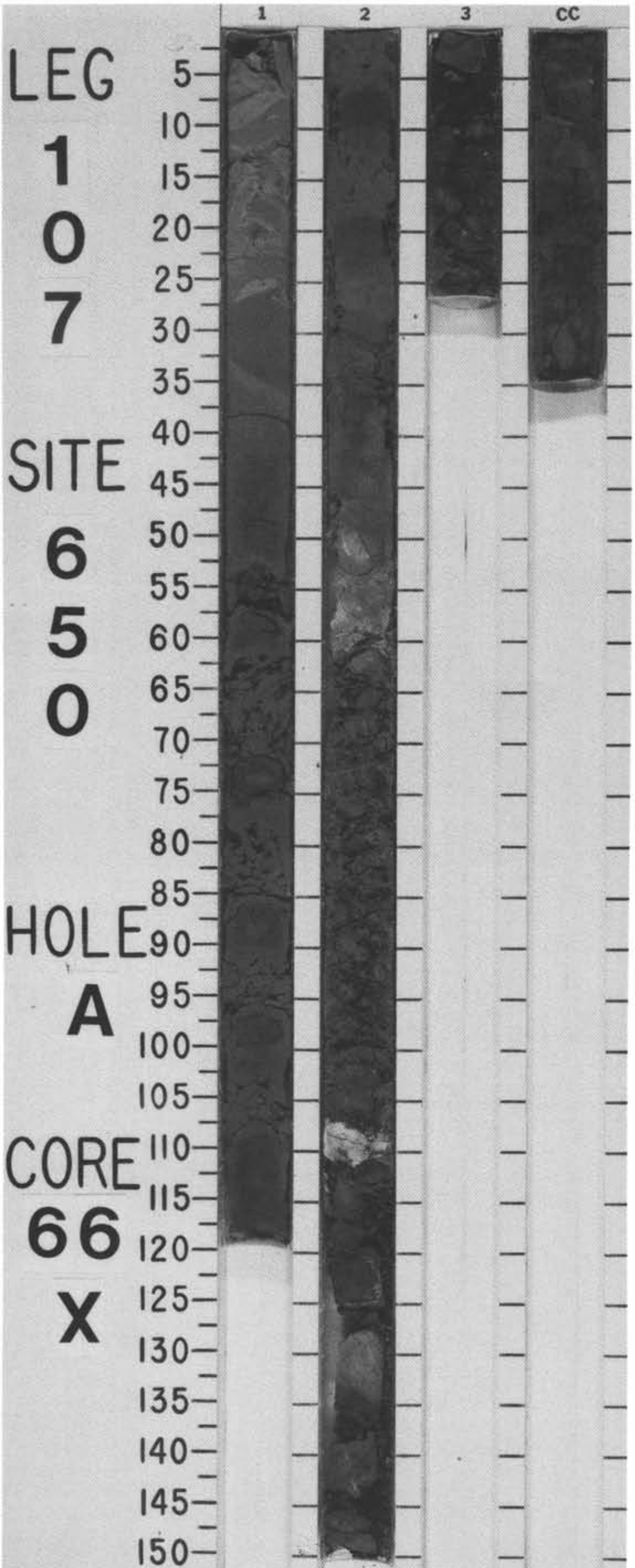
LEG
1
0
7
SITE
6
5
0
HOLE
A
CORE
66
X
1
2
3
CC

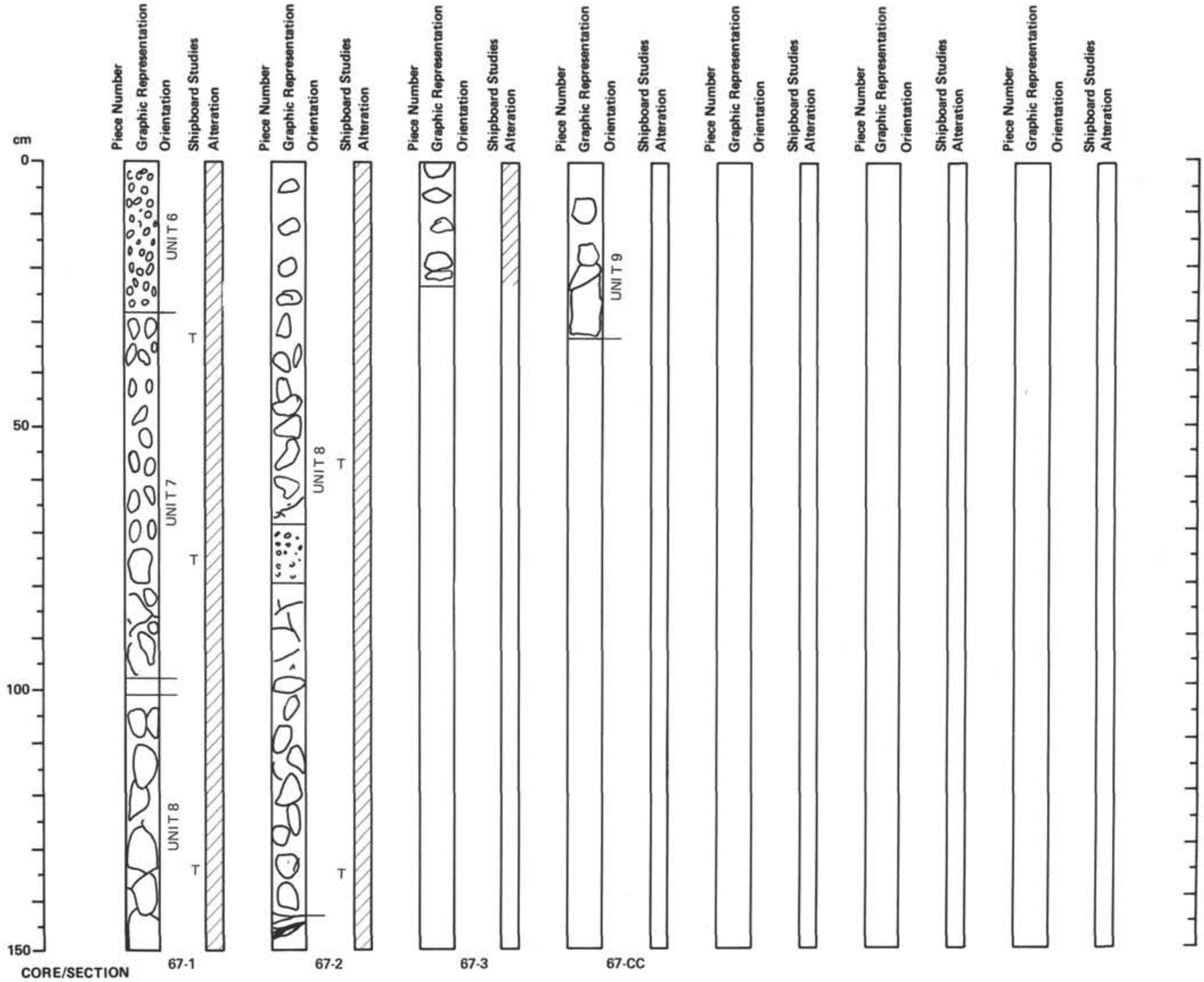

UNIT 6

Basalt. Finely crushed during drilling and mixed with drilling mud.

UNIT 7

Vesicular basalt. Intergranular texture. Ca-plagioclase (labradorite) laths in altered matrix. Olivine pseudomorphs are present in the Interval 650A-67X-1, 30-60 cm. Interval 650A-67X-1, 70-95 cm is altered vesicular basalt. Large (up to 2-3 mm diameter) vesicles are partially filled with carbonates, zeolites and Fe-hydroxides. Texturally similar to other units. Yellowish band of baked sediment(?) observed in Interval 650A-67X-1, 98-102 cm.

UNIT 8

Vesicular basalt. Intersertal texture. Highly altered. Plagioclase laths are the only recognizable primary phase. Vesicles >10%. Interval 650A-67X-2, 0-30 cm, contains fragmented pebbles embedded in drilling mud. Interval 650A-67X-2, 30-70 cm, is basalt with vesicles partiallly filled by carbonates and zeolites. Intersertal texture, with plagioclase laths dispersed in a highly altered matrix.

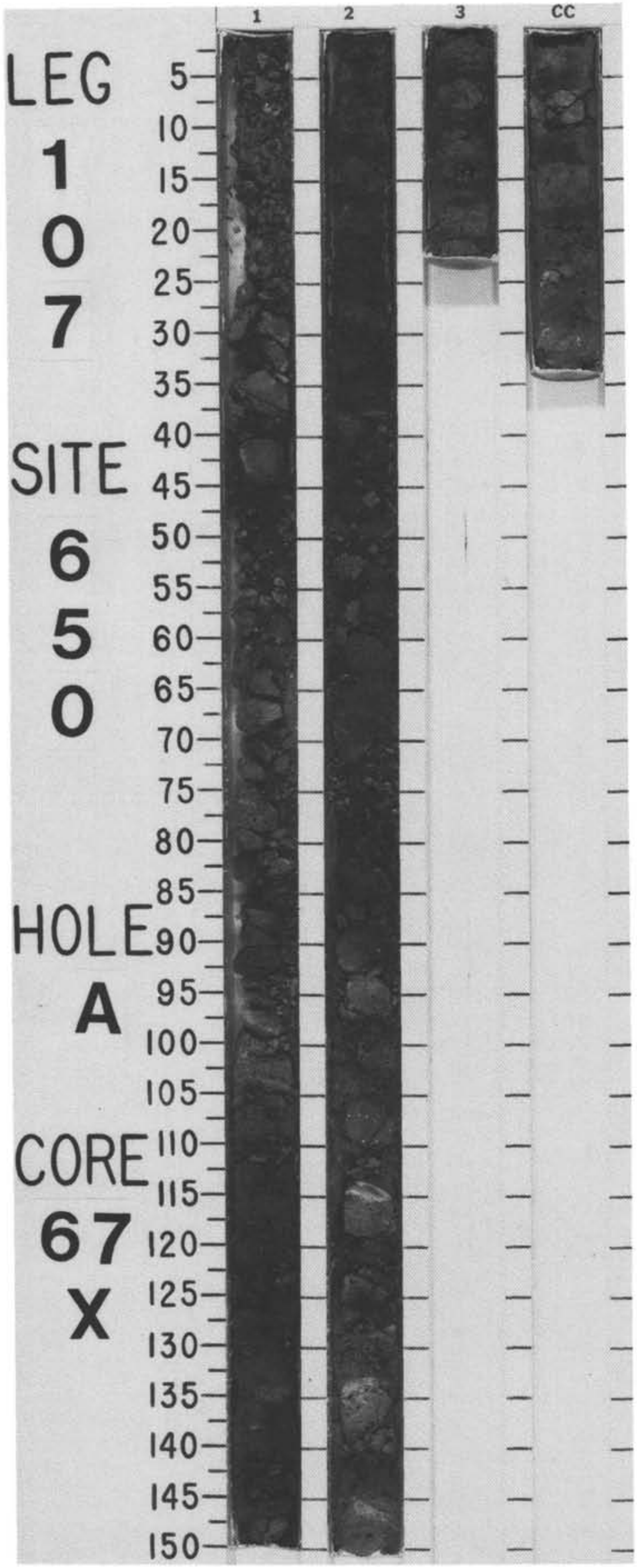
LEG
107
SITE
650
HOLE
A
CORE
67
X
1
2
3
CC
5
10
15
20
25
30
35
40
45
50
55
60
65
70
75
80
85
90
95
100
105
110
115
120
125
130
135
140
145
150

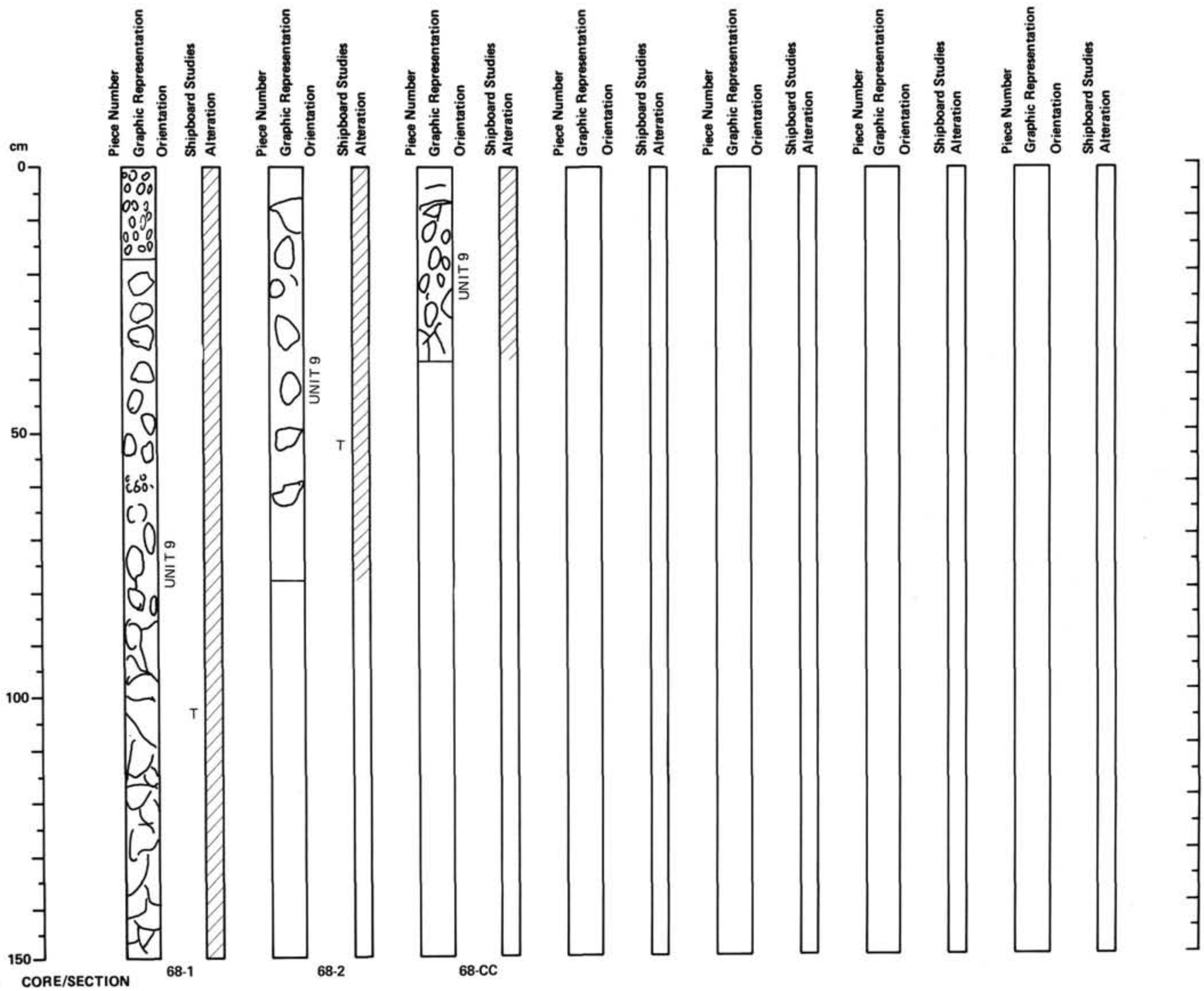

UNIT 9

Vesicular basalt. Intersertal to intergranular texture. Olivine pseudomorphs not observed. Ca-plagioclase laths are in a highly altered groundmass. A few clusters of microphenocrysts of Ca-plagioclase observed.

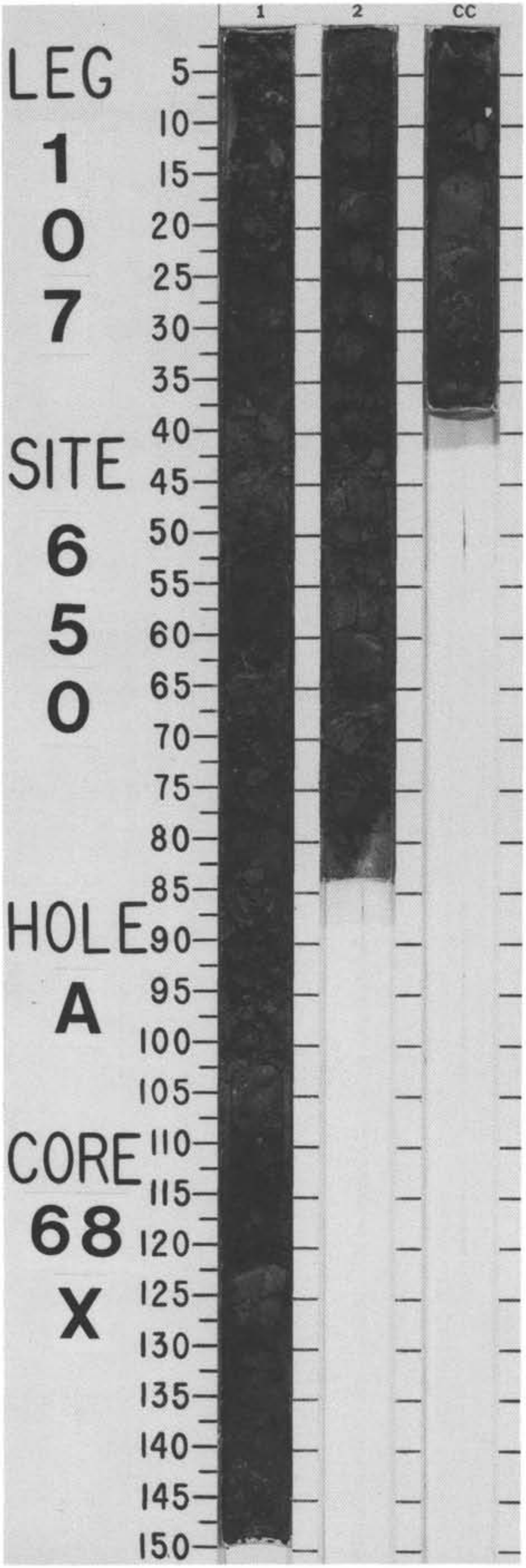
LEG
1
0
7
SITE
6
5
0
HOLE
A
CORE
68
X
1
2
CC

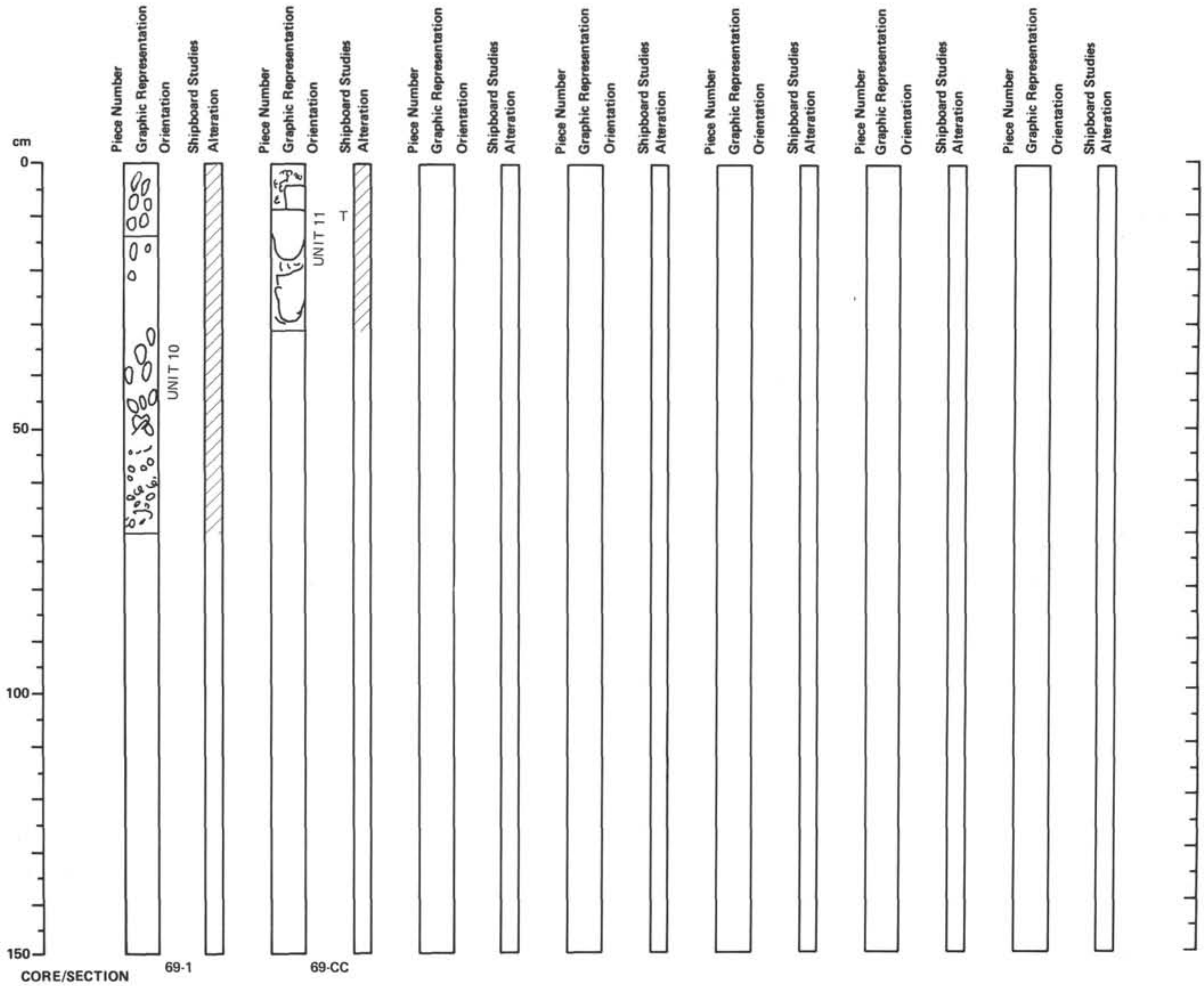

UNIT 10

Unit 10 is composed of crushed pebbles mixed with drilling mud. Fragments of indurated sediments were observed at the base of this unit, Interval 650A-69X-CC, 0-7 cm .

UNIT 11

This unit is composed of less altered, relatively non-vesicular basalt. Intersertal texture. Ca-plagioclase laths in a matrix of clay plus secondary Fe-hydroxide. Pseudomorphs after euhedral olivine also present.

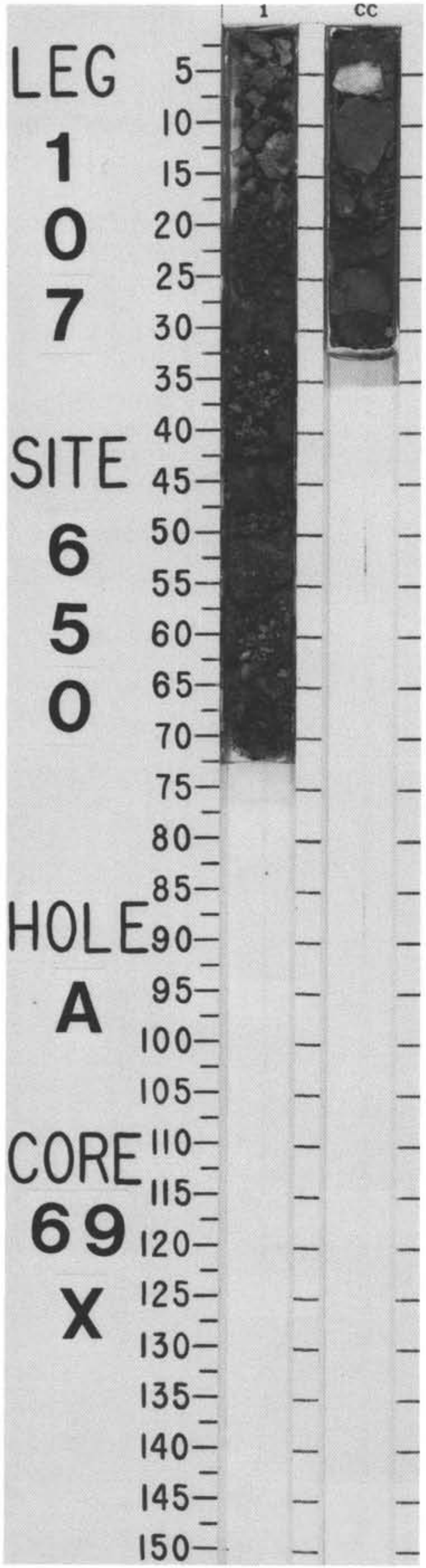
LEG
1
0
7
SITE
6
5
0
HOLE
A
CORE
69
X
1
CC
5
10
15
20
25
30
35
40
45
50
55
60
65
70
75
80
85
90
95
100
105
110
115
120
125
130
135
140
145
150